AN ABSTRACT OF THE DISSERTATION OF

Bradley W. Pitcher for the degree of Doctor of Philosophy in Geology presented on June 9, 2017.

Title: The Deschutes Formation: Evidence of Extension-Enhanced Explosivity in the Early High Cascades

Abstract approved:

_____

Adam J.R. Kent

The eruptive history of the Quaternary Cascades arc has been relatively well characterized. However, much less is known about the frequency and sizes of explosive eruptions produced by earlier stages of the arc. The Late Neogene Deschutes Formation of Central Oregon preserves a remarkable record of heightened pyroclastic activity during the initial stages of High Cascades volcanism, following an eastward shift in volcanic activity ~7.5 Ma. Extensive fieldwork, $^{40}Ar/^{39}Ar$ geochronology, and geochemical analyses allow us to reconstruct this unusually explosive phase of the earliest Central Oregon High Cascades.

Plagioclase $^{40}Ar/^{39}Ar$ ages for eight laterally-extensive marker ignimbrites that stratigraphically bracket the many pyroclastic deposits exposed within the Deschutes Formation, indicate that almost all of these explosive eruptions occurred within only ~800 k.y., between 6.25± 0.07 and 5.45± 0.04 Ma. Combining these age data with multivariate statistical tephra correlation methods, I establish a comprehensive tephrostratigraphy of the Deschutes Formation. These correlations suggest that at least 67 distinct explosive eruptions (possibly as many as 120) occurred within the 800 k.y. explosive pulse.

Using a new ArcGIS-based method that I developed for calculating ignimbrite volumes, I find that a total volume of 82 km^3 (62 km^3 DRE) for just 26 of the ignimbrites deposited distally into the Deschutes Basin. If these ignimbrites also deposited an equal volume to the west and had a tephra fall:flow ratio of between

0.5:1 and 1.9:1 (similar to Mount Pinatubo and Valley of Ten Thousand Smokes), the total volume of all 26 eruptions was likely between 246 and 475 km^3, or a rate of 6-12 km^3/m.y./km. This rate is approximately 2-8 times higher than the production rate of all compositions over the entire Quaternary Cascades and is the highest rate in Oregon over at least the last 17 Ma.

The unique timing and location of this pulse, approximately 1 m.y. after an eastward shift of the arc axis, and in a region undergoing extension, may explain the anomalous explosivity recorded in the Deschutes Formation. I suggest that such extension allowed for penetration of hot, low-K tholeiitic basalt magmas into shallow levels of the crust, which induced a period of enhanced shallow crustal melting and the production of large volumes of hot-dry-reduced rhyolites (high Fe, Na, Y, MREE, and low Eu/Eu* and Sr). Thus, the anomalously high production of silicic magma and rate of explosive volcanism recorded in the Deschutes Formation is mirrored by the unusual geochemistry of the eruptive products, and are together indicative of magmatic processes driven by extension, that no longer operate during the Quaternary.

In addition to constraining changes in geochemistry and style of volcanism through time, I used rigorous statistical methodology to assess the geochemical variability along-arc for the Quaternary Cascades. To do this, I compiled a dataset of over 11,000 samples and utilized a Monte Carlo approach with weighted bootstrap resampling to reduce the bias that over-sampled volcanoes have on overall trends. In in doing so, I assessed regional, rather than local processes. Our study develops a novel approach to assessing along-arc geochemical variability using entirely objective and statistically-based methodology. Using this new approach, I separated the Cascades arc into 5 segments such that the geochemical differences between each is maximized. This new segmentation scheme, which includes the North, Washington, Graben, Mazama, and South Segments is more statistically robust than previous segmentation schemes. By separating the arc into the most statistically distinct regions, one can better assess the spatially disparate processes that lead to geochemical heterogeneity. This, in turn, provides a better understanding of the fundamental processes involved in arc magma generation.

The Deschutes Formation:
Evidence of Extension-Enhanced Explosivity in the Early High Cascades

by
Bradley W. Pitcher

A DISSERTATION

submitted to

Oregon State University

in partial fulfillment of
the requirements for the
degree of

Doctor of Philosophy

Presented June 9, 2017
Commencement June 2018

Doctor of Philosophy dissertation of Bradley W. Pitcher presented on June 9, 2017

APPROVED:

Major Professor, representing Geology

Dean of the College of Earth, Ocean, and Atmospheric Sciences

Dean of the Graduate School

I understand that my dissertation will become part of the permanent collection of Oregon State University libraries. My signature below authorizes release of my dissertation to any reader upon request.

Bradley W. Pitcher, Author

ACKNOWLEDGEMENTS

First, I would like to express my sincerest gratitude to my advisor, Adam Kent. I am grateful to have been given the opportunity to come to Oregon State University and to work on an exciting project that was already funded. His knowledge of geochemistry provided a wealth of inspiration for this project. He has helped me to learn to be self-motivated and to become a better writer and scientist. I also want to express tremendous thanks to Anita Grunder and Bob Duncan, who are Co-PIs on the Deschutes Formation Grant and acted as 2nd and 3rd advisers, not just committee members. I felt that every one of our Deschutes Group meetings were quite fruitful and the many rounds of edits on the first manuscript are greatly appreciated. Specifically, Anita's passion for geology, field work, and willingness to drop everything, despite her incredibly busy schedule, just to have a discussion with me, is greatly appreciated. I want to thank Bob for being so kind and supportive through the entire process, even housing me when I came in 2012 for the perspective student weekend. I would also like to thank Andrew Meigs for our brief, slightly confusing, but very helpful discussion and for agreeing to be on my committee. Finally, I want to thank Nick Pisias for being my GCR despite having recently retired. I look forward to many mathematical discussions in the future.

I owe an incredible debt of gratitude to all my amazing field assistants over the years. In rough order of appearance, thank you to: Kurt Winner, Bud Torcum, Ben Christensen, Ben Kane, Allan Lerner, Heather Winslow, My Dad and Mom (David and Lisa Pitcher), Taryn K. Bye, Bobby Cruze, Ellen Svadlenak, and Thomas Madden. I put you all through a lot: thunderstorms, sketchy cliffs, long 10 hour hikes, 100°F heat, flat tires, rattlesnakes, lack of field-naps, and constant uncertainty as to where we were or what we were looking at. So, thank you!

Thank you to the many helpful people that I met while in the field. First and foremost, thank you to Phil and Bobby. Without you and your boat, there is no way I would have been able to get all of that field work done on Lake Billy Chinook. I am lucky to call you my friends!

I would also like to acknowledge Frank Tepley, Dale Burns, and Melissa Drignon for their help with the Electron Microprobe. Constant help from Dan Miggins and Anthony Koppers with the 40Ar/39Ar sample preparation is greatly appreciated. Finally, thank you to Jim Palandri for all of your help with collecting excellent oxygen isotope data at University of Oregon.

I would also like to thank Rick Conrey and Dave Sherrod for their insight on locations of key Deschutes Formation units and other useful discussions. Their thorough reviews and detailed suggestions helped to immensely improve chapter 2 before publication. Daniel Eungard is also acknowledged for introducing the author to the Deschutes Formation and for sharing field site locations and measurements.

Thank you to all of the VIPERs. I appreciate all of the discussions that we had and enjoyed our meetings that helped keep me well rounded in igneous petrology. Specifically, thank you to Allan Lerner, who was there for me to discuss scientific results, to encourage me and to complain about graduate school. Additionally, thank you to my fellow VIPERs, Nikki Moore, Henri Sanville and Richard Bradshaw, who helped me to grow as a scientist throughout my full five years of graduate school. I owe a special thank you to Jenny DiGuilio for making me dinner and editing my thesis! I can never thank you enough.

Most of all, I want to thank my friends and family. All of my friends here in Corvallis and elsewhere, thank you for keeping me sane and helping me to still enjoy life. Thank you to my whole family, including my Grandparents, Aunt Cathe, my Brother, The Burt, and the lovely Sarah Pitcher! Thank you all for your kind support. I owe so much to my incredible parents. All of the many phone calls and texts reminding me of how proud you are of me really helped me get through this. You have always been so supportive, and you have always been my biggest fans. You have always taught me to strive for academic excellence, and I thank you both for the teaching genes that you passed on to me! Thank you so much for helping to encourage that little 4-year-old who decided he wanted to be a geologist. You truly helped me to nurture the passion that I still have today!

Finally, I owe the sincerest gratitude to my incredible wife, Marina. You have been so supportive through this whole experience and have helped me to remember that I am doing what I truly love. I have always enjoyed our nerdy discussions and I am lucky to have my life partner share in a passion for science, and to care about what I am doing. Thank you so much for everything, Marina, I love you.

CONTRIBUTION OF AUTHORS

Dr. Adam Kent, Dr. Anita Grunder, and Dr. Robert Duncan all helped tremendously with the editing of the chapter 2 manuscript. In addition, their discussions on interpretation of data, specifically chapter 2 and 4 were very beneficial.

TABLE OF CONTENTS

LIST OF FIGURES

LIST OF FIGURES (continued)

Figure Page

LIST OF FIGURES (continued)

Figure Page

LIST OF TABLES

1. Introduction and Background

1.1 Introduction

The common juxtaposition of highly populated areas and active arc volcanoes worldwide poses a serious threat to millions of people. More than 550 million people are estimated to live within 100 km of a volcano that has erupted during the Holocene (Small and Naumann, 2001). Volcanoes that erupt explosively are especially dangerous because pyroclastic flows, lahars and ash fallout, hazards predominantly associated with explosive volcanoes, are responsible for 88% of the nearly 92,000 estimated volcano-related deaths in the 20th Century (Witham, 2005). Explosive eruptions commonly occur in arc volcanoes, but such eruptions are irregularly distributed worldwide both spatially and temporally, and vary widely in their eruptive volumes. Larger caldera-forming eruptions (generally >5 km^3) have occurred more frequently in some Quaternary arcs such as Kamchatka, New Zealand, and northeast Japan, compared to other arcs such as the Aleutians or Southern Philippines (Hughes and Mahood, 2011). Furthermore, explosivity within a single arc tends to be highly variable through time and space. For example, while the central portion of the Taupo Volcanic Zone (TVZ) of New Zealand is characterized by the highest density of calderas of any arc in the world (Hughes and Mahood, 2011; Rowland et al., 2010), yet such eruptions are rare in the northern or southern segments of the arc, and rarely occurred in the central segment before 0.9 Ma (Deering et al., 2010, 2011).

Thus, to better understand hazards of an arc we must constrain that arcs full eruptive history, and not just that of the recent past. It is particularly important to document the geochemistry, eruptive frequency, and volumetric production during unusually explosive periods. This allows us compare them to those of the steady-state arc, and to infer the processes responsible for temporal variations in explosivity and silicic magma generation. In addition, to understand along-arc changes in composition and eruptive style, we must explore correlative spatial changes in parameters such as the geometry and composition of the slab, mantle and/or crust. Documenting spatial and temporal changes within a single arc can help constrain the effects that these geodynamic, tectonic, and geochemical factors have on magmatic

compositions and eruptive style, thus addressing one of the fundamental questions of igneous petrology.

Volcanic arcs are typically characterized by widely spaced composite volcanoes, which generally erupt tephra volumes of less than 1 km^3, (VEI 2-5) (Newhall and Self, 1982). Although less common, larger silicic (>63 wt. % SiO_2) caldera-forming eruptions (CFEs), with erupted volumes of 1-100 km^3 (VEI 5-7), have occurred in arcs world-wide (Hughes and Mahood, 2011). These eruptions can be extremely hazardous and have the potential for major climatic effects (e.g. the 1815 eruption of Tambora and the subsequent "year without a summer") and thus must be well studied and understood. Supervolcanic eruptions, which have volumes greater than 1000 km^3 (VEI 8), are rare in arcs and only occur where an unusually high flux of mantle melts results in thermal and mechanical maturation of the crust, thereby allowing for the storage of large intrusive complexes (de Silva, 2008). An extensive compilation by Hughes and Mahood (2011) of 108 Quaternary calderas within arcs around the world has revealed some general features that tend to favor the formation of silicic calderas. Not surprisingly, the authors found that large rhyolitic calderas tend to occur in thick and evolved crust, as thicker crust acts as a density filter for ascending mafic melts, leading to more fractionation, as well as a source for evolved melts (Hughes and Mahood, 2008). In addition, arcs situated at subduction zones with faster convergence rates, particularly between 7.0 and 9.5 cm/yr, tend to contain more silicic calderas, indicating that higher magmatic flux is also likely crucial for silicic magma generation at volumes sufficient to produce caldera systems (Hughes and Mahood, 2011). In addition, arcs that are experiencing an extensional stress regime, and those that have migrated or initiated within the last 30 million years, tend to have a higher caldera density (Hughes and Mahood, 2011).

The Cascades arc of western North America lacks most of the criteria found by Hughes and Mahood (2011) to nurture the growth of calderas. Over the last 40 Ma, the rate of convergence of the Juan De Fuca plate has slowed from 16 to 3.2 cm/year, and has become increasingly oblique, progressing from nearly orthogonal (85°) to 23°, resulting in a 5-fold decrease in orthogonal convergence rate from 8.5 to

1.6 cm/year (Verplanck and Duncan, 1987). Over this time period, the Cascades arc has experienced an overall decrease in volcanic production (Priest, 1990), consistent with a decrease in the overall magmatic flux resulting from a slowing convergence rate (Fig. 1). Additionally, because the Juan De Fuca Ridge is located so proximally to the Cascadia trench, the slab that is subducted is very young, less than 10 Ma, and thus unusually hot (Green and Harry, 1999). As a result, the anomalously hot slab tends to dehydrate at shallow depths trenchward of the arc and the volatile budget for flux melting beneath the arc is reduced, as evidenced by depletion in fluid-mobile elements (Green and Harry, 1999; Leeman et al., 2004), as well as relatively low H_2O contents of melt inclusions in primitive basalt tephras (Walowski et al., 2013). In addition, the crust beneath the Central Oregon Cascades arc is only ~41 km thick (Trehu et al., 1994) and isotopic studies and seismic data indicate that the Oregon Cascades arc may be predominantly built atop accreted Mesozoic to early Tertiary mafic terrains (Church et al., 1986) and the Siletzia terrain, a Paleocene to Eocene large igneous province (Schmidt et al., 2008; Trehu et al., 1994). Thus, according to the findings of Hughes and Mahood (2011), it seems that an arc such as the Cascades, which sits atop mafic crust, at a subduction zone characterized by relatively slow convergence of a hot slab would be unlikely to foster the growth of significant silicic magma bodies.

The Quaternary Cascades arc of western North America has had relatively few caldera-forming eruptions, and has a caldera density that places it in the lowest 40th percentile of arcs worldwide (Hughes and Mahood, 2011). During the Quaternary, the arc has produced only 20 explosive eruptions with volumes >1 km^3 (Hildreth, 2007). The Cascades consist predominantly of monogenetic basaltic-andesite to andesite shield volcanoes and stratocones, with only a small number of more evolved, long-lived composite volcanoes (Hildreth, 2007). Nevertheless, there is evidence that Oregon experienced an episode of elevated amounts of explosive volcanism during the Oligocene, seen in the John Day Formation (Mclaughry et al., 2009), and again during the Late Neogene (~7.5-4 Ma), seen in the Deschutes Formation (e.g. Conrey, 1985; Smith, 1986; Priest, 1990). The Deschutes Formation

contains hundreds of ignimbrite and tephra-fall deposits which were all erupted during a relatively short pulse between 6.25± 0.07 and 5.45± 0.04 Ma (Pitcher et al., 2017a) (Fig. 2). This pulse records the highest volumetric rate of pyroclastic volcanism within the Cascades arc since at least 17 Ma (Pitcher et al., 2017a).

The timing of this pulse of silicic volcanism occurred immediately after an eastward shift in the locus of the arc activity from the older Western Cascades (~35-17 Ma) to the modern High Cascades at 7.5 Ma, and occurs during a period of syn-volcanic rifting (Priest, 1990) (Fig. 1). This major reorganization of the Cascades arc is also marked by a shift from primarily effusive andesite lava flows to the eruption of both low-K tholeiitic lavas and dacitic to rhyodacitic explosive eruptions (Priest, 1990; Taylor, 1990). Thus, the Deschutes Formation records a transitional period of volcanism characterized by magmatic compositions (basalt and rhyolite) and frequent explosive eruptions, which are atypical of the arc as a whole.

This study establishes a comprehensive chronology of the explosive volcanism recorded in Deschutes Formation to infer magmatic processes that lead to its occurrence. Understanding these processes and how they differ from those of the Quaternary is critical to our understanding of the complete magmatic evolution of the Cascades arc. Determining the cause for such unusual volcanism requires investigation into: the timing of its initiation, cotemporaneous events, the pace of volcanism during the episode, and the magmatic geochemistry. Taken together, these data provide key evidence that allow us to unravel the petrogenetic causes for this extraordinary period of Cascades arc history.

In addition to investigating the causes for temporal changes in the geochemistry and eruptive style of the Cascades arc, I also begin to explore spatial variability in Quaternary arc geochemistry. The composition of magmas erupted at arc volcanoes bear evidence of the complex interplay between geochemical contributions from the subducted oceanic crust and sediment, liberated fluids, mantle wedge, and the overlying lithosphere. Comparing along-arc changes in geochemistry of the Cascades arc to disparities in these parameters provides an excellent tool to constrain those that may be most responsible for production of heterogenous magmas

within a single arc system. This, in turn, provides a more comprehensive understanding of the complex magmatic processes that occur within arcs.

Following this introduction and background chapter, my dissertation is organized into four main chapters (2-5). In chapter two, I use $^{40}Ar/^{39}Ar$ dating of marker ignimbrites to establish a chronostratigraphic framework from which I can build our comprehensive tephrostratigraphy. Also in this chapter, I calculate the volumes of these 13 marker ignimbrites and compare the volumetric rate to that of the Quaternary. I use the relative timing of the pulse of volcanism to infer its relationship to intra-arc extension. In chapter three, I use multivariate statistics to establish geochemical correlations between ignimbrite and tephra fall units and determine the number of distinct volcanic eruptions that occurred. Furthermore, I compile a comprehensive, basin-wide tephrostratigraphy and calculate the eruptive frequency as recorded by the Deschutes Formation. I then use this tephrochronology to address whether explosive volcanism was declining prior to graben formation, and further comment on the intimacy of extensional tectonics and magmatism in central Oregon during Deschutes time. In chapter four I present major and trace element as well as oxygen and lead isotopic data to determine potential causes for the production of unusually large volumes of silicic magma during this time. I use these data to propose a magmatic system that is highly affected by extension, and compare these compositions and magmatic processes to those of the Quaternary arc. In chapter six I address along-arc geochemical variability and segmentation of the Quaternary Cascades arc. To do this, I compile a comprehensive geochemical dataset and use multivariate statistics to test the segmentation scheme proposed by Schmidt et al. (2008). I then develop a new statistically-based segmentation scheme and use this to begin to explore differences in the slab, mantle, or overriding plate which may have led to such segmentation.

1.2 Brief Volcanic History of the Cascades volcanic arc

The onset of Cascades arc volcanic activity occurred approximately 45 Ma, approximately 5 Ma after accretion of the mafic Siletzia terrane at ~49-51 Ma (Wells

et al., 2014). However, activity was focused mainly in southwest Washington (du Bray and John, 2011). Evidence of this initial volcanism in Oregon is primarily preserved as a stark increase, approximately 45 Ma, in non-metamorphosed volcanic lithic fragments within marine sandstones of the Coaledo Formation in southern Oregon and the Spencer and Eugene Formations of west-central Oregon, as well as minor subaerial flows within the Fisher Formation of west-central Oregon (Sherrod and Smith, 2000). Volcanic rocks erupted during the onset of Cascades activity are predominantly basalt to andesite, and no plutonic units have been found (du Bray and John, 2011).

The best record preserved in eastern Oregon of the earliest Cascades volcanic history are the calc-alkaline andesite to dacite tephra fall and tuffaceous clay units of the John Day Formation, which began accumulating approximately 39 Ma and may have been sourced from early Cascades volcanoes in northern Oregon (Sherrod and Smith, 2000). By approximately 35 Ma, the entire arc became established and was active from southern Oregon to present-day Mt. Rainier, with the exception of the area near present-day Mt. Hood (du Bray and John, 2011). The Cascades arc has remained constantly active since 35 Ma, but has undergone significant changes since that time (Verplank and Duncan, 1987; Priest, 1990; Taylor, 1990; Sherrod and Smith, 2000; du Bray and John, 2011).

By convention, the Cascades are divided into the Western Cascades, which erupted over a wide area until around 2 Ma, and the more recent High Cascades, which initiated approximately 7.5 Ma and erupted over a much narrower belt east of the Western Cascades (Priest, 1990) (Figure 2). The evolution of the Cascades arc can be summarized by breaking its history into 5 volcanic episodes, where each episode represents distinct characteristics in the style, composition, and locations of eruptions. The following divisions are a modified after the work of Priest (1990) and du Bray and John (2011).

1.2.1 Early Western Cascades Volcanism: 35-26 Ma

The early Western Cascades were active along a volcanic belt that was approximately three to four times wider than the Quaternary arc, and extended from northern California to present-day Mt. Rainier (Priest, 1990). The erupted large volumes of predominantly tholeiitic basalt to andesite lava with minor local andesite stratovolcanoes and dacite to rhyolite domes (du Bray and John, 2011). Cascades volcanism was also explosive during this time, producing several tens of ignimbrite sheets, with a few calderas (Seligman et al., 2014) identified within the Western Cascades arc (e.g. ~25 km diameter Mohawk River Caldera, 32 Ma), as well as east of the arc, associated with the John Day Formation (e.g. 41 x 27 km Crooked River caldera, 38-32 Ma) (McClaughry, 2009; McClaughry et al., 2010). However, source calderas for some of the John Day Formation ignimbrites are far from the arc (e.g. Tower Mountain caldera is over 220 km east of the modern arc axis) (McClaughry et al., 2009). In addition, trace element (elevated Nb, Th, Y) and isotopic ($\delta^{18}O_{zircon}$ and εHf) data for these ignimbrites have been interpreted to result from back-arc or intraplate processes rather than those related directly to arc magmatism (Seligman et al., 2014). The higher volcanic production during this time is consistent with higher convergence during the Oligocene. (Verplanck and Duncan, 1987).

1.2.2 Middle Western Cascades Volcanism: 26-17 Ma

A transition from primarily tholeiitic compositions to more calc-alkaline compositions marks the transition to the middle Western Cascades (Sherrod and Smith, 2000). During this episode, volcanism shifted northwards and was active from southern Oregon up to an area north of present-day Mt. Rainier, again with a magmatic gap in the area near present-day Mt. Hood (du Bray and John, 2011). Volcanic productivity was also relatively high during this time, and compositions became more evolved, dominated by andesite lavas and tephra (du Bray and John, 2011). Dacite, and even rhyolite, primarily as local ignimbrites, became much more voluminous during this time, and large volumes of distal pyroclastic deposits continued to be deposited within the John Day Formation (Sherrod and Smith, 2000).

Plutonic rocks also became a volumetrically significant for the first time during this episode (du Bray and John, 2011). This episode of Western Cascades volcanism ended approximately 17 Ma with a period of uplift (~5-10° east) and low volcanic activity, creating a marked unconformity above these units in most locations (Taylor, 1990).

1.2.3 Late Western Cascades Volcanism: 17- 7.5 Ma

The last 10 m.y. of Western Cascades development are characterized by very low rates of volcanic activity (Priest, 1990). Eruption rates were approximately three times lower than they were during the previous episode, possibly reflective of the decreasing convergence rate between the Juan de Fuca and North American plates (Priest, 1990). Columbia River Basalts flowed into northwest Oregon during this time, and the lack of significant interbedded volcaniclastic sediment is evidence of the relative inactivity in the northern Oregon and Southern Washington Cascades in this time period (Sherrod and Smith, 2000). The northern two-thirds of Oregon, including the magmatic gap near present-day Mt. Hood which had prevailed for the previous 20 million years, became the only areas to experience volcanism during this time, and the active arc became focused over a narrower band (Priest, 1990). Eruptions were primarily effusive, and 2-pyroxene andesite lava flows became the dominant composition (Priest, 1990). Dacite to rhyolite compositions are almost completely absent, with the exception of the silicic volcaniclastic deposits of the Simtustus Formation (15.5-12 Ma) located in the Deschutes Basin of central Oregon (du Bray and John, 2011; Smith, 1986).

1.2.4 Early central Oregon High Cascades Volcanism: 7.5- 4 Ma

Volcanic activity increased dramatically in central Oregon beginning approximately 7.5 Ma, and was focused within a new arc axis, the High Cascades, located east of the ancestral Western Cascades (Priest, 1990).The initiation of the High Cascades was marked by the eruption of significant volumes of MORB-like Low-K tholeiitic basalt (0.1-0.5 wt. % K_2O) and basaltic andesite, a change from the almost exclusively calc-alkaline andesite compositions that dominated the previous

10 m.y. (Conrey et al., 2004; Conrey et al., 1997). An 800 k.y. pulse of explosive volcanism also occurred during this time, producing hundreds of ignimbrites and tephra-fall layers which account for the highest volumetric rate of silicic magmatism in the Oregon Cascades since at least 17 Ma (Pitcher et al., 2017). Near-source rocks from this episode have all been buried by subsequent lava flows of the Late High Cascades. With the exception of some ridge-capping basalts and rare ignimbrites within the Outerson Formation above the central Oregon ancestral Cascades (Taylor, 1990), the stratigraphic record of the Early High Cascades is poorly preserved on the western side for most of the arc. Instead, the volcanic record of the Early High Cascades is best recorded within the well-preserved Deschutes Formation, located east of the Central Oregon segment of the arc, within the greater Deschutes Basin (Taylor,1990; Smith, 1986). The formation is a thick sequence of sub-horizontal fluvial sediment, mass flow deposits, lacustrine sediment, lava flows, and numerous interbedded pyroclastic flow and fall deposits (Smith, 1986). The deposits resulted from a prolonged period of volcanism-induced aggradation that began around 7.5 Ma and continued until the formation of the High Cascades graben, beginning ~5.3 Ma, which ultimately cut off supply from the arc and arrested aggradation (Smith et al., 1987). Uplift of the Western Cascades also occurred during this time, possibly due to erosion (Lopez et al., 2016), and volcanism was relatively rare.

1.2.5 Late central Oregon High Cascades Volcanism (<4 Ma)

In central Oregon, all subsequent volcanism was constrained within the newly formed High Cascades graben. During the Pliocene, a broad mafic platform was built up by numerous overlapping shield volcanoes (Taylor, 1990). Much of the Pliocene graben filling volcanism is buried, but drill cores reveal that it consists mostly of basalt to basaltic andesite (Taylor, 1990). Quaternary volcanism continues to be characterized primarily by overlapping monogenetic basalt to basaltic andesite shield volcanoes which form the third highest volcanic vent density in the entire Quaternary arc (Hildreth, 2007). Larger, more evolved stratocones include, from north to south, Mt. Jefferson, Three-Fingered Jack, Mt Washington, and the Three Sisters, and evolved composition at these centers range up to true rhyolites (e.g. South Sister).

Felsic eruptions are more common in central Oregon than in most of the Quaternary arc. There have been eight explosive eruptions since 700 ka, large enough to produce tephra-fall deposits, and five of these were larger than 0.1 km^3 (DRE) (Hildreth, 2007, and references therein). This includes pyroclastic eruptions from the Tumalo Volcanic Center, located 15-20 km east of the main arc axis (Sherrod et al., 2004). Overall, volcanic production rates of all compositions are lower than during the early High Cascades (Priest, 1990).

1.3 Previous Work

Although it has been referred to by many names, the Deschutes Formation has been studied by various scientists for over 125 years. The formation was first described by Captain Clarence E. Dutton (1889), a geologist with the USGS, who described "waterlaid tuff" interbedded with basalt while surveying along the Metolius River. The Deschutes Formation was first named the "Deschutes Sands," by Russell (1905), who described units within the Deschutes and Crooked Rivers during a trip concerned with water resources. Russell recognized that the units were of Tertiary age, and described channel-filling basalts and ignimbrites, which he referred to as "white volcanic dust." While searching for a potential site for a future dam on the Deschutes River, Williams (1924) insisted on the name, "Deschutes Formation" rather than "Sands", because of the prevalence of basalt and units other than sandstone. He also named the Pelton Basalt, which forms the base of the Deschutes Formation. Stearns (1930) was the first to suggest that the Deschutes Formation has its origin in the Cascades. In 1940, Hodge suggested the name, "Madras Formation," arguing that because there were many other formations within the Deschutes River Canyon, the former name was not specific enough. Two years later, Hodge (1942) changed the name to the "Dalles Formation," mistakenly correlating it with a formation in northern Oregon. Williams (1957) was the first to describe the ignimbrites in great detail, and suggested that they were all erupted from the Quaternary volcano, Broken Top. Stensland (1969) revived the name Deschutes Formation, which was used to describe all units within the Deschutes basin above the Columbia River Basalt Group and unconformably underlying Pliocene and

Pleistocene basalts. However, Smith and Hayman (1983) noted a slight angular unconformity and distinct lithologic break between the older Simtustus Formation and the Younger Deschutes Formation, and Smith (1986) described in detail the differences between the strata and suggested a 5.5 Ma hiatus between them.

The first reconnaissance geologic maps of the Deschutes Basin were by Wells and Peck (1961), and then Waters (1968). A series of theses by Oregon State University graduate students under the direction of Dr. Edward Taylor in the 1970s and 1980s included extensive mapping of the Deschutes Basin. Mapping north of Lake Billy Chinook, primarily on older Deschutes Formation units and the Simtustus Formation was completed by Jay (1982), Hayman (1983), and Smith (1986). Mapping in the middle of the Deschutes Basin near Lake Billy Chinook was undertaken by Hewitt (1970), and Dill (1985). Hales (1975), Conrey (1985), Yogodzinski (1986), and Wendland (1988) mapped the northwestern portion of the basin, including Green Ridge, and the area around the Whitewater and Metolius Rivers. Stensland (1970) mapped almost the entire southern half of the basin, and McDannel (1989)focused on the southernmost portion, which contains Quaternary ignimbrites such as the Tumalo Tuff. Cannon (1984) focused on mapping the extent of two large ignimbrites in the southern portion of the Deschutes basin, the McKenzie Canyon and Lower Bridge Tuffs. Maps were published by the USGS for the Steelhead Falls 7.5 minute quadrangle (Ferns, 1996), Hinkle Butte 7.5 minute quadrangle (Taylor, 1998), and the Bend 30 minute quadrangle (Sherrod et al., 2004). Despite this work, only the maps of Cannon (1984), Dill (1985), Conrey (1985), and Sherrod and others (2004) have put an emphasis on correlating and mapping the extent of some of the marker ignimbrite units. In addition, several field trip guides have been published, some primarily focusing on the area within Cove Palisades State Park (Smith, 1983; Bishop, 1990; Peterson and Groh, 1991; Smith, 1991) and others that encompass a wider area including the Western and High Cascades (Taylor, 1991; Conrey et al., 2004).

Although these aforementioned workers did describe ignimbrite units and mentioned the existence of multiple pumice fall deposits within their individual

mapping areas, most did not attempt to correlate these ignimbrites within their field area or with ones in adjacent mapping areas. Thus, for the most part, ignimbrites are listed as disparate units with a confusing nomenclature and no regard to a basin-wide compilation. One contrast to this is the work of Smith (1986), who correlated 14 laterally extensive marker ignimbrites throughout the Deschutes Basin, based largely on field observations. In addition to providing consistent names for these marker ignimbrites, Smith (1986) described the distinguishing characteristics of the units and provided some geochemical data. Dill (1992) used, for the most part, the nomenclature of Smith (1986), but also correlated and mapped 26 other more minor ignimbrites surrounding Lake Billy Chinook. Five of the ignimbrites described by both Smith (1986) and Dill (1992) were studied and further characterized by Aubin (2000).

Geochemical data, especially trace elements for units within the Deschutes formation are largely lacking and are almost completely unpublished. Smith (1986) compiled XRF and atomic absorption whole rock major element data from previous unpublished theses, and added additional XRF major element and limited trace element data. A few theses also present Electron Microprobe data for minerals. Largely these data focus on the basalts and basaltic andesites of the Deschutes Formation, and with the exception of sparse data from Hales (1975), Jay (1982), Cannon (1984), and Conrey (1985), very little data were collected on ignimbrites. Aubin (2000) collected a significant amount of major and trace element data on bulk pumice from 5 ignimbrites using both the XRF and solution ICP-MS. Additionally, this author collected major element data on minerals using the Electron Microprobe, and $^{87}Sr/^{86}Sr$ data were collected on whole rock pumices using TIMS. Eungard (2012) collected whole pumice XRF trace element data, as well as extensive *in situ* major and trace element data on pumice glass from the McKenzie Canyon and Lower Bridge Tuffs, using the Electron Microprobe and the Laser Ablation-ICP-MS. Eungard (2012) also showed that bulk XRF analyses of pumice often had more restricted compositions than *in situ* analyses of glass within pumice clasts, indicating the importance of analyses of pumice glass by *in situ* techniques. With the exception

of Conrey et al. (1991,1997), geochemical data for the Deschutes Formation remains largely unpublished or available only in the "grey" literature.

Russell (1905) was the first to suggest that the Deschutes Formation is of Tertiary age, which was further constrained to early or middle Pliocene by Chaney (1938) using fossil flora and then to early Pliocene by Hodge (1940). Early K-Ar dating in the 1960s and 1970s revealed inconsistent ages, but recent advances in radiometric dating, including the $^{40}Ar/^{39}Ar$ method, since the 1980s provided improved age constraints (Table 1). Everden and James (1964) suggested the formation was 4.3 to 5.3 Ma, on the basis of K-Ar dating. Hales (1975) dated the top and bottom of the section exposed on Green Ridge using the K-Ar method, constraining the formation to 4.5 to 9.2 Ma. However, Armstrong (1975) reported K-Ar ages of 3.3 to 15.9 Ma and Farooqui and others (1981) and Bunker and others (1982) reported K-Ar ages for Deschutes Formation basalts ranging 10.7 ± 1.2 to 22.0 ± 8 Ma. $^{40}Ar/^{39}Ar$ dating of the Pelton basalt gave an age of 7.6 Ma, consistent with K-Ar ages given by previous authors (Smith and Snee, 1983). Smith (1986) reported $^{40}Ar/^{39}Ar$ ages of 12 units within the Deschutes Formation, as well as 3 that unconformably overlie it, thus constraining the formation to 4.0 ± 0.1 to 7.6 Ma. Finally, Smith and others (1987) refined the age of the Pelton basalt at the base of the formation to 7.42±0.22 Ma and uppermost lava on Green Ridge at 5.27 ± 0.08 Ma, suggesting a majority of the Deschutes Formation was deposited between these times. Aubin (2000) presents the only two $^{40}Ar/^{39}Ar$ ages of ignimbrites within the formation, reporting ages of 5.38 ± 0.06 Ma for the Six Creek Tuff and 5.56 ± 0.06 for the Balancing Rocks Tuff. A compilation of these radiometric ages is provided in Appendix 2.6.

FREQUENCY AND VOLUMES OF IGNIMBRITE ERUPTIONS FOLLOWING THE LATE NEOGENE INITIATION OF THE CENTRAL OREGON HIGH CASCADES

Bradley W. Pitcher, Adam J. R. Kent, Anita L. Grunder, and Robert A. Duncan

Journal of Volcanology and Geothermal Research
Elsevier, Inc
1600 John F Kennedy Blvd #1800
Philadelphia, PA 19103

Volume 339 (2017) pp. 1-22

Abstract

The late Neogene Deschutes Formation of central Oregon preserves a remarkable volcanic and sedimentary record of the initial stages of High Cascades activity following an eastward shift in the locus of volcanism at ~7.5 Ma. Numerous ignimbrite and tephra-fall units are contained within the formation, and since equivalent deposits are relatively rare for the Quaternary Cascades, the eruptions of the earliest High Cascades volcanoes were likely more explosive than those of the Quaternary arc. In this study, the timing and frequency of eruptions which produced 14 laterally extensive marker ignimbrites within the Deschutes Formation are established using $^{40}Ar/^{39}Ar$ geochronology. Plagioclase $^{40}Ar/^{39}Ar$ ages for the lowermost (6.25 ± 0.07 Ma) and uppermost (5.45 ± 0.04 Ma) marker ignimbrites indicate that all major explosive eruptions within the Deschutes Formation occurred within a period of 800 ± 54 k.y. (95% confidence interval). Minimum estimates for the volumes of the 14 ignimbrites, using an ArcGIS-based method, range from 1.0 to 9.4 km^3 and have a total volume of 62.5 km^3. Taken over the 50 km of arc length, the explosive volcanic production rate of the central Oregon High Cascades during Deschutes Formation time was a minimum of 1.8 km^3/m.y./km of arc length. By including estimates of the volumes of tephra-fall components, as well as ignimbrites that may have traveled west, we estimate a total volume range, for these 14 eruptions alone, of 188 to 363 km^3 (~121 to 227 km^3 DRE), a rate of 4.7-9.1 km^3/m.y./km arc length. This explosive volcanic production rate is much higher than the average Quaternary eruption rates, of all compositions, estimated for the entire Cascades arc (1.5-2.5), Alaska Peninsula segment of the Aleutian arc (0.6-1.0), and the Andean southern volcanic zone (1.1-2.0). We suggest that this atypical explosive pulse may result from the onset of regional extension and migration of the magmatic arc, which had the combined effect of increasing magmatic flux and temporarily enhancing melting of more fusible crust.

2. Frequency and Volumes of Ignimbrite Eruptions Following the Late Neogene Initiation of the Central Oregon High Cascades

2.1 Introduction

Large explosive volcanic eruptions (>1 km^3, dense rock equivalent, [DRE]) create substantial natural hazards due to their potentially disastrous effect on human populations, infrastructure, and climate (e.g. Newhall and Self, 1982; Witham, 2005). These eruptions are typically associated with eruption columns that are 10 km or higher and thus can result in large pyroclastic flows, widespread ash fall and injection of aerosol into the upper atmosphere. Such eruptions can also be associated with a range of other hazardous volcanic phenomena such as pyroclastic surges, lahars, and debris avalanches (e.g. Doocy et al., 2013). Larger explosive eruptions with volumes greater than 5 km^3 (DRE) typically produce calderas, and many of the world's known Quaternary caldera-forming eruptions (CFEs) have occurred at subduction margins (Hughes and Mahood, 2011) where the common juxtaposition of highly populated areas and arc volcanoes make these eruptions especially dangerous. CFEs also occur more frequently in some subduction zones than others, and even in individual arcs the frequency of CFEs can vary greatly through time (Hughes and Mahood, 2008; 2011). Understanding the extent and timing of explosive eruptions, the petrogenetic processes that lead to the formation of explosively erupted magmas within arcs, and the processes that lead to periods of elevated eruption rates are important research goals.

In a study of 108 Quaternary calderas within arcs around the world, Hughes and Mahood (2011) evaluate the general features of subduction zones that favor the formation of explosive silicic CFEs. Large rhyolitic CFE tend to occur in areas of thick and evolved crust, as thicker crust acts as a density filter for trapping ascending mafic melts, resulting in differentiation and crustal melting to produce silicic magma (Hughes and Mahood, 2008). In addition, arcs with faster convergence rates, particularly between 7.0 and 9.5 cm/yr, contain a higher abundance of silicic calderas, indicating that higher magmatic fluxes also favor generation of silicic magma at volumes sufficient to produce caldera systems (Hughes and Mahood, 2011). Arcs that

are experiencing extensional stresses, and those that have migrated or initiated within the last 30 m.y., also tend to have higher caldera density.

The Cascadia subduction zone is an example of an arc system with an overall low incidence of CFEs in the Quaternary; it has less than three calderas per 1000 km of arc length, which is below the 40th percentile of arcs worldwide (Hughes and Mahood, 2011). The only known Quaternary Cascades CFEs are the 1.15 Ma Kulshan eruption (erupted volume ~30 km^3 DRE), the 7.7 ka climactic eruption of Mount Mazama (33 km^3 DRE), the 610 ka eruption of the Rockland Ash, and the 300 ka eruption (Donnelly-Nolan et al., 2004) of the Tuff of Tepee Draw (~10 km^3) (Hildreth et al., 2004, Bacon and Lanphere, 2006, Lanphere et al., 2004, and Macleod et al., 1995, respectively). Quaternary ignimbrites of small to moderate scale (< 5 km^3 DRE), but that did not appear to form calderas, have been found only in the vicinity of Mount Meager, Mount Garibaldi, Glacier Peak, Mount St. Helens, Mount Jefferson, the Tumalo volcanic center, Mount Shasta, and Mount Lassen (Hildreth, 2007).

The low incidence of CFEs and other large silicic eruptions in the Cascades arc is consistent with the nature of subduction. During the last 40 m.y., the rate of convergence of the Juan de Fuca plate has slowed, and direction of convergence has become increasingly oblique to the plate boundary, resulting in a fivefold decrease in orthogonal convergence rate from 8.5 cm/year to the current value of 1.3 cm/year (Verplanck and Duncan, 1987). Over this time period, the central Oregon Cascades arc has also experienced an overall decrease in volcanic production (Priest, 1990), consistent with a decrease in magmatic flux from slowing orthogonal convergence rates (Fig. 1). Additionally, because the Juan de Fuca Ridge is located so close to the Cascadia trench, the subducting oceanic crust is very young, less than 10 Ma, and thus unusually hot compared to other arcs (Green and Harry, 1999). The anomalously hot slab dehydrates at shallow depths trenchward of the arc and the volatile budget for flux melting beneath the arc is thus reduced, as evidenced by depletion in fluid-mobile elements (Green and Harry, 1999; Leeman et al., 2004), and somewhat lower H_2O contents of melt inclusions in primitive basalts relative to global average values

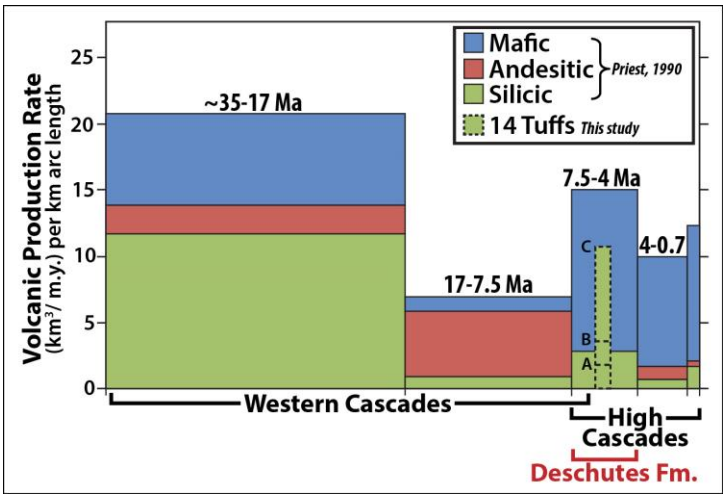

Figure 2.1: Volcanic production rate through time for the central Oregon Cascades arc between 44°N and 44°52'30''N (modified after Priest, 1990). Green dashed column shows our estimated total volume (per million years, per km arc length) of 14 marker ignimbrites. The lower limit, marked "A," is the conservative estimate based only on the volume erupted eastward into the Deschutes Basin over 50 km arc length. "B" depicts the rate if an equal volume of each ignimbrite traveled west. "C" is the extrapolated volume of the 14 ignimbrites if a similar spatial distribution of each tuff was erupted in all directions from the assumed source. Tephra-fall and intracaldera volumes are not included.

(Ruscitto et al., 2010; Plank et al., 2013; Walowski et al., 2013). Isotopic studies and seismic data indicate that the 41 km-thick crust (Eagar et al., 2011) beneath the central Oregon Cascades arc consists predominantly of accreted young mafic terrains (Schmidt et al., 2008; Trehu et al., 1994; Church et al., 1986). Thus, the modern Cascades arc, with slow convergence of young, hot slab beneath a mafic crust of average thickness, appears unlikely to produce large volumes of silicic crustal melt and attendant caldera-forming eruptions (Hughes and Mahood, 2011).

However, the extent and frequency of large explosive eruptions within an arc can also vary substantially in time. In the Cascades arc, the pre-Quaternary history reveals several distinct phases of eruptive output, composition, and eruptive style (Fig. 1; Verplanck and Duncan, 1987; Priest, 1990; Taylor, 1990). The central Oregon region experienced two episodes of elevated explosive volcanism (Conrey, 1985; Smith, 1986; Priest, 1990; McClaughry et al., 2010) since the Cascadia subduction zone assumed its current geometry after accretion of the mafic Siletzia terrane at ~49-51 Ma (Wells et al., 2014). In the Oligocene, Cascades volcanism was exceptionally explosive, producing several tens of ignimbrite sheets, with a few calderas (Seligman et al., 2014) identified within the Western Cascades arc (e.g. ~25

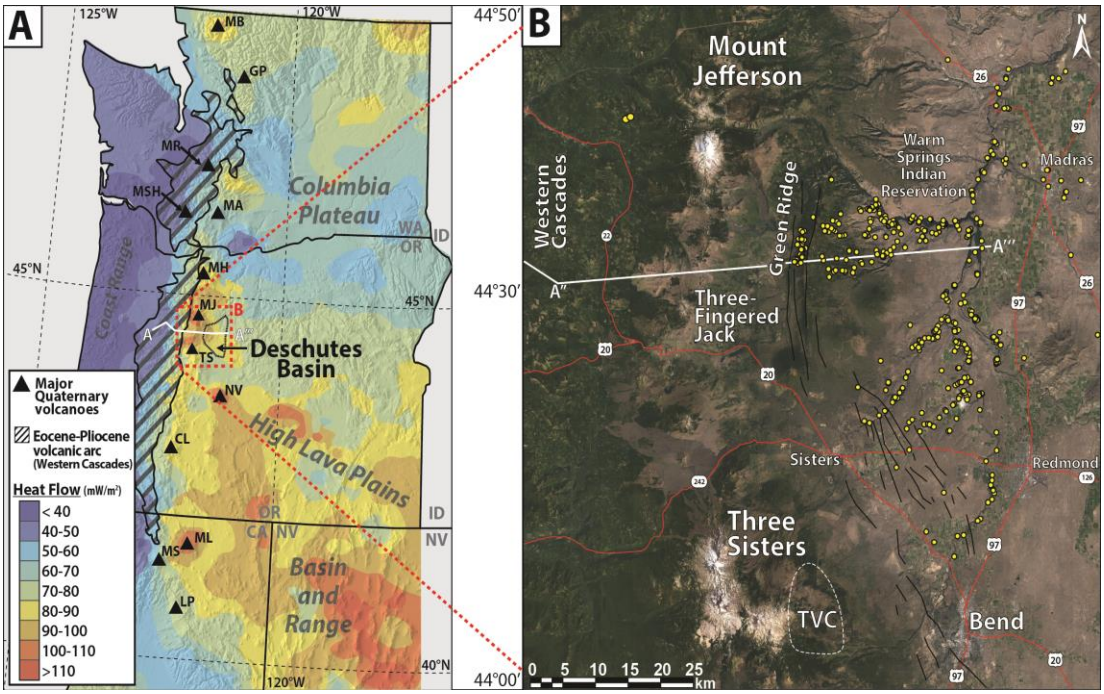

Figure 2.2: **(A)** Map indicating the locations of the Deschutes Basin (dashed outline), Western Cascades (striped area, du Bray and John, 2011) and major Quaternary High Cascades volcanoes (triangles), (MB=Mt. Baker, GP=Glacier Peak, MR=Mt. Rainier, MSH=Mt. St. Helens, MA=Mt. Adams, MH=Mt. Hood, MJ=Mt. Jefferson, TS=Three Sisters, NV=Newberry Volcano, CL=Crater Lake, ML=Medicine Lake, MS=Mt. Shasta, LP=Lassen Peak). Some major geologic provinces such as the Basin and Range and High Lava Plains are also labeled. Heat flow contours are from Ingebritsen and Mariner (2010). Yellow dots in **(B)** are locations where tuff thicknesses were measured for this study. The Green Ridge and Sisters Fault zones mark the boundary of the High Cascades graben, wherein all Deschutes-age strata have been buried. TVC is the approximate location of the Tumalo volcanic center (Hill and Taylor, 1990; Sherrod et al., 2004). Cross section A-A''' is shown in Fig 2.6.

km diameter Mohawk River Caldera, 32 Ma), as well as east of the arc, associated with the John Day Formation (e.g. 41 x 27 km Crooked River caldera, 38-32 Ma) (McClaughry, 2009; McClaughry et al., 2010). However, source calderas for some of the John Day Formation ignimbrites are far from the arc (e.g. Tower Mountain caldera is over 220 km east of the modern arc axis), and trace element (elevated Nb, Th, Y) and isotopic ($\delta^{18}O_{zircon}$ and εHf) data for these ignimbrites have been interpreted to result from back-arc or intraplate processes rather than those related directly to arc magmatism (Seligman et al., 2014). The higher incidence of Oligocene explosive silicic volcanism associated with the Western Cascades and the near-arc part of the John Day Formation is consistent with higher convergence during

Oligocene time (Verplanck and Duncan, 1987), as well as the relatively recent shift of volcanism following accretion of Siletzia (Gao et al., 2011).

Another episode of explosive Cascades silicic volcanism occurred during the late Neogene (~5.45-6.25 Ma, this study). Products of this episode are preserved in the Deschutes Formation (~4-7.5 Ma) of central Oregon and to a lesser extent in parts of the Western Cascades (e.g. Conrey, 1985; Smith, 1986; Priest, 1990) (Fig. 1). The cause of heightened explosive volcanism in the Deschutes Formation is also more enigmatic, given that orthogonal convergence rates at this time were low (~1.6 cm/yr, Verplanck and Duncan, 1987) and the Deschutes Formation episode postdates volcanism associated with Siletzia accretion by at least 25 million years. To address this, we present new constraints on the timing and erupted volumes of major ignimbrite units preserved within the Deschutes Formation. These results provide the basis for comparison to the Quaternary Cascades arc and provide insight on the cause of an episode of explosive silicic volcanism in a predominantly mafic and effusive arc.

2.1.1 The Deschutes Formation: an extraordinary record

The Deschutes Formation, which is found primarily within the modern Deschutes Basin of central Oregon (Fig. 2), is a thick sequence of subhorizontal fluvial sediment, mass flow deposits, lacustrine sediment, lava flows, and numerous interbedded pyroclastic flow and fall deposits (Smith, 1986). The Deschutes Basin lies to the east, and by analogy to the present, downwind, of the Cascades arc (Fig. 2A). The deposits resulted from a prolonged period of volcanism-induced aggradation that began around 7.5 Ma and continued until the formation of the High Cascades graben, beginning at 5.4 Ma, arrested aggradation (Smith et al., 1987). The Deschutes Formation has been subsequently incised by the Deschutes River and its tributaries. The surface of the landscape is armored by extensive lava flows from late Neogene Cascades arc sources (Smith, 1986) and Pleistocene Newberry Volcano (Sherrod et al., 2004); these contribute to development of steep and deep exposures of the Deschutes Formation As a result, the formation preserves an unsurpassed stratigraphic record as thick as 700 m of volcanic activity from the High Cascades

between ~7.5 and 4.0 Ma (Smith, 1986), and it provides the best opportunity to establish the chronology of the unusual pulse of explosive eruptions that occurred during the infant stages of the High Cascades arc.

2.2 Methods

2.2.1 Field work

The field area for this study includes over 1700 km^2 of the Deschutes Basin, between the cities of Bend and Madras (Fig. 2). Exposures are almost exclusively restricted to river canyons and drainages, as well as some road cuts. Although previous work indicates that numerous tuffs can be found north of the Metolius River (Smith, 1986), we were not granted permission to access these locations on the Warm Springs Indian Reservation. Previous geologic mapping provided useful unit descriptions and aided in locating some of the major marker ignimbrite units (Hewitt, 1969; Cannon, 1984; Conrey, 1985; Smith, 1986; McDannel, 1989; Dill, 1992). We focus on the 14 largest and most prominent ignimbrites, which we designate as *marker* ignimbrites. We document the thickness, compositional components, and imbrication (where recognizable) at each tuff outcrop. Representative outcrops were sampled for geochemical analysis and correlation. We measured thicknesses of units with a tape measure, a Jacob staff with a mounted Brunton compass, or by trigonometric methods. Where a precise contact could not be located, we used the disappearance of pumice float or change in slope to estimate contact location, and minimum possible thickness.

2.2.2 $^{40}Ar/^{39}Ar$ geochronology

Ten new $^{40}Ar/^{39}Ar$ ages (nine plagioclase and one glass) were obtained by laser step-heating techniques. The entire procedure of mineral separation, irradiation and mass spectrometric analysis was completed at Oregon State University. For analysis, we separated pumice clasts from ignimbrite hand samples, removed altered or hydrated surfaces, and crushed them using a hammer and mortar and pestle. The crushed sample was sieved and the 212-500 μm fraction was washed in deionized

water to remove dust. Plagioclase separates were magnetically separated and acid-leached following methods of Koppers et al. (2011). Inclusion-free plagioclase was then hand-picked under a binocular microscope at 6-7x magnification on a glass plate with a white background to ensure they were clear and inclusion-free from all angles. Neither quartz nor alkali feldspar were found in any of the samples. The 300-500 µm size fraction was used for most samples; however, for those with abundant melt inclusions, the 212-300 µm size was used. Glass was separated from pumice of the Six Creek Tuff, using a lithium heteropolytungstate (LST) heavy liquid with density of 2.4 g/cm^3. The floating portion was then cleaned, sonicated, and dried, and denser, purer glass was found to be magnetic using a Franz LB-1 separator at 0.4 amps and 15° tilt. Finally, we hand-picked dense, dark-brown to black transparent glass fragments using a binocular microscope and placed these in 5% HF for 45 seconds to remove any adhered less-dense glass.

We irradiated prepared samples along with Fish Canyon Tuff sanidine (28.201± 0.046 Ma, 2σ; Kuiper et al. 2008) flux monitor for six hours in the TRIGA CLICIT nuclear reactor using methods previously described by Koppers et al. (2011). Laser step-heating $^{40}Ar/^{39}Ar$ age determinations were performed using a multi-collector ARGUS-VI mass spectrometer at Oregon State University, following methods described by Balbas (2016).

2.2.3 Volume estimation

Estimating the volumes of the ignimbrites within the Deschutes Formation is critical to establishing the magnitude of explosive volcanic activity that occurred during the initial stages of the High Cascades arc. To calculate tuff volumes, the field attributes of each unit – including outcrop thicknesses, estimated uncertainty in thickness, and the outcrop GPS coordinates – were imported into an attribute table within ArcGIS 10.2 software. Source vents for these eruptions likely were located along the current Cascades arc, although now hidden by Quaternary volcanic and related fill (Smith et al., 1987) (Fig. 2). Thus, we estimated source vent locations for each ignimbrite from imbrication (where present), welding facies, and geometry of thickness variations (Fig. 3).

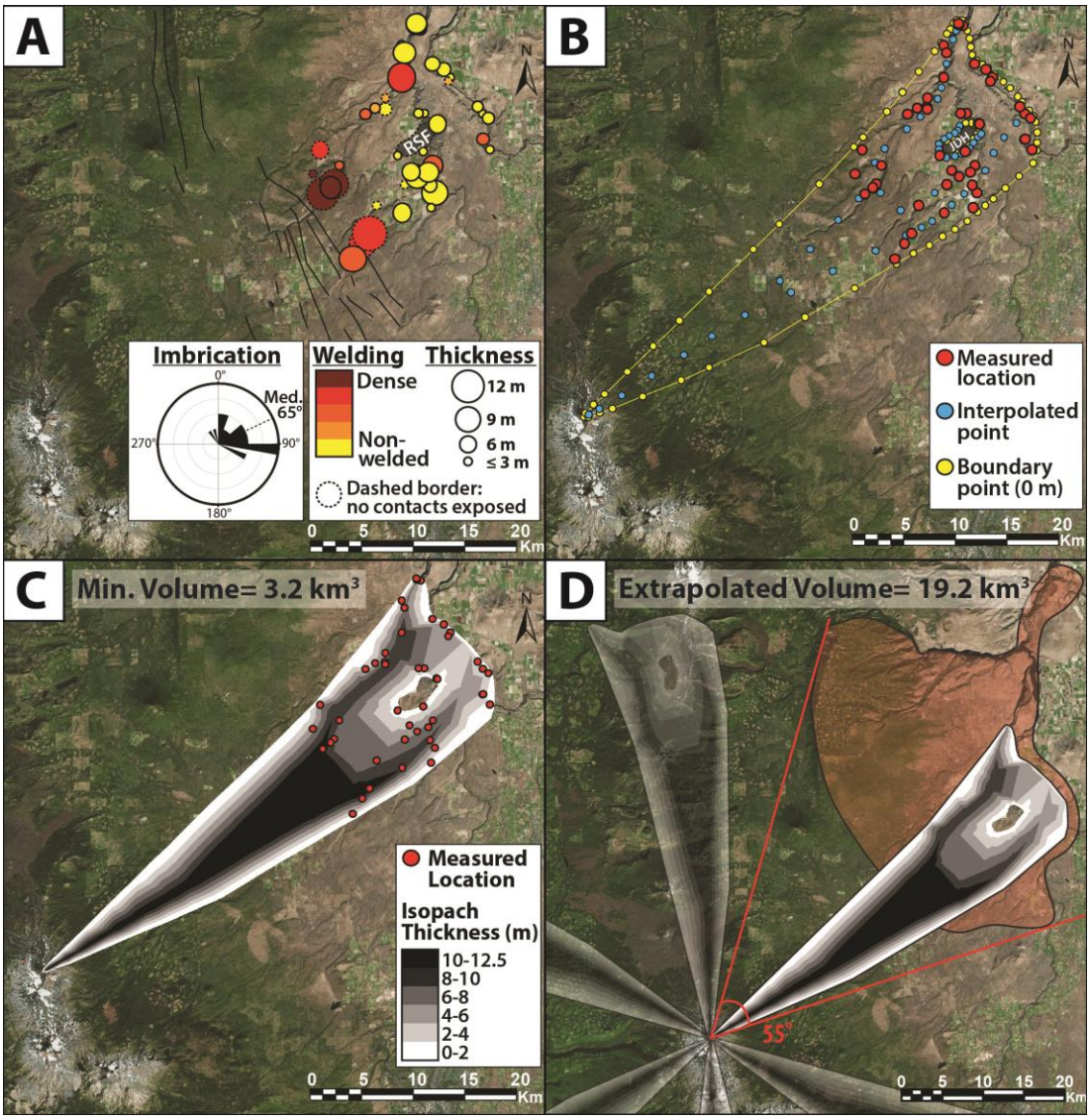

Figure 2.3: An example of the process used to calculate the volume of the McKenzie Canyon Tuff (MCT) using ArcMap 10.2 software. **(A)** Measured thickness and degree of welding of MCT at each location are indicated by size and colors of circles, respectively, and are used to infer source direction. A compilation of measured imbrication directions from 24 different locations (each an average of three measurements) is presented on the inset rose diagram. Bin size is 10°, and the maximum is four locations within a given bin. Field evidence suggests that the MCT flowed around the area designated on the map as "RSF," a 6.74± 0.2 Ma rhyodacite lava flow at least 180 m thick (Sherrod et al., 2004). **(B)** A conservative, fan-shaped ignimbrite outline is drawn **(C)** The ArcMap 10.2 software creates isopachs of the gridded surface defined by the points shown in panel B to calculate a volume=3.2 km^3. **(D)** A rough estimate of the maximum volume of an eruption that produced ignimbrites which flowed in all directions. Deschutes Basin (red area) represents only 55° sector area from source. See text for further explanation.

For all ignimbrites, the source was assumed to lie along the current arc axis, but a separate volume calculation was also carried out assuming a source just west of the eastern High Cascades graben boundary. Once the general source direction was established, the precise point-source that was used for volume calculations was estimated using the spatial pattern of measured thickness, such that the tuff thicknesses were roughly symmetrical on either side of a line drawn from the location of maximum tuff thickness to the assumed source (Fig. 3A). It should be noted that although the latitude of this assumed source is subject to considerable error, the choice of latitude has little effect on the final volume. After estimating the vent location, the boundary of the ignimbrite was defined by adding points of zero thickness (yellow points, Fig. 3B).

Ignimbrites were assumed to be fan-shaped when deposited, and boundaries were drawn conservatively. For example, if the outermost outcrop was X meters thick, the boundary of the tuff was drawn 100 times X meters away from that outcrop. This is consistent with thickness measurements of the 11 km^3 ash-flow tuff from the 1912 eruption of Novarupta, where the termini of the flow were an average of approximately 80 m away from positions with 1 m thickness (Curtis, 1968). The maximum measured thickness was projected in a straight line back to the assumed source location, such that no assumptions of thinning or thickening towards source were made. In cases where the maximum thickness was anomalously high compared to nearby measurements (likely indicating local channelization), this maximum value was discarded and replaced with the value of the next thickest location. In creating this shapefile, some points had to be added in between measurements that are located large distances from each other in order to create a continuous fan-shape and prevent the software from isolating these points from the rest of the ignimbrite (blue points, Fig. 3B). Finally, locations with anomalously thin tuff compared to nearby measurements were discarded if both contacts had not been found, as their measured thickness represented a minimum estimate. This step allowed for more consistent and logical shapes for the ignimbrite. In some cases, (e.g. Chinook Tuff, Appendix 2.4) distal portions of the ignimbrite were drawn as narrow channels following the path of

the ancestral Deschutes River, as defined by Smith (1986). During all steps, care was taken to ensure that final volume estimates were minima.

The shapefile containing thickness measurements and zero-thickness boundary points was then used to create a triangulated irregular network (TIN) file, a vector representation of a ground surface. The "elevation" (tuff thickness) of the TIN, at any given location is interpolated on a 3D triangular surface whose endpoints are defined by the three nearest actual thickness measurements or boundary (zero-thickness) points. This step is necessary because the locations at which we have thickness measurements are irregularly spaced from each other, and thus, a raster could not be used. Then the TIN was converted to a raster, and a floating-point output data type, linear interpolation method, and a sampling distance of cell size 30 m were used. This step creates a gridded dataset where the center of each grid is given a linearly interpolated elevation (thickness), which can then be used to create isopach contours (Fig. 3C). From this, the ArcGIS software calculates the volume below this rastered surface.

Dense rock equivalent (DRE) volumes of ignimbrites were estimated based on the welding facies and density ratios (measured bulk rock density of each facies divided by density of densely welded rhyolitic Rattlesnake Tuff [2.34 g/cm^3] measured by Streck and Grunder,1995). For each Deschutes Formation tuff, the fraction of outcrops characterized by each welding facies was estimated. Then the average density ratios (e.g. nonwelded=0.63, partially welded with pumice=0.79) found for each of the welding facies of the Rattlesnake Tuff (Streck and Grunder, 1995) were multiplied by these fractions to get a weighted average of the density ratio, which was then multiplied by the volume of that ignimbrite to get DRE volume. For example, half of Fremont Canyon Tuff outcrops are densely welded (density ratio=1.0) and half are partially welded with fiamme (0.93). Thus, the estimated volume of the tuff (2.4 km^3) was multiplied by the average density ratio (0.96), to get a DRE volume of 2.3 km^3. We did not account for a likely increase in welding towards the source, and no attempt was made to directly measure bulk rock density or

to correct for (sparse) accidental lithic contents of the Deschutes Formation tuffs. Thus, DRE volume estimates are also minima in this regard, as welding typically increases toward the source. In addition, we made no attempt to estimate the volume of magma lost to downwind tephra-fall deposits, tuff that was trapped in a caldera, or tuff that flowed down westward drainages. For this reason, all our volume estimates are considered minima.

2.3 Results

Our focus is the chronology and volumes of the eruptions that produced 14 marker ignimbrites, described in some detail by Smith (1986). Although a number of other ash fall and ignimbrite units occur within the formation, the marker ignimbrites have the greatest lateral extent, and the $^{40}Ar/^{39}Ar$ ages presented herein provide a useful stratigraphic framework for all Deschutes Formation eruptions. These units also correspond to the largest eruptions preserved, and their volumes help constrain the total volume of volcanic output of material erupted in the central Oregon Cascades during this time.

2.3.1 Marker ignimbrite field characteristics

The 14 marker ignimbrites of this study are laterally extensive and have distinctive characteristics such as pumice populations, crystallinity, and overall color which allowed them to be easily identified in the field (Table 1). Most ignimbrites contain a dominant population of rhyolite pumice, and commonly have at least one more mafic pumice population, typically andesite or dacite; banded pumice is sparse but present in ignimbrites with multiple pumice populations. Two marker ignimbrites, the Six Creek Tuff and the McKenzie Canyon Tuff, have roughly bimodal compositions, with common andesite and rhyolite pumice, but few of dacitic composition. Crystallinity ranges from < 1% to 10% (Table 1), and the most common mineral assemblage observed in the ignimbrites is plagioclase and two pyroxenes; amphibole is rare or absent. Most ignimbrites are nonwelded in the field area, but the McKenzie Canyon Tuff, Fremont Canyon Tuff and Fly Creek Tuff also have partially to densely welded facies exposed.

2.3.2 $^{40}Ar/^{39}Ar$ ages and composite stratigraphy

The ten new $^{40}Ar/^{39}Ar$ ages on nine ignimbrites significantly expand the geochronological data available for the Deschutes Formation, which heretofore included 12 $^{40}Ar/^{39}Ar$ ages for lava flows and only 2 for ignimbrites. Our new dates span from 6.25± 0.07 Ma to 5.45± 0.04 Ma (Table 2). A table of calculated ages, intercepts and MSWD for plateau, total fusion, and normal and reverse isochron results, as well as sample locations are given in Appendix 2.1. Step-heating age spectra are in Appendix 2.2. Age plateaus were chosen to include as many contiguous, concordant step ages as possible (without violating statistical significance [MSWD]) and were defined by 5-20 heating steps (median of 10) which included 57-97% (median of 81%) of the $^{39}Ar_K$ released. Our approach resulted in high precision ages, with 2σ uncertainty ranging between 0.01 and 0.09 Ma, including J-value errors. MSWD (mean square of weighted deviations) values range from 0.43 to 1.89, with the two highest being associated with the two oldest samples. Only the Chinook Tuff, the oldest unit dated, exhibits significantly lower apparent ages for initial

Table 2.1: Field characteristics of the 14 marker ignimbrites, as well as the Outerson Formation lithic-rich tuff, located west of the modern arc axis, which has an $^{40}Ar/^{39}Ar$ age (5.55± 0.03 Ma, this study) that is consistent with a Deschutes Formation origin.

Ignimbrite	Source	Max. thick-ness	Common outcrop color	Pumice populations	Composition	Welding	Crystallinity	Flow units	Other prominent features
Six Creek	North	82 m	Grey-yellow, buff	Black, grey, white, banded	Bimodal: andesite, rhyolite	None	1-3%	2-3	Large black pumice; only marker tuff traced to Green Ridge
Meadow Creek	North	15 m	Light grey	Black, grey	Dacite to rhyolite	None	2-3%	7	Similar appearance to Six Creek Tuff
Deep Canyon	South	33 m	Olive grey or light brown	Black	Dacite	None to moderate	< 1%	Multiple	Contains black vitrophyre clasts
Fremont Canyon	South	19 m	Dark brown to red-brown	Black	Rhyolite	Moderate to dense	1-2%	1	Dense vitrophyre in some locations
Peninsula	South	12 m	Brown to grey	Grey, black	Andesite to trachydacite	Weak in places	< 1%	1	Very channelized; contains large black bombs
Steelhead Falls	North	25 m	Pink-grey	White, grey	Rhyolite	Partial in one area	4-8%	1	Always overlies 1-2 m co-genetic fall unit; Similar in all aspects to Fly Creek Tuff lower flow unit. Likely correlated.
Fly Creek	North	49 m	Light grey to orange-grey	White, grey	Rhyolite	Partial to dense	7-10%	Multiple	Often welded; most crystal-rich unit; 1-2 m fall unit when base is exposed
Balanced Rocks	North	56 m	Light to dark grey (top)	Grey, black	Dacite to rhyolite	None	≤ 1%	2-3	Forms hoodoos capped by Fly Creek Tuff
McKenzie Canyon	South	23 m	White to red-orange (top)	White, black, banded	Bimodal: andesite, rhyolite	Partial to dense	2-3%	>5	Columnar where welded
Cove	North	18 m	White	Grey	Rhyolite	None	3-5%	1	Similar stratigraphic position as McKenzie Canyon Tuff
Lower Bridge	South	18 m	Pink-light grey	White, grey	Rhyolite	None	4-8%	2	Usually overlies 1-1.5 m accretionary lapilli
Jackson Buttes	North	23 m	Light grey to pink	Grey	Rhyolite	Partial in places	2-4%	>2	1st flow unit: large orange, pink and purple pumice, 2nd flow unit: fine white pumice; often welded (columns in places)
Osborne Canyon	South	28 m	Orange	Orange, black	Rhyolite	None	1-2%	2	Large orange pumice; forms hoodoos
Chinook	North	38 m	Grey-pink, white	White, grey	Rhyolite	None	3-4%	Multiple	Found at shoreline of Lake Billy Chinook; often contains rounded river cobbles
Outerson Fm. Lithic-rich tuff	North	62 m	Medium grey	White, dark grey	Bimodal: andesite, dacite	None	2-5%	2	Rich in volcanic lithics throughout; 1 m cobble-rich layer separates flow units

heating steps, indicating argon loss. Normal and inverse isochron ages are all within 2σ uncertainty of the plateau age. All samples except the Steelhead Falls Tuff have isochrons with $^{40}Ar/^{36}Ar$ intercepts that overlap the atmospheric value of 295.5 within 2σ uncertainty. For the Steelhead Falls Tuff the intercept values were 264.8 and 270.0 for the normal and inverse isochrons, respectively.

Our new ages are consistent with the stratigraphic position of each marker ignimbrite within the sequence (Fig. 4) and with published ages (Smith, 1986 revised in Smith et al., 1987) for Deschutes Formation lava flow units within the sequence, after recalculating these ages using the Kuiper et al., 2008 age for the Fish Canyon Tuff flux monitor (Appendix 2.6). Aubin (2000) gives the only two $^{40}Ar/^{39}Ar$ dates for Deschutes Formation ignimbrites, Six Creek Tuff (5.38± 0.12 Ma) and Balanced Rocks Tuff (5.56± 0.12 Ma). After recalibrating these dates, the new age for Six Creek tuff (5.41± 0.12 Ma) is within error of our age for the same unit, and the new age for Balanced Rocks Tuff (5.60± 0.12 Ma) is consistent, within error, with its position beneath Fly Creek Tuff (5.68± 0.01 Ma, our study). Given the high precision

Table 2.2: Age, volume and distance traveled for each of the 14 marker ignimbrites. Minimum distances were calculated by measuring the straight-line distance from the easternmost outcrop to the faults that define the eastern edge of the High Cascades graben. *Steelhead Falls Tuff is likely correlated to the lower flow unit of Fly Creek Tuff. Its volume in this table represents that of a separate flow unit volume, not included in the Fly Creek Tuff volume.

Ignimbrite	^{40}Ar-^{39}Ar age ±2σ (Ma)	Source	Min. Volume (km^3)	DRE volume	Min. distance traveled (km)
Six Creek	5.45 ± 0.04	North	4.3	2.6	20
Meadow Creek	--	North	3.2	2.0	26
Deep Canyon	--	South	5.0	3.2	17
Fremont Canyon	--	South	2.4	2.3	14
Peninsula	--	South	2.7	1.7	27
Fly Creek	5.68 ± 0.01	North	5.2	4.0	30
Steelhead Falls*	5.68 ± 0.02	North	2.7	1.7	33
Balanced Rocks	--	North	8.8	5.4	25
McKenzie Canyon	5.76 ± 0.02	South	3.2	2.7	26
Cove	--	North	1.0	0.6	29
Lower Bridge	5.93 ± 0.02	South	3.6	2.2	25
Jackson Buttes	5.98 ± 0.01	North	6.3	4.2	42
Osborne Canyon	5.99 ± 0.02	South	9.4	5.7	31
Chinook	6.25 ± 0.07	North	4.7	2.9	44

of plateau ages, the lack of evidence for argon loss or excess argon, and the concordance of the ages with stratigraphic position, we conclude that all $^{40}Ar/^{39}Ar$ dates in our study accurately represent the eruption ages of the ignimbrites.

For the Six Creek Tuff, the dense glass yielded a $^{40}Ar/^{39}Ar$ plateau age of 5.34± 0.09 Ma, within 2σ uncertainty of the plagioclase age of 5.45± 0.04 Ma. Although this indicates that dense pumice glass can be used successfully to date ignimbrites by the $^{40}Ar/^{39}Ar$ method, it should be noted that a smaller fraction of the total gas was used in calculating the weighted average plateau age (68% for glass vs. 95% ^{39}Ar released for plagioclase). For consistency, we rely on the plagioclase age of this unit throughout this study.

Steelhead Falls and Fly Creek Tuffs are the same age (5.68 ± 0.02 Ma and 5.68 ± 0.01 Ma, respectively) and appear to be identical (i.e., mineralogy, glass and plagioclase compositional range). The Steelhead Falls Tuff, which is only exposed over a short distance (<7.5 km) along the Deschutes River in the middle latitudes of the field area, is tentatively correlated to the lowermost flow unit of the Fly Creek tuff.

The Chinook and Six Creek Tuffs stratigraphically bracket almost all tuffs within the Deschutes Formation (Fig. 4). Only two tuffs (one ignimbrite and one tephra-fall) were found stratigraphically below the Chinook Tuff, and only two ignimbrites and four tephra-fall deposits were found to be stratigraphically higher than Six Creek Tuff. However, these tuffs are not laterally extensive and are not considered in this study. We note that the relative lack of ignimbrite units that are older and younger than these units is not simply a result of differences in preservation, as good stratigraphic exposures exist above and below these ignimbrites. For example, on Green Ridge, a 600-m normal fault scarp exposes approximately 115 m of section (44.541°N, 121.603°W) in which no tuffs are exposed between the Six Creek Tuff (5.45± 0.04 Ma, Table 1) and a 5.27± 0.04 Ma basalt on the crest of the ridge (Smith et al., 1987). Additionally, a 2.5 km long landslide scarp in the northernmost portion of the field area (44.741°N, 121.222°W) exposes over 100 m of tuff-free strata beneath the Chinook Tuff.

Using a Welch's t-interval calculation (Appendix 2.5), we estimate, with 95% confidence that almost all Deschutes Formation explosive eruptions occurred over a span of only 800± 54 thousand years. This relatively short time interval was characterized by a marked increase in explosive volcanic activity relative to the periods immediately before and after.

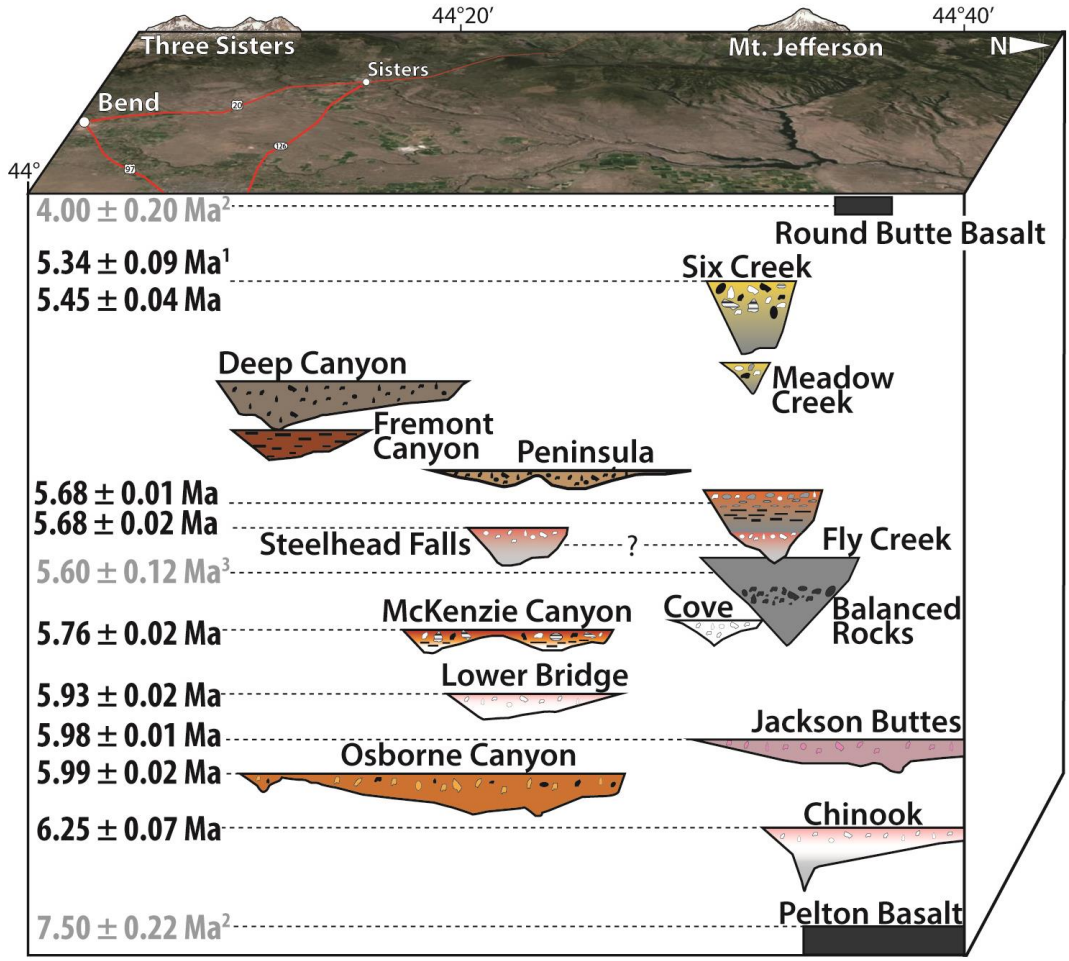

Figure 2.4: Schematic cross section showing the stratigraphic relations, thickness profiles, north-south extent, and ages of the 14 marker ignimbrites of this study. Names of the ignimbrites are shown next to an actual thickness profile (140x vertical exaggeration) of the ignimbrite shape at its widest point, defined using ArcMap 10.2 (see volume calculation methods). For reference, Balanced Rocks Tuff has a maximum thickness of 56 m. Vertical distance between units is not shown to scale. Plagioclase $^{40}Ar/^{39}Ar$ ages (±2σ uncertainty) of ignimbrites from this study (black) are shown on the left, along with one ignimbrite from Aubin, 2000[3] and two Deschutes Formation lavas (both grey) from Smith et al., 1987[2] (all recalibrated using the Kuiper et al., 2008 Fish Canyon Tuff age) are shown on the left. The 5.34 ± 0.09[1] age is from dense pumice glass. Steelhead Falls Tuff may be correlated to lower flow unit of the Fly Creek Tuff.

It is plausible that ignimbrites from Deschutes Formation eruptions also traveled westward. Several ignimbrites described from the Western Cascades have K-Ar ages of Deschutes Formation age, including the dacitic tuff of Tipsoo Butte (6.3-8.7 Ma, K-Ar age, Priest et al., 1988) and the north-south trending mafic ignimbrite of Trailbridge Reservoir (5.5± 0.2 Ma, K-Ar age, Armstrong et al., 1975). For this study, we have sampled and dated one ignimbrite on the western flank of the Cascades, the Outerson Tuff (of the Outerson Formation), mapped and described by Clayton (1976) and Priest et al, 1987. The tuff has an $^{40}Ar/^{39}Ar$ plagioclase age of 5.55± 0.03 Ma (Appendix 2.1), which is consistent with the timing of Deschutes Formation eruptions, and our imbrication measurements from two different outcrops are largely consistent with a source in the direction of the area just south of modern Mount Jefferson. Greater erosion and denser vegetation make the western ignimbrite record hard to reconstruct, but our new age for the Outerson Tuff may indicate that ignimbrites of Deschutes Formation age also flowed west from their sources. However, we presume that the wind direction was largely eastward as it is now, so that most tephra fell preferentially on the east side, with opportunity to be preserved in the Deschutes Basin.

Although this study focuses on the laterally extensive marker ignimbrites within the Deschutes Formation, we note that there are at least 50 other less laterally extensive ignimbrites and at least 30 distinct tephra-fall units, that erupted from approximately 50 km of arc length over a span of 800± 54 thousand years. Thus, the Deschutes Formation preserves an exceptionally explosive and productive period of the Cascades arc at this latitude.

2.3.3 Ignimbrite volumes and temporal trends

Each of the 14 marker ignimbrites of this study flowed tens of kilometers and covered hundreds of square kilometers of area within the Deschutes Basin (Table 2). In general, pumice imbrication in ignimbrites in the northern portion of the field area indicate eastward flow; and the tuffs have westward increases in welding and thickness, consistent with a source to the west or west-southwest (between Mount Jefferson and Three-Fingered Jack) (Fig.4A). Ignimbrites in the southern portion of

the field area have imbrication, welding, and thickness changes that suggest sources to the southwest, near the position of the North Sister volcano. Similar source directions were estimated by Conrey (1985), Smith (1986), McDannel (1989) and Dill (1992). Assuming volcanic sources that lie on the modern arc axis, we calculate that the 14 ignimbrites traveled between 31 and 58 km (Table 2). However, if we instead assume sources that are just west of the fault zones that mark the edge of the Cascades graben, the minimum distance that these ignimbrites flowed ranges from 16 to 44 km (Table 2).

Minimum volume estimates for the eruptions that produced the 14 marker ignimbrites range from 1.0 to 9.4 km^3, indicating eruption magnitudes of VEI 5-6 (Newhall and Self,1982) (Table 2). Conservative calculation of the areal extent of each ignimbrite by GIS methods range from 117 to 442 km^2. Our best estimate for the cumulative volume of the 14 marker ignimbrites in total is 62.5km^3 (~41 km^3 DRE)

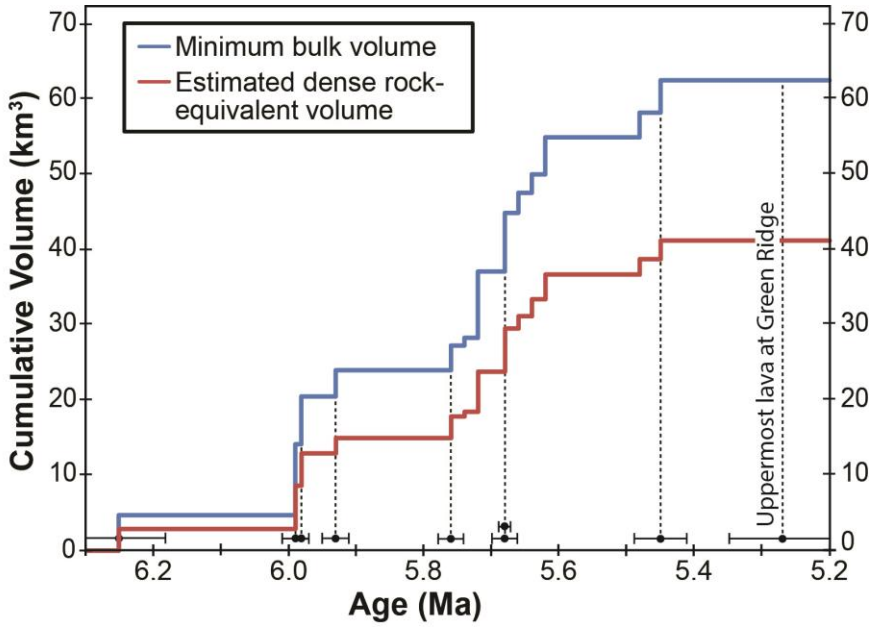

Figure 2.5: Cumulative volume through time for the 14 marker ignimbrites of this study. $^{40}Ar/^{39}Ar$ ages are represented by the normal curves at the bottom of the figure, and dashed lines are drawn to the corresponding tuff volume for reference. Approximate ages of undated ignimbrites were linearly interpolated based on the number of units stratigraphically between bracketing dated units. The age of the uppermost lava on Green Ridge (5.27± 0.04 Ma) from Smith et. al (1987) is also shown, as no tuff outcrops exist within the 115 m of exposed strata between it and Six Creek Tuff.

(Fig. 5). These estimates ignore pyroclastic fall facies of the eruption, any caldera fill, and the potential distribution down westward drainages of the arc. It should be noted, however, that the lack of Deschutes-age exposure within the High Cascades graben, which encompasses the most proximal 15-25 km east of the volcanic axis, leads to considerable uncertainty in these estimates. Assuming a volcanic source that is just west of the graben boundary reduces individual ignimbrite volumes by 25 to 60%.

2.4 Discussion

2.4.1 Erupted volumes and uncertainty

The total volume of the marker ignimbrite components of the 14 eruptions in this study is 62.5 km^3 (~ 41km^3 DRE), based on calculation methods above. We consider each estimated ignimbrite volume, and thus the total, to be minimum estimates, as they do not include pyroclastic fall components of the eruptions, nor caldera fill volumes (if any), or pyroclastic flows that traveled any direction other than east into the Deschutes Basin. Accounting for such volumes more than doubles the initial estimate.

Substantial volumes of tephra were deposited as coeval tephra-fall units for many of the ignimbrites of this study. For example, at all of its outcrops the Lower Bridge Tuff directly overlies a coarse co-genetic tephra-fall deposit that ranges from 40 to 130 cm thick. This component of the eruption is likely to be volumetrically significant, but it is not included in the volume estimate above for the ignimbrite (3.6 km^3). Using the exponential thinning model of Pyle (1989), we estimate the volume of the coeval Lower Bridge tephra-fall deposit to be 4.2 km^3 (based on 11 thickness measurements from the field). This approximately 1:1.2 ratio of tephra fall to flow is consistent with bulk rock ratios estimated for the modern eruptions of Novarupta (1.3:1 to 1.9:1, Hildreth and Fierstein, 2012) and Pinatubo (0.5:1 to 0.9:1 Scott et al., 1996; 1:1 to 1.7:1, Koyaguchi, 1996). Since the bulk ignimbrite volumes for Novarupta (9-13 km^3) and Pinatubo (5-6 km^3) are of similar magnitude to the volumes presented herein (1-10 km^3), we may assume, based on these modern

analogues, that the tephra-fall components of the Deschutes Formation eruptions are 0.5 to 1.9 times the volume of the marker ignimbrites.

The marker ignimbrite volumes presented above are also considered minima because they do not account for ignimbrites that flowed any direction other than east into the Deschutes Basin. Five million years of volcanic and sedimentary accumulation has covered all proximal Deschutes Formation tuffs that were deposited within the 30-km-wide High Cascades graben, and only the ignimbrites deposited outside of the graben (predominantly eastward, within the modern Deschutes Basin) are exposed (Fig. 6). It is unlikely that eruptions capable of producing ignimbrites that flowed almost 50 km from their assumed source would flow in only one direction. More likely is that ignimbrites flowed in several directions from the vent, as exemplified by the modern eruptions of Mount Mazama (Bacon, 2008), the Valley of Ten Thousand Smokes (VTTS) (Hildreth and Fierstein, 2012), and Mount Pinatubo (Scott et al., 1996). Although not yet correlated to any marker units, at least three ignimbrites of Deschutes Formation age, mentioned previously, are found just west of the faults that define the western boundary of the High Cascades graben and imbrication measurements for one tuff indicate a source in the direction of Mt. Jefferson. Formation This indicates that the Deschutes Formation eruptions dispersed pyroclastic flows also to the west. As a result of drainage distribution, we may expect to find larger volumes of flows perpendicular to the arc axis than parallel to it, as seen for Valley of the Ten Thousand Smokes (VTTS) ignimbrite (Hildreth and Fierstein, 2012). A more symmetric distribution of ignimbrites warrants multiplying the Deschutes Formation ignimbrites volume by a factor of two. Were the distribution radial, as approximated by the Mount Mazama eruption (Bacon, 2008), then the ignimbrite volume could be as much as six times greater, as the Deschutes Basin represents 1/6 (55°) of the radial potential outflow from a point source in the arc (Fig. 3D).

By estimating the volumes of tephra-fall components (0.5:1 to 1.9:1 fall: flow ratio) as well as ignimbrites which may have traveled west (symmetric distribution), we estimate a total volume, for just these 14 eruptions alone, of ~188 to 363 km^3 (121

to 227 km^3 DRE). We make no assumptions of intracaldera tuff volumes; however, the volumes of the individual tuffs we have documented are unlikely to have caused syneruptive coherent (piston) collapse of the caldera floor (e.g. Roche and Druitt, 2001) and extensive ponding of intracaldera tuff. Additionally, these ignimbrites are unlikely to thicken toward the source, as the source was on the topographically high arc.

2.4.2. An unusual pulse of explosive silicic volcanism for the central Oregon Cascades

In contrast to Quaternary volcanism in the central Oregon Cascades (43.75°N to 44.75°N), which is dominantly mafic (Priest,1990; Hildreth, 2007), the Deschutes Formation preserves an episode of increased volcanic productivity characterized by much higher proportions of explosive eruptions of silicic compositions (Table 1). Much of the Quaternary volcanic output is dominated by smaller basaltic and basaltic andesite lava flows that collectively account for > 90% of the total volume erupted (Sherrod et al., 2004; Hildreth, 2007). The Quaternary arc also includes several central volcanoes, including Mount Washington and North Sister, which have basaltic andesite to andesite compositions (Schmidt and Grunder, 2011), and three which are mostly andesite to rhyodacite with rare rhyolite compositions (Mount Jefferson, South Sister, and the Tumalo volcanic center (TVC), as compiled by Hildreth, 2007). The 14 silicic eruptions of the Deschutes Formation described here have a cumulative volume much greater than the entire edifice volumes of the three regional Quaternary silicic volcanoes (including the TVC) combined (70-86 km^3) (Hildreth, 2007). Taken over the 50 km of arc length that the inferred sources span, these 14 eruptions equate to a silicic eruptive rate of 4.7-9.1 km^3/m.y./km arc length. Even the minimum rate estimated for these 14 eruptions is three times greater than the silicic (dacite-rhyolite) production rate of Brunhes-age central Oregon Cascades (1.6 km^3/m.y./km, Priest, 1990), and is thus the highest silicic eruption rate this region has experienced in the last 17 million years (Fig. 1). The Deschutes Formation also contains numerous mafic lava flows, which occur throughout the entire stratigraphic sequence (Smith, 1986; 4-7.5 Ma) and further contribute to the high volcanic productivity of the period. In

figure 6 we compare the cross-sectional area of Brunhes age rocks in the central Oregon High Cascades, as constrained by drill holes, to that of Deschutes-age rocks, and find that the former had rates that were 3 to 6 times higher. Furthermore, the eruptive rate contributed by just these 14 explosive eruptions (4.7-9.1 km^3/m.y./km) far exceeds the average Quaternary eruption rates, of all compositions, calculated by Hildreth (2007) for the entire Cascades arc (1.5-2.5 km^3/m.y./km), Alaska Peninsula (0.6-1.0 km^3/m.y./km), and the Andean southern volcanic zone (33°-46°S) (1.1-2.0 km^3/m.y./km).

In addition to erupting higher proportions of silicic magma than during the Quaternary, Late Neogene (5.45-6.25 Ma), central Oregon volcanoes were also more explosive. Explosive eruptions are relatively rare in the central Oregon segment of the Quaternary Cascades (Sherrod and Smith, 1990; Hildreth 2007), and volumes of known Quaternary explosive eruptions are much smaller than those that produced the Deschutes marker ignimbrites. There are several known explosive eruptions from Mount Jefferson, one of which produced a ~1 km^3 pyroclastic flow (20-60 ka) that traveled approximately 19 km down the Whitewater River valley (Yogodzinski, 1985), and another rhyodacite pyroclastic flow deposit from Mount Jefferson can be found along the Deschutes River, more than 45 km away (Smith and Hayman, 1987; Conrey, 1991). In addition, tephra from unit Qrdw reached as far east as Yellowstone (Conrey, 1991). The South Sister region produced two explosive eruptions 2000-2300 ^{14}C years ago, with a total tephra-fall volume of 1.6 km^3 (0.5 km^3 DRE) and minor pyroclastic flows that flowed less than 1 km (Scott, 1987). The highest rate of Quaternary explosive volcanism in central Oregon occurred during the Pleistocene (~700 to 175 ka), likely originating from the TVC (Sherrod et al., 2004). During this time, the region produced at least three pyroclastic deposits, including the Desert Spring Tuff (600-700 ka, Sarna-Wojcicki et al., 1989), the Tumalo Tuff and Bend Pumice fall deposit (440± 6 ka, Lanphere et al., 1999) and the Shevlin Park Tuff (between 225± 10 ka and 175± 3 ka, Hildreth et al., 2012)), which are rhyolite, rhyodacite and andesite, respectively (Sherrod et al., 2004). The erupted volume of these deposits is uncertain, but estimates suggest each of these three ignimbrites is as

large as ~3 km^3 (Hill, 1984; Conrey et al., 2001). Thus, the total pyroclastic volume erupted by the Quaternary central Oregon Cascades (44°N to 45°N) is less than 15 km^3, which is less than 25% of the minimum estimated volume of the 14 eastward-deposited ignimbrites of this study. This comparison is appropriate as they were erupted over similar time intervals (~800 k.y.), and as noted above, the actual volumes of both the Quaternary and Deschutes Formation pyroclastic deposits are likely larger due to lack of exposures and unconstrained tephra-fall volumes. In addition, the Deschutes Basin contains at least an additional 50 ignimbrites and 30 distinct tephra-fall units, which add substantially to the total volume erupted during Deschutes Formation time. Overall our data shows that the central Oregon Cascades Range was more volcanically productive as well as more explosive between 5.45 and 6.25 Ma than during the Quaternary or any other time in the last 17 m.y. (Figs. 1, 6).

2.4.3 Extension and arc axis migration as possible drivers for explosive volcanism

To understand the causes of the atypical pulse of explosive silicic volcanism that is preserved within the Deschutes Formation, we consider: (i) why the pulse occurred specifically within central Oregon (ii) why it began at 6.25 Ma, (iii) why it lasted only ~800 k.y., and (iv) why it was much more silicic than Quaternary volcanism in this area. In the following sections, we explore the idea that the explosive pulse may result from the onset of regional extension and migration of magmatic activity. We will begin with evidence for regional extension, which continues in the modern arc, and then propose that the timing and short duration of the Deschutes Formation silicic pulse resulted from more efficient melting shortly after the onset of extension and the migration of magmatic activity into temporarily more fusible crust.

The central Oregon Cascades are currently experiencing intra-arc extension (McCaffrey et al., 2007; Wells and McCaffrey, 2013), and such extension has likely persisted since for at least 7.5 m.y. (Conrey et al., 2004). Given the association between extension and increased explosive silicic volcanism in other arc systems, including the central Taupo Volcanic Zone (Deering et al., 2011), the Tepic-Zacoalco Rift (Frey et al., 2007), and the Sierra Madre Occidental (Ferrari et al., 2002), this

appears a viable mechanism to cause Deschutes Formation explosive volcanism. Many authors have recognized that extension may drive decompression mantle melting, increase basaltic magma flux into the crust, enhance shallow crustal partial melting, and allow such silicic melts to coalesce into large volumes (e.g. Hildreth, 1981; Jellinek and DePaolo, 2003; Price et al., 2005). De Silva (2008) suggests that an increase in mantle-derived flux, actuated by changes in regional tectonics (i.e. extension), may cause an arc to switch from its steady-state behavior (dominantly stratovolcanoes) to a flare-up mode in which numerous caldera-forming eruptions occur. Indeed, a majority of Quaternary arc calderas worldwide have formed within locally extensional settings, and extension and the presence of a fault zone and (or) graben favor higher incidence of silicic explosive eruptions (Hughes and Mahood, 2011).

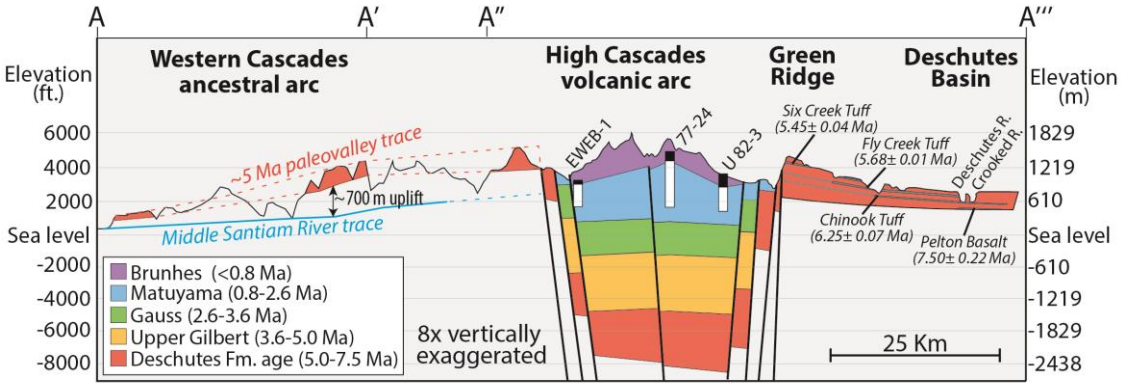

Figure 2.6: Cross-section (A-A’’’, Figure 2) through the Western Cascades ancestral arc, High Cascades arc, and the Deschutes Basin, depicting relative volcanic production through time. Cross-sectional area was constrained for Brunhes age rocks with three drill holes (EWEB-1, SP 77-24, and Unocal 82-3). We estimated the cross-sectional area for within-graben Deschutes-age rocks by projecting a 5° slope (Smith, 1986) to the modern arc axis, and added this to the cross-sectional area of actual exposures of Deschutes-age rocks on both sides of the graben. We calculated the area per million years for both time periods and assuming a linear decrease in volcanic production rate, we interpolated the cross-sectional areas for Matuyama, Gauss, and Upper Gilbert rocks. Ages and stratigraphic positions of Deschutes Fm. ignimbrites from this study are shown (thickness exaggerated), as well as the age of the Pelton Basalt (7.50± 0.22, Smith et al., 1987) which forms the base of the formation. Paleovalley-constrained Deschutes-age lavas now form inverted topographic ridgecaps atop the older Western Cascades 700 m above the modern Middle Santiam River, providing an estimate for the amount of uplift in the Western Cascades since ~5 Ma (Conrey et al., 2002). Figure modified from two cross-sections in Conrey et al. (2002) and other information from Black et al., 1987, Hill and Priest, 1992, Sherrod et al., 2004, and McClaughry et al., 2010.

2.4.3.1 Extension and increased magmatic flux to the central Oregon Cascades

Abundant evidence suggests that the central Oregon Cascades arc has undergone extension and that this is associated with an increased magmatic flux. North-striking graben faults propagate into the arc, including the Green Ridge and Sisters fault zones, that form the eastern boundary of the 30-km wide High Cascades graben which hosts the buried sources of the Deschutes Formation (Fig. 6). Extension is inferred to terminate near Mount Hood (Conrey et al., 2004). Formation GPS studies show that the Oregon forearc is rotating clockwise as much as 2.0°/m.y. (McCaffrey et al., 2007), and paleomagnetic studies indicate similar rotation rates have persisted since at least the mid-Miocene (e.g. Wells and Heller, 1988; Wells and McCaffrey, 2013). Thus, unlike the Washington and British Columbia portions of the arc, which are experiencing overall compression, the Oregon Cascades arc adjoining the Basin and Range province is experiencing regional extension (~1 mm/yr, Wells et al., 1998), with rates increasing southward (Wells and McCaffrey, 2013). In addition, a marked increase in crustal heat flow and hydrothermal heat discharge occurs within the arc southward of 45°15’ (Fig. 2A), and over 25% of the total hydrothermal heat discharge for the entire Cascades arc comes from just five hot springs located near Mount Jefferson (Blackwell et al., 1990; Ingebritsen and Mariner, 2010). This anomalous heat flow within the central Cascades is further evidence for the effect of crustal thinning and regional extensional tectonics, which allows for deep circulation of fluids (Ingebritsen and Mariner, 2010).

Although regional crustal extension rates, may be insufficient to drive large-scale decompression melting of the mantle beneath the arc, previous work has demonstrated the role of extension in focusing decompression melts of mantle upwelling induced by slab rollback and steepening (Long et al., 2012; Till et al., 2013; Wannamaker et al., 2014; Long, 2016, and references therein). Laboratory experiments coupled with geodynamic models indicate that when combined with even moderate extension (1.7 mm/yr), thermal anomalies in the upper mantle wedge resulting from slab-induced flow are more than two orders of magnitude greater than with rollback alone (Druken et al., 2011; Long et al., 2012). A magnetotulluric (MT)

profile at the latitude of Mount Jefferson shows a lack of low resistivity within the subarc mantle compared to profiles across the rest of the arc, which has been interpreted to result from the dominance of east-west tensional stresses within the mantle and a north-south alignment of decompression mantle melt pathways (Wannamaker et al., 2014). Furthermore, an along-arc shear-velocity profile from ambient-noise tomography reveals a marked decrease in velocity within the upper mantle south of 45°N latitude (Mount Jefferson), which is interpreted to be the result of increased melt production and focusing caused by extension within the southern half of the arc (Porritt et al., 2011). Thus, intra-arc extension likely contributes to decompression melting and controls when and where these melts propagate into the crust (Till et al., 2013), thereby generating an increased magmatic flux to the central Oregon Cascades.

Potential segmentation of the downgoing Juan de Fuca slab may also play a role in the spatial organization of regions of increased decompression melting. A common finding of many recent upper mantle tomography models is a segmented slab at approximately 100-150 km depth, with two gaps located approximately beneath the Washington-Oregon border (46°N) and southern Oregon (43°N) (Porritt et al., 2011; Gao and Shen, 2014; Long, 2016 and references therein). According to these results, the central Oregon portion of the Cascades arc lies above the center of one intact segment of the Juan de Fuca slab. Laboratory experiments (MacDougall et al., 2014) indicate that although slab gaps allow subslab mantle material to pass into the overlying wedge, slab gaps are not likely to be the locations of increased decompression melting because vertical motions are not observed. Instead, experiments by Druken et al (2011) suggest that beneath an extending arc, the highest degree of vertical mantle upwelling occurs above the center of a slab segment (beneath the axis of extension); it is away from the axis that toroidal flow around the slab edges reduces this extension-driven vertical mantle motion. These results, which have been further modeled to indicate higher thermal anomalies in the uppermost mantle above the center of slab segments (Long et al., 2012), are also consistent with along-arc shear wave tomography profiles, which seem to indicate low-velocity upper

mantle melting structures centered above high-velocity (slab) segments, not between them (Porritt et al., 2011). Thus, despite evidence that intra-arc extension continues along the entire southern half of the Cascades volcanic arc, decompression melting may be highly focused in central Oregon (~43.75-44.75°N) due to its location above the center of a slab segment.

Increased regional flux of decompression-driven mantle melts is also consistent with the existence of over 600 overlapping Quaternary mafic vents in central Oregon, , which has one of the highest volcanic vent densities in the Cascades volcanic arc (Hildreth, 2007, and references therein). Although basaltic andesite compositions are more common than true basalts in the central Oregon segment of the Quaternary arc, basalts were much more common during Deschutes Formation time (Hughes and Taylor, 1986), and were predominantly low K tholeiites (LKTs, also known as High-alumina olivine tholeiites, HAOTs). These basalts have major and trace element compositions that indicate the prevalence of dry decompression melting of depleted, but subduction fluid-modified, mantle (Conrey et al., 1997; Rowe et al., 2009; Till et al., 2012; Till et al., 2013). The crystal-poor (<10%) nature and anhydrous mineral assemblage (plagioclase and two pyroxenes) of the Deschutes Formation tuffs (Table 1) likewise suggest the involvement of "hot-dry-reduced" magmas rather than arc-typical "cold-wet-oxidized" magmas (after Deering et al., 2011), consistent with an extensional influence on regional volcanism. Geochemical investigations of these ignimbrites are ongoing; however, initial results indicate the tuffs share geochemical similarities (e.g. high FeO*, FeO*/MgO, Y, MREE, and Zr/Sr) (Pitcher et al., Unpublished results) to dry rhyolites of intraplate origins such as the High Lava Plains province (Till et al., 2012; Ford et al., 2013), as well as transitional ("damp") back-arc rhyolites from Newberry volcano (Mandler et al., 2014), both located southeast of the Central Oregon Cascades Range.

2.4.3.2 Timing of the explosive pulse following the 7.5 Ma onset of extension and arc migration

We suggest that although extension continues in the modern central Oregon Cascades arc, the timing of a short pulse of Deschutes Formation explosive volcanism

is a result of the onset of extension and arc migration, which occurred simultaneously ~7.5 Ma (Smith et al., 1987; Priest, 1990). A marked change from relatively low production rates of primarily andesite lavas (17-7.5 Ma) to much higher extrusion rates of mafic lava which included LKTs beginning 7.50 ±0.22 Ma (Fig. 1) suggests an increasing influence of extension began during this time (Smith et al., 1987; Priest, 1990). In the High Lava Plains of eastern Oregon, LKT volcanism followed Columbia River Basalt Group volcanism and is ascribed to Cascades slab rollback, incursion of Pacific mantle related to slab rollback, plume-head spreading or combinations thereof (Hart et al., 1984; Carlson and Hart, 1987; Draper, 1991; Camp and Ross, 2004). However, a major eruptive pulse of LKT volcanism occurred between 7.8 and 7.5 Ma across the entire High Lava Plains province, signaling a shift in tectonic and mantle upwelling regime reaching across central Oregon into the Cascades Range (Jordan et al., 2004). These changes are coincident with a distinct change in Pacific plate motion to a more northerly direction at ~8 Ma (Atwater and Stock, 1998), which would have caused more oblique subduction of the Juan de Fuca plate, leading to increased forearc block rotation and subsequent extension in central Oregon (DeMets, 1995). Although current rates of extension are estimated to be ~1mm/yr, the rate of extension during Deschutes time, may have been three times greater (Conrey et al., 2002).

While there is ample evidence for the influence of extension beginning ~7.5 Ma, there are difficulties constraining the exact timing of the migration of arc activity because more than 5 m.y. of subsequent volcanism has completely covered the Deschutes Formation source volcanoes within the High Cascades graben (Smith et al., 1987). Although volcaniclastic sediments and sparse pyroclastic flows were shed eastward into the Deschutes Basin to form the Simtustus Formation (12-15 Ma), the Simtustus Formation lacks lava flows (Smith, 1986). Deschutes Formation lavas, on the other hand, were deposited to the east of the current Cascades axis, and although thick sections of these lavas are found on the crest of the older Western Cascades, most of these are found just west of the graben boundary, with the exception of a few paleovalley-constrained distal flows (e.g. Fig. 6) (Conrey, 1991; Priest et al., 1987,

1988). This suggests that the LKTs of the Deschutes Formation were likely sourced from a more eastward source than that of Western Cascades volcanism (Smith, 1986; du Bray and John, 2011). Thus, the contemporaneous change in volcanic production and the composition and location of erupted lavas is consistent with the onset of extension and eastward migration of arc activity from the Western Cascades to the current High Cascades axis approximately 7.5 Ma.

Although we make the case that regional extension, coupled with slab-rollback induced mantle flow, caused increased magmatic flux within the central Oregon Cascades arc since ~ 7.5 Ma, this does not explain the ~1.25 m.y lag before the onset of a pulse of silicic and explosive volcanism during Deschutes time, nor the short duration of this pulse. This may be partially explained by the cotemporaneous eastward migration of activity ~7.5 Ma (Smith et al., 1987; Priest, 1990). Arc migration associated with the transition to the High Cascades would have resulted in access to more fusible crust, temporarily promoting production of higher volumes of silicic magma. Hughes and Mahood (2011) recognize that arcs with the highest volcano and caldera densities (e.g. New Zealand, Central America, Kamchatka) have all migrated axis positions within the last ~10 m.y. Over time, magma supply decreases in stagnant arcs as they deplete the lithosphere and mantle wedge of the most fusible material and/or volatiles (Hughes and Mahood, 2011).

If arc migration is the cause of the pulse of silicic volcanism we observe in the Deschutes Formation, then the interval between arc migration at ~7.5 Ma and the onset of Deschutes ignimbrite activity (6.25± 0.07 Ma) is consistent with a ~1.25 Ma period of thermal maturation of the crust before substantial silicic magma is produced and erupted. Annen et al (2006) suggest that after initial injection of basalt into a region of the lower crust, a thermal incubation time of up to 1 m.y. is required to establish a deep crustal hot zone, from which silicic crustal melts of lower crust can be extracted. In addition, Annen et al. (2006) also propose that, for a given intrusion depth (for any intrusion rate) the thickness of the partially melted crust is limited by heat diffusivity, since at a certain distance, the conductive heat transfer from the underlying basalt becomes insufficient to partially melt the cool overlying crust.

Those authors propose that after establishing a deep crustal hot zone, crustal melting productivity reaches a maximum and then declines. Using a thermo-mechanical model, Karakas and Dufek (2015) focus on modeling the thermodynamic and petrologic effects of extensional kinematics on crust-magma interactions. Their model indicates that for relatively high basaltic flux rates into an amphibolite arc crust which is undergoing extension, the maximum crustal melt volume is reached 1.2 to 1.8 m.y. after the initiation of extension. After this time, the authors suggest that crustal melt efficiency decreases as the melting region becomes saturated by mafic intrusions and fertile crust is displaced away from the melting zone by continued intrusion and extension. This timing corresponds well with the timing of Deschutes Formation ignimbrites, all of which were erupted between 1.25 and 2.05 m.y. after the advent of the LKTs in the region and thus the approximate timing of initiation of arc migration and intra-arc extension. The cessation of explosive eruptions after 5.25 Ma and shift to more mafic volcanism within the Deschutes Formation (Conrey, 1985; Smith et al., 1987) is consistent with the expected decline in crustal melting and saturation of the lower crust by mafic intrusions predicted by both Annen et al. (2006) and Karakas and Dufek (2015).

2.4.4 Comparison with other young extensional Arcs

The volcanic behavior of the central Oregon High Cascades arc during its infancy may be used to infer possible changes in volcanic activity at other young and extensional arcs around the world. Of the 29 arcs that Hughes and Mahood (2011) examined, five are undergoing extension and have migrated axial locations more recently than the Cascades (<7 Ma). Of these, only the Aegean and New Zealand arcs have trench-normal convergence rates similar to the Cascades arc (3-4 cm/yr.) (Hughes and Mahood, 2011). Although these arcs differ in many ways, similarities in arc immaturity, extensional stress, and slow convergence may be predictors for the longevity of pulses of explosive volcanism.

Volcanic activity in the Aegean Sea shifted southward at approximately 4 Ma, forming the Southern Aegean active volcanic arc (SAAVA) (Pe-Piper and Piper, 2005). The arc is characterized by extensional deformation, and current rates increase

to a maximum of 7 mm/yr in the central portion of the arc (Papazachos and Kiratzi 1996), which includes the most explosive volcanoes such as Santorini and Kos. The advent of tholeiitic compositions in the region, which marks the initial influence of extension, began approximately 0.8 Ma, and the earliest stages of explosive volcanism began only 0.36 Ma (Francalanci et al., 2005). The timing of explosive volcanism approximately 0.8 m.y. after extension agrees well with numerical modeling results by Karakas (2011), which predict that at moderate extension rates like that of the central SAAVA (7 mm/yr), maximum crustal melting efficiency begins at 0.9 m.y. and should decline 1.3 m.y. after initiation of extension.

The Taupo volcanic zone (TVZ) has been active for 2 m.y., and extension increases northward from 3 to 13 mm/yr (Deering et al., 2011, and references therein). A marked change from andesitic to rhyolitic volcanism occurred approximately 0.7 Ma, following an acceleration in rifting velocity and the formation of the Taupo Rift beginning 0.9 Ma (Deering et al., 2011). The cause of this petrologic transition is still highly debated, and has been attributed to crustal anatexis and re-melting andesitic precursors (e.g. Price et al., 2005) or assimilation and fractional crystallization (AFC) processes (Deering et al., 2011), but the temporal and spatial correlation of the compositional transition with the onset of TVZ extension is undeniable.

We may infer from the short pulse of increased explosivity in the central Oregon Cascades arc and numerical modeling results of Karakas and Dufek (2015) that the current period of explosive volcanism in the SAAVA and TVZ arcs may be short-lived. A similar short-lived pulse (between 5 Ma and 3 Ma) of rhyolitic ignimbrite volcanism, 10 times greater than the Quaternary rate of the region, occurred in western Mexico following the initiation of the Tepic-Zacoalco rift (Frey et al., 2007). It is noted, however, that all of these extensional arc systems are different from the Cascades arc (e.g. different thickness and compositions of crust), and volumes of Deschutes Formation ignimbrites are one to two orders of magnitude smaller than those of Santorini, Kos and the TVZ. However, if the explosive flare-ups in these arcs were to have the same overall duration as that of central Oregon

(800± 54 k.y.), our results suggest that explosive activity may sharply decrease in the TVZ in approximately 100-200 k.y., and within 340-540 k.y. in the SAAVA.

2.5 Conclusions

A high-productivity relatively short ~800,000-year pulse of dominantly silicic explosive volcanism occurred in central Oregon following the late Neogene initiation of the High Cascades volcanic arc. New $^{40}Ar/^{39}Ar$ ages for eight of the ignimbrites that stratigraphically bracket the many pyroclastic deposits exposed immediately east of the arc indicate that almost all of these eruptions occurred within only 800± 54 k.y., between 6.25± 0.07 and 5.45± 0.04 Ma. Field evidence indicates that all these eruptions were likely sourced from two approximate locations: 7-15 km south of modern Mount Jefferson and just north of modern North Sister volcanoes. Estimation of volumes of just 14 of the many ignimbrites contained within the Deschutes Formation yields a minimum cumulative volume of 62.5 km^3 (~41 km^3 DRE). The corresponding eruptive rate is greater than any silicic eruptive rate in the central Oregon Cascades in the last 17 m.y. Estimated total volume of these 14 eruptions, if including westward-flowing ignimbrites and tephra-fall contributions, ranges from 188 to 363 km^3 (~121 to 227 km^3 DRE). The large pyroclastic volumes and geochemical trends, which suggest the influence of hot and dry decompression melting, are likely the consequence of regional extension that promoted increased magmatic flux, crustal melting, and magma storage. The central Oregon Cascades arc may have experienced this short pulse due to a temporary increase in crustal melting efficiency following both the onset of intra-arc rifting and the migration of the locus of volcanic activity into more fusible crust approximately 7.5 Ma.

In addition, we develop a new GIS-based methodology for calculating the volumes of ignimbrites. The method linearly interpolates thickness between measured locations, thereby accounting for spatial patterns of thickness variation. This is much more robust to irregular tuff distributions than the method of multiplying average thickness by areal extent which is more useful for sheet-like ignimbrites (cf. Salisbury et al., 2010). Our method allows for large ranges in thickness measurements and is

thus more logical for ignimbrites with non-sheet-like morphologies and can be applied to ignimbrites of all sizes.

Acknowledgements

We would like to express gratitude to Daniel Miggins and Anthony Koppers in the $^{40}Ar/^{39}Ar$ geochronology lab at Oregon State University for their help and patience in teaching the entire preparation and analysis procedure. We would also like to thank Rick Conrey and Dave Sherrod for their insight on locations of key Deschutes Formation units and other useful discussions. Their thorough reviews and detailed suggestions helped to immensely improve this manuscript. Daniel Eungard is also acknowledged for introducing the author to the Deschutes Formation and for sharing field site locations and measurements. This project was supported by the GeoPRISMS program of the National Science Foundation [Award number 1144555].

References

Annen, C., Blundy, J.D., Sparks, R.S.J., 2006. The genesis of intermediate and silicic magmas in deep crustal hot zones. J. Petrology 47, 505–539. doi:10.1093/petrology/egi084

Armstrong, R.L., Taylor, E.M., Hales, P.O., Parker, D.J., 1975. K-Ar dates for volcanic rocks, central Cascades Range of Oregon. Isochron/West 13 5–10.

Atwater, T., Stock, J., 1998. Pacific-North America plate tectonics of the NeogenesSouthwestern United States: an update. International Geology Review 40, 375–402. doi:10.1080/00206819809465216

Aubin, W., 2000. Ignimbrites of the Deschutes Formation: A record of Crustal Melting and Magma Mixing (M.S.). Washington State University, Pullman, WA.

Bacon, C.R., 2008. Geologic Map of Mount Mazama and Crater Lake Caldera, Oregon. Scientific Investigations Map 2832.

Bacon, C.R., Lanphere, M.A., 2006. Eruptive history and geochronology of Mount Mazama and the Crater Lake region, Oregon. Geological Society of America Bulletin 118, 1331–1359. doi:10.1130/B25906.1

Balbas, A.M., 2016. Application of Cosmogenic Nuclides and Argon Geochronology to Paleoclimate, Paleomagnetism, and Paleohydrology (Ph. D.). Oregon State University, Corvallis, Oregon.

Black, G.L., Woller, N.M., Ferns, M.L., Neuhaus, M.E., 1987. Geologic Map of the Crescent Mountain Area, Linn County, Oregon. Oregon Dept. of Geology and Mineral Industries Geological Map, GMS-47.

Blackwell, D.D., Steele, J.L., Frohme, M.K., Murphey, C.F., Priest, G.R., Black, G.L., 1990. Heat flow in the Oregon Cascades Range and its correlation with regional gravity, Curie point depths, and geology. Journal of Geophysical Research: Solid Earth 95, 19475–19493. doi:10.1029/JB095iB12p19475

Cannon, D.M., 1984. The stratigraphy, geochemistry, and mineralogy of two ash-flow tuffs in the Deschutes Formation, central Oregon (M.S.). Oregon State University, Corvallis, Oregon.

Carlson, R.W., Hart, W.K., 1987. Crustal genesis on the Oregon Plateau. Journal of Geophysical Research: Solid Earth 92, 6191–6206. doi:10.1029/JB092iB07p06191

Church, S.E., Lehuray, A.P., Grant, A.R., Delevaux, M.H., Gray, J.E., 1986. Lead-isotopic data from sulfide minerals from the Cascades Range, Oregon and Washington. Geochimica et Cosmochimica Acta 50, 317–328. doi:10.1016/0016-7037(86)90180-8

Clayton, C.M., 1976. Geology of the Breitenbush Hot Springs area, Cascades Range, Oregon (M.S.). Portland State University, Portland, Oregon.

Conrey, R.M., 1991. Geology and Petrology of the Mt. Jefferson Area, High Cascades Range, Oregon (Ph.D.). Washington State University, Pullman, WA.

Conrey, R.M., 1985. Volcanic stratigraphy of the Deschutes Formation—Green Ridge to Fly Creek—north-central Oregon (M.S.). Oregon State University, Corvallis, Oregon.

Conrey, R.M., Donnelly-Nolan, J., Taylor, E.M., Champion, D., Bullen, T., 2001. The Shevlin Park Tuff, Central Oregon Cascades Range: Magmatic Processes Recorded in an Arc-Related Ash-Flow Tuff. AGU Fall Meeting Abstracts 32.

Conrey, R.M., Grunder, A.L., Schmidt, M.E., 2004. SOTA field trip guide, State of the Cascades arc: Stratocone persistence, mafic lava shields, and pyroclastic volcanism associated with intra-arc rift propagation. DOGAMI Open-File Report O-2004-04 39.

Conrey, R.M., Sherrod, D.R., Hooper, P.R., Swanson, D.A., 1997. Diverse primitive magmas in the Cascades arc, northern Oregon and southern Washington. The Canadian Mineralogist 35, 367–396.

Curtis, G.H., 1968. The Stratigraphy of the Ejecta from the 1912 Eruption of Mount Katmai and Novarupta, Alaska. Geological Society of America Memoirs 116, 153–210. doi:10.1130/MEM116-p153

de Silva, S.L., 2008. Arc magmatism, calderas, and supervolcanoes. Geology 36, 671–672. doi:10.1130/focus082008.1

Deering, C.D., Bachmann, O., Dufek, J., Gravley, D.M., 2011. Rift-Related Transition from Andesite to Rhyolite Volcanism in the Taupo Volcanic Zone (New Zealand) Controlled by Crystal–melt Dynamics in Mush Zones with Variable Mineral Assemblages. J. Petrology 52, 2243–2263. doi:10.1093/petrology/egr046

DeMets, C., 1995. Plate motions and crustal deformation. Reviews of Geophysics 33, 365–369. doi:10.1029/95RG00120

Dill, T.E., 1992. Stratigraphy of the Neogene volcanic rocks along the lower Metolius River, Jefferson County, central Oregon (M.S.). Oregon State University, Corvallis, Oregon.

Donnelly-Nolan, J.M., Champion, D.E., Lanphere, M.A., Ramsey, D., 2004. New Thoughts About Newberry Volcano, Central Oregon USA. Eos Trans. AGU, Fall Meeting Suppl. 85(47).

Doocy, S., Daniels, A., Dooling, S., Gorokhovich, Y., 2013. The Human Impact of Volcanoes: a Historical Review of Events 1900-2009 and Systematic Literature Review. PLoS Curr 5. doi:10.1371/currents.dis.841859091a706efebf8a30f4ed7a1901

Draper, D.S., 1991. Late Cenozoic bimodal magmatism in the northern basin and range province of southeastern Oregon. Journal of Volcanology and Geothermal Research 47, 299–328. doi:10.1016/0377-0273(91)90006-L

Druken, K.A., Long, M.D., Kincaid, C., 2011. Patterns in seismic anisotropy driven by rollback subduction beneath the High Lava Plains. Geophysical Research Letters 38, L13310. doi:10.1029/2011GL047541

du Bray, E.A., John, D.A., 2011. Petrologic, tectonic, and metallogenic evolution of the Ancestral Cascades magmatic arc, Washington, Oregon, and northern California. Geosphere 7, 1102–1133. doi:10.1130/GES00669.1

Eagar, K.C., Fouch, M.J., James, D.E., Carlson, R.W., 2011. Crustal structure beneath the High Lava Plains of eastern Oregon and surrounding regions from receiver function analysis. Journal of Geophysical Research: Solid Earth 116, B02313. doi:10.1029/2010JB007795

Eungard, D.W., 2012. Early High Cascades Silicic Volcanism: Analysis of the McKenzie Canyon and Lower Bridge Tuff (M.S.). Oregon State University, Corvallis, Oregon.

Ferrari, L., López-Martínez, M., Rosas-Elguera, J., 2002. Ignimbrite flare-up and deformation in the southern Sierra Madre Occidental, western Mexico: Implications for the late subduction history of the Farallon plate. Tectonics 21, 17–1--17–24. doi:10.1029/2001TC001302

Ford, M.T., Grunder, A.L., Duncan, R.A., 2013. Bimodal volcanism of the High Lava Plains and northwestern Basin and Range of Oregon: distribution and tectonic implications of age-progressive rhyolites. Geochemistry, Geophysics, Geosystems 14, 2836–2857. doi:10.1002/ggge.20175

Francalanci, L., Vougioukalakis, G.E., Perini, G., Manetti, P., 2005. A west-east traverse along the magmatism of the south Aegean volcanic arc in the light of volcanological, chemical and isotope data, in: Vougioukalakis, M.F. and G.E. (Ed.), Developments in Volcanology. Elsevier, pp. 65–111.

Frey, H.M., Lange, R.A., Hall, C.M., Delgado-Granados, H., Carmichael, I.S.E., 2007. A Pliocene ignimbrite flare-up along the Tepic-Zacoalco rift: Evidence for the initial stages of rifting between the Jalisco block (Mexico) and North America. Geological Society of America Bulletin 119, 49–64. doi:10.1130/B25950.1

Gao, H., Humphreys, E.D., Yao, H., van der Hilst, R.D., 2011. Crust and lithosphere structure of the northwestern U.S. with ambient noise tomography: Terrane accretion and Cascades arc development. Earth and Planetary Science Letters 304, 202–211. doi:10.1016/j.epsl.2011.01.033

Gao, H., Shen, Y., 2014. Upper mantle structure of the Cascades from full-wave ambient noise tomography: Evidence for 3D mantle upwelling in the back-arc. Earth and Planetary Science Letters 390, 222–233. doi:10.1016/j.epsl.2014.01.012

Green, N.L., Harry, D.L., 1999. On the relationship between subducted slab age and arc basalt petrogenesis, Cascadia subduction system, North America. Earth and Planetary Science Letters 171, 367–381. doi:10.1016/S0012-821X(99)00159-4

Hart, W.K., Aronson, J.L., Mertzman, S.A., 1984. Areal distribution and age of low-K, high-alumina olivine tholeiite magmatism in the northwestern Great Basin. Geological Society of America Bulletin 95, 186–195. doi:10.1130/0016-7606(1984)95<186:ADAAOL>2.0.CO;2

Hewitt, S., 1969. Geology of the Fly Creek Quadrangle and theNorth Half of the Round Butte Dam Quadrangle, Oregon (M.S.). Oregon State University, Corvallis, Oregon.

Hildreth, W., 2007. Quaternary Magmatism in the Cascades - Geologic Perspectives. U.S. Geological Survey Professional Paper 1744, Professional Paper.

Hildreth, W., 1981. Gradients in silicic magma chambers: Implications for lithospheric magmatism. Journal of Geophysical Research: Solid Earth 86, 10153–10192. doi:10.1029/JB086iB11p10153

Hildreth, W., Fierstein, J., 2012. The Novarupta-Katmai eruption of 1912—largest eruption of the twentieth century, Centennial Perspectives: U.S. Geological Surv. Professional Paper 1791.

Hildreth, W., Fierstein, J., Calvert, A., 2012. Geologic map of Three Sisters volcanic cluster, Cascades Range, Oregon. U.S. Geological Survey Scientific Investigations Map 3186.

Hildreth, W., Lanphere, M.A., Champion, D.E., Fierstein, J., 2004. Rhyodacites of Kulshan caldera, North Cascades of Washington: Postcaldera lavas that span the Jaramillo. Journal of Volcanology and Geothermal Research 130, 227–264. doi:10.1016/S0377-0273(03)00290-7

Hill, B.E., 1984. Petrology of the Bend pumice and Tumalo tuff, a Pleistocene Cascades eruption involving magma mixing (M.S.). Oregon State University, Corvallis, Oregon.

Hill, B.E., Taylor, E.M., 1990. Oregon Central High Cascades pyroclastic units in the vicinity of Bend, Oregon. Oregon Geology 52, 125-126; 139-140.

Hughes, G.R., Mahood, G.A., 2011. Silicic calderas in arc settings: Characteristics, distribution, and tectonic controls. Geological Society of America Bulletin 123, 1577–1595. doi:10.1130/B30232.1

Hughes, G.R., Mahood, G.A., 2008. Tectonic controls on the nature of large silicic calderas in volcanic arcs. Geology 36, 627–630. doi:10.1130/G24796A.1

Hughes, S.S., Taylor, E.M., 1986. Geochemistry, petrogenesis, and tectonic implications of central High Cascades mafic platform lavas. Geological Society of America Bulletin 97, 1024–1036. doi:10.1130/0016-7606(1986)97<1024:GPATIO>2.0.CO;2

Ingebritsen, S.E., Mariner, R.H., 2010. Hydrothermal heat discharge in the Cascades Range, northwestern United States. Journal of Volcanology and Geothermal Research 196, 208–218. doi:10.1016/j.jvolgeores.2010.07.023

Jellinek, A.M., DePaolo, D.J., 2003. A model for the origin of large silicic magma chambers: precursors of caldera-forming eruptions. Bulletin of Volcanology 65, 363–381. doi:10.1007/s00445-003-0277-y

Jordan, B.T., Grunder, A.L., Duncan, R.A., Deino, A.L., 2004. Geochronology of age-progressive volcanism of the Oregon High Lava Plains: Implications for the plume interpretation of Yellowstone. Journal of Geophysical Research: Solid Earth 109, B10202. doi:10.1029/2003JB002776

Karakas, O., 2011. Modulation of crustal magmatic systems by external tectonic forcing (M.S.). Georgia Institute of Technology, Atlanta, Georgia.

Karakas, O., Dufek, J., 2015. Melt evolution and residence in extending crust: Thermal modeling of the crust and crustal magmas. Earth and Planetary Science Letters 425, 131–144. doi:10.1016/j.epsl.2015.06.001

Koppers, A.A.P., Gowen, M.D., Colwell, L.E., Gee, J.S., Lonsdale, P.F., Mahoney, J.J., Duncan, R.A., 2011. New $^{40}Ar/^{39}Ar$ age progression for the Louisville hot spot trail and implications for inter–hot spot motion. Geochemistry, Geophysics, Geosystems 12, Q0AM02. doi:10.1029/2011GC003804

Koyaguchi, T., 1996. Volume Estimation of Tephra-Fall Deposits from the June 15, 1991, Eruption of Mount Pinatubo by Theoretical and Geological

Methods, in: Newhall, C.G., Punongbayan, R.S. (Eds.), Fire and Mud: Eruptions and Lahars of Mount Pinatubo, Philippines. Philippine Institute of Volcanology and Seismology, pp. 545–575.

Kuiper, K.F., Deino, A., Hilgen, F.J., Krijgsman, W., Renne, P.R., Wijbrans, J.R., 2008. Synchronizing Rock Clocks of Earth History. Science 320, 500–504. doi:10.1126/science.1154339

Lanphere, M.A., Champion, D.E., Christiansen, R.L., Donnelly-Nolan, J.M., Fleck, R.J., Sarna-Wojcicki, A., Obradovich, JD, Izlett, GA, 1999. Evolution of tephra dating in the western United States. Geological Society of America Abstracts with Programs 31.

Lanphere, M.A., Champion, D.E., Clynne, M.A., Lowenstern, J.B., Sarna-Wojcicki, A.M., Wooden, J.L., 2004. Age of the Rockland tephra, western USA. Quaternary Research 62, 94–104. doi:10.1016/j.yqres.2004.03.001

Leeman, W.P., Tonarini, S., Chan, L.H., Borg, L.E., 2004. Boron and lithium isotopic variations in a hot subduction zone—the southern Washington Cascades. Chemical Geology, Lithium Isotope Geochemistry 212, 101–124. doi:10.1016/j.chemgeo.2004.08.010

Long, M.D., 2016. The Cascadia Paradox: Mantle flow and slab fragmentation in the Cascadia subduction system. Journal of Geodynamics. doi:10.1016/j.jog.2016.09.006

Long, M.D., Till, C.B., Druken, K.A., Carlson, R.W., Wagner, L.S., Fouch, M.J., James, D.E., Grove, T.L., Schmerr, N., Kincaid, C., 2012. Mantle dynamics beneath the Pacific Northwest and the generation of voluminous back-arc volcanism. Geochemistry, Geophysics, Geosystems 13, Q0AN01. doi:10.1029/2012GC004189

MacDougall, J.G., Kincaid, C., Szwaja, S., Fischer, K.M., 2014. The impact of slab dip variations, gaps and rollback on mantle wedge flow: insights from fluids experiments. Geophysical Journal International 197, 705–730. doi:10.1093/gji/ggu053

MacLeod, N.S., Sherrod, D.R., Chitwood, L.A., Jensen, R.A., 1995. Geologic map of Newberry Volcano, Deschutes, Klamath, and Lake Counties, Oregon. U.S. Geological Survey Miscellaneous Investigations Series Map I-2455.

Mandler, B.E., Donnelly-Nolan, J.M., Grove, T.L., 2014. Straddling the tholeiitic/calc-alkaline transition: the effects of modest amounts of water on magmatic differentiation at Newberry Volcano, Oregon. Contributions to Mineralogy and Petrology 168, 1066. doi:10.1007/s00410-014-1066-7

McCaffrey, R., Qamar, A.I., King, R.W., Wells, R., Khazaradze, G., Williams, C.A., Stevens, C.W., Vollick, J.J., Zwick, P.C., 2007. Fault locking, block rotation and crustal deformation in the Pacific Northwest. Geophysical Journal International 169, 1315–1340. doi:10.1111/j.1365-246X.2007.03371.x

McClaughry, J.D., Ferns, M.L., Gordon, C.L., Partridge, K.A., 2009. Field trip guide to the Oligocene Crooked River caldera: central Oregon's supervolcano, Crook, Deschutes, and Jefferson counties, Oregon. Oregon Geology 69, 25.

McClaughry, J.D., Wiley, T.J., Ferns, M.L., Madin, I.P., 2010. Digital geologic map of the southern Willamette Valley, Benton, Lane, Linn, Marion, and Polk

Counties, Oregon. Oregon Dept. Geol. and Mineral Industries Open-File Report O-10-03.

McDannel, A., 1989. Geology of the southernmost Deschutes basin, Tumalo quadrangle, Deschutes County, Oregon (M.S.). Oregon State University, Corvallis, Oregon.

Nathenson, M., Donnelly-Nolan, J.M., Champion, D.E., Lowenstern, J.B., 2007. Chronology of Postglacial Eruptive Activity and Calculation of Eruption Probabilities for Medicine Lake Volcano, Northern California (No. 2007–5174–B), U.S. Geol. Surv. Scientific Investigations Report 2007-5174-B.

Newhall, C.G., Self, S., 1982. The volcanic explosivity index (VEI) an estimate of explosive magnitude for historical volcanism. Journal of Geophysical Research: Oceans 87, 1231–1238. doi:10.1029/JC087iC02p01231

Papazachos, C.B., Kiratzi, A.A., 1996. A detailed study of the active crustal deformation in the Aegean and surrounding area. Tectonophysics 253, 129–153. doi:10.1016/0040-1951(95)00047-X

Pe-Piper, G., Piper, D.J.W., 2005. The South Aegean active volcanic arc: relationships between magmatism and tectonics, in: Vougioukalakis, M.F. and G.E. (Ed.), Developments in Volcanology. Elsevier, pp. 113–133.

Plank, T., Kelley, K.A., Zimmer, M.M., Hauri, E.H., Wallace, P.J., 2013. Why do mafic arc magmas contain ~4 wt% water on average? Earth and Planetary Science Letters 364, 168–179. doi:10.1016/j.epsl.2012.11.044

Porritt, R.W., Allen, R.M., Boyarko, D.C., Brudzinski, M.R., 2011. Investigation of Cascadia segmentation with ambient noise tomography. Earth and Planetary Science Letters 309, 67–76. doi:10.1016/j.epsl.2011.06.026

Price, R.C., Gamble, J.A., Smith, I.E.M., Stewart, R.B., Eggins, S., Wright, I.C., 2005. An integrated model for the temporal evolution of andesites and rhyolites and crustal development in New Zealand's North Island. Journal of Volcanology and Geothermal Research 140, 1–24. doi:10.1016/j.jvolgeores.2004.07.013

Priest, G.R., 1990. Volcanic and tectonic evolution of the Cascades Volcanic Arc, central Oregon. Journal of Geophysical Research: Solid Earth 95, 19583–19599. doi:10.1029/JB095iB12p19583

Priest, G.R., Black, G.L., Woller, N.M., Taylor, E.M., Neuhaus, M.E., 1988. Geologic Map of the McKenzie Bridge Quadrangle, Lane County, Oregon. GMS-048.

Priest, G.R., Woller, N.M., Ferns, M.L., 1987. Geologic Map of the Breitenbush River Area, Linn and Marion Counties, Oregon. GMS-060.

Pyle, D.M., 1989. The thickness, volume and grainsize of tephra fall deposits. Bulletin of Volcanology 51, 1–15. doi:10.1007/BF01086757

Renne, P.R., Swisher, C.C., Deino, A.L., Karner, D.B., Owens, T.L., DePaolo, D.J., 1998. Intercalibration of standards, absolute ages and uncertainties in $^{40}Ar/^{39}Ar$ dating. Chemical Geology 145, 117–152. doi:10.1016/S0009-2541(97)00159-9

Roche, O., Druitt, T.H., 2001. Onset of caldera collapse during ignimbrite eruptions. Earth and Planetary Science Letters 191, 191–202. doi:10.1016/S0012-821X(01)00428-9

Rosner, B., 2011. Fundamentals of biostatistics, 7th ed. ed. Brooks/Cole, Cengage Learning, Boston.

Rowe, M.C., Kent, A.J.R., Nielsen, R.L., 2009. Subduction Influence on Oxygen Fugacity and Trace and Volatile Elements in Basalts Across the Cascades Volcanic Arc. J. Petrology 50, 61–91. doi:10.1093/petrology/egn072

Ruscitto, D.M., Wallace, P.J., Johnson, E.R., Kent, A.J.R., Bindeman, I.N., 2010. Volatile contents of mafic magmas from cinder cones in the Central Oregon High Cascades: Implications for magma formation and mantle conditions in a hot arc. Earth and Planetary Science Letters 298, 153–161. doi:10.1016/j.epsl.2010.07.037

Salisbury, M.J., Jicha, B.R., Silva, S.L. de, Singer, B.S., Jiménez, N.C., Ort, M.H., 2010. $^{40}Ar/^{39}Ar$ chronostratigraphy of Altiplano-Puna volcanic complex ignimbrites reveals the development of a major magmatic province. Geological Society of America Bulletin B30280.1. doi:10.1130/B30280.1

Samson, S.D., Alexander, E.C., 1987. Calibration of the interlaboratory ^{40}Ar□^{39}Ar dating standard, MMhb-1. Chemical Geology: Isotope Geoscience section 66, 27–34. doi:10.1016/0168-9622(87)90025-X

Sarna-Wojcicki, A.M., Meyer, C.E., Nakata, J.K., Scott, W.E., 1989. Age and correlation of mid-Quaternary ash beds and tuffs in the vicinity of Bend, Oregon. U.S. Geological Survey Open-File Report 89, 55–66.

Schmidt, M.E., Grunder, A.L., 2011. Deep Mafic Roots to Arc Volcanoes: Mafic Recharge and Differentiation of Basaltic Andesite at North Sister Volcano, Oregon Cascades. J. Petrology egq094. doi:10.1093/petrology/egq094

Schmidt, M.E., Grunder, A.L., Rowe, M.C., 2008. Segmentation of the Cascades arc as indicated by Sr and Nd isotopic variation among diverse primitive basalts. Earth and Planetary Science Letters 266, 166–181. doi:10.1016/j.epsl.2007.11.013

Schmidt, M.E., Grunder, A.L., Rowe, M.C., Chesley, J.T., 2013. Re and Os isotopes of the central Oregon Cascades and along the arc indicate variable homogenization and mafic growth in the deep crust. Geochimica et Cosmochimica Acta 109, 345–364. doi:10.1016/j.gca.2013.02.003

Scott, W.E., 1987. Holocene rhyodacite eruptions on the flanks of South Sister volcano, Oregon. Geological Society of America Special Papers 212, 35–54. doi:10.1130/SPE212-p35

Scott, W.E., Hoblitt, R.P., Torres, R.C., Self, S., Martinez, M.L., Nillos Jr., T., 1996. Pyroclastic Flows of the June 15, 1991, Climactic Eruption of Mount Pinatubo, in: Newhall, C.G., Punongbayan, R.S. (Eds.), Fire and Mud: Eruptions and Lahars of Mount Pinatubo, Philippines. Philippine Institute of Volcanology and Seismology, pp. 545–575.

Seligman, A.N., Bindeman, I.N., McClaughry, J., Stern, R.A., Fisher, C., 2014. The earliest low and high $\delta^{18}O$ caldera-forming eruptions of the Yellowstone plume: implications for the 30–40 Ma Oregon calderas and speculations on

plume-triggered delaminations. Volcanology 2, 34. doi:10.3389/feart.2014.00034

Sherrod, D. R., Taylor, E. M., Ferns, M. L., Scott, W. E., Conrey, R. M., Smith, G. A., 2004. Geologic Map of the Bend 30-× 60-Minute Quadrangle. Central Oregon. US Geological Survey Geologic Investigations Series Map I-2683.

Sherrod, D.R., Smith, J.G., 1990. Quaternary extrusion rates of the Cascades Range, northwestern United States and southern British Columbia. Journal of Geophysical Research: Solid Earth 95, 19465–19474. doi:10.1029/JB095iB12p19465

Smith, G.A., 1986. Stratigraphy, sedimentology, and petrology of Neogene rocks in the Deschutes basin, central Oregon : a record of continental-margin volcanism and its influence on fluvial sedimentation in an arc-adjacent basin (Ph.D.). Oregon State University, Corvallis, Oregon.

Smith, G.A., Hayman, G.A., 1987. Geologic Map of the Eagle Butte and Gateway Quadrangles, Jefferson and Wasco Coiunties, Oregon. GMS-43.

Smith, G.A., Snee, L.W., Taylor, E.M., 1987. Stratigraphic, sedimentologic, and petrologic record of late Miocene subsidence of the central Oregon High Cascades. Geology 15, 389–392. doi:10.1130/0091-7613(1987)15<389:SSAPRO>2.0.CO;2

Streck, M.J., Grunder, A.L., 1995. Crystallization and welding variations in a widespread ignimbrite sheet; the Rattlesnake Tuff, eastern Oregon, USA. Bulletin of Volcanology 57, 151–169. doi:10.1007/BF00265035

Taylor, E.M., 1990. Volcanic history and tectonic development of the Central High Cascades Range, Oregon. Journal of Geophysical Research: Solid Earth 95, 19611–19622. doi:10.1029/JB095iB12p19611

Till, C.B., Grove, T.L., Carlson, R.W., Donnelly-Nolan, J.M., Fouch, M.J., Wagner, L.S., Hart, W.K., 2013. Depths and temperatures of <10.5 Ma mantle melting and the lithosphere-asthenosphere boundary below southern Oregon and northern California. Geochemistry, Geophysics, Geosystems 14, 864–879. doi:10.1002/ggge.20070

Till, C.B., Grove, T.L., Krawczynski, M.J., 2012. A melting model for variably depleted and enriched lherzolite in the plagioclase and spinel stability fields. Journal of Geophysical Research: Solid Earth 117, B06206. doi:10.1029/2011JB009044

Trehu, A.M., Asudeh, I., Brocher, T.M., Luetgert, J.H., Mooney, W.D., Nabelek, J.L., Nakamura, Y., 1994. Crustal Architecture of the Cascadia Forearc. Science 266, 237–243. doi:10.1126/science.266.5183.237

Verplanck, E.P., Duncan, R.A., 1987. Temporal variations in plate convergence and eruption rates in the Western Cascades, Oregon. Tectonics 6, 197–209. doi:10.1029/TC006i002p00197

Walowski, K.J., Wallace, P.J., Hauri, E.H., Clynne, M.A., Rea, J., Rasmussen, D.J., 2013. Magma formation in hot-slab subduction zones: Insights from hydrogen isotopes in Cascades arc melt inclusions. Eos Trans. AGU, Fall Meeting Suppl.

Wannamaker, P.E., Evans, R.L., Bedrosian, P.A., Unsworth, M.J., Maris, V., McGary, R.S., 2014. Segmentation of plate coupling, fate of subduction fluids, and modes of arc magmatism in Cascadia, inferred from magnetotelluric resistivity. Geochemistry, Geophysics, Geosystems 15, 4230–4253. doi:10.1002/2014GC005509

Welch, B.L., 1947. The Generalization of `Student's' Problem when Several Different Population Variances are Involved. Biometrika 34, 28–35. doi:10.2307/2332510

Wells, R., Bukry, D., Friedman, R., Pyle, D., Duncan, R., Haeussler, P., Wooden, J., 2014. Geologic history of Siletzia, a large igneous province in the Oregon and Washington Coast Range: Correlation to the geomagnetic polarity time scale and implications for a long-lived Yellowstone hotspot. Geosphere 10, 692–719. doi:10.1130/GES01018.1

Wells, R.E., Heller, P.L., 1988. The relative contribution of accretion, shear, and extension to Cenozoic tectonic rotation in the Pacific Northwest. Geological Society of America Bulletin 100, 325–338. doi:10.1130/0016-7606(1988)100<0325:TRCOAS>2.3.CO;2

Wells, R.E., McCaffrey, R., 2013. Steady rotation of the Cascades arc. Geology 41, 1027–1030. doi:10.1130/G34514.1

Wells, R.E., Weaver, C.S., Blakely, R.J., 1998. Fore-arc migration in Cascadia and its neotectonic significance. Geology 26, 759–762. doi:10.1130/0091-7613(1998)026<0759:FAMICA>2.3.CO;2

Witham, C.S., 2005. Volcanic disasters and incidents: A new database. Journal of Volcanology and Geothermal Research 148, 191–233. doi:10.1016/j.jvolgeores.2005.04.017

Yogodzinski, G., 1985. The Deschutes Formation-- High Cascades transition in the Whitewater River area, Jefferson County, Oregon (M.S.). Oregon State University, Corvallis, Oregon.

3. Statistical Correlation of Pyroclastic Units and Revision of Tephrostratigraphy within the Deschutes Formation, Central Oregon

3.1 Introduction

Explosive eruptions commonly occur in arcs around the world and pose a serious threat to large populations that live close to these volcanic chains. Such eruptions are irregularly distributed worldwide both spatially and temporally, and vary widely in their eruptive volumes. Larger caldera-forming eruptions (generally >5km^3) have occurred more frequently in some Quaternary arcs such as Kamchatka, New Zealand, and northeast Japan, when compared to other arcs such as the Aleutians or Southern Philippines (Hughes and Mahood, 2011). Furthermore, explosivity within a single arc tends by be highly variable through time and space. For example, while the northern and southern portions of the Taupo Volcanic Zone (TVZ) of New Zealand contain primarily andesitic composite cones with no calderas, the central TVZ is characterized by the highest density of calderas of any arc in the world (Hughes and Mahood, 2011; Rowland et al., 2010). Prior to ~0.9 Ma, eruptions from the central TVZ were predominantly andesitic, but multiple cycles of increased explosivity have occurred since (Deering et al., 2010, 2011). Thus, to better understand hazards of an arc we must constrain its full eruptive history, not just that of the recent past. It is particularly important to elucidate the eruptive frequency and volumetric production during unusually explosive periods, in order to compare them background level and to infer processes responsible for temporal variations in explosivity and silicic magma generation.

Compared to arcs like the TVZ, the Quaternary Cascades arc of western North America has had relatively few caldera-forming eruptions, and has a caldera density that places it in the lowest 40th percentile of arcs worldwide (Hughes and Mahood, 2011). During the Quaternary, the arc produced only 20 explosive eruptions with volumes >1 km^3 (Hildreth, 2007). The Cascades consist predominantly of monogenetic basaltic-andesite to andesite shield volcanoes and stratocones, with only a small number of more evolved, long-lived composite volcanoes (Hildreth, 2007). However, this has not always been the case. The Deschutes Formation of Central

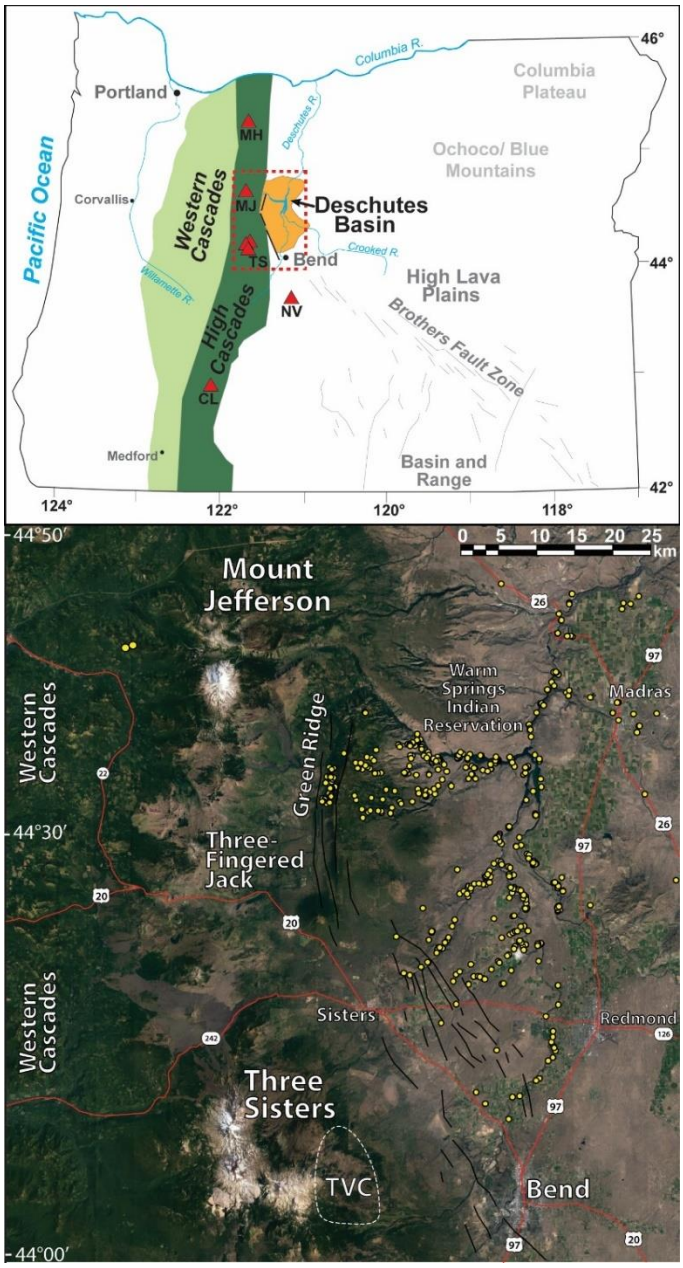

Figure 3.1: (A) Map indicating the location of the Deschutes Basin in central Oregon. Approximate areas of the Western Cascades (after du Bray and John, 2011) and the High Cascades are depicted. Red triangles represent major Quaternary stratovolcanoes (MH= Mount Hood, MJ= Mount Jefferson, TS= Three Sisters, NV= Newberry Volcano, CL= Crater Lake/ Mount Mazama). Other important geologic and tectonic regions of Oregon, including NW Basin and Range and the High Lava Plains, are also shown for reference. (B) Map of the Deschutes Basin field area, with sampling locations shown in yellow. The Green Ridge and Sisters Fault zones are also shown, as they represent the boundary of the Cascades Graben, wherein only Quaternary stratigraphy is exposed. Approximate outline of the Tumalo Volcanic Center and faults are from Sherrod et al., 2004.

Oregon (Fig. 3.1) preserves a record of unusually high mafic and silicic productivity following the ~7.5 Ma initiation of the High Cascades volcanic arc (Priest, 1990; Smith, 1986). Before this time, arc volcanism in Oregon was focused to the west, within the Western Cascades ancestral arc (Fig. 3.1), which produced very little pyroclastic material between ~17 and 7.5 Ma (du Bray and John, 2011). In stark contrast, the Deschutes Formation (~4-7.5 Ma) contains hundreds of ignimbrite and tephra-fall deposits which were all erupted during a relatively short pulse between

6.25± 0.07 and 5.45± 0.04 Ma (Pitcher et al., 2017a) (Fig. 3.2). This pulse records the highest volumetric rate of pyroclastic volcanism within the Cascades arc since at least 17 Ma (Pitcher et al., 2017a).

To understand the nature of this unusual transitional period of Cascades arc volcanism, we must document its full eruptive history. However, formation of the High Cascades graben at ~5.3 Ma (Fig.3.1), has constrained all subsequent volcanism from the central Oregon portion of the High Cascades (44.25-44.75°N) to the graben, burying the entire Deschutes record within 15 km of the arc axis (Smith et al., 1987). Although Deschutes-age lava flows are exposed as ridge caps across the Western Cascades, the poorly preserved ignimbrite record west of the graben may result from a lack of preservation in steep river valleys and significant uplift-induced erosion (Conrey et al., 2002; Smith, 1986). In addition, regions to the north and south of the Deschutes Basin lack a contemporaneous record, indicating that such volcanism was limited to central Oregon during this time (Conrey et al., 2002). Thus, the best record of this important transitional period of Cascades volcanic history lies to the east of the arc, within the Deschutes Formation.

Although the Deschutes Formation was mapped by numerous graduate students from Oregon State University during the 1980s, significant gaps in knowledge about the basin-wide tephrostratigraphy still exist. Several of these studies focused on mapping and constraining the stratigraphy of larger, laterally-extensive "marker" ignimbrite units across the Deschutes Formation (e.g. Pitcher et al., 2017a; Sherrod et al., 2004; Smith, 1986) (Fig. 3.2). Hundreds of other tuff outcrops have been mapped within individual sections by numerous previous researchers. However, there has not been an effort to systematically catalog and correlate these outcrops between individual map areas and across the entire Deschutes Basin. For example, Green Ridge, a 600-m high normal fault tilt block that defines the eastern edge of the High Cascades graben, preserves over 20 ignimbrite outcrops that represent the most proximal exposures to the eruptive source (Conrey, 1985). However, previous studies have traced only one ignimbrite unit from the ridge to the Deschutes Basin (Conrey,

1985; Smith, 1986). Without correlating ignimbrite and tephra-fall outcrops across the basin, we cannot establish the number of distinct eruptions that occurred nor their spatial distribution or volumes. Furthermore, although previous workers have

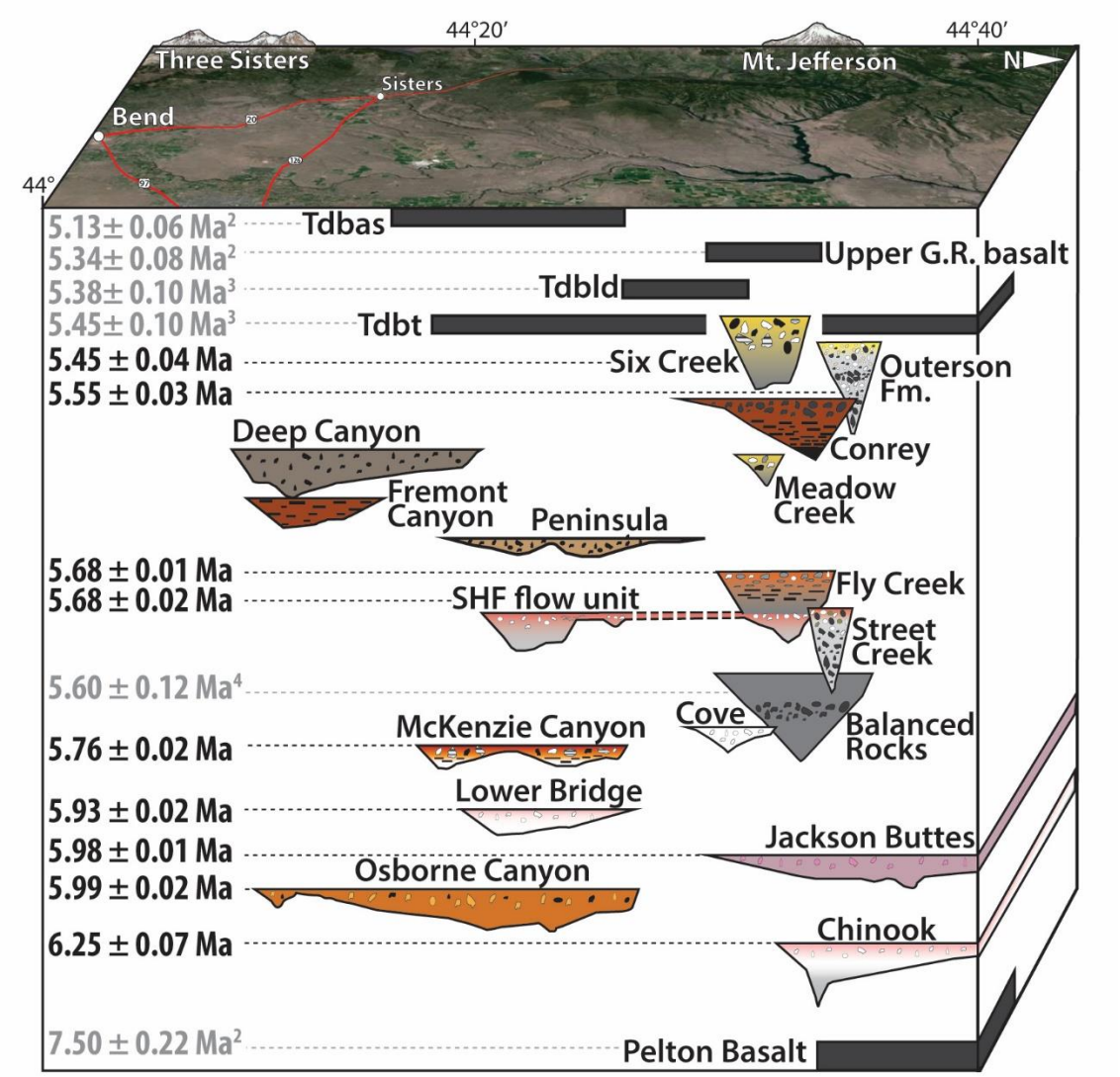

Figure 3.2: Schematic cross section (modified from Fig. 2.4) showing the stratigraphic relations, thickness profiles, north-south extent, and ages of the 14 marker ignimbrites from Pitcher et al., 2017, as well as the three additional marker units discussed in this study. Distance from arc is not depicted. Names of the ignimbrites are shown next to an actual thickness profile (140x vertical exaggeration) of the ignimbrite shape defined using ArcMap 10.2 (Pitcher et al., 2017) For reference, Balanced Rocks Tuff has a maximum thickness of 56 m. Vertical distance between units is not shown to scale. The left side lists plagioclase $^{40}Ar/^{39}Ar$ ages (±2σ uncertainty) of ignimbrites from Pitcher et al., 2017 (black), one ignimbrite from Aubin, 2000[4], and five Deschutes Formation lavas (grey) from Smith et al., 1987[2,3], which have all been recalibrated using the Kuiper et al., 2008 Fish Canyon Tuff age. The two Smith et al., 1987[3] ages are Bayesian ages. See text for methods of calculation.

established that the Deschutes Formation pyroclastic units originated from two separate source regions, a northern source near modern Mount Jefferson and a southern source near Three Sisters volcanoes (Conrey et al., 2002; Smith, 1986; Pitcher et al., 2017a), no comprehensive comparison of the chronology and frequency of volcanism between these two sources has been undertaken. Thus, a complete basin-wide chronology of the eruptive history during this time is lacking, and our understanding of the rates, volumes and temporal trends in volcanism during this time remains incomplete.

These major gaps in the current knowledge about the pyroclastic deposits of the Deschutes Formation lead us to ask three questions about the nature of this explosive pulse: (1) How frequent and how large were the eruptions? (2) Were the eruptions sporadic or were eruption rates broadly constant through time? And finally, (4) was the decline in deposition of pyroclastic material across the Deschutes basin the result of waning explosive volcanism or was it terminated as a result of normal faulting occluding the basin from its supply source?

To answer these questions, this study focuses on correlating ignimbrite and tephra-fall units, and establishes for the first time a comprehensive tephrochronology of the entire Deschutes Formation. To do this, we performed extensive fieldwork, *in situ* major and trace element analyses of tephra glass, and multivariate statistical analysis of geochemical correlations to establish a basin-wide stratigraphy. When combined with a new set of $^{40}Ar/^{39}Ar$ age determinations (Pitcher et al., 2017a), the resulting chronological sequence allows us to establish the number of distinct eruptions that occurred during Deschutes time and determine the size and frequency of individual eruptive events. This, in turn, allows us to compare the rate of explosive volcanism in the High Cascades arc during the late Miocene to that of the Quaternary and comment on the relationship of this eruptive frequency to regional tectonic forces. By establishing a detailed tephrostratigraphic record and elucidating a more comprehensive history of the initial stages of the High Cascades volcanic arc, our study fills a major gap in knowledge that is critically important to our understanding of the evolution of the Cascades arc.

3.1.1 Geological Setting: The Deschutes Formation

The layer-cake stratigraphy of lava flows, pyroclastic deposits and volcaniclastic sediments preserved in Deschutes Formation offers a unique window into the earliest High Cascades eruptive history. High eruptive rates allowed for a prolonged period of aggradation between ~7.5 and ~5 Ma, and these deposits were later armored by widespread late Miocene and Pleistocene lava flows that preserve the formation (Sherrod et al., 2004). Subsequent incision by the Deschutes River and its tributaries has provided excellent access to the stratigraphy that spans over 300 vertical meters in places. These outcrops are exposed over an area of >2000 km^2 within the greater Deschutes River Basin. Within the basin, there is limited faulting and units exhibit a relatively shallow-dipping paleoslope (<5°, Smith, 1986). In addition, Green Ridge contains 400 m of outcrop exposure and represents the westernmost and most proximal Deschutes Formation stratigraphy (Figs. 1 and 6C). Near Green Ridge, the formation has a relatively high abundance of lava flows, whereas ignimbrites and volcaniclastic sediment dominate the eastern 2/3 of the basin (Smith, 1986).

3.2 Methods

Tuff correlations were established using major and trace element data collected by *in situ* analyses of pumice glass by electron microprobe (EMP) and laser ablation inductively coupled plasma mass spectrometer (LA-ICP-MS). Geochemical similarity was assessed statistically using multivariate analysis of variance (MANOVA) and the Hotelling's T^2 test.

3.2.1 Field work and general description of tuff units

Field work was conducted within the Deschutes Bain over the course of three months, during which we collected over 400 samples and took over 300 measurements of ignimbrite and tephra-fall thickness. Thicknesses were measured either directly with a tape measure, using a Jacob staff and Brunton compass, or occasionally using triangulation methods. Care was taken to avoid hydrated pumice, and to collect samples of each pumice population within a unit, visually-identifiable

by color. Ignimbrites are exposed as both cliff-forming and slope-forming outcrops and are primarily nonwelded to incipiently welded. Less than 10 ignimbrites exhibit welding beyond incipient, but four units are densely welded in places.

Thickness ranges up to 82 m on Green Ridge and up to 60 m within the Deschutes Basin, with declining thicknesses eastward. Large changes in thickness between outcrops of a single tuff over a short distance, and general lack of continuous exposures indicate that many ignimbrites were highly channelized. Ignimbrites are crystal-poor, with most containing <5% crystals. The most common assemblage consists of two pyroxenes and plagioclase, and amphibole is very rare. Numerous ignimbrites have a basal pumice-fall layer preserved. Most units contain multiple pumice populations identifiable by color, often containing both white and grey to black pumice. Numerous tuffs contain banded pumice, and some contain accretionary lapilli. Abundance and size of volcanic lithics are highly variable both between units and within single flows. Most tephra-fall outcrops are less than 0.5 m thick, but some range up to 3.5 m. Most are medium to coarse-grained pumice lapillistone deposits, but some fine-grained ash and accretionary lapilli layers exist. Many tephra-fall units are zoned, either marked by changes in pumice population proportions or by changes in pumice size or lithic abundance. A table with field descriptions of each unit is given in Appendix 3.6.

3.2.2 Sample selection and geochemical data collection

In order to establish correlations among Deschutes Formation tuff units, 89 non-marker ignimbrites and 59 pumice fall samples were chosen for geochemical analysis out of the 144 non-marker ignimbrite and 111 pumice fall samples taken in the field. In addition, 42 samples of the 14 marker ignimbrites discussed in Pitcher et al (2017a) were analyzed in order to fully characterize all pumice populations within these units. Ignimbrites and tephra fall units were selected for analysis if they were thicker than 1 meter and 20 cm, respectively. In addition, six thinner tephra fall samples were analyzed because they appeared especially important stratigraphically or were hypothesized to be correlated to another sample. Tuffs were also selected only if their stratigraphic position relative to at least one marker ignimbrite could be

established. We did, however, include six ignimbrites and two tephra fall samples that we hypothesized were correlated to other units, despite having no stratigraphic context. All non-hydrated tuff units on Green Ridge were selected for geochemical and statistical analysis, despite having limited chronologic context due to the exposure of only one marker unit (Six Creek Tuff) on the ridge. These outcrops were chosen because correlating samples from the Deschutes Basin to those on Green Ridge, the most proximal location to the High Cascades axis, was a major objective of this study.

For tuff units with multiple pumice populations identifiable by eye, the white pumice population was chosen for analysis and correlation work. This was done to maximize the possibility of correlation without having to analyze all pumice populations within a given unit. At least five different pumice from each tuff sample were selected for analysis in order to increase the likelihood of adequately characterizing compositional heterogeneity.

Pumice was separated from ignimbrite matrix using a hammer and chisel, and outer rims were removed using clean shears to avoid analysis of hydrated glass. These were then crushed using mortar and pestle, sieved, and the 106-212 μm size fraction was washed w/ DI water to remove dust. Epoxy mounts of six samples each were made and polished using the methods outlined in Lowe (2011).

Electron Microprobe (EMP) analysis of pumice glass was completed at Oregon State University with a Cameca SX-100. The best practices for EMP analysis of tephra glass, as outlined in Kuehn et al. (2011) were used, including the use of a 10μm rastered beam. At least seven EMP analyses per sample were made initially and samples with significant compositional heterogeneity were analyzed again for a total of up to 15 spots. Where possible, bubble wall glass areas at least 30 μm wide were chosen to allow for future LA-ICP-MS analysis of the same spot. However, micro-vesicularity was common and made it difficult to find large glass areas in many samples. Care was taken to avoid microphenocrysts, visible in backscatter electron (BSE) images or detectable by blue fluorescence under the EMP beam. In some microlite-rich samples, however, these were impossible to avoid. Analyses with

anomalously high FeO and TiO_2 or high CaO and Al_2O_3, those with values further than 1.5 times the interquartile range (IQR) from the median, were assumed to be the result of analysis of oxides or plagioclase, respectively, and were removed from the dataset. In addition, analyses with totals less than 90% were also removed, as lower totals likely indicate either a high degree of hydration or the analysis of a large proportion of epoxy (WoldeGabriel et al., 2005).

Plagioclase phenocrysts separated from ignimbrite pumice were also analyzed with EMP. For this study, 10 plagioclase crystals from both the Steelhead Falls Tuff (DB-083) and Fly Creek Tuff (DB-156) were analyzed *in situ*. For each crystal, we collected major element data from the core and rim, as well as 1-5 intermediate points, depending on zoning complexity seen in back -scatter electron (BSE) images. In total, we analyzed 49 spots on plagioclase from Steelhead Falls and 45 from Fly Creek Tuff. Two rim analyses were discarded due to having analytical totals lower than 90%.

In situ trace element data for tephra glass were collected using the LA-ICP-MS method. A Photon Machines ArF Excimer laser and a Thermo-Fischer X2 quadrupole ICP-MS at Oregon State University were used. SiO_2, as determined by EMP, was used for the internal calibration, and GSE-1G was used as the calibration standard. We also analyzed BCR-2G, T1-G and ATHO-G as secondary standards to check accuracy. The exact spots that were analyzed by EMP were ablated with a 50 µm spot at 5 Hz and 225 shots. During data processing, at least eight seconds of analysis time were always included while integrating. Analyses were discarded if they had anomalous trace element signatures that indicated the analysis of subsurface crystals (e.g. Ba and Sr spike due to plagioclase) within the first eight seconds. Standard errors were calculated by propagating the uncertainty associated with repeated analysis of the calibration standard, uncertainty in the SiO_2 value (assumed to be ±1%), and the standard error of the normalized counts over the time interval selected.

3.2.3 Statistical correlation methodology

The multivariate analysis of variance (MANOVA) and Hotelling's T^2 test statistical techniques that we used to assess geochemical similarity are relatively robust methods compared to more simple correlation techniques such as Similarity Coefficient and visual analysis, but are strongly affected by outliers (Tryon et al., 2011). Thus, great care was taken to remove outliers, while trying not to remove extreme, but valid points, using Chauvenet's criterion for rejection (Taylor, 1982). Analyses were removed if they had major or trace element values that were more than τ standard deviations away from the mean, where τ is the critical Z-score for which the probability $P(\tau)=1-0.25/N$ and N is the number of analyses. Two iterations were used in order to account for outliers' effect on the mean and standard deviation.

Data were first log-ratio transformed using the additive log-ratio (ALR) transformation technique and Al_2O_3 as the divisor. Compositional data must be log-ratio transformed before multivariate analysis due to the autocorrelation between elements resulting from summing to 100% (Aitchison, 1986). Pairwise Hotelling's T^2 test was performed to assess geochemical similarities and potential correlations between all samples. Hotelling's T^2 test is the multivariate equivalent of Student's t test and is an extension of a pairwise MANOVA. Unlike other statistical methods of correlation often used in the literature, such as statistical distance (Perkins, 1995) and similarity coefficient (e.g. Kuehn and Foit Jr., 2006), which simply compare the means of two samples, Hotelling's T^2 test compares the means, variance and multivariate covariance (i.e. multivariate trends) of each sample (Tryon et al., 2011). This is especially useful for multimodal tuffs or units with significant compositional heterogeneity where a mean value doesn't accurately capture the true compositions or the compositional variability of the sample (Fig. 3.3). For each pair of samples, the MANOVA procedure creates a new set of dependent variables that are a linear combination of the original log-transformed variables, such that differences between samples are maximized (Weinfurt, 1995). Then, on this new set of variables, Hotelling's T^2 test is used to evaluate whether the mean vectors different enough to reject the null hypothesis that the two samples came from the same population.

For small sample sizes (N<30), the test statistic follows an F distribution, which allows us to calculate a p value (Weinfurt, 1995). The p value between two samples, A and B, represents the probability of finding another pair of samples from the same eruption with larger differences than A and B. Thus, if A and B have a p<0.05, they are considered statistically distinct, since there is a <0.5% probability of finding another pair of samples that have a greater difference than A and B. Statistically, higher p values simply mean that we do not have enough evidence to reject the null hypothesis (that the two samples came from the same population), and although higher p values indicate more multivariate similarity, it cannot state definitively that two samples are correlated.

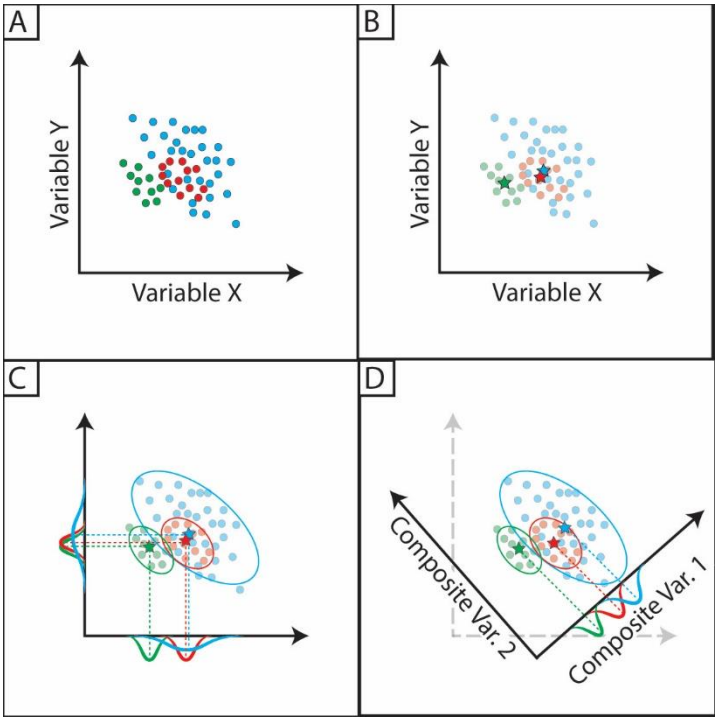

Figure 3.3: Rationale for using the MANOVA technique for tephra correlation. A bivariate diagram with synthetic data for three different samples (blue, red, green) is shown in (A). Note that, a simple method of assigning correlations based on overlap in bivariate diagrams would not be useful in this case, as all three overlap. (B) shows the mean (X,Y) values for each sample (stars). Note that although the blue and red samples have different distributions, their means are very close to one another, and may be considered correlated if the Statistical Distance method were to be used. In (C) the normal distributions for each variable are shown. Simply performing separate single-variable ANOVAs for each element would indicate that red and green samples are identical for variable Y but not for variable X. (D) illustrates the MANOVA, where a new set of "composite variables" are created as combinations of the other variables, such that there is the largest between-group differences and the smallest within-group variance. This allows multivariate differences between the means and variances of samples to be discerned in a way that would be impossible using the other methods of correlation.

Because the T^2 value relies on the calculation of the inverse covariance matrix, this matrix must be non-singular, requiring there to be more observations per sample than variables. Since we had 225 pairs of ignimbrites and 35 pairs of

pumice fall units with only seven total analyses, we had to use six or less variables during our analyses. In order to still incorporate many elements, we completed three Hotelling's T^2 tests for each pair of samples, each utilizing six or fewer variables. The three tests were based on: major elements (SiO_2, FeO, TiO_2, K_2O, MgO, MnO), the four "best trace elements" with the smallest uncertainty for the GSE-1G standard (Nb, Ba, Ce, Nd) and the five "moderate trace elements" with slightly higher uncertainty.

To complete the statistical analysis, we wrote a script in MATLAB that calculated the p values for each possible pair of samples and accepted as possible correlatives only pairs with p>0.05 for both the major elements and the best trace elements (Fig. 3.4). This criterion for possible correlation was based on the results of our test on known tuff units, detailed in the section below. The MATLAB script then disregarded any potential correlations between tuffs that have known age ranges that do not overlap. Age ranges were assigned to each tuff based on positions relative to dated marker ignimbrites and lava flows (Fig. 3.2). The six ignimbrites and two tephra fall units for which we could not establish stratigraphic context were given age ranges of 4-7.5 Ma, the entire age range for the Deschutes Fm. We also calculated the statistical distance and associated Chi-squared p value (Perkins et al., 1995, 1998)

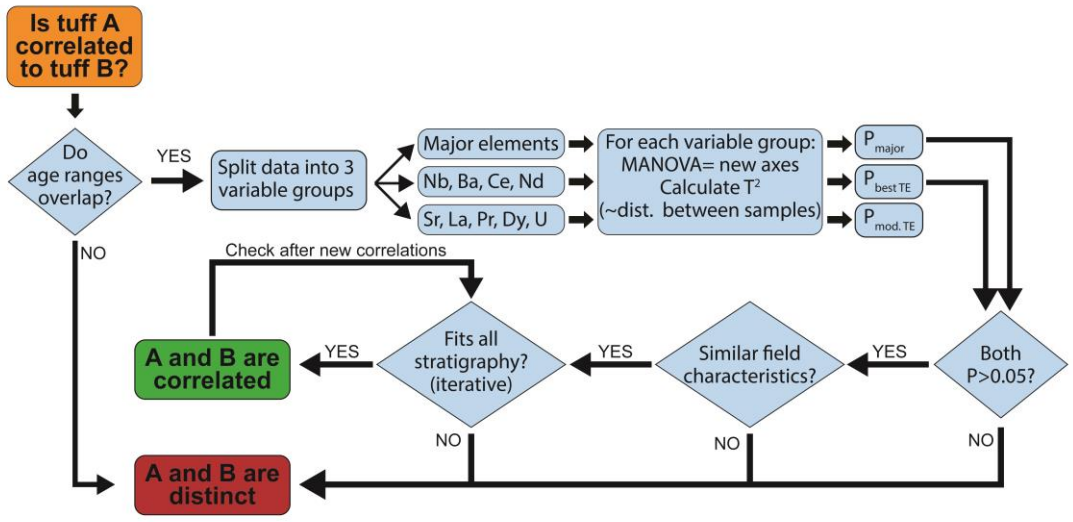

Figure 3.4: Flow chart of the MATLAB procedure that we created to assess geochemical correlations between tuff units. After all possible pairs were checked, each correlative pair was checked to see if correlation was still possible based on new stratigraphy. Thus, this was an iterative approach.

between the means of each tuff pair in order to compare results to our multivariate methodology.

We then manually checked each possible correlation to ensure that they were consistent with stratigraphy, field descriptions and geography. In addition to the dated marker ignimbrite and lava flow units that were used to constrain age ranges for each of the unknown tuff units, there are numerous other smaller tuff units that are laterally extensive enough to further constrain stratigraphic relations between the unknown tuffs. Furthermore, as correlations were made, relative stratigraphic positions were revised and all potential correlations were checked again in an iterative approach. Tuffs that had moderate p values between 0.05 and 0.20, but had field characteristics, such as crystallinity, pumice populations, and matrix lithic (sand) abundances that differed significantly, were considered non-correlated. Other characteristics, such as thickness, color, welding, and cobble lithic abundance are known to vary significantly with distance from the source (Branney and Kokelaar, 2002) and were not used to discriminate between potentially correlative tuffs. Conflicts in which a single sample was found to be similar in geochemistry and stratigraphic position to multiple others, were resolved by choosing the pair with the highest p value.

3.2.3.1 Testing the accuracy of the correlation method on known samples

To test the accuracy of our Hotelling's T^2 methodology for tuff correlations, we assessed the proportions of samples from known marker ignimbrites that were successfully correlated to other samples from that same unit. We analyzed 32 felsic samples (all analyses >65 wt. % SiO_2) from 16 known ignimbrites. We constrained this test to include only felsic samples because mafic pumice analyses would be unlikely to be successfully correlated to felsic pumice from the same ignimbrite, and would thus give an unrealistically low success rate. There were a total of 29 correlated pairs of (10 Balanced Rocks, 1 Chinook, 1 Deep Canyon, 6 Fly Creek, 3 Lower Bridge, 2 McKenzie Canyon, 3 Meadow Creek, 1 Tdt-20 and 2 Six Creek Tuff pairs) and 426 pairs that we know are not correlated. In addition to the proportion of correct correlations, we also wanted to assess the proportion of type I errors, situations where statistical tests indicated that two correlative samples were distinct,

and type II errors, situations in which the tests indicated possible correlation between two tuffs that are known to be different.

In addition, as discussed above, we performed Hotelling's T^2 tests using three different subsets of variables (major elements, "best" trace elements, and "moderate" trace elements) to test which combination of these three tests was most effective. That is, we wanted to determine which criterion to use for acceptance of correlation. Should we accept pairs as being correlated only if they have high p values for all three subsets of elements, or just for two of the three subsets? We tested the efficacy of six different criteria for correlation, using two critical p values (0.05 and 0.10) for each of three different combinations of Hotelling's T^2 results: (1) "conservative": all three subsets of elements, (2) "moderate": at least the major elements and best trace elements, and (3) "liberal": any two of the three elemental subsets. In addition, we assessed the accuracy of using the statistical distance method of Perkins (1995, 1998), utilizing both p values (0.05 and 0.10).

3.2.4 Calculating eruption frequency with time

Statistical analysis and geochemical correlation allowed us to establish the number of distinct tuff units and therefore the minimum number of discrete eruptions that are preserved within the Deschutes Formation. Combining this tephrostratigraphy with $^{40}Ar/^{39}Ar$ dates of marker ignimbrites, also allowed us to elucidate changes in the frequency of explosive eruptions through time. To do this, tuffs were given uniform probabilities of occurrence between the ages of those dated units contained within their stratigraphic section (Fig. 3.5). These probabilities were then discretized into 10 k.y. time intervals for ease of calculations and interpretation. For example, in Figure 3.5, tuff B (orange) is found between Jackson Buttes Tuff (5.98± 0.01 Ma) and Fly Creek Tuff (5.68± 0.01 Ma) and is therefore assigned a uniform probability (1/30) of having occurred within each of the 10 k.y. time intervals (n=30) between 5.98 and 5.68 Ma. However, since tuff D was found in a location where Fly Creek Tuff was absent, and only the lava flow Tdbt (5.45± 0.10 Ma) overlies it, it was given a uniform probability of having occurred between 5.98 and 5.45 Ma. Thus, because this tuff is less constrained and could have been erupted over a longer period than tuff B,

the probability of occurrence within any given 10 k.y. time interval (1/47) is lower than that of tuff B (1/30) (Fig. 3.5). To avoid subjective weighting, uniform probabilities were assigned even if a tuff was observed to be much closer to one marker unit than another. Thus, tuff D was given a uniform probability even though it is found much closer to Jackson Buttes tuff than basalt flow Tdbt. Although we can be certain that the tuff was emplaced between 5.98 and 5.45 Ma, we cannot be certain that the distance from either of the marker tuffs is an exact proxy for the time between their emplacement. The existence of thick packages of lahars and hyperconcentrated flows (Smith, 1986) indicates that local sedimentation rates were not constant, and channel incision and subsequent fill by ignimbrites could lead to erroneous conclusions about distance-time relationships. Tuffs for which we could not establish stratigraphic position were given uniform probability distributions over the entire time interval between the oldest and youngest dated units in their region (i.e. 6.25-5.34 Ma in the north, and 5.99-5.13 Ma in the south).

The normal probability distributions for each dated tuff, defined by the mean ^{40}Ar-^{39}Ar age and 2σ, were also discretized into 10 k.y. time bins. All discretized probabilities were then added together to give an estimate of the approximate number of explosive eruptions preserved in the Deschutes Formation per 10 k.y (Fig. 3.5). However, these are minimum estimates, as they are based on only the 148 samples that we analyzed, and may not include eruptions represented by the 107 additional unanalyzed samples. To estimate the number of additional distinct eruptions represented by these samples, we first removed all that were hypothesized, based on field evidence, to be correlative with analyzed samples. We then assigned the remaining unanalyzed tuffs to time bins, discretized, and summed their probabilities within each 10 k.y. time interval using the same methodology described above. However, since we cannot ensure that all unanalyzed samples are uncorrelated and therefore represent separate eruptions, we multiplied by 48%, the proportion of analyzed tuff samples that were found to be geochemically distinct. By adding this to the number of eruptions per 10 k.y. that we calculated for analyzed samples, we can give our best estimate for the total Deschutes Fm. eruption frequency through time.

We also calculated a maximum eruptive frequency, in which all unanalyzed samples were distinct, and a minimum, in which all unanalyzed samples were correlated to

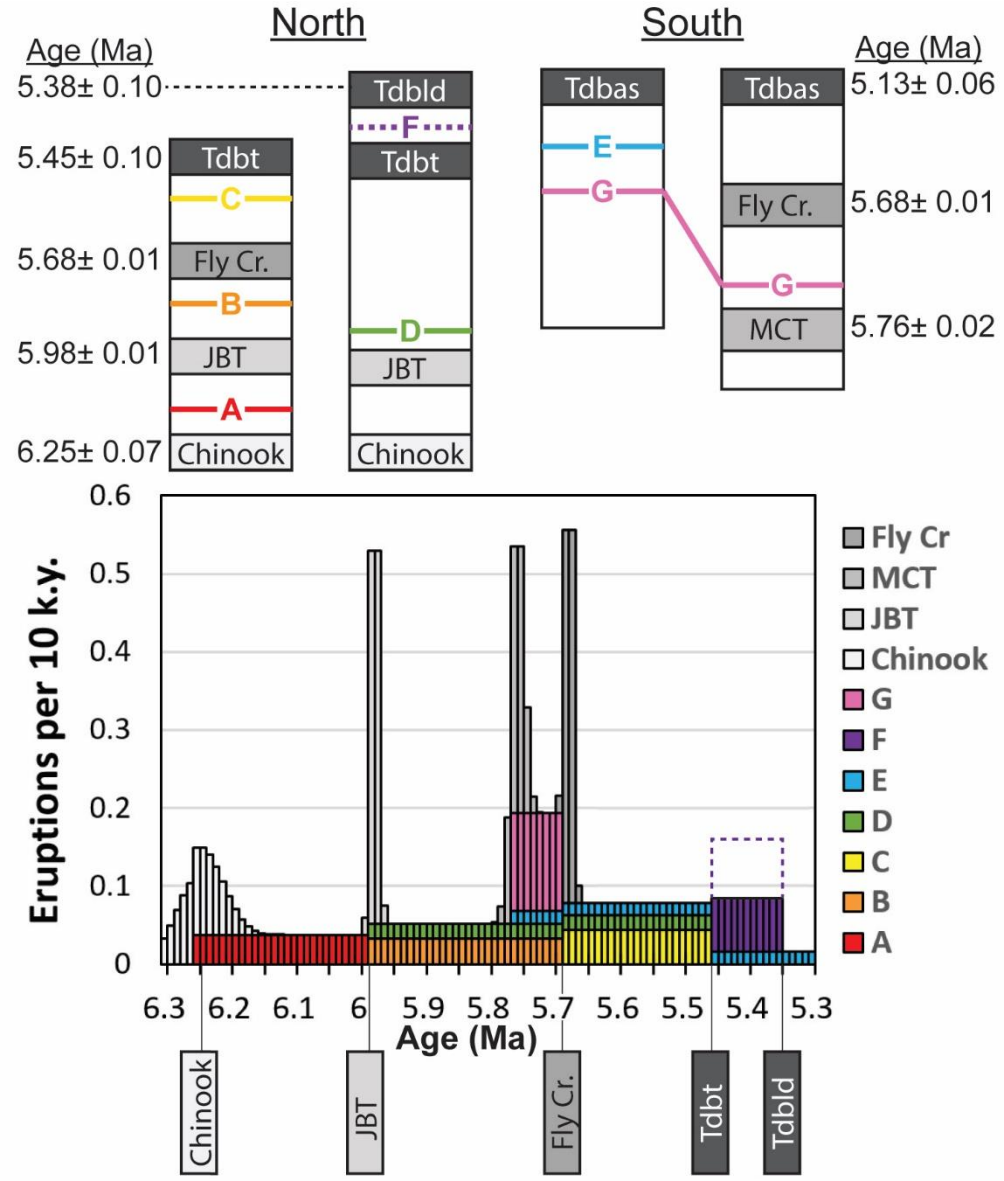

Figure 3.5: Our methodology for calculating eruption frequency with time. The positions of seven synthetic tuff units (A-G) relative to dated tuffs and lava flows are shown on the four stratigraphic sections. Each undated tuff is given a uniform probability of occurrence between the underlying and overlying dated unit. This probability is discretized into 10 k.y. intervals as seen in the figure below. See text for discussion. Also note that unit G is correlated between two sections, and since it must be younger than MCT, provides an lower age constraint for unit E. A discretized normal probability distribution is given to each dated tuff, as defined by its mean and standard deviation $^{40}Ar/^{39}Ar$ age. The probabilities for all tuffs are summed up for each 10 k.y. interval to give the approximate number of eruptions per 10 k.y. through time. Each unanalyzed tuff (e.g. tuff F) was given a best guess probability distribution (purple bars) that is 48% of the original probability for each interval (dashed purple box).

one that we had analyzed.

To provide chronologic constraints on the uppermost Deschutes Formation stratigraphy, we utilized three basalt units, the uppermost lava on Green Ridge (5.27± 0.08 Ma), Tetherow Butte Basalt (5.31± 0.10 Ma), and Lower Desert Basalt (5.43± 0.10 Ma) from Smith et al. (1987). After recalibrating these $^{40}Ar/^{39}Ar$ ages using the Kuiper et al (2008) age for the Fish Canyon Tuff sanidine flux monitor, these ages are 5.34± 0.08, 5.38± 0.10, and 5.50± 0.10 Ma, respectively. However, Smith (1986) states that in two locations, the Lower Desert Basalt (Tdbld) overlies the Tetherow Butte Basalt (Tdbt), thus conflicting with the mean $^{40}Ar/^{39}Ar$ ages for the units. In addition, the Six Creek Tuff (5.45± 0.04 Ma) is observed beneath the Lower Desert Basalt, again indicating that the mean $^{40}Ar/^{39}Ar$ ages are inconsistent with stratigraphy. To resolve this, we used a Bayesian estimation method, in which we randomly selected an age for all three units from the normal distribution defined by their mean $^{40}Ar/^{39}Ar$ age and standard deviation, and repeated this 100,000 times. We then accepted only those ages that satisfy our *apriori* constraints, that both Six Creek Tuff and Tetherow Butte Basalt must be older than Lower Desert Basalt, to create a posterior distribution of ages for each unit that are consistent with stratigraphy. After doing so, the new Bayesian ages for Tetherow Butte Basalt and Lower Desert Basalt are 5.45± 0.10 and 5.38± 0.10 Ma, respectively, and Six Creek remains 5.45± 0.04 Ma. We use these Bayesian age estimates for all calculations in this study.

3.2.5 Calculating volumes of eruptions

To calculate the volumes of ignimbrite eruptions, we utilized the ArcGIS method described in Pitcher et al. (2017a), where we calculate the volumes of 14 regionally extensive marker ignimbrites. We calculate the volumes of 10 additional ignimbrites that have a minimum of three thickness measurements separated by at least 1 km. To estimate dense rock equivalent (DRE) volumes, we used the method outlined in Pitcher et al. (2017a).

3.3 Results

3.3.1 Results of our test of the accuracy of correlation methodology

Our test of the accuracy of the Hotelling's T^2 method indicates that it is an effective technique for correlation based on its ability to correctly identify samples that are known to be correlative and its low rate of Type I (false positive of correlation) and Type II (false negative) errors. We found that out of the six different criteria for correlation that we tested, the "moderate" criterion that accepts correlations only if $p>0.05$ for both major elements and the "best" trace elements (Nb, Ba, Ce, Nd), was most effective in this regard (Table 3.1).

There are 496 different possible pairings among the 32 known felsic ignimbrite samples in our case study, of which there were 33 pairs, which are known *a priori* to be correlated. During our test, we disregarded stratigraphy to observe the efficacy of the method performed without the assistance of stratigraphic constraints. Although the "liberal" Hotelling's T^2 criterion (accepting correlation if $p>0.05$ for any two of the three subsets of variables) correctly identified the highest proportion of all correlative samples (33%), it also had the highest Type II error rate (Table 3.1). That

Table 3.1: Hotelling's T^2 and Statistical Distance results for our case study of 32 known felsic ignimbrite samples, using different confidence levels (a) and acceptance criterion. There were 33 correlative pairs and 463 pairs of distinct samples. Type I error rate gives the proportion of sample pairs that the test suggested were distinct, but were actually correlated=N(Type I error)/N(Type I error+ correctly distinct)*100. Type II error rate gives the % of occurrences where the test suggested two samples were correlated, but actually weren't= N(Type II error)/N(Type II error+ correctly correlated)*100.

	Correctly correlated (N)		Type I error (says distinct, actually corr.)		Type II error (says corr., but not)	
Criterion:	a=0.10	a=0.05	a=0.10	a=0.05	a=0.10	a=0.05
Conservative (p>a, all 3 tests)	5	7	28	26	0	0
Moderate (p>a, majors and bestTE)	7	8	26	25	0	0
Liberal (p>a, any 2 tests)	11	13	22	20	5	12
StatD (p>a, majors+bestTE)	21	21	12	12	126	151

	Sucessfully correlated (% of 33)		Type I error rate (%)		Type II error rate (%)	
Criterion:	a=0.10	a=0.05	a=0.10	a=0.05	a=0.10	a=0.05
Conservative (p>a, all 3 tests)	15	21	5.7	5.3	0	0
Moderate (p>a, majors and bestTE)	21	24	5.3	5.1	0	0
Liberal (p>a, any 2 tests)	33	39	4.6	4.2	31	48
StatD (p>a, majors+bestTE)	64	64	3.4	3.7	86	88

is, 52% of pairs that the criterion suggested were correlated, were actually from different ignimbrites. This is relatively useless. While it is important for a statistical correlation technique to correctly identify correlative samples, we must also maximize confidence that the correlations designated are actually sourced from the same eruption (VanVooris and Morgan, 2007). The "moderate" criterion was most useful in this regard. Although this criterion successfully correlated a slightly lower proportion of samples (24%) than the "liberal" criterion, all suggested correlations were real (i.e. zero Type II errors), and it is therefore most preferable. For all six criteria, ~4-5% of sample pairs designated as distinct were known to be correlated (Type I error proportion).

However, for the unknown samples, we chose to analyze only the lightest colored (white or light grey) pumice population from each sample in order to maximize the potential for correlation. If we instead use the 20 white or light grey pumice populations from the known ignimbrites, the test is more indicative of how the techniques will perform with the unknown (light pumice) samples. With this test, our acceptance criterion ($p>0.05$ for both major and best trace elements) correctly identified six of the seven (86%) pairs of light-colored pumice. Thus, we can be more confident that our statistical method will correctly identify a relatively high proportion of correlated samples.

The Statistical Distance method of Perkins et al (1995, 1998) correctly identified 63% of correlative pairs, but had type II error rates of 86 and 88% ($p=0.10$ and 0.05, respectively). Thus, for our samples, that often have similar mean geochemical values but different variance or trends of data, the Hotelling's T^2 technique is much more useful than the Statistical Distance.

Although our tests on known samples provide a measure of the relative accuracy between our correlation methods, the proportion of accurate results may vary with unknown samples depending on a variety of factors. A few examples include compositional heterogeneity or bimodality within samples or overall similarities between samples from different eruptive episodes of a single source.

3.3.2 Pairwise Hotelling's T^2 results for unknown samples

We first conducted separate pairwise Hotelling's T^2 tests for the 131 ignimbrite samples (89 unknown and 42 known) and for the 59 pumice fall samples, and then completed a third test comparing ignimbrites to pumice fall samples. In all cases, we applied the additional criteria that a similar stratigraphic position relative to dated marker units was a necessity for correlation. These constraints helped to filter results, reducing the number of possible correlations of ignimbrites down from 611 to 216. After checking each potential correlative pair to ensure that they had comparable field characteristics (e.g. crystallinity, pumice populations and small lithic content), and iteratively checking for similar stratigraphic positions relative to all other tuffs, we accepted 149 correlations. We found 67 statistically similar pairs that were not correlative (Type II errors) based on disparate field characteristics or stratigraphic conflicts. We accepted 26 tephra-fall correlations out of the 57 pairs that were statistically similar. We correlated only 19 tephra-fall samples to ignimbrites.

In total, our geochemical correlation work, together with stratigraphic and field constraints, indicates a minimum of 67 different explosive eruptions large enough to deposit pyroclastic material in the Deschutes Basin between 6.25 and 5.45 Ma. However, this does not include eruptions represented by the 107 additional unanalyzed samples. Assuming that, like the 139 analyzed samples, 48% of the unanalyzed samples are from distinct eruptions, we suggest a more reasonable estimate of 118 different explosive eruptions. We also estimate that at least three Deschutes Formation explosive eruptions occurred before 6.25 Ma and at least 8 occurred after 5.45 Ma.

3.3.3 New ignimbrite volumes

Establishing geochemical correlations between outcrops allows us to distinguish an additional 13 ignimbrites that are laterally extensive enough for us to calculate volumes (Table 3.2). Although most are smaller in volume than the 13 marker ignimbrites of Pitcher et al. (2017a), together they contribute approximately 20 km^3 to the total volume of ignimbrites that were deposited eastward into the

Deschutes Basin. Eight of these non-marker ignimbrites have outcrop distributions that form a relatively narrow band, less than 1 km wide, indicative of limited deposition within relatively narrow paleovalleys and have estimated minimum volumes of 0.2-1.0 km^3 within the Deschutes Basin. However, five units, the Outerson Formation Tuff, Spring Creek Tuff, Street Creek Tuff, Tdt22, and BKT-316 each have volumes greater than 2 km^3 (6.0, 2.9, 2.0, 2.2, and 2.7 km^3, respectively). All of these newly correlated ignimbrites are nonwelded in all locations, except for the Spring Creek Tuff, and dense rock equivalent (DRE) volumes range from 0.1 to 3.7 km^3. In total, the volume of 26 ignimbrites deposited into the Deschutes basin between 6.25 and 5.45 Ma is 82 km^3 (62 km^3 DRE) (Fig. 3.6).

Table 3.2: Correlative samples, volume, and distance traveled for 26 Deschutes Formation ignimbrites. * indicates samples with volumes that were presented in Pitcher et al. (2017).

Age (Ma)	Ignimbrite	Correlative samples	Bulk volume (km^3)	DRE volume (km^3)	Min. dist. Traveled (km)	Max. Thickness (m)	Source region
5.45±0.04	Six Creek*	DB.005, 006, 008, 119, 159, 177, 121, *216*	4.3	2.6	19	60	North
	Deep Canyon*	DB.093, 100	5.0	3.2	17	33	South
	Tdt28	DB.242, 319, 118, 166	0.6	0.4	21	13	North
	Fremont Canyon*	DB.095,	2.4	2.3	14	19	South
5.55±0.03	Outerson Fm.	DB.251, 219, 275, 311, 312, 317	6.0	3.7	6	62	North
	Spring Creek (Tdt26)	DB.149, 145, 147, 170, 273, 271, 344, 236, 192, 161	2.9	2.5	27	39	North
	Meadow Creek*	DB.163, 254, *270, 143, 280 344*	3.2	2.0	22	44	North
	Peninsula*	DB.070, 88, 81,	1.9	1.7	25	12	South
	BKT-316	DB.297,301,329	2.7	1.6	27	16	South
	Tdt22	DB.237	2.2	1.3	13	48	North
	Tdt21		0.9	0.5	10	49	North

Age (Ma)	Ignimbrite	Correlative samples	Bulk volume (km^3)	DRE volume (km^3)	Min. dist. Traveled (km)	Max. Thickness (m)	Source region
	Tdt19 +(Tdt20/Tdt 25)	DB.001, 002, 004, 256, 122, 245	0.4	0.3	24	24	North
5.68± 0.01	Fly Cr.*	DB.019, 135, 156, 224, 066, 331, 343, 117, 083, 334; PF-072, 059, 087, 300, 173, 332	7.9	5.8	33	50	North
	Tdt18	DB.143, 270	0.2	0.1	14	15	North
	Street Creek (Tdt17)	DB.142, 150, 222, 313, 314, 168, 345, 342, 221	2.0	1.2	14	61	North
	Balancing Rocks*	DB.009, 010, 011, 013 0,20, PF-173	8.8	5.4	19	59	North
	Cove*	DB.052,337, *279*	1.0	0.6	27	18	North
5.76± 0.02	McKenzie Canyon*	DB.043; MCTA.206, 209, 88; MCTB.209, 88; MCTL.88, 206, 208	3.2	2.7	26	23	South
5.93± 0.02	Lower Bridge*	LBTP.146, 156, 159, 185.1,LBTT.146, 159, 183, 185; DB.PF.069, 084	3.6	2.2	25	18	South
5.98± 0.01	Jackson Buttes*	DB.198, 048, 127, 290, 292, 322, PF-44, 60, 228	6.3	4.2	42	23	North
5.99± 0.02	Osborne Canyon*	DB.061	9.4	5.7	31	28	South
	Tdt9	DB.179	0.5	0.3	12	18	North
	Tdt8	DB.141, 182	0.8	0.5	12	18	North
	Tdt7	DB.180, 264	0.8	0.5	15	31	North
	Tdt4	DB.185	0.2	0.1	20	12	North
6.25±0. 07	Chinook*	DB.126, 187, 184, 125, 124, 207	4.7	2.9	44	39	North

3.3.4 Eruptive frequency

By establishing a comprehensive tephrostratigraphy of the Deschutes Formation, we have calculated the rate of distinct explosive eruptions per 10 k.y. that

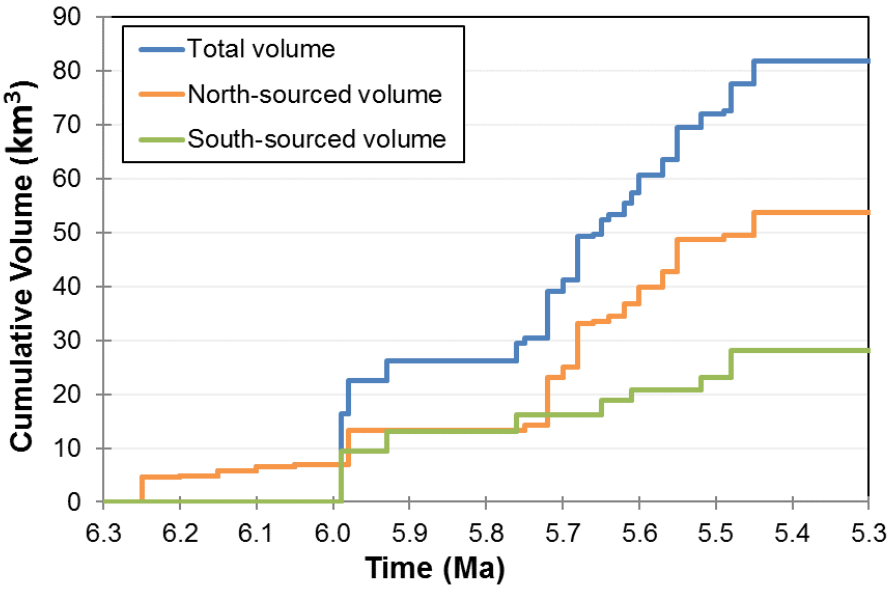

Figure 3.6: Cumulative volume through time for 26 Deschutes Formation ignimbrites. See Table 4 for individual volumes. Ages of non-dated units were linearly interpolated between constraining dated tuffs.

deposited pyroclastic debris within the Deschutes Basin during Deschutes time (Fig. 3.10). In the south, the eruptive history is not as well constrained, as no strata older than 5.99± 0.07 Ma are exposed, there are far fewer canyons to provide exposure, and age constraints on the top of sections in the southwest portion of the field area are lacking. However, we are confident in our calculated rates for the south between 6 and 5.45 Ma. While the eruptive frequency in the north and south are roughly similar between 6 and 5.75 Ma, eruptions become much more frequent in the north after this time (Fig. 3.10). Our best estimate for the highest eruptive rate in the north, which takes place between 5.67 and 5.68 Ma, is approximately 2.3 eruptions per 10 k.y., although this number could be as high as 3.2. In the south, however, the rate rarely exceeds 1 eruption per 10 k.y (Fig. 3.10).

In the south, only ~35% of eruptions deposited ignimbrites into the Deschutes Basin, whereas ignimbrites are recorded in over 80% of northern eruptions. This may indicate that the source was more proximal in the north. This is consistent with the fact that in the north, Deschutes Formation tuffs are exposed only 15 km east of the modern axis, whereas in the south, the most proximal tuff outcrop lies over 30 km northeast of the axis. Even if the Tumalo Volcanic Center (previously, Bend Silicic

Highland of Smith, 1986) was the source area for the southern tuffs, as proposed by Smith (1986) and Sherrod et al. (2004), the most proximal outcrop is still over 20 km to the northwest.

3.4 Discussion

3.4.1 Sources of uncertainty in statistical correlations and eruptive frequency

Several factors may have contributed some uncertainty to our statistical correlations. Because many Deschutes tuffs are compositionally heterogeneous or even polymodal, we hold that the MANOVA technique, which accounts for within-sample variability, is preferable over other means-comparison methods of correlation, as discussed in the methods section. However, the MANOVA technique is less effective with smaller datasets because the technique relies on adequate characterization of the variance (Weinfurt, 1995). After removing outliers, including analyses of microphenocrysts or those with low analytical totals, more than half of the Deschutes samples had less than seven analyses. Vanvooris and Morgan (2007) recommend that ideally sample sizes should be $n>30$ to fully utilize the power of MANOVA, but suggest a minimum of $n=7$. Thus, in compositionally heterogeneous samples with few analyses, the variance of the small subset may not be representative of the true population variance, leading to a degree of uncertainty (VanVooris and Morgan, 2007). These highly heterogenous samples tended to have high p values with many different samples, including samples that could not be correlative due to conflicting stratigraphy. For these samples, we were very cautious with these tentative correlations, and accepted only those pairs that had the highest p values and nearly identical field characteristics (e.g. crystallinity, pumice populations and small lithic content). Furthermore, as mentioned previously, small sample sizes required us to perform three separate MANOVA analyses for different subsets of elements, which may have introduced some uncertainty, particularly in Type I error rate, and reduce the overall effectiveness of the multivariate method (Weinfurt, 1995).

Our estimates of eruptive rates are also subject to multiple sources of uncertainty. Age constraints are poor for the upper part of southern stratigraphy, and

the lack of exposure compared to that of the north, particularly before 6 Ma, makes it difficult to confidently compare the rates of the two regions. In addition, these rates are affected by our estimates of the proportion (48%) of unanalyzed samples that are from distinct eruptions (see methods). For example, if every unanalyzed sample were correlated to one that we have already analyzed, the maximum eruptive rate (5.67-5.68 Ma) for the whole basin would decrease from 3.3 to 2.1 eruptions/ 10 k.y. If, instead, every unanalyzed sample were from a separate eruption, an equally unlikely scenario, this maximum eruptive rate would become 4.5 for the same 10 k.y. interval. However, we hold that our estimate is reasonable, and is more likely an overestimate, since prior to multiplying by 48%, we removed any unanalyzed sample that we had hypothesized (based on field evidence) to be potential correlatives. We did not do the same for the samples that we did analyze, and in fact, many samples were chosen for analysis because we wanted to confirm our field-based hypotheses of correlations. Thus, there was likely a higher correlation percentage of analyzed samples than may be expected for the unanalyzed samples. Uncertainty in the ages of the basalts that constrain the uppermost stratigraphy also has a large effect on the estimated eruptive rates of the upper Deschutes Formation. If these basalts are younger than our Bayesian ages, rates prior to the basalt eruption would increase, since the same number of eruptions would have occurred within a shorter interval, and if the ages are older, rates would decrease. Furthermore, because the rates depend on elucidating the number of distinct eruptions, and failure to recognize a correlative pair means that a single eruption is counted twice, our correlations also contribute to uncertainty. If, as our tests of the known ignimbrite samples demonstrated, our MANOVA technique succeeds in recognizing 86% of correlations, our best estimate for the maximum rate would decrease from 3.3 to 2.8 eruptions/ 10 k.y.

3.4.2 Revisions to Deschutes Formation tephrostratigraphy

Based on our statistical correlations, we can make several important contributions to the stratigraphy of the Deschutes Formation. In the following section, we demonstrate that two of the 14 marker ignimbrites discussed by Pitcher et al (2017a) and Smith (1986) are correlated. In addition, we establish two new extensive

marker units that play important roles in constraining stratigraphic relations, and we provide the first evidence of deposition of a single Deschutes Formation ignimbrite on both sides of the High Cascades graben. Finally, we establish the relative stratigraphic positions of several major Deschutes Formation ignimbrites not determined by previous authors.

3.4.2.1 Correlation of Steelhead Falls and Fly Creek Tuffs

Our results show that two marker ignimbrites, the Steelhead Falls Tuff and the Fly Creek Tuff, which heretofore have been considered separate units, were produced by the same eruption. The Steelhead Falls Tuff (SHFT), which was first described by Stensland (1969) as "ash-flow tuff 3" and later named the "Steelhead Falls Ignimbrite member" by Smith (1986), outcrops nearly continuously for 2.5 km north of Steelhead Falls along the Deschutes river and in isolated outcrops in the Crooked River Canyon (Figure 3.7A). Other marker ignimbrites that appear in the same stratigraphic sequence with the SHFT, such as the McKenzie Canyon and Peninsula Tuffs, have spatial distributions, welding facies, and imbrication that indicates an eruptive source to the southwest (Smith, 1986; Eungard, 2012; Pitcher et al., 2017a). Although SHFT exposures are limited to the southern half of the Deschutes Basin, no previous workers have proposed a source direction for the tuff (Stensland, 1969; Smith, 1986; Eungard, 2012). In contrast, Fly Creek Tuff (FCT) is exposed throughout the northern part of the field area, along the Metolius arm of Lake Billy Chinook and its tributary canyons (Fig. 3.7A). Welding facies and outcrop distributions indicate a source region just south of modern Mount Jefferson (Pitcher et al., 2017a; Smith, 1986). Although our correlation work has located additional outcrops that act to spatially connect the two ignimbrite flow units, the most proximal previously mapped exposures of the two tuffs are separated by over 11 km (Fig. 3.7A).

Despite differences in spatial distributions of outcrops, our analysis indicates that SHFT and FCT are correlated based on their $^{40}Ar/^{39}Ar$ ages (5.68± 0.02 and 5.68± 0.01 Ma, Pitcher et al., 2017a), similarity of glass and plagioclase compositions, and common physical characteristics in the field. Sample DB-019

(FCT) and DB-083 (SHFT) have p values of 0.12 and 0.32 for major elements and trace elements indicative of possible correlation (Appendix 3.3). Both tuffs nearly always overlie a 0.5-2 m thick pumice-fall layer, and glass compositions of these are statistically correlated, with p values that range up to 0.92. In addition, multiple samples from both units are correlated to the same unnamed tuffs (DB-066-W, 331, and 334) with p values ranging from 0.05 to 0.63 for both major elements and trace elements. Additionally, SHFT and FCT have nearly identical plagioclase compositions, with average ($\pm 1\sigma$) An contents of 33.2± 5.9 and 33.1± 6.0, and FeO weight % of 0.31± 0.05 and 0.31± 0.05, respectively (Appendix 3.2). Finally, these tuffs have crystal contents (5-12%) that are unusually high compared to all other Deschutes Formation tuffs, and contain sparse hornblende crystals (<5% of total mineral content), a mineral phase that is absent in most other units.

We suggest that the Steelhead Tuff is the lowermost flow unit of the Fly Creek Tuff. Detailed studies of the FCT indicate that the tuff has at least two flow units; a pumice-rich zone overlain by a pumice-poor zone marks the flow unit boundary. In addition, this flow unit boundary is marked by an upward change from only white rhyolite pumice in the lower unit to containing both white pumice and crystal-rich black scoria in the upper unit (Conrey, 1985). This upper flow unit is rarely found east of the Fly Creek canyon (Fig. 3.7B), even in outcrops where the uppermost pumice-rich zone of the lower unit is preserved (Dill, 1992). The lower flow unit, however, is found much more distally (Fig. 3.7A), and had been previously mapped as far as the west wall of the Deschutes River canyon (Dill, 1992). The flow unit transitions from containing fiamme and basal vitrophyre within 10 km west of Green Ridge to being entirely nonwelded beyond 20 km west of the ridge.

Like the lower flow unit of FCT, the Steelhead Falls unit contains only white rhyolite pumice. SHFT is welded only in its most northwestern location (44.46°N, 121.33°W), 24 km southwest of Green Ridge, where it unusually thick (18m) and fills a relatively narrow channel incised into the McKenzie Canyon Tuff (Fig. 6A). All southern and eastern outcrops of the tuff are nonwelded, even in one 25 m thick location; consistent with SHFT having cooled significantly by the time it reached at

these more distal southwestern locations. In summary, significant similarities in ages, crystallinity, welding patterns, and plagioclase and glass compositions, suggest that the Steelhead Tuff is the lowermost flow unit of the Fly Creek Tuff. We calculate a total volume of 7.9 km^3 (5.8 km^3 DRE) for the Fly Creek Tuff.

3.4.2.2 Spring Creek Tuff

Previous work has identified 14 extensive "marker" ignimbrite units that are useful in determining the stratigraphic positions of other Deschutes Formation units. We propose integrating two new marker ignimbrites that outcrop over a laterally

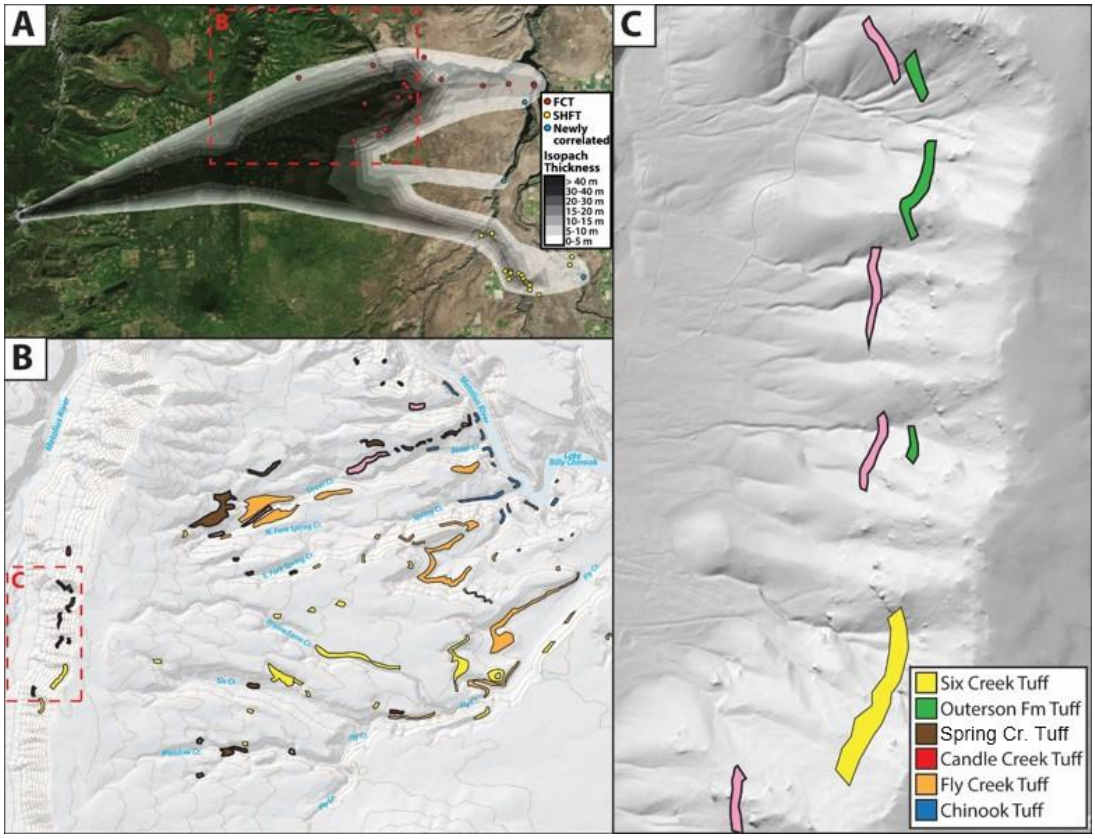

Figure 3.7: (A) Isopachs used to calculate the volume of Fly Creek Tuff. Yellow dots are thickness measurements of the Steelhead Falls flow unit of the Fly Creek Tuff, and blue points are samples which were found to be geochemically correlated to the tuff. Methods for ignimbrite shape and volume estimation is given in Pitcher et al., 2017. (B) Map showing the distribution of the two new marker units, Street Creek Tuff and the Spring Creek Tuff (legend is the same as in C). The distribution of three other marker tuffs, Six Creek, Fly Creek and Chinook Tuffs are shown for reference. (C) LiDAR image of Green Ridge showing the distribution of Outerson Formation, Street Creek, Candle Creek, and Six Creek Tuffs. Note that there are very few outcrops, of any lithology, lower than Street Creek Tuff on Green Ridge

extensive area and occupy key stratigraphic positions that help to constrain Deschutes Formation stratigraphy.

We name the first new marker unit the Spring Creek Tuff, due to its exposure in two outcrops near the head of Spring Creek (Fig. 3.7). Conrey (1985) first mapped and described multiple outcrops of the unit, that he had simply named the "W" (welded) tuff (Conrey, 1985). We choose to assign it a new name, as the tuff is not welded in all locations and to avoid ambiguity with other welded ignimbrites in the formation. Aubin (2000) gave the tuff the informal name Candle Creek II tuff, but we choose to avoid this name as our correlation work indicates the unit is geochemically distinct from the Candle Creek I ignimbrite, and the Spring Creek Tuff does not crop out near the Candle Creek campground for which the other unit is named. We correlated samples from nine outcrops (Fig. 3.7B), of which five had been mapped as "W" by Conrey (1985) and three that had not been mapped as correlative, including the southernmost outcrop (Fig. 3.7B). In addition, we have confirmed that the tuff is correlated to the unit Tdt29 of Dill (1992). We also suggest, on the basis of statistical dissimilarity, that two outcrops that were erroneously mapped as "W" and "W?" by Conrey (1985), are not actually correlated.

The Spring Creek tuff forms a distinctive marker unit just east of the crest of Green Ridge and can be mapped throughout the northwestern-most region of the field area, where it overlies most tuffs. Dated units such as the Six Creek Tuff (5.45± 0.04 Ma) are absent in this region, but because the Spring Creek Tuff is observed directly below Six Creek Tuff in two southerly locations, it acts to constrain the ages of the northwestern tuffs to be older than 5.45± 0.04 Ma.

The tuff is light grey in fresh surfaces, but weathers to an orange-brown or yellow-tan color, and often forms cliffs or pinnacles. In multiple locations, the ignimbrite is partially welded with fiamme, but even in nonwelded outcrops the black scoria tends to be dense and glassy, sometimes forming non-flattened, barely vesicular, vitrophyre. Scoria is often very large, up to 15x15 cm, and is unusually crystal-rich, containing up to 20% plagioclase and pyroxene crystals, compared to other Deschutes ignimbrites that generally contain <5% crystals. While the black

scoria is most abundant component (85-90%), the tuff also contains medium to dark grey pumice (5-10%) and rare (<5%) white pumice that are always smaller than the scoria. The matrix is both crystal and lithic rich.

We further propose a tentative correlation of the Spring Creek Tuff to Dill's (1992) Tdt26, equivalent to Hewitt's (1969) "ash flow tuff number six," that is exposed only in cliff-forming outcrops up to 12 m thick near the confluence of the Metolius and Deschutes Rivers. The latter tuff has p values that indicate likely correlation to four different Spring Creek Tuff samples (0.11-0.49 and 0.08-0.82 for major elements and best trace elements, respectively) and has similar field characteristics to nonwelded portions of the Spring Creek Tuff, such as large glassy crystal-rich scoria and a lithic and crystal rich matrix containing obsidian fragments. Our correlation greatly increases the estimated distance traveled for the Spring Creek Tuff, from a maximum of 8 km from the crest of Green Ridge to nearly 28 km (Fig. 3.7B). Smith (1986) shows the Peninsula Tuff in two locations where Dill (1992) had mapped Tdt26 near the confluence of the Deschutes and Metolius Rivers. Although the tuffs have similar field characteristics, we suggest that they are not correlated on the basis of differing geochemistry ($p<0.05$). We calculate a volume of 2.9 km^3 (2.5 km^3 DRE) for this unit.

3.4.2.3 Street Creek Tuff

A second marker ignimbrite unit, which we name the Street Creek Tuff due to its numerous exposures throughout the Street Creek canyon, is correlated to Dill's (1992) Tdt17 and Conrey's (1985) LRT-170 ($p=0.22-0.82$ and 0.06-0.45). It is one of the few units that can be successfully traced back to the west flank of Green Ridge (Fig. 3.7), where it is correlated in four outcrops ($p=0.25-0.997$ and 0.07-0.50) that are exposed at approximately the same elevation on the ridge (1120-1160 m), but separated over a horizontal distance of 3 km. Because it outcrops just beneath Fly Creek Tuff (5.68± 0.01 Ma) in one location (44.579°N, -121.537°W), Street Creek Tuff acts as a critical constraint on the ages of tuffs in the northwestern portion of the field area where the dated tuffs do not outcrop (Fig. 3.7B). Since there are only two tuff outcrops lower than Street Creek Tuff on Green Ridge, we can constrain that

almost all exposures on Green Ridge are younger than approximately 5.68 Ma (Fig. 3.7C).

Street Creek tuff is light grey in fresh surfaces but can be yellow-grey in weathered surfaces; the top is occasionally vapor-phase altered to an orange-pink color. The most distinctive characteristic is the high abundance of angular volcanic lithics, including black glassy breadcrust blocks and grey platy-jointed plagioclase-rich andesite lithics, that can range up to 1 m in size in outcrops on and near Green Ridge. The tuff contains, in decreasing abundance, white to light grey, medium olive-grey, and large (up to 50 cm) black pumice within a sandy and moderately crystal-rich (~2-5%) matrix. On Green Ridge, outcrops range 9 to 40 m in thickness but east of the ridge, the tuff is up to 61 m thick and is therefore one of the thickest ignimbrites in the Deschutes Formation. However, due to its relatively limited distance of deposition, the Street Creek Tuff has a volume of 2.0 km^3 (1.2 km^3 DRE).

3.4.2.4 The Tuff of Outerson Formation: deposited on both sides of the High Cascades graben

Although lava flows of Deschutes Formation age are exposed on ridge tops west of the High Cascades graben, very few ignimbrites of equivalent age are preserved to the west, relative to the extensive outcrops in the Deschutes Basin. Priest et al. (1987) suggested that one ignimbrite, the Tuff of Outerson Formation (unit Tt), which is found west of the Graben, was likely lithologically similar to Deschutes formation tuffs. A recent $^{40}Ar/^{39}Ar$ age for this unit of 5.55± 0.03 Ma is consistent with its eruption during Deschutes Formation time (Pitcher et al., 2017a). We have located three outcrops on the west flank of Green ridge (Fig. 3.7) and one that is five km east of the ridge crest that are statistically correlated to the Tuff of Outerson Formation (p=0.33-0.81 and 0.12-0.40). This study is the first to successfully correlate any Deschutes Formation unit to both sides of the High Cascades graben. The tuff also plays a critical role in constraining the ages of units exposed on the northern half of Green Ridge, since Six Creek Tuff is not exposed there (Fig. 3.7). Only one ignimbrite and two tephra-fall tuffs (DB-312, DB-310A, DB-310B) outcrop above the Tuff of Outerson Formation, indicating that almost all tuffs in the northern

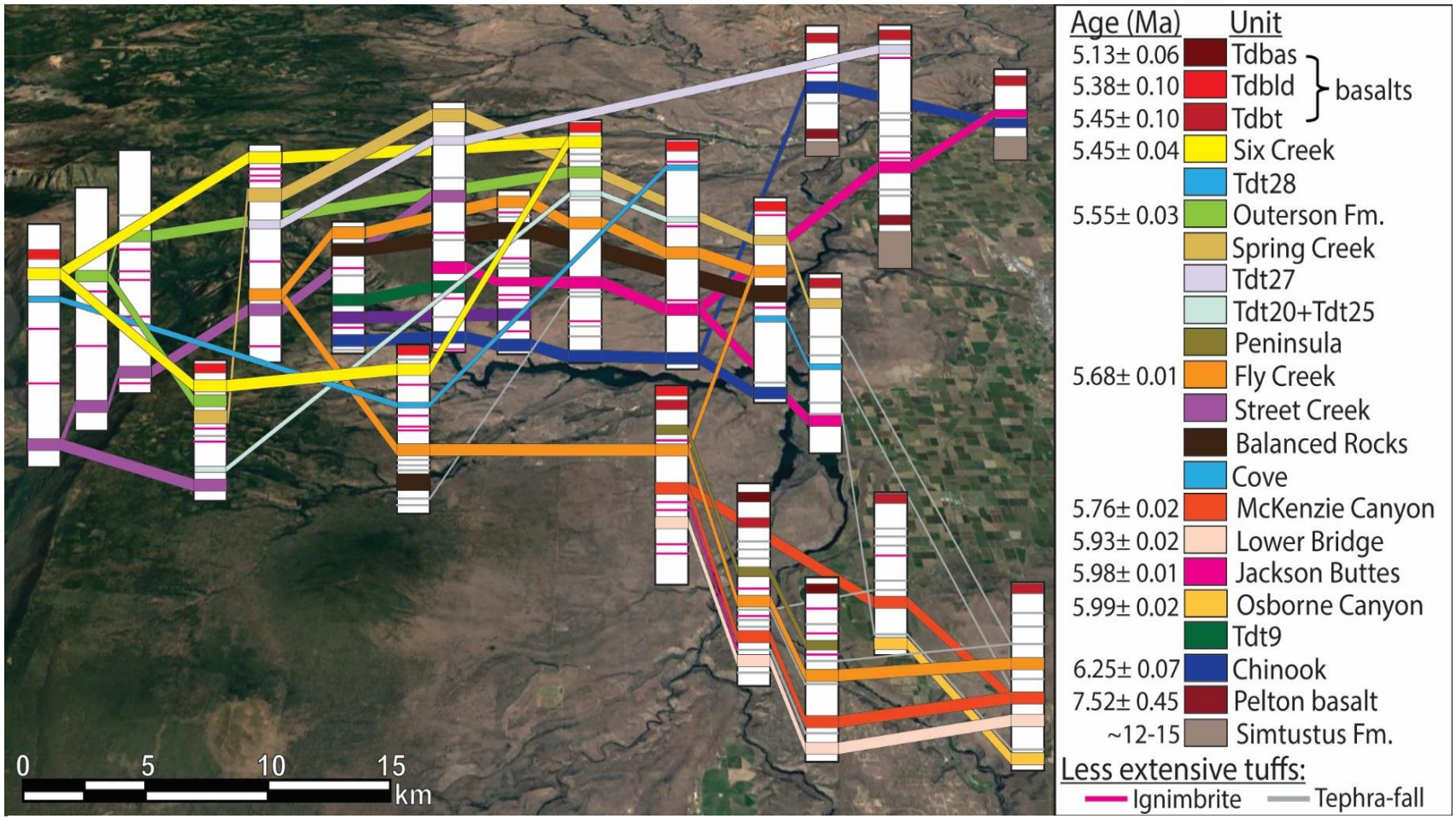

Figure 3.8: Correlation (fence) diagram. Relative positions of major ignimbrites are shown, but thickness and distance between them are not to scale. Stratigraphic positions of less extensive ignimbrites and tephra-fall units (pink and grey lines, respectively) are also shown. These correlations provide the comprehensive tephrostratigraphy of the Deschutes Formation. 21 representative stratigraphic sections are shown, with the base of the section indicating their approximate locations within the Deschutes basin. Many of these combine 2-3 nearby stratigraphic sections. Appendix 3.5 shows correlations of units between 48 stratigraphic sections throughout the basin.

half of the ridge are older than 5.55± 0.03 Ma. We have also correlated the ignimbrite unit to two tephra-fall deposits (DB-133 and DB-084), that are located 18 and 24 km from the crest of Green Ridge, respectively.

The Tuff of Outerson Formation is light to medium grey in fresh and weathered surfaces but grades to a yellow-grey color near the top. The tuff is lithic rich throughout (>30%), containing cobbles and small boulders up to 40x40cm even near the top of outcrops and consists of at least two flow units. The tuff contains abundant white pumice, altered to a cream color, and less abundant but larger dark grey to black pumice (up to 8x6cm), within a sand-rich, crystal-poor matrix.

On the west side of the High Cascades graben, the tuff is located (44.720°N, -121.955°W) 14 km north-northeast of the summit of modern Mount Jefferson, where the base is 200 m higher (1435 m) than its eastside equivalents, possibly as a result of the uplift of the Western Cascades (e.g. Conrey et al., 2002; Priest, 1990; Lopez, 2016). In this location, it ranges between 42 and 62 m thick and can be traced over a horizontal distance of 2.4 km. The tuff is also mapped in two other locations on the west side of the graben, (44.720°N, -121.872°W) and (44.655°N, -121.982°W), 7 km and 15 km from Mount Jefferson, respectively (Priest et al., 1987).

On the east side of the graben (Green Ridge), which is located 20 km southeast of Mount Jefferson, the tuffs are thinner, between 26 and 37 m, and contain slightly smaller lithics (maximum 40x40 cm) than on the west-side (maximum 30x30 cm). These characteristics are consistent with the eruptive source being near the modern High Cascades axis, such that the Green Ridge samples are more distal than their west-side equivalents.

3.4.2.5 Other notable correlations

Conrey (1985) originally mapped one ignimbrite outcrop on Green Ridge as the lowermost flow unit of his “W” tuff (our “Spring Creek Tuff”). Conversely, Aubin (2000) claims, based on “careful field work, petrography, and chemical variations,” that the outcrop belongs to a different ignimbrite that he informally named Candle Creek ignimbrite. Evidence for this claim is not presented in detail, and thus cannot be evaluated. Our correlation work agrees with Aubin (2000);

although the Spring Creek tuff is found directly overlying the Candle Creek tuff in multiple field locations, the two are geochemically distinct.

Furthermore, our correlation work has resolved the relative stratigraphic positions of the Candle Creek, Spring Creek, and Meadow Creek Tuff, which heretofore had been ambiguous (Aubin, 2000). The Meadow Creek Tuff lies directly beneath the Six Creek Tuff within the Fly Creek Canyon. In more northerly locations near the crest of Green Ridge, the Candle Creek Tuff directly underlies the Spring Creek Tuff, which, in turn, is found directly beneath Six Creek other locations. However, as Aubin (2000) points out, Meadow Creek Tuff is never found in the same stratigraphic section as either the Spring Creek Tuff of Candle Creek Tuff and thus their relative stratigraphic order was previously unknown. We have correlated the Candle Creek Tuff to an ignimbrite (DB-164) that overlies the Meadow Creek Tuff, separated by 4 m of tuffaceous sandstone. The Candle Creek Tuff (DB-309) and DB-164 are identical in the field and have high p values (0.64 and 0.75 for major elements and best trace elements, respectively) providing a high level of confidence in the correlation. Thus, the stratigraphic order of these relatively extensive ignimbrites is, from oldest to youngest: Meadow Creek Tuff, Candle Creek Tuff, Spring Creek Tuff, and Six Creek Tuff (Figs. 3.2 and 3.8).

We also determined the relative age of two other marker ignimbrites, the McKenzie Canyon Tuff and the Cove Tuff. Smith (1986) suggests that the Cove Tuff to the north occupies approximately the same stratigraphic level as the McKenzie Canyon Tuff, and that the two units could act as useful markers to tie the two regions together. However, because they are never found within the same stratigraphic section, their relative ages were previously unknown. A separate, compositionally zoned tephra fall unit has one correlated outcrop that underlies Cove ignimbrite and another that directly overlies McKenzie Canyon Tuff (Fig. 3.8). We have demonstrated that the Cove Tuff is younger than the McKenzie Canyon Tuff (5.76± 0.02 Ma), thus providing further age constraints on tuffs that outcrop above Cove Tuff in the northern part of the field area.

3.4.3 Comparison of Deschutes Formation eruptive frequency and volumes

Pitcher et al. (2017a) calculated the volumes of 14 marker ignimbrites within the Deschutes Formation. We update the total volume to include that of an additional 13 ignimbrites made possible by the correlation work in this study. If we assume, as in Pitcher et al (2017a), that the 13 additional ignimbrites from our study also deposited an equal volume to the west and had a tephra fall:flow ratio of between 0.5:1 and 1.9:1, the total volume of all 26 eruptions was likely between 246 and 475 km^3, or a rate of 6-12 km^3/m.y./km. This new rate is approximately 2-8 times higher than the production of all compositions over the entire Quaternary Cascades (1.5-2.5 km^3/m.y./km arc length), and is also much higher than that of the Alaska Peninsula (0.6-1.0 km^3/m.y./km), and the Andean southern volcanic zone (33°-46°S) (1.1-2.0 km^3/m.y./km) (Hildreth, 2007).

While it has already been demonstrated by Pitcher et al. (2017a) that the Deschutes Formation pulse represents the highest volumetric rate of silicic magma erupted in the Central Oregon Cascades within the last 17 Ma, our upper estimate now rivals that of the 35-17 Ma arc (11.7 km^3/m.y./km) (Priest, 1990). Furthermore, our correlation work indicates that there were at least 20 additional uncorrelated ignimbrite eruptions as well as 27 distinct tephra-fall deposits that would have contributed additional volumes to the total erupted during Deschutes Formation time. Thus, although subject to significant uncertainty, the short 800 k.y. pulse of Deschutes Formation explosive volcanism may represent the highest silicic volumetric rate since the inception of the Cascades ~45 Ma.

In addition to producing relatively large volumes of pyroclastic material compared to the Quaternary, explosive eruptions also occurred more frequently during Deschutes Formation time. We have demonstrated that during the 800 k.y. pulse of Deschutes Formation explosivity, there were approximately 120 different eruptions large enough (>0.1 km^3) to deposit pyroclastic material into the Deschutes Basin. This equates to an *overall average* of 1.7 eruptions/ 10k.y. However, the eruption rate was not constant through time, and the region reached a maximum rate of nearly 3 eruptions per 10 k.y between 5.7 and 5.55 Ma (Fig. 3.10A). In Central

Oregon (44-45°N), there have been only eight explosive eruptions since 700 ka large enough to produce tephra-fall deposits, of which only five were larger than 0.1 km^3 (DRE) (Hildreth, 2007, and references therein). Thus, the central Oregon High Cascades had explosive eruptions (>0.1 km^3) approximately 24 times more frequently during Deschutes time than they have in the last 700 k.y.

Overall, there are only 46 tephra-fall deposits from the entire Quaternary Cascades arc that record explosive eruptions of >0.1 km^3 of magma (Hildreth, 2007, and references therein). This equates to an approximate eruptive frequency of 0.18 eruptions/ 10 k.y., or 10 times less frequent than Deschutes Formation source volcanoes, alone. Of these Quaternary eruptions, only 20 of them erupted more than 1 km^3 of magma (Hildreth, 2007). We estimate that at least 18 of the eruptions recorded within the Deschutes Formation alone had volumes greater than this. However,

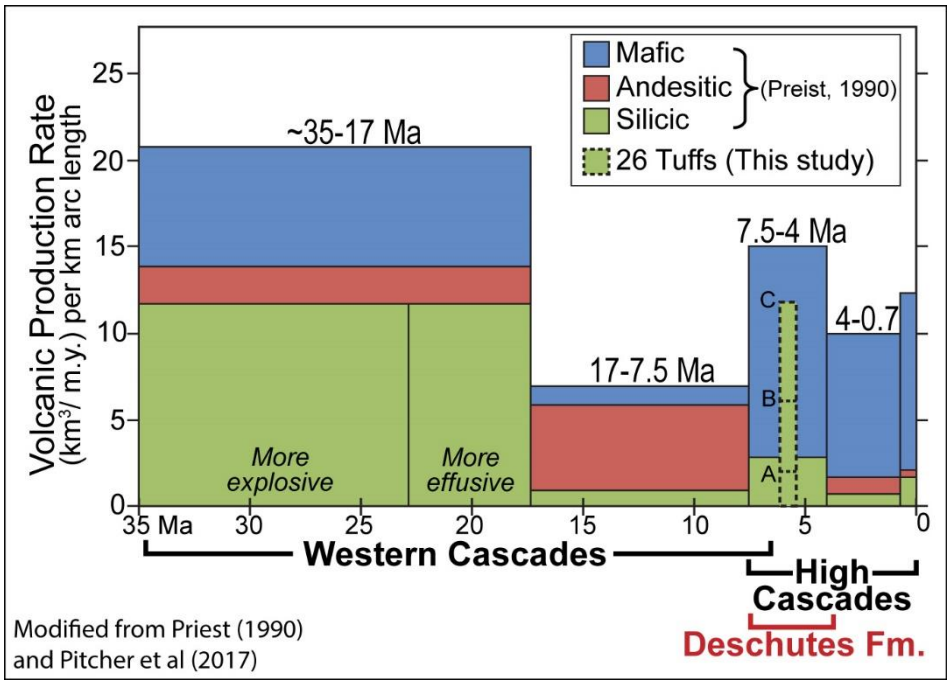

Figure 3.9: Volcanic production rate through time for the central Oregon Cascades, modified from Pitcher et al. (2017) to include volumes from 13 additional tuffs from this study. All data except the dashed column are from Priest (1990). Dashed column represents volumetric rate from just 26 ignimbrites of the Deschutes Formation. (A) gives the minimum rate if only the eastward ignimbrite volumes are used. (B) represents an estimate if an equal ignimbrite volume is deposited westward and an additional tephra fall volume that is half that of the ignimbrite component. (C) is an estimate assuming the tephra fall component is twice that of the ignimbrite. See text for justification.

during the Holocene, the frequency of Cascades arc explosive eruptions appears 1.5 times higher than the maximum rate reached during the Deschutes Formation, with six eruptions >1 km^3 (Hildreth, 2007). However, Mt. St. Helens is the only single volcano with more frequent explosive eruptions than the Deschutes Formation sources, with 20 eruptions larger than 0.1 km^3 (8 larger than 1 km^3) during the last 50 k.y. (Mullineaux, 1996). This rate of 4 eruptions per 10 k.y., is nearly two times more frequent than the highest average rate recorded by the *northern* Deschutes Formation volcanic source (2.7/10 k.y.).

3.4.4 Decline of the Deschutes Formation: Graben subsidence and/ or waning volcanism?

While numerous authors have proposed that intra-arc extension played a vital role in increasing magmatic flux driving this period of unusually productive magmatism in the central Oregon Cascades (Conrey et al., 2002; Conrey, 1991; Smith et al., 1987), there is some uncertainty as to the role that tectonics may have played in its decline. The youngest lava at the crest of Green Ridge has an $^{40}Ar/^{39}Ar$ age of 5.34± 0.08, indicating that normal faulting became extensive enough after this time to prevent further deposition of lava into the basin (Smith et al., 1987). Previous work by Conrey et al. (2002) and Smith (1986) also indicates that the deposition of ignimbrites within the Deschutes Basin ceased sometime before ~5.34 Ma, leading researchers to postulate that the formation of the graben formed a barrier that trapped ignimbrite volumes and prevented their passage into the basin.

Six Creek Tuff was the last large ignimbrite deposited within the Deschutes formation (5.45± 0.04 Ma, Pitcher et al., 2017a). Smith (1986) suggests that a marked lithological break occurs above the level of the Six Creek Tuff, from sheet-flood and ignimbrite-dominated to paleosol dominated facies in the upper 50-100m of many sections. Similarly, the uppermost 100-150 m of strata above Six Creek Tuff on Green Ridge is almost entirely lava flows and contains no ignimbrites (Conrey, 1985). Smith (1986) argues that this distinct lithological break was the result of the formation of the High Cascades graben that cut-off supply of ignimbrites and volcaniclastic material from the Cascades to the Deschutes Basin, but that frequent

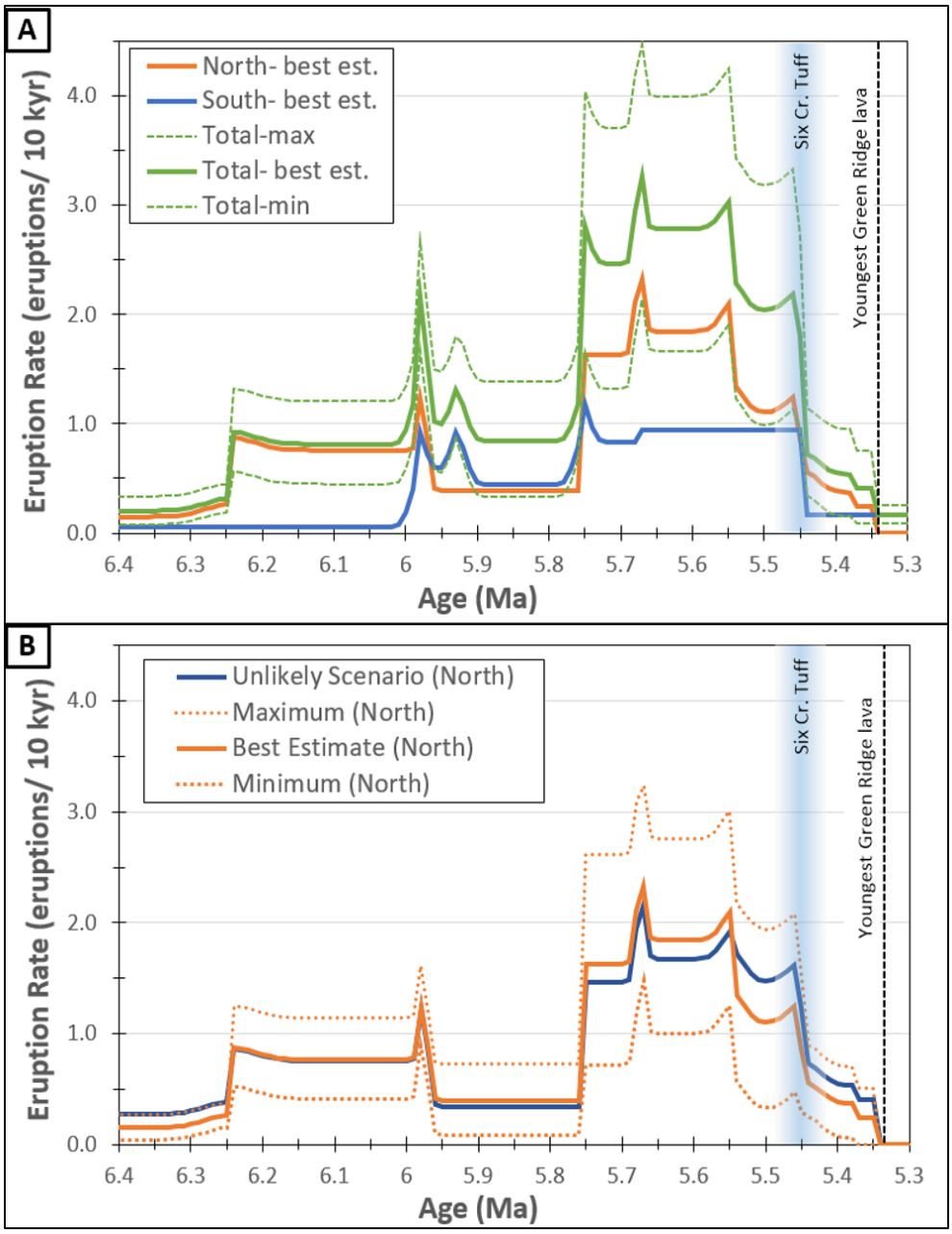

Figure 3.10: Eruptive frequency vs. time. (A) shows our best estimate of the eruptive frequency if all units are given uniform probability distributions and 53% of unanalyzed tuffs are assumed to be distinct. The maximum and minimum total frequencies are also shown. Blue area represents the age of Six Creek Tuff ±2σ (5.45± 0.04 Ma), demonstrating that eruptive frequency decreased prior to eruption of Six Creek Tuff. See text for discussion. (B) Shows the "unlikely scenario" in which we assume all 11 tuffs that outcrop less than 50 m below Tdbt were given ages between 5.55 and 5.45 Ma. In addition, this scenario assumes that all 5 eastern basin tephra-fall units for which no stratigraphic context could be established are younger than Tdbt. Note that for all scenarios, there is a decrease in eruptive frequency prior to graben subsidence ~5.34 Ma.

explosive eruptions continued to occur for some time. The existence of numerous tephra-fall deposits above Six Creek Tuff indicates that explosive volcanism did continue to occur after 5.4 Ma. Although this subsidence almost certainly lead to the ultimate termination of ignimbrite deposition within the Deschutes Basin, Conrey et al. (2002) suggests that a concurrent decrease in volcanism may also have been partially responsible for decreased ignimbrite frequency in the upper Deschutes Formation. This leads us to ask another question: Was the notable decrease in deposition across the Deschutes Basin entirely the result of subsidence and graben-formation, or was volcanism waning prior to subsidence?

Since the post-subsidence ignimbrite record is not accessible via exposed outcrop or other direct observation methods, we attempt to answer this question by noting trends in eruptive frequency prior to the initiation of subsidence. If subsidence was solely responsible, we would expect to see a continuously high eruption rate just prior to normal faulting and then an abrupt decrease thereafter. The highest eruptive frequency in both the north and south occurred 5.70-5.55 Ma, during which time the total frequency was more than 2.7 eruptions per 10 k.y (Fig. 3.10). Between 5.55 Ma and 5.45 Ma, the eruptive frequency in the north decreased by 40% (1.9 to 1.1), and the rate declined significantly in both the north and south thereafter. Although formation of the graben certainly prevented ignimbrite deposition within the basin, our eruption rate calculations indicate that the frequency of explosive eruptions was already decreasing ~100 k.y. prior to the eruption of Six Creek Tuff (5.45± 0.04 Ma) (Fig. 3.10, blue vertical area), and ~200 k.y. before the eruption of the uppermost Green Ridge lava (5.34± 0.08 Ma).

Our conclusion that waning volcanism predated graben subsidence is important for several reasons. First, this indicates that the ignimbrite record preserved within the Deschutes Basin is relatively complete, and that it is not missing a significant post-graben ignimbrite record. Thus, the 800 k.y. interval of pyroclastic deposits recorded within the Deschutes Formation does represent a short pulse of explosive volcanism (Pitcher et al., 2017a) and the duration is not simply a relic of preservation within the basin. This conclusion has petrogenetic implications. Waning

volcanism is consistent with the thermomechanical modeling by Karakas and Dufek (2015) that asserts that for a relatively high basaltic flux within a region undergoing crustal extension, the maximum crustal melting efficiency is reached 1.2 to 1.8 m.y. after it initiation, and wanes thereafter. Our results indicate that the highest silicic eruption rate in the Deschutes Formation occurred approximately 1.75 to 2 m.y. after the first eruption of low K tholeiitic lava in the region ~7.5 Ma. This supports the conclusions of Pitcher et al (2017a) who suggest that the short interval of heightened explosive volcanism was the result of increased magmatic flux resulting from extension and temporarily enhanced crustal melting of more fusible crust.

3.4.4.1 Addressing uncertainty in declining eruptive frequency trend

Based on new $^{40}Ar/^{39}Ar$ age constraints (Pitcher et al., 2017a) and the detailed tephrochronology established by this study, we disagree with the conclusion of Smith (1986) and Smith et al. (1987), that the rate of explosive volcanism remained high prior to, during and immediately following graben formation. Instead, from our observations we conclude that the rate of explosive volcanism began waning ~100 k.y. before the initiation of graben subsidence. Smith et al. (1987) based their claim on the existence of numerous thick tephra-fall deposits within the uppermost paleosol-rich sections of the Deschutes Basin, particularly in the east. However, since exposures of Six Creek tuff are limited to the western 18 km of the basin, and the marker tuff had not been previously dated, the stratigraphic positions of eastern tephra-fall units relative to the Six Creek Tuff were poorly constrained. Only Jackson Buttes tuff (5.98± 0.01 Ma, Pitcher et al., 2017a) and Tetherow Butte basalt (Tdbt) (5.45± 0.10 Ma) can be used as chronologic markers in the eastern basin. Almost all tephra-fall deposits underlie Tetherow Butte Basalt, which forms a cap over most of the basin east of the Deschutes River. On the eastern boundary of the Deschutes Basin, near Madras, there are four distinct tephra fall units and one fine-grained ignimbrite that are located too far from Tetherow Butte Basalt to establish relative position; we can be certain only that they are younger than the Big Canyon basalt (<5.76 Ma, by stratigraphic relations). In order to be completely objective, these units were assigned a uniform probability of erupting between 5.76 and 5.33 Ma. If we had

instead assumed that all five of these tuffs were younger than the basalt, the eruptive rate after 5.45 Ma would increase slightly, from 0.55 to 0.75 in the interval of 5.40-5.41 Ma, however, this is still 3.5 times less frequent than during 5.67-5.57 Ma.

Additionally, there are four ignimbrites and seven tephra-fall tuffs in the eastern basin that outcrop less than 50 m below Tetherow Butte Basalt. If we assumed that all of these were distinct and all erupted between 5.55 and 5.45 Ma and continued to assume, as above, that the five aforementioned tuffs are younger than 5.45 Ma, the frequency of eruptions between 5.55 and 5.45 Ma would increase by 20% from 2.0 to 2.4. However, despite this increase, the rate during this interval is still 10% lower than that of the previous 100 k.y. (Fig. 3.10B). Although this difference is likely within uncertainty, this scenario is unlikely, as accumulation rates in the regions near these samples (calculated using the vertical distance between Tetherow Butte Basalt and Chinook Tuff or Jackson Buttes Tuff) are such that 10 k.y. prior to the eruption basalt should only include the uppermost 5-23 m rather than the 50m that we used in this scenario.

Although there is uncertainty in the age of Tetherow Butte Basalt, this has no effect on the conclusion of waning volcanism. Both increasing and decreasing the age of the basalt unit cause an even greater decrease in the rate of volcanism prior to subsidence. As discussed above, other sources of uncertainty exist, such as the proportion of unanalyzed samples that we assume are distinct, however, these are likely to affect all time intervals similarly, and would have little effect on the apparent decrease in eruptive frequency. After testing numerous scenarios to address uncertainty in our estimated eruptive rates, we are confident that our conclusion, that waning volcanism predated subsidence, is robust and is corroborated by the data in all cases.

3.5 Conclusions

3.5.1 Contributions of this study

In this study, we established a comprehensive tephrostratigraphy of the Deschutes Formation made possible through detailed field work, geochemical

analysis and multivariate statistical correlations. We suggest that at least 67 distinct explosive eruptions (possibly as many as 120) occurred within the 800 k.y. explosive pulse of the Deschutes Formation. In addition, we correlated two existing marker ignimbrite units, the Fly Creek and Steelhead Falls Tuffs, established two new marker ignimbrites, the Spring Creek and Street Creek Tuffs, and correlated the Tuff of Outerson Formation to both the eastern and western sides flanks of the High Cascades graben. We combined this detailed stratigraphy with $^{40}Ar/^{39}Ar$ ages (Pitcher et al., 2017a) and addressed temporal variations in volume and frequency of explosive volcanic events. In addition, we established that the eruptive rate of the early central Oregon High Cascades began to wane at least 100 k.y. before initiation of graben subsidence. Thus, our correlation work allowed us to reconstruct the earliest volcanic history of the incipient High Cascades arc.

3.5.2 Eruptive and tectonic history of the early central Oregon High Cascades

The advent of low potassium tholeiite eruptions into the eastward Deschutes Basin approximately 7.5 Ma marked the initial influence of extension and migration of arc activity. After this time, basalt injection accommodated extension and began to thermally prime the upper and middle crust, which consists of more fusible material than that of the depleted crust beneath the Western Cascades. After a period of ~1 m.y., melting of the thermally-primed fusible crust produced significant volumes of silicic magma. Between 6.25 and 5.55 Ma, the frequency of explosive eruptions large enough to deposit tuffs within the Deschutes Basin increased from <1 to over 3 eruptions per 10 k.y. At least 82 km^3 of felsic magma was explosively erupted during this 800 k.y. period.

After the ~1 m.y. interval of most efficient crustal melting (Karakas and Dufek, 2015), production of silicic magma began to slow and pyroclastic volcanism began to wane after the eruption of the Tuff of Outerson Formation, 5.55 Ma. Resultant cooling at the periphery of the magmatic system cause the upper crust to become more brittle, and initiation of normal faulting occurred shortly after the eruption of Six Creek Tuff (5.45 Ma).

Between 5.45 and 5.34 Ma, continued brittle faulting, and initial formation of the High Cascades graben prevented further ignimbrite deposition in the Basin. However, lavas did erupt on the periphery of the mid-crustal melt (shadow) zone east of the extensional fault zone, and emplaced 100-150m of lava over the present-day crest of Green ridge. Basalt lavas also began to erupt within the Deschutes Basin now (Smith et al., 1987; Smith, 1986). Explosive volcanism continued to occur but eruptive frequency declined rapidly. After ~5.34 Ma normal faulting and graben formation became extensive enough cut off basalt supply to the Deschutes Basin. Volcanism, including pyroclastic eruptions, continued during this time at decreased rates within the High Cascades graben and sporadic lava flows erupted within the Deschutes Basin until ~4.0 Ma (Smith, 1986). Rates of volcanism continued to decrease into the Quaternary (Pitcher et al., 2017a; Conrey, 2002), and were punctuated by smaller pulses of explosive volcanism from the Tumalo Volcanic Center during the Pleistocene (Sherrod et al., 2004 and references therein).

3.5.3 Future work

Although we established the tephrochronology of the Deschutes Basin, our estimates of the eruptive volume and frequency could be further constrained with future work. Uncertainty in the number of distinct eruptions could be improved with geochemical and statistical analysis of all tuffs within the Deschutes formation, including the 107 samples that we collected but were unable to analyze due to time constraints. Collection of additional analyses of the samples from this study, such that each sample has at least 15 analyses, would greatly improve the resolving power of our MANOVA technique for correlation. In addition, collecting new, higher precision $^{40}Ar/^{39}Ar$ ages for Tetherow Butte Basalt and Lower Desert basalt, as well as some of the uppermost tephra-fall units for which we have no tephrostratigraphic constraints, would help to greatly reduce uncertainty in the relationship between volcanic history and graben subsidence. Finally, access to Warm Springs Indian Reservation would allow us to further constrain eruptive volumes of ignimbrites deposited into the northern third of the Deschutes Basin field area.

References

Aitchison, J., 1986. The statistical analysis of compositional data.

Aubin, W., 2000. Ignimbrites of the Deschutes Formation: A record of Crustal Melting and Magma Mixing (M.S.). Washington State University, Pullman, WA.

Branney, M.J., Kokelaar, B.P., 2002. Pyroclastic Density Currents and the Sedimentation of Ignimbrites. Geological Society of London.

Bray, E.A. du, John, D.A., 2011. Petrologic, tectonic, and metallogenic evolution of the Ancestral Cascades magmatic arc, Washington, Oregon, and northern California. Geosphere 7, 1102–1133. doi:10.1130/GES00669.1

Brocher, T.M., Wells, R.E., Lamb, A.P., Weaver, C.S., 2017. Evidence for distributed clockwise rotation of the crust in the northwestern United States from fault geometries and focal mechanisms. Tectonics 2016TC004223. doi:10.1002/2016TC004223

Buck, W.R., 2004. Consequences of asthenospheric variability on continental rifting, in: Karner, G., Taylor, B., Driscoll, N. (Eds.), Rheology and Deformation of the Lithosphere at Continental Margins. Columbia University Press, pp. 1–30.

Conrey, R.M., 1985. Volcanic stratigraphy of the Deschutes Formation—Green Ridge to Fly Creek—north-central Oregon (M.S.). Oregon State University, Corvallis, Oregon.

Conrey, R.M., Grunder, A.L., Schmidt, M.E., 2004. SOTA field trip guide, State of the Cascades arc: Stratocone persistence, mafic lava shields, and pyroclastic volcanism associated with intra-arc rift propagation. DOGAMI Open-File Report O-2004-04 39.

Conrey, R.M., Sherrod, D.R., Hooper, P.R., Swanson, D.A., 1997. Diverse primitive magmas in the Cascades arc, northern Oregon and southern Washington. The Canadian Mineralogist 35, 367–396.

Conrey, R.M., Taylor, E.M., Donnelly-Nolan, J.M., Sherrod, D.R., 2002. North-central Oregon Cascades: Exploring petrologic and tectonic intimacy in a propagating intra-arc rift. Field guide to geologic processes in Cascadia 36 47–90.

Deering, C.D., Bachmann, O., Dufek, J., Gravley, D.M., 2011. Rift-Related Transition from Andesite to Rhyolite Volcanism in the Taupo Volcanic Zone (New Zealand) Controlled by Crystal–melt Dynamics in Mush Zones with Variable Mineral Assemblages. J. Petrology 52, 2243–2263. doi:10.1093/petrology/egr046

Deering, C.D., Gravley, D.M., Vogel, T.A., Cole, J.W., Leonard, G.S., 2010. Origins of cold-wet-oxidizing to hot-dry-reducing rhyolite magma cycles and distribution in the Taupo Volcanic Zone, New Zealand. Contrib Mineral Petrol 160, 609–629. doi:10.1007/s00410-010-0496-0

Dill, T.E., 1992. Stratigraphy of the Neogene volcanic rocks along the lower Metolius River, Jefferson County, central Oregon (M.S.). Oregon State University, Corvallis, Oregon.

du Bray, E.A., John, D.A., 2011. Petrologic, tectonic, and metallogenic evolution of the Ancestral Cascades magmatic arc, Washington, Oregon, and northern California. Geosphere 7, 1102–1133. doi:10.1130/GES00669.1

Eungard, D.W., 2012. Early High Cascades Silicic Volcanism: Analysis of the McKenzie Canyon and Lower Bridge Tuff (M.S.). Oregon State University, Corvallis, Oregon.

Everts, R.C., Conrey, R.M., Fleck, R.J., Hagstrum, J.T., 2009. The Boring Volcanic Field of the Portland-Vancouver area, Oregon and Washington: Tectonically anomalous forearc volcanism in an urban setting, in: Volcanoes to Vineyards: Geologic Field Trips Through the Dynamic Landscape of the Pacific Northwest. Geological Society of America.

Garibaldi, N., Tikoff, B., Hernández, W., 2016. Neotectonic deformation within an extensional stepover in El Salvador magmatic arc, Central America: Implication for the interaction of arc magmatism and deformation. Tectonophysics, Special issue on Tectonics of oblique plate boundary systems 693, Part B, 327–339.

Grove, T., Parman, S., Bowring, S., Price, R., Baker, M., 2002. The role of an H2O-rich fluid component in the generation of primitive basaltic andesites and andesites from the Mt. Shasta region, N California. Contrib Mineral Petrol 142, 375–396. doi:10.1007/s004100100299

Hewitt, S., 1969. Geology of the Fly Creek Quadrangle and theNorth Half of the Round Butte Dam Quadrangle, Oregon (M.S.). Oregon State University, Corvallis, Oregon.

Hildreth, W., 2007. Quaternary Magmatism in the Cascades - Geologic Perspectives. U.S. Geological Survey Professional Paper 1744, Professional Paper.

Hughes, G.R., Mahood, G.A., 2011. Silicic calderas in arc settings: Characteristics, distribution, and tectonic controls. Geological Society of America Bulletin 123, 1577–1595. doi:10.1130/B30232.1

Karakas, O., Dufek, J., 2015. Melt evolution and residence in extending crust: Thermal modeling of the crust and crustal magmas. Earth and Planetary Science Letters 425, 131–144. doi:10.1016/j.epsl.2015.06.001

Kendall, J.-M., Stuart, G.W., Ebinger, C.J., Bastow, I.D., Keir, D., 2005. Magma-assisted rifting in Ethiopia. Nature 433, 146–148. doi:10.1038/nature03161

Kuehn, S.C., Foit Jr., F.F., 2006. Correlation of widespread Holocene and Pleistocene tephra layers from Newberry Volcano, Oregon, USA, using glass compositions and numerical analysis. Quaternary International, Linking African palaeoenvironments and modern environments: PAGES Workshop 148, 113–137. doi:10.1016/j.quaint.2005.11.008

Kuehn, S.C., Froese, D.G., Shane, P.A.R., 2011. The INTAV intercomparison of electron-beam microanalysis of glass by tephrochronology laboratories: Results and recommendations. Quaternary International, Enhancing tephrochronology and its application (INTREPID Project): Hiroshi Machida commemorative volume 246, 19–47. doi:10.1016/j.quaint.2011.08.022

Kuiper, K.F., Deino, A., Hilgen, F.J., Krijgsman, W., Renne, P.R., Wijbrans, J.R., 2008. Synchronizing Rock Clocks of Earth History. Science 320, 500–504. doi:10.1126/science.1154339

Lopez, W., 2016. Post 4.5 Ma Erosionally Driven Rock Uplift and Landscape Evolution of the Cascades Range in the Pacific Northwest. Presented at the AGU Faqll Meeting, San FRancisco, CA.

Lowe, D.J., 2011. Tephrochronology and its application: A review. Quaternary Geochronology 6, 107–153. doi:10.1016/j.quageo.2010.08.003

Meigs, A., Scarberry, K., Grunder, A., Carlson, R., Ford, M.T., Fouch, M., Grove, T., Hart, W.K., Iademarco, M., Jordan, B., Milliard, J., Streck, M.J., Trench, D., Weldon, R., 2009. Geological and geophysical perspectives on the magmatic and tectonic development, High Lava Plains and northwest Basin and Range. Field Guides 15, 435–470. doi:10.1130/2009.fld015(21)

Mullineaux, D.R., 1996. Pre-1980 tephra-fall deposits erupted from Mount St. Helens, Washington. U.S. Geological Survey Professional Paper 1563.

Perkins, M.E., Brown, F.H., Nash, W.P., Williams, S.K., McIntosh, W., 1998. Sequence, age, and source of silicic fallout tuffs in middle to late Miocene basins of the northern Basin and Range province. Geological Society of America Bulletin 110, 344–360. doi:10.1130/0016-7606(1998)110<0344:SAASOS>2.3.CO;2

Perkins, M.E., Nash, W.P., Brown, F.H., Fleck, R.J., 1995. Fallout tuffs of Trapper Creek, Idaho—A record of Miocene explosive volcanism in the Snake River Plain volcanic province. Geological Society of America Bulletin 107, 1484–1506. doi:10.1130/0016-7606(1995)107<1484:FTOTCI>2.3.CO;2

Phipps Morgan, J., Ranero, C.R., Vannucchi, P., 2008. Intra-arc extension in Central America: Links between plate motions, tectonics, volcanism, and geochemistry. Earth and Planetary Science Letters 272, 365–371. doi:10.1016/j.epsl.2008.05.004

Pitcher, B.W., Kent, A.J.R., Grunder, A.L., Duncan, R.A., 2017. Frequency and volumes of ignimbrite eruptions following the Late Neogene initiation of the Central Oregon High Cascades. Journal of Volcanology and Geothermal Research 339, 1–22. doi:10.1016/j.jvolgeores.2017.04.019

Pollard, A.M., Blockley, S.P.E., Ward, K.R., 2003. Chemical alteration of tephra in the depositional environment: theoretical stability modeling. J. Quaternary Sci. 18, 385–394. doi:10.1002/jqs.760

Priest, G.R., 1990. Volcanic and tectonic evolution of the Cascades Volcanic Arc, central Oregon. Journal of Geophysical Research: Solid Earth 95, 19583–19599. doi:10.1029/JB095iB12p19583

Priest, G.R., Woller, N.M., Ferns, M.L., 1987. Geologic Map of the Breitenbush River Area, Linn and Marion Counties, Oregon. GMS-060.

Rowland, J.V., Wilson, C.J.N., Gravley, D.M., 2010. Spatial and temporal variations in magma-assisted rifting, Taupo Volcanic Zone, New Zealand. Journal of Volcanology and Geothermal Research, Making and Breaking the Arc: a volume in honour of Professor John Gamble 190, 89–108. doi:10.1016/j.jvolgeores.2009.05.004

Scarberry, K.C., Meigs, A.J., Grunder, A.L., 2010. Faulting in a propagating continental rift: Insight from the late Miocene structural development of the Abert Rim fault, southern Oregon, USA. Tectonophysics, Extensional Tectonics in the Basin and Range, the Aegean, and Western Anatolia 488, 71–86. doi:10.1016/j.tecto.2009.09.025

Sherrod, D. R., Taylor, E. M., Ferns, M. L., Scott, W. E., Conrey, R. M., Smith, G. A., 2004. Geologic Map of the Bend 30-× 60-Minute Quadrangle. Central Oregon. US Geological Survey Geologic Investigations Series Map I-2683.

Smith, G.A., 1986. Stratigraphy, sedimentology, and petrology of Neogene rocks in the Deschutes basin, central Oregon : a record of continental-margin volcanism and its influence on fluvial sedimentation in an arc-adjacent basin (Ph.D.). Oregon State University, Corvallis, Oregon.

Smith, G.A., Snee, L.W., Taylor, E.M., 1987. Stratigraphic, sedimentologic, and petrologic record of late Miocene subsidence of the central Oregon High Cascades. Geology 15, 389–392. doi:10.1130/0091-7613(1987)15<389:SSAPRO>2.0.CO;2

Stensland, D.E., 1970. Geology of part of the northern half of the Bend quadrangle, Jefferson and Deschutes counties, Oregon (M.S.). Oregon State University, Corvallis, Oregon.

Stensland, D.E., 1969. Geology of part of the northern half of the Bend quadrangle, Jefferson and Deschutes counties, Oregon (M.S.). Oregon State University, Corvallis, Oregon.

Tanton, L.T.E., Grove, T.L., Donnelly-Nolan, J., 2001. Hot, shallow mantle melting under the Cascades volcanic arc. Geology 29, 631–634. doi:10.1130/0091-7613(2001)029<0631:HSMMUT>2.0.CO;2

Taylor, J.R., 1982. An introduction to error analysis: the study of uncertainties in physical measurements. University Science Books.

Trench, D., Meigs, A., Grunder, A., 2012. Termination of the northwestern Basin and Range province into a clockwise rotating region of transtension and volcanism, southeast Oregon. Journal of Structural Geology 39, 52–65. doi:10.1016/j.jsg.2012.03.007

Trimble, J., Meigs, A.J., Wannamaker, P.E., 2015. A REFINED STRUCTURAL MODEL OF THE OREGON CASCADES ARC-BACKARC TECTONIC PROVINCE. Presented at the Geologic Society of America Annual Meeting, Geological Society of America Abstracts with Programs, Baltimore, MD, p. 150.

Tryon, C.A., Kuhn, S.L., Slimak, L., Logan, M.A.V., Balkan-Atlı, N., 2011. Scale in tephrostratigraphic correlation: An example from Turkish Pleistocene archaeological sites. Quaternary International, Enhancing tephrochronology and its application (INTREPID Project): Hiroshi Machida commemorative volume 246, 124–133. doi:10.1016/j.quaint.2011.05.039

VanVooris, C.W., Morgan, B.L., 2007. Understanding power and rules of thumb for determining sample sizes. Tutorials in Quantitative Methods for Psychology 3, 43–50.

Wallace, L.M., Beavan, J., McCaffrey, R., Darby, D., 2004. Subduction zone coupling and tectonic block rotations in the North Island, New Zealand. J. Geophys. Res. 109, B12406. doi:10.1029/2004JB003241

Weinfurt, K.P., 1995. Multivariate analysis of variance, in: Grimm, L.G., Yarnold, P.R. (Eds.), Reading and Understanding Multivariate Statistics. American Psychological Association, Washington, DC, US, pp. 245–276.

WoldeGabriel, G., Hart, W.K., Heiken, G., 2005. Innovative tephra studies in the East African Rift System. Eos Trans. AGU 86, 255–255. doi:10.1029/2005EO270003

Wolfenden, E., Ebinger, C., Yirgu, G., Renne, P.R., Kelley, S.P., 2005. Evolution of a volcanic rifted margin: Southern Red Sea, Ethiopia. Geological Society of America Bulletin 117, 846–864. doi:10.1130/B25516.1

4. Geochemical Evidence for Extension-driven Magmatic Processes in the Late Miocene Deschutes Formation, Central Oregon

4.1 Introduction

The chemical composition of primitive magmas from a single arc may be highly variable both spatially and temporally, and may result from differences in tectonic influences, subduction rate, or composition of the slab or mantle wedge (e.g. Schmidt et al., 2008). Changes to any of these variables may lead to significant differences in the primitive mantle melts that enter the subarc crust which can affect all aspects of the magmatic system. It is now well accepted by the geologic community that the primary driver for arc volcanism is fluid-flux melting of the mantle wedge due to the transfer of volatiles from the slab (e.g. McColloch and Gamble, 1991). The high H_2O content of melt inclusions in arc basalts (average ~4 wt. %, Plank et al., 2013), common hydrous liquid lines of descent (Sisson and Grove, 1993), and enrichment in fluid-mobile elements (e.g. Ayers, 1998; Pearce and Parkinson, 1993) in arcs worldwide corroborate this model.

Conversely, some studies have provided evidence of nearly anhydrous mantle melting beneath arcs, including the Indonesian arc (Sisson and Bronto, 1998) and the Aleutian arc (Draper and Johnston, 1992), indicating that decompression melting may also play a role in mantle melting beneath arcs. Numerical and geophysical modeling demonstrates that slab-induced flow of hot mantle material into the wedge results in decompression melting that can be focused beneath the arc due to erosion of the sub-arc lithosphere and the existence of a cold corner that can block mantle flow trenchward of the arc (e.g. Conder et al., 2002; Eberle et al., 2002; Kelemen et al., 2003). While the role of decompression in back arc volcanism is widely demonstrated (Kellie et al., 2006; Pearce and Stern, 2006; Saunders and Tarney, 1984), there is geochemical evidence from numerous arc fronts that both flux melting and decompression melting occurred contemporaneously and in close spatial association, including in Guatemala, New Zealand, Mexico, and California (Cameron et al., 2003; Cervantes and Wallace, 2003; Grove et al., 2002; Righter, 2000).

The relative contributions of flux and decompression melting mechanisms on arc systems greatly impact the water content of primary magmas, oxidation states of magmatic systems and the magmatic and volatile flux into the arc crust (Arculus, 1994). These processes, in turn, influence the geochemistry, magmatic evolution, and eruptive style of an arc (e.g. Deering et al., 2010).

The immense influence of water content on crystallizing assemblages and differentiation trends (i.e. tholeiitic vs. calc-alkaline) of arc magmas has been demonstrated by many authors for over a half-century (Yoder and Tilley, 1962; Miyashiro, 1974; Sisson and Grove, 1993). Although calc-alkaline basalts, indicative of flux melting (Sisson and Grove, 1993) are nearly ubiquitous in arcs world-wide, tholeiitic basalts are also common at many arcs, indicative of the drier process of decompression melting (Jakes and Gill, 1970). In addition to affecting mantle melts, studies have also shown that the H_2O content and oxygen fugacity (fO_2) of a magmatic system has a significant effect on the composition of more silicic melts, whether derived by crustal melting (Sisson et al., 2005) or fractional crystallization processes (Deering et al., 2010). Thus, felsic magmas can by roughly characterized by two end-member rhyolite types, those indicating formation within "arc-typical" cold-wet-oxidizing environments (R1), and those indicating formation within hot-dry-reduced environments (R2). Although R2 rhyolites are typically associated with continental rift or hot spot tectonic settings (Bachmann and Bergantz, 2008), they are also demonstrated to occur within arcs experiencing significant extension such as the Taupo Volcanic Zone (TVZ) (Deering et al., 2011) and NW Costa Rica (Deering et al., 2012). Temporal and spatial variations in the proportion of these endmember rhyolite types erupted in intra-arc rift settings indicate differences in the temperature, H_2O content and/or fO_2 conditions of the magmatic system, and may reflect the relative influx of cold-wet-oxidized primitive basalts produced by fluid-flux melting of the mantle, or hot-dry-reduced basalts from decompression mantle melting.

In addition to potentially effecting the composition of silicic magmas, intra-arc extension may also initiate increased production of silicic magmas. For example, the Sierra Madre Occidental (Ferrari et al., 2002), Tepic-Zacoalco Rift (Frey et al.,

2007), Southern Aegean active volcanic arc (Francalanci et al., 2005; Papazachos and Kiratzi 1996) and the TVZ (Deering et al., 2011) systems all experienced heightened silicic magma generation and increased explosive volcanic activity following an increase in or initiation of extension. In fact, approximately 70% of all arc calderas worldwide (n=108) and 84% of calderas >15km diameter are found in regions with extensional stress regimes (Hughes and Mahood, 2011). Extension may cause increased basaltic flux into the upper to middle crust, which leads to more crustal melting and/or fractionation, thereby producing larger volumes of silicic magma (e.g. Jellinek and DePaolo, 2003; Price et al., 2005).

Extension is also occurring within the Oregon and Northern California portion of the Cascades arc, with extension rates increasing southwards (Wells et al., 1998). The Oregon forearc is rotating clockwise approximately 2°/m.y. (McCaffrey et al., 2007) around a pole located in eastern Oregon or Washington (Trench et al., 2012 and references therein). Pluton migration studies coupled with paleomagnetic evidence indicate that this rotation has been continuous since the mid-Miocene (Wells and Heller, 1988; Wells and McCaffrey, 2013). A marked increase in hydrothermal heat discharge and crustal heat flow (Fig. 4.1) south of the 44.75°N latitude (slightly south of Mt. Jefferson volcano) is consistent with extensional stresses (Ingebritsen and Mariner, 2010). The central Oregon High Cascades, which stretches between Mt Jefferson volcano and the Sisters volcanic complex, is located within an extensional depression, called the High Cascades graben. This intra-arc extensional feature is bounded to the east by Green ridge, a 600-meter westward dipping normal fault scarp, and to the west by the Horse Creek fault system (Sherrod et al. 2004). Conrey et al. (2002, 2004) propose that this graben represents a northward-propagating intra-arc rift that terminates south of Mt. Hood, while others have asserted that the Central Oregon High Cascades graben actually represents the northwestern-most expression of Basin and Range extension based on the evidence that major westward-dipping normal faults similar to Green Ridge are lacking in northern Oregon (Scarberry et al., 2010; Trench et al., 2012). Regardless of the tectonic cause, the current extension rate within the central Oregon portion of the arc is ~1 mm/yr, (Wells et al., 1998).

However, Conrey et al. (2002) suggest the extension rate may have been ~3 mm/yr between 7.5 and 5 Ma.

Approximately 7.5 Ma, the central Oregon Cascades arc underwent a marked change from relatively low eruptive rates of andesitic lava flows to eruptions of large volumes of LKT basalts, signaling the onset of intra-arc extension (Smith et al., 1987; Priest, 1990). At this time, volcanism also shifted eastward from the Western Cascades (~35-7 Ma), to the High Cascades arc axis along which volcanism continues today (du Bray and John, 2011; Priest, 1990). Approximately 1.25 m.y. after the initiation of the High Cascades, the arc began erupting significant volumes of pyroclastic material that was deposited in the aggrading Deschutes Basin to the east of the arc and preserved within the Deschutes Formation (Fig. 4.1). The

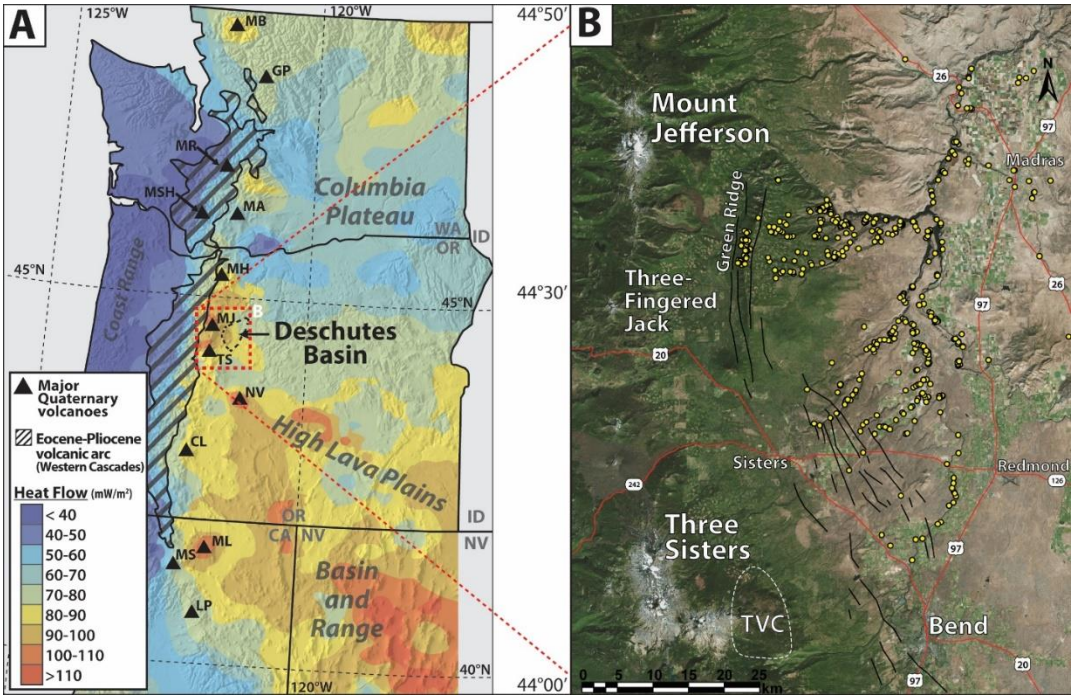

Figure 4.1: Location of Deschutes Basin field area in central Oregon, USA. (A) Heat flow map indicating the positions of the Western Cascades ancestral arc and the major Quaternary High Cascades volcanoes. Position of Deschutes Basin to the east of the central Oregon Cascades, is near the intersection with the High Lava Plains province of southeastern Oregon. Heat flow map (Ingebritsen and Mariner, 2010) shows the highest heat flow in the Cascades is between Mount Jefferson and Three Sisters. (B) Sampling locations for geochemical analyses are shown by yellow dots. Green Ridge, which marks the eastern edge of the High Cascades Graben is shown along with faults to the south which belong to the Sisters Fault zone. The approximate position of the Tumalo Volcanic Center (TVC) is also depicted.

Deschutes Formation, a well-preserved layer-cake stratigraphy of lava flows, tuffs and volcanoclastic sediments (e.g. Smith, 1986), provides an excellent record of the initial ~2.2 m.y. of High Cascades volcanism (~7.5-5.3 Ma). However, the Deschutes Basin was largely cutoff from the arc approximately 5.3 Ma due to normal faulting and subsidence along Green Ridge, which prevented further accumulation of ignimbrites and arc-derived lavas within the Deschutes Formation (Smith et al., 1987). Despite truncation from the High Cascades arc axis ~5.3 Ma, the Deschutes formation stratigraphic sequence contains tuff deposits from nearly 150 different explosive eruptions, all between 6.25 and 5.45 Ma. This accumulation of eruptive material equates to the highest silicic production rate in the region since at least 17 Ma (Pitcher et al., 2017a, 2017b). The timing of this pulse of silicic magmatism, approximately 1.25 Ma after the onset of extension, is consistent with thermo-mechanical modeling that suggests that in an arc undergoing extension. a maximum crustal melting efficiency is reached after a thermal maturation period of ~1.2 m.y. (Karakas and Dufek, 2015). Thus, Pitcher et al. (2017a) suggest, based on the timing of these events, that an extension-driven increase in basaltic flux to a more fusible portion of crust, east of where volcanism had previously been focused, could have been responsible for the atypical pulse of silicic volcanism.

The purpose of this study is to determine the magmatic processes that led to the production and eruption of these unusually large volumes of silicic magma during the initial stages (6.25-5.45 Ma) of the High Cascades arc, and assess what influence intra-arc extension had on these processes. Here we compare the geochemistry of Deschutes Formation tuffs to the eruptive products of the Quaternary High Cascades volcanoes and Early to mid-Miocene Western Cascades to determine temporal changes in the tectonic influences and magmatic processes leading to such an unusual pulse of volcanism. Understanding these processes and how they differ from those of the Quaternary, is critical to our understanding of the complete magmatic evolution of the Cascades arc.

4.2 Methods

4.2.1 Major and trace element analysis of tephra glass

For this study, we used tephra glass major and trace element data presented in Pitcher et al. (2017b). This dataset includes *in situ* electron microprobe (EMP) data and laser ablation inductively coupled plasma mass spectrometer (LA-MC-ICPMS) data collected on fresh pumice glass from 159 ignimbrite samples and 70 tephra-fall samples from the Deschutes Formation. We collected approximately 10-15 analyses for each sample, and care was taken to analyze the same glass spot with LA-ICP-MS as was analyzed with EMP. Analyses with major element totals <90% and those that had major or trace elements indicative of analysis of crystalline phases were removed, as described in Pitcher et al. (2017b). After removing these outliers, the dataset includes a total of 1,313 major element analyses and 1,289 trace element analyses. All analysis parameters are given in Pitcher et al. (2017b).

4.2.2 Major element analysis of plagioclase

We collected major element data for plagioclase using the EMP method; analysis parameters are described in Pitcher et al. (2017b). For this study, we collected data from 218 plagioclase crystals within 22 samples of 11 different laterally extensive "marker" ignimbrite units, including 2 from the regional Simtustus Formation (12-15 Ma, Smith, 1986). Our subset of samples was carefully chosen such that it included: 5 units from each source region (north and south), the whole stratigraphic range, and the whole compositional range.

For each plagioclase, we analyzed the core and rim, and at least 1 intermediate point. More analyses were collected for crystals with significant zoning patterns apparent in backscatter electron (BSE) images. We removed 47 analyses that had totals <90% or had anomalously high FeO* and low Al_2O_3 indicative of analysis of a high proportion of glass inclusions. After removing these data, our plagioclase dataset contains 654 analyses.

4.2.2 Plagioclase Oxygen isotopes- Laser Fluorination

We collected oxygen isotope data from plagioclase phenocrysts using the laser fluorination method. Analyses were performed at the University of Oregon stable isotope laboratory using a 35W NewWave IR laser and a Thermo-Scientific MAT 253 mass spectrometer. Specific analysis parameters and description of the filtering processes and laboratory set up can be found in Bindeman et al. (2014).

We analyzed plagioclase from the same 22 samples of 11 ignimbrite units for which we collected plagioclase major element data. Separation and acid leaching of plagioclase was completed using the same methods described in Pitcher et al. (2017a). Once separated, plagioclase were examined under binocular microscope and only crystals (250-500 μm) that were completely free of melt inclusions and adhered glass were chosen for analysis. For each sample, 1.25-1.35 mg (~10-15 plagioclase crystals) were chosen. We analyzed two separate aliquots from each sample, and for those samples with a standard error >0.04, we analyzed 1-2 additional aliquots. Analysis occurred over the course of three days, and on each day, 4-7 UOG garnet standards ($\delta^{18}O$=6.52‰) were analyzed along with the unknowns. Standard error of repeat analyses of UOG standard each day was <0.1% Unknown $\delta^{18}O$ were adjusted using the average value of the standards for the day.

4.2.3 In situ plagioclase and glass Pb isotopes by LA-MC-ICPMS

We collected plagioclase and glass Pb isotope data using the Laser ablation multi-collector inductively coupled plasma mass spectrometer (LA-MC-ICP-MS) method in W. M. Keck Collaboratory for Plasma Spectrometry at Oregon State University. A Photon Machines 193nm ArF laser was used to ablate in situ plagioclase, and was connected to a NuPlasma MC-ICP-MS with parallel Faraday cup and ion counter detectors, located in a clean lab. Specific operating conditions can be found in Table 4.1, and further explanation of the MC-ICP-MS setup can be found in Kent (2008).

Since Pb concentrations in plagioclase (~An30) tend to be relatively low, we conducted a series of experiments, altering the repetition rate (10-25 Hz), scan speed

(5-15 µm/s), and spot size (50-85µm) to maximize Pb signal on plagioclase. Not surprisingly, we found that larger spot sizes, higher rep rates, and faster scan speed produced higher counts (e.g. 85 µm, 25 Hz, and 15 µm/sec generally yielded 5-10 mV of ^{208}Pb). Thus, for all plagioclase analyses, we used 25 Hz and 85 µm spots, and tried to maximize the scan speed, such that we still had >35 seconds of analysis time. Integrating over longer analysis time leads to smaller standard errors of analysis. Where possible, we also analyzed tephra glass. Since Pb concentration is higher in glass (2-6 times higher 208Pb mV than with plagioclase), slower speeds and shorter distances could be used in these cases. We analyzed pure epoxy and found that there was a signal only for masses 202 and 205, with no signal for 206, 207 or 208. Thus, analysis of epoxy during ablation of pumice glass is not likely to introduce any contaminant; it just simply reduces counts associated with glass. Prior to analysis, we did a pre-ablation laser scan, such that the uppermost ~3-5µm was removed from the analysis area of each plagioclase to avoid problems with contamination. Before each analysis, there was 30 seconds of wash time and then 30 seconds of background collection.

Table 4.1: Acquisition settings for Pb isotopes.

Instrumentation	NuPlasma MC-ICP-MS double focusing mass spectrometer with ESA, fixed collector array and Edwards E2 M80"Big80" 80 L min^{-1} rotary pump
Forward power	1300 W
Reflected power	<5 W
Cones	Nickel (NuPlasma Type B)
Accelerating voltage	4000 V
Analyzer vacuum	~5 × 10^{-9} mbar
Argon gas flows	
Plasma	13.00 L min^{-1}
Cool	~0.70 L min^{-1}
Mix	~0.75 L min^{-1}
Sample introduction (laser)	Photon Machines ArF Excimer laser
Sweep gas	He
Flow rate	0.40 L min^{-1}
Laser parameters	
Spot size	85 µm
Translation rate	5 µm s^{-1}
Pulse frequency	25 Hz
Pulse energy	~12 J cm^{-2}

In addition to NIST-612 glass, which we used as the calibration standard, we also collected data for the USGS basalt glass BCR-2G as a secondary standard to check the accuracy of our calibration. For each experimental run, we analyzed both standards between every two unknowns; average runs included ~6-8 analyses of each standard and ~10-15 unknowns. We corrected for instrumental mass bias by calculating the fractionation factor from analysis of the NIST-612 standard during each run using an exponential correction factor as in Kent (2008). In general, no consistent instrument drift was observed in standards over the 48 hours of analysis. ^{204}Pb counts were so low for plagioclase, this data is unusable, and thus no correction for isobaric interference by ^{204}Hg was necessary.

Uncertainty in these Pb isotope data come from a variety of sources. There is the variability of counts during analysis, uncertainty involved in calculation of the fractionation factor, and uncertainty in the accepted value for the calibration standard. To account for all of these, we used calculus-based methods to propagate the uncertainty. Details of such calculations can be found in Appendix 4.1.

Raw measured ^{208}Pb/^{206}Pb for NIST-612 (published value=2.1651) generally ranged from 2.1942 to 2.1997 (1.3-1.6% higher than the accepted value), and standard errors within a given run (~6-8 analyses) were always <0.0002 (Table 4.2). After mass bias correction, BCR-2G ^{208}Pb/^{206}Pb and ^{20}7Pb/^{206}Pb values were < ±0.2% from the published values (2.063 and 0.832, respectively).

Table 4.2: Primary and secondary standard analyses for each of 11 runs on the LA-MC-ICPMS. Values represent averages of n analyses for that run, with n given in the table.

Run	^{208}Pb/^{206}Pb	% error	Std error	n	corrected ^{208}Pb/^{206}Pb	% error	corrected ^{208}Pb/^{206}Pb	%error
1	2.1942	1.34	0.0002	6	2.0670	0.19	0.8312	-0.10
2	2.1950	1.38	0.0002	7	2.0642	0.06	0.8324	0.05
3	2.1951	1.39	0.0002	6	2.0643	0.06	0.8332	0.14
4	2.1955	1.40	0.0001	6	2.0634	0.02	0.8328	0.10
5	2.1957	1.41	0.0001	7	2.0630	0.00	0.8322	0.02
6	2.1957	1.41	0.0001	6	2.0634	0.02	0.8328	0.10
7	2.1969	1.47	0.0002	5	2.0639	0.04	0.8322	0.02
8	2.1976	1.50	0.0001	6	2.0636	0.03	0.8328	0.10
9	2.1951	1.39	0.0001	5	2.0645	0.07	0.8330	0.12
10	2.1972	1.48	0.0001	5	2.0653	0.11	0.8330	0.12
11	2.1982	1.53	0.0001	3	2.0624	-0.03	0.8320	0.00
12	2.1997	1.60	0.0002	5	2.0642	0.06	0.8329	0.11

We collected a total of 75 Pb isotope analyses on 62 plagioclase phenocrysts, as well as 15 glass analyses, from 6 Deschutes Formation ignimbrites and 1 Simtustus Formation ignimbrite. We analyzed 2 different pumice populations of Six Creek Tuff (60 and 68 wt.% SiO_2), and 4 samples of 2 different flow units of McKenzie Canyon Tuff (57, 70, 71 and 71 wt. % SiO_2). Three ignimbrites from each source region (north and south) were analyzed and pumice compositions spanned the whole ignimbrite compositional range (57, 59, 64, 68,70,71,71, 73, 75 wt.% SiO_2). In addition, we collected 3 groundmass analyses on a Deschutes Formation basalt, and 6 analyses on each of two granulite-facies metamorphic xenoliths and a granodiorite xenolith, all found within the Balanced Rocks Tuff (provided by Richard Conrey).

4.2.4 MELTS modeling

We used MELTS thermodynamic phase equilibria modeling (Ghiorso and Sack, 1995) to investigate, to a first order, whether Deschutes Formation rhyolites could be produced by pure FC processes. We tested three different parental compositions from the Deschutes Formation: the most primitive calk-alkaline basalt, the Juniper Canyon Basalt (MgO=11.62 wt. %, FeO*/MgO=0.78, Al_2O_3/TiO_2=17.5), the most primitive LKT (MgO=9.03 wt.%, FeO*/MgO=1.06, K_2O/TiO_2=0.26), and a 50:50 mix of the two (Smith, 1986; Schmidt et al., 2008). In addition, we did 5 runs using average MORB (Gale et al., 2013) as a parental composition. We began with the LKT magma and attempted various combinations of pressure (0.1, 0.5, 1, 2.5, and 5 kbar), H_2O content (0, 1, 2, 3, and 4 wt. %) and oxygen fugacity (NNO, QFM, and QFM-1). We found that only 5 combinations of pressure and H_2O, at all three fO_2 (15 total combinations) were feasible and only tested these conditions on the other parental melts. In total, we had 45 successful models that ran to completion without reaching a quadratic minimization error (Appendix 4.4). We then visually compared calculated melt compositions to data from all tuffs erupted from the northern source.

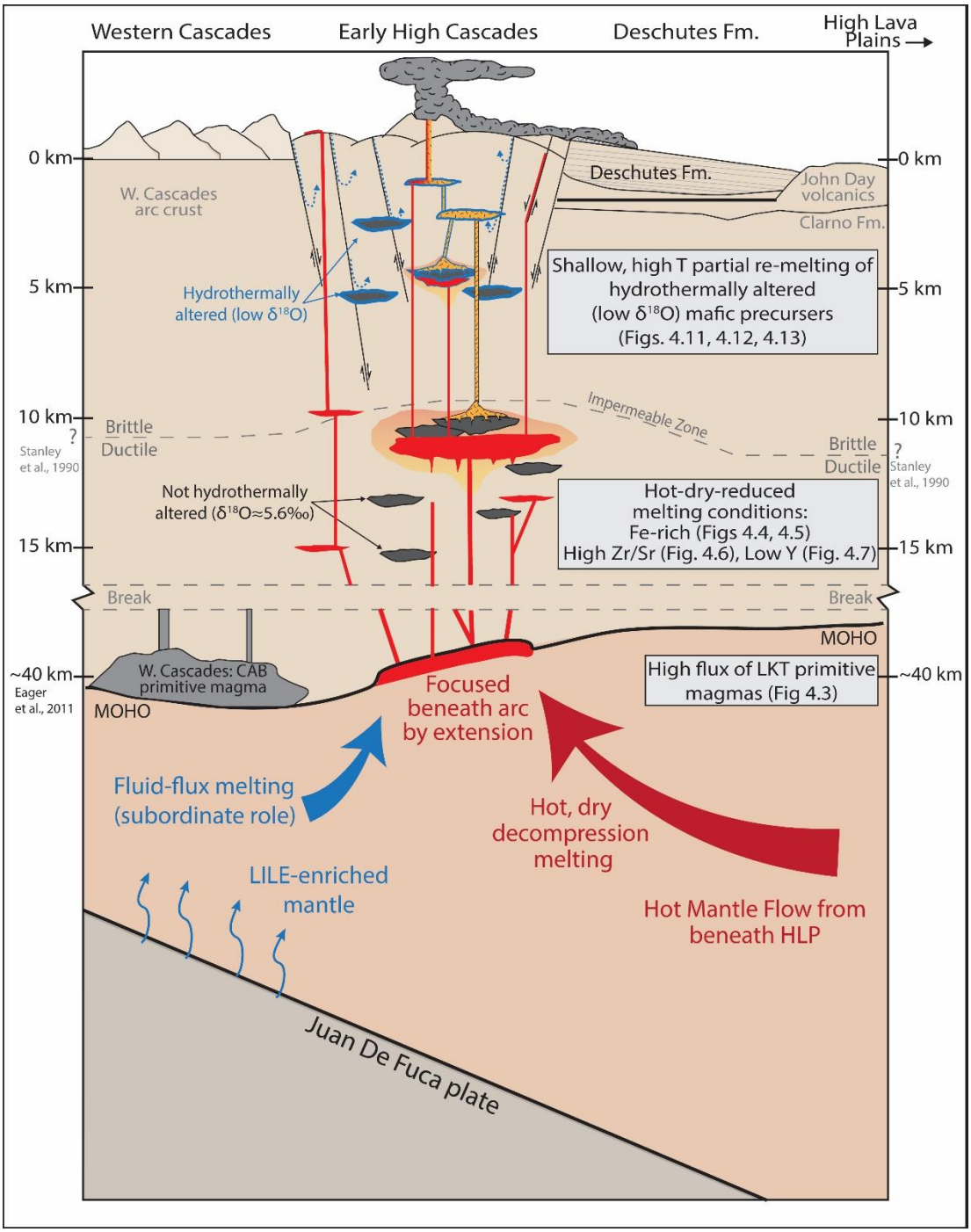

Figure 4.2: Schematic diagram depicting the inferred petrogenesis of Deschutes Formation silicic magmas. Evidence for each portion of this diagram is provided in the referenced figures. Note that extension plays an important role at all levels of the magmatic system. Actual depths are not well-constrained.

4.3 Results and Discussion

4.3.1 The influence of extension on the Deschutes Formation magmatic system

In the following sections, we will move progressively upwards in the magmatic system providing geochemical evidence of the influence that extension had on all aspects of magmatic evolution (Fig. 4.2). We will begin with evidence of decompression mantle melting, then discuss the dry and reduced state of the magmatic system, and then substantiate shallow crustal melting as the dominant process to produce Deschutes Formation rhyolites.

4.3.1.1 Influence of decompression mantle melting

Although flux melting of the mantle is the primary driver of many arc magmatic systems, geochemical evidence from basalts of the Deschutes Formation suggests that decompression melting played a critical role in producing the high magmatic flux into the crust during this time.

Primitive arc basalts (SiO_2<52 wt.%, MgO>6%, and Mg#>55, Leeman et al., 2005) offer insight into the composition and melting processes of the mantle beneath arcs because they are relatively unmodified by assimilation and fractional crystallization (AFC) processes. Compositional heterogeneity of High Cascades primitive basalts along-arc and even within a given volcano have been recognized by many authors (e.g. Bacon et al. 1997; Conrey et al. 1997; Leeman et al., 1990, 2005; Mullen et al. 2017; Rowe et al., 2009; Schmidt et al. 2008). These primitive basalts are largely defined by three compositional end-members: low-K tholeiites (LKTs, also known as high-alumina olivine tholeiites, HAOTs), calc-alkaline basalts (CABs), and intraplate-type basalts (IPBs, also known as HFSE-type and ocean island basalt, OIB-types) (Mullen et al., 2017) (Table 4.3). The origin of these endmember types across the Cascades arc is the subject of debate, and while many authors have invoked heterogenous mantle compositions (e.g. Bacon et al., 1997; Schmidt et al., 2008), recent high-precision isotopic and trace element work suggests that most of compositional heterogeneity is the result of differing slab/ sediment compositions and input (Mullen et al., 2017). In general, CABs are typical of arcs, and have higher

Al_2O_3, SiO_2, K_2O LILE, LREE, and melt inclusion water content, but lower MgO, FeO, HFSE and HREE, indicative of the involvement of slab fluids and their production primarily by fluid-flux melting of the mantle (Grove et al., 2002; Mullen et al., 2017). In contrast, LKTs have lower K_2O and trace element compositions similar to N-MORB, but with slightly higher LILE, and is generally associated with decompression mantle melting of mantle that has been partially influenced by fluids (Schmidt et al., 2008; Mullen et al., 2017). IPBs tend to have higher LILE and LREE than CABs, with no HFSE-depletion (Table 4.3), and tend to be associated with low degree melting of enriched mantle with little to no slab influence (Mullen et al., 2017). These primitive magma types can provide insight into the relative importance of different mantle melting processes that occur beneath the Cascades arc.

To compare the relative proportions of primitive basalt types erupted in the Cascades through time, we compiled major and trace element data from the literature for the Deschutes Formation, Quaternary High Cascades, Newberry volcano, and Middle Eocene-Late Miocene Western Cascades, using the EarthChem and GeoRoc databases, as well as manual data entry. For the Western Cascades, we used the database provided in du Bray and John (2011). In all, we compiled data from 1,224 primitive basalt samples, including 105 Deschutes Formation, 851 from the High Cascades arc, 71 from Newberry volcano and 197 from the Western Cascades. To divide these into the 3 endmember primitive basalt types, we used criteria modified from those of Leeman et al. (2005) and Schmidt et al. (2008) (Table 4.3).

Table 4.3: Criteria used to classify primitive basalts from the literature

	K_2O wt.%	K_2O/TiO_2	Sr/Y	Ba/Nb	Al_2O_3/TiO_2	Nb/Zr
LKT	< 0.5	< 0.4	< 20	< 20	< 11	< 0.15
CAB	> 0.5	> 0.5	>15	> 20	> 9	< 0.09
IPB	> 0.5	0.4-0.6	< 20	< 20	< 11	> 0.09

Our compilation demonstrates that LKTs were the most common Deschutes Formation primitive basalt type (74%) with significantly lower proportion of CABs (26%), and no IPB-type lavas (Fig. 4.3). These LKT lavas lack the high subduction fluid signature (e.g. high Ba/Nb, low Sr/Y) that is typical of arcs (Leeman et al., 2005; Pearce and Stern, 2006). This is very different from the Quaternary High Cascades, that erupted higher proportions of CABs (44%) as well as an appreciable proportion of IPBs (16%). Newberry, a rear-arc Quaternary volcano located 60 km east of the Cascades arc (Fig. 4.1), also has higher proportions of LKTs (51%) compared to CABs (34%), consistent with the importance of decompression melting within the rear-arc (e.g. Till et al., 2013). LKT lavas from the Cascades have been demonstrated to be the product of 6-30% partial melting of dry spinel lherzolite (Baker et al., 1994; Conrey et al., 1997) at high temperatures (1300°C) and shallow depths (11 kbar), close to the base of the crust ~33 km (Bartels et al., 1991). This is consistent with their formation by decompression, rather than flux-melting. Numerous studies have proposed that LKT magma generation beneath the Cascades arc is the result of decompression melting of back-arc mantle source that is

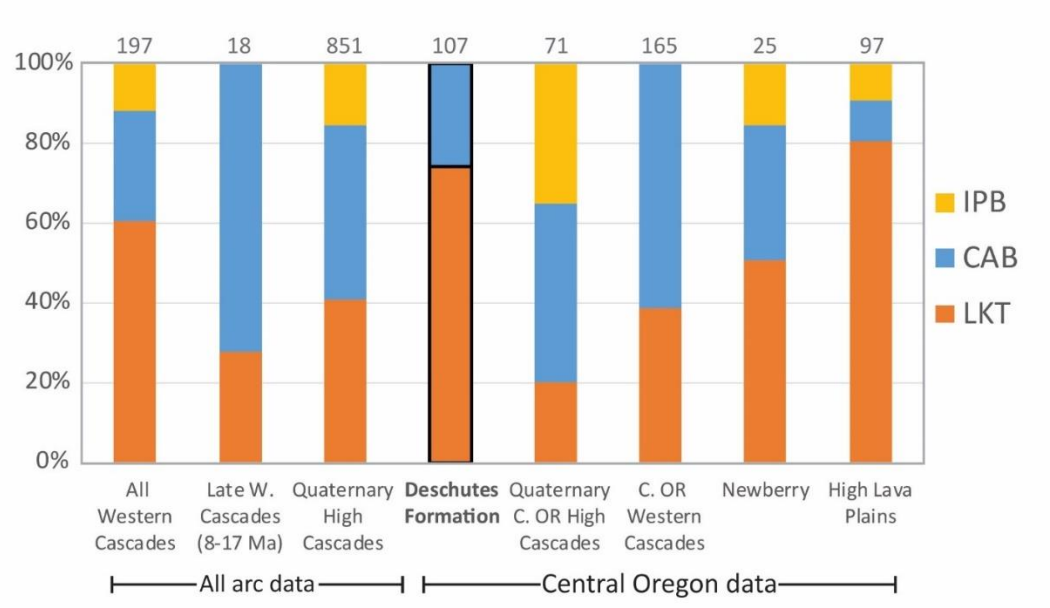

Figure 4.3: Stacked histogram showing proportions of primitive basalt types erupted through time in the Cascades and High Lava Plains. Numbers at top indicate the number of primitive basalt samples which could be confidently classified into one of the three basalt types. Classification scheme is given in Table 1.

significantly less modified by modern subduction fluids, and is driven into the region beneath the arc by subduction-induced corner flow (e.g. Grove et al., 2002; Elkins-Tanton et al., 2001; Till et al., 2013). Thus, these basalts tend to have much lower water contents. Melt inclusions from High Cascades LKT lavas range from 0.04 to 0.2 wt. % H_2O (Le Voyer et al., 2010, and Sisson and Layne, 1993, respectively), compared to those from CABs that, in central Oregon, contain 1.7-3.6 wt.% H_2O (Ruscitto et al., 2010). In summary, unlike the Quaternary High Cascades, lavas of the Deschutes Formation were primarily LKTs indicating that hot and dry decompression was likely the most important mantle melting mechanism during that time.

Ultimately, basaltic flux into the crust is responsible for production of most rhyolites, whether it acts simply as an underplate that provides heat to partially melt overlying crust, or acts as a primary magma that is fractionated to a rhyolite composition (e.g. Vigneresse, 1999, and references therein). The water content of this basalt, then, plays a major role in determining the composition of any felsic magmas that may be produced (Mandler et al., 2014). Thus, the hot and dry nature of the decompression mantle melts (LKTs) that seem to dominate the Deschutes Formation likely have a great influence on the compositions of all magmas within the system.

4.3.1.2 Deschutes Formation Rhyolites: hot, reduced, and "damp"

The magmatic system within the sub-arc crust, including magma, mush zones, and solidified plutons, is generally characterized as being relatively wet and oxidized compared to that of continental rift or hotspot settings (Bachmann and Bergantz, 2008). However, some arcs erupt felsic magmas that reflect processes of generation and modulation within a relatively dry and reduced magmatic system (Deering et al., 2008). Many authors have demonstrated that a relatively hydrous basalt will tend to fractionate along a hydrous (calk-alkaline) liquid line of descent (LLD), while basalts with low water contents will tend to follow a tholeiitic LLD (e.g. Miyashiro, 1974; Sisson and Grove, 1993). Experiments have also demonstrated that partial melting a moderately hydrous (1.7-2.3 wt.% H_2O) medium to high-K basalt in a reduced fO_2 environment (QFM), will produce reduced (NNO to NNO-0.5 log units) dacitic to

rhyolitic liquids (Sisson et al., 2005) that have FeO*/MgO contents that plot within the tholeiitic field of Myashiro (1974). Thus, regardless of whether fractional crystallization or crustal melting is primarily responsible for the production of felsic magmas, the composition of that magma will likely reflect the water content, temperature and oxidation state of the environment in which it formed (Mandler et al., 2014; Sisson and Grove, 1993; Sisson et al., 2005).

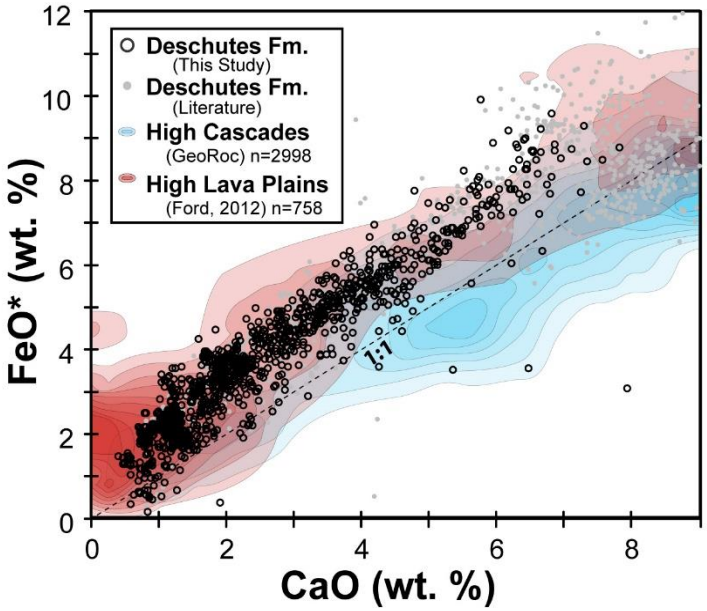

Figure 4.4: FeO* vs CaO of Deschutes Formation (symbols), and fields for the Quaternary High Cascades and High Lava Plains. Darker portions of the fields contain higher density of points.

Deschutes Formation felsic rocks tend to be iron-enriched, which is more typical of tholeiitic differentiation trends than of more arc-typical calk-alkaline trends. Lower H_2O contents of the former type allow for earlier crystallization of plagioclase and later crystallization of Fe-Ti Oxides, and causes such rocks to evolve along a more Fe and Ti-rich LLD (Mandler et al., 2014). The Deschutes rocks have higher FeO* for a given CaO compared to the Quaternary Cascades, and instead, plot much closer to the Fe-rich compositions of High Lava Plains volcanics (Fig. 4.4). The High Lava Plains (HLP) of central and southeastern Oregon form a northwestward-younging trend of bimodal volcanism that swept across Oregon since ~10 Ma and ended near Newberry volcano ~1 Ma, where volcanism continues today (Jordan et al., 2004). Volcanism has been attributed to decompression melting of the mantle due to subduction-induced corner flow of the mantle (Ford et al., 2013; Long et al., 2012; Till et al., 2013). Like the HLP, Deschutes Formation rocks have higher FeO*/MgO

than the Quaternary High Cascades (Fig. 4.5) and plot near the tholeiitic/ calc-alkaline boundary as defined by Myashiro (1974). These rocks plot within the "medium Fe" field of Arculus (2003) compared to the Quaternary High Cascades that plot mostly within the arc-typical "low-Fe" field (Fig. 4.5).

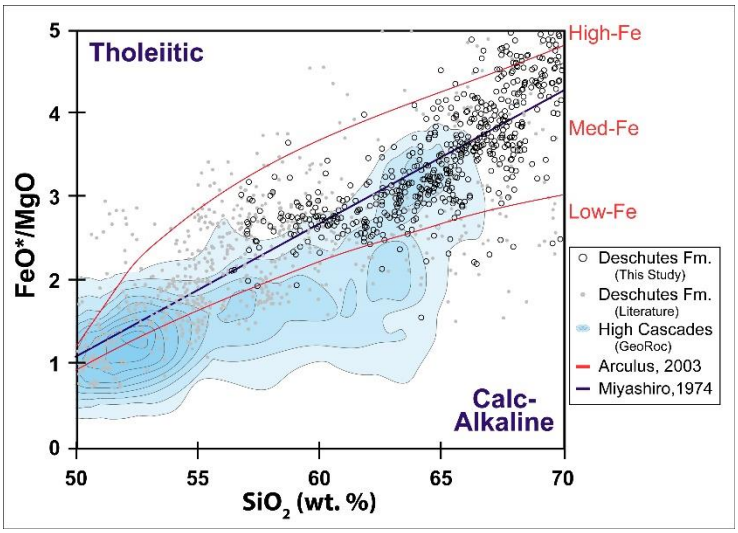

Figure 4.5: Deschutes Formation tends to be higher in FeO*/MgO than most Quaternary High cascades (shown in blue field), and straddle the tholeiitic/calc-alkaline line of Miyashiro (1974).

In addition to being relatively enriched in iron, Deschutes Formation rhyolites demonstrate many other geochemical and petrological characteristics that indicate formation within a relatively hot, dry, and reduced system. Deering et al. (2008, 2010) used multivariate analysis to demonstrate that rhyolites in the Taupo Volcanic Zone (TVZ) fall along a continuum between two endmembers, R1 and R2, that correspond to the "cold-wet-oxidized" and "hot-dry-reduced" source mush types, respectively, of Bachmann and Bergantz (2008). These rhyolite types are also demonstrated to occur in other arcs besides the TVZ, such as NW Costa Rica (Deering et al., 2012). Cold-wet-oxidized (R1) rhyolites tend to be crystal-rich (up to 45%), contain dominant hydrous phases (amphibole ± biotite), have high Sr, but low FeO*/MgO, Y, Zr, Eu/Eu*, and MREE (Deering et al., 2008, 2010). In contrast, hot-dry-reduced (R2) rhyolites tend to be crystal poor (<10%) with an anhydrous mineral assemblage (i.e. 2 pyroxenes), have low Sr, but high FeO*/MgO, Y, Zr, Eu/Eu*, and MREE.

Deschutes Formation rhyolites exhibit all of these R2-type characteristics. Ignimbrites are crystal poor, ranging from <1% to 10% crystallinity (most are <5%), with an anhydrous assemblage of plagioclase and two pyroxenes; amphibole is

extremely rare (Pitcher et al., 2017a). Despite having lower water contents, the higher temperature of R2 rhyolites result in much lower viscosity, more efficient crystal-melt separation, and thus eruption with lower crystal contents (Christiansen, 2005). High Y content of Deschutes Formation tuffs indicates that amphibole is not stable due to the dry LLD or melting conditions, and that the paucity of amphibole phenocrysts is not simply a result of the phase being efficiently fractionated or left behind as a restite during melting (Fig. 4.6). In addition, Deschutes Formation felsic rocks have high Zr/Sr contents (>2), more similar to those of the HLP, Iceland, and Miocene Colorado Rift (Miller, 2014), compared to the low Zr/Sr (<<1) of the High Cascades (Fig.4.7). Higher water contents in the latter result in less plagioclase fractionation (higher Sr), and lower temperatures allow for earlier zircon saturation (lower Zr) (Deering et al., 2010; Miller, 2014).

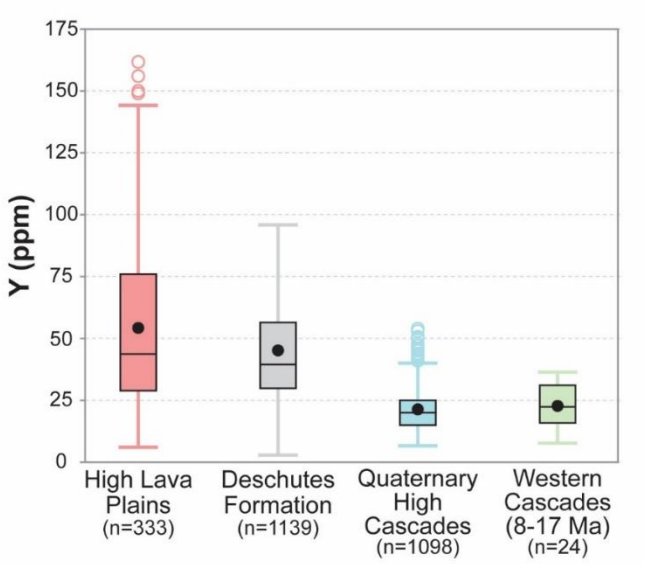

Figure 4.6: Boxplots of Y (ppm) for Felsic volcanic rocks (>63 wt.% SiO_2) from HLP, Deschutes Formation, all Cascades and Western Cascades. C. Oregon Cascades have nearly identical distribution. Open circles represent outliers that are > median+ (1.5*IQR). Mean values are shown by black closed circle. Number of analyses are shown beneath each boxplot. Felsic rocks were rarely erupted in the Western Cascades 8-17 Ma.

Additionally, the REE pattern of Deschutes Formation rhyolites is consistent with classification as R2 type rhyolites. These rhyolites demonstrate a "seagull-shaped" pattern (Glazner et al., 2008), with generally higher REE abundances (Fig. 4.8), indicative of incompatible REE behavior, but with a pronounced Eu/Eu* anomaly resulting from increased plagioclase stability within hot-dry-reduced rhyolites (Bachmann and Bergantz, 2008; Deering et al., 2010). In contrast, the High Cascades demonstrate a more arc-typical, cold-wet-oxidizing "U-shaped" REE

pattern (Glazner et al., 2008), with lower MREE due to the presence of amphibole and titanite, and a less pronounce Eu/Eu* anomaly because the suppression of plagioclase crystallization in the presence of water (Bachmann and Bergantz, 2008; Sisson and Grove, 1993). To quantify the shape of the REE patterns, we use ratios Dy/Dy* (lower indicates more U-shaped, MREE depletion), and Dy/Yb (lower indicates more depletion of MREE than HREE) (Davidson et al., 2009). While the Quaternary Cascades have Dy/Dy*=0.35 and Dy/Yb=0.65, (U-shaped) indicative of amphibole fractionating or being left behind as a residual, these values are much higher for the Deschutes Formation (0.63 and 1.0), indicating that pyroxene rather than amphibole must be the stable phase (FC or residual during melting). In summary, the Deschutes Formation rhyolites are characterized as R2-type, indicative of hot, dry, and reduced conditions of formation, and are more similar to those of the HLP than the High Cascades.

Although Deschutes Formation tuffs can be characterized as being most similar to the dry R2 rhyolitic endmember of Deering et al. (2008, 2010, 2011), it should be noted that they are not entirely anhydrous, and still have evidence of subduction fluids (e.g. higher LILE than anhydrous locations such as Iceland).

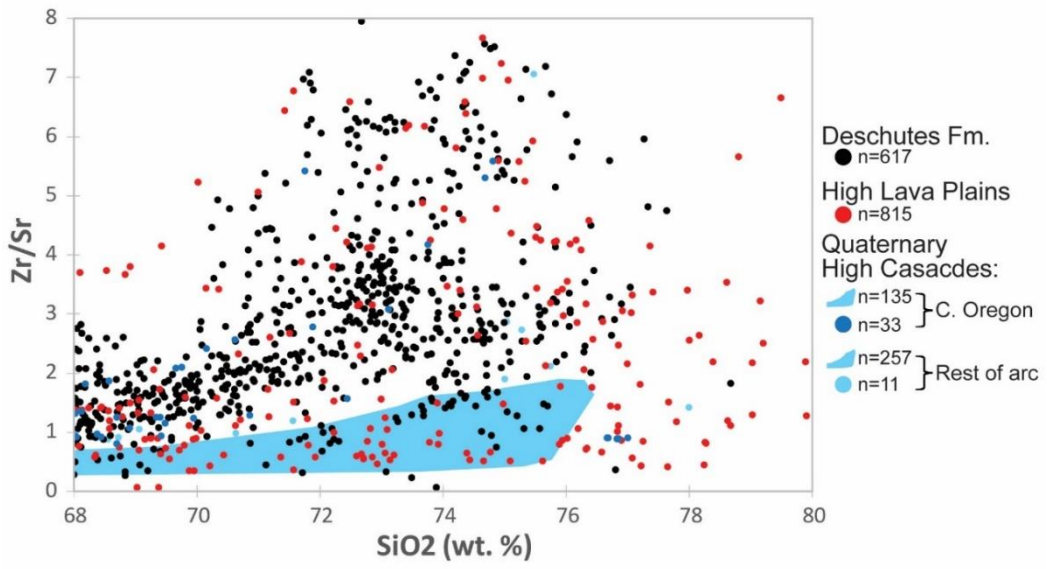

Figure 4.7: Zr/Sr vs. SiO_2 for felsic rocks from the Deschutes Formation, High Lava Plains, and Quaternary High Cascades. Light blue field encompasses all Quaternary Cascades (including 135 from central Oregon). 33 additional points from central Oregon and 11 from the rest of the arc have values outside this field.

Furthermore, Deschutes Formation ignimbrites straddle the tholeiitic/calc-alkaline line of Miyashiro (1974) and do not plot entirely within the tholeiitic field as might be expected for an entirely anhydrous system. Thus, Deschutes Formation rhyolites are not "wet" like the High Cascades (3-4 wt. % H_2O, Ruscitto et al., 2010), and are not entirely "dry" like Icelandic rhyolites (<1wt.% H_2O, Nichols et al., 2002). Instead, these rhyolites are similar to those of Newberry volcano, that is described by Mandler et al. (2004) as demonstrating "damp" differentiation trends. Melting experiments at a variety of pH_2O indicate that pumice compositions from the ~75 ka Tuff of Newberry Caldera (TNC) follow a distinctive differentiation trend most consistent with the presence of a modest amount of water (1.5 wt. %) at upper crustal pressures (Mandler et al., 2014). The authors suggest that a coupled enrichment in Fe, Ti and Na relative to the trend of calk-alkaline, like what is observed in TNC pumice is indicative of a damp (1-2 wt. % H_2O) differentiation trend. A sodium enrichment trend requires moderate water contents because if the magma is too dry, plagioclase is abundant and is more albitic, leading to a depletion in Na; if the magma is too wet, Na-bearing amphibole becomes stable, and the low-SiO_2 and moderate Na_2O assemblage leads to only a small Na-enrichment. Thus, a damp system prevents amphibole stability but also temporarily delays plagioclase crystallization, such that when it does come on the liquidus it tends to be more anorthitic, leading to a Na enrichment in the magma between 65 and 70 wt. % SiO_2 (Mandler et al., 2014). Deschutes ignimbrites exhibit a similar Na-enrichment trend as TNC pumice. A similar compositional trend is also seen in pumice from the ~200 ka Shevlin Park Tuff, that likely erupted from the Tumalo Volcanic Center (TVC), approximately 20 km east of the Quaternary arc axis (Hildreth et al., 2012; Sherrod et al., 2004). The Deschutes Formation rhyolites, therefore, exhibit "damp" trends that are transitional between what is typical of the Cascades arc and what is seen at entirely anhydrous tectonic settings, consistent with the interplay between extensional decompression melting and arc-typical flux melting.

There is also direct evidence of the reduced nature of Deschutes Formation rhyolites. Ilmenite-magnetite oxygen fugacity and temperature data from the literature for eight different Quaternary High Cascades volcanoes tend to be relatively oxidized, mostly plotting between the NNO and NNO+1 (log unit) buffers (Fig. 4.9). Deschutes Formation rhyolitic tuffs, however, tend to be more reduced, than the High Cascades rhyolites, plotting below the NNO buffer (Conrey, 1991; Eungard, 2012). However, temperatures of Deschutes formation rhyodacite to rhyolite tuffs are approximately the same as High Cascades samples of similar compositions, mostly between 825 and 900°C.

4.3.1.3 Evidence for shallow crustal melting

We have provided evidence for a damp and reduced magmatic system from which Deschutes Formation felsic magmas are produced. These compositions could have been produced by either fractional crystallization (FC) of a tholeiitic basalt along a dry LLD (e.g. Bachmann and Bergantz et al., 2008) or by melting mafic crust within a hot-dry-reduced environment (i.e. underplated by a dry tholeiitic basalt) (e.g. Sisson et al., 2005). Although undoubtedly a combination of both FC and melting or assimilation processes likely occur during the generation of most felsic magma, discerning the process that plays a larger role is often cryptic and is the subject of

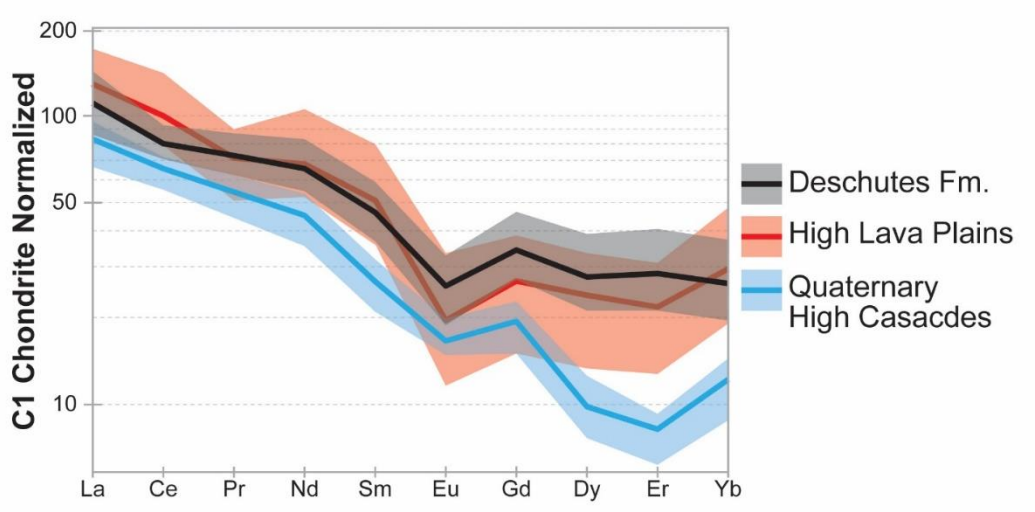

Figure 4.8: Chondrite-normalized (Sun and McDonough, 1995) REE patterns of the Deschutes Formation, High Lava Plains and Quaternary High Cascades. Opaque line represents the median value, and transparent fields enclose 50% of data (IQR).

wide debate (e.g. Annen et al., 2006; Bachmann and Bergantz, 2004; Borg and Clynne, 1998; Grove et al., 2003; Vigneresse, 2004). Discerning the relative contributions of these processes is made especially difficult in settings such as the Cascades, where the crust is predominantly young and mafic, and therefore geochemically similar to the basalts that intrude it (Mullen et al., 2017).

In the following sections, we present MELTS results that indicate pure FC is unlikely to produce the Deschutes Formation rhyolites, and then provide evidence that crustal melting played an important role in their production. We then suggest, based on oxygen isotope and trace element data, that this melting occurred at relatively shallow depths in the crust.

4.3.1.3.1 MELTS evidence against closed-system FC

We used MELTS thermodynamic modeling to determine if the Fe-rich rhyolites of the Deschutes Formation could be reproduced using simple FC. We tested 45 different combinations of pressure, initial H_2O content, and fO_2 buffer for each of three primitive basalts from the Deschutes Formation (LKT, CAB, and a 50% LKT+50% CAB mixture). We found that none of these models adequately fit all Deschutes Formation compositional trends (Fig. 4.10). The conditions that came the

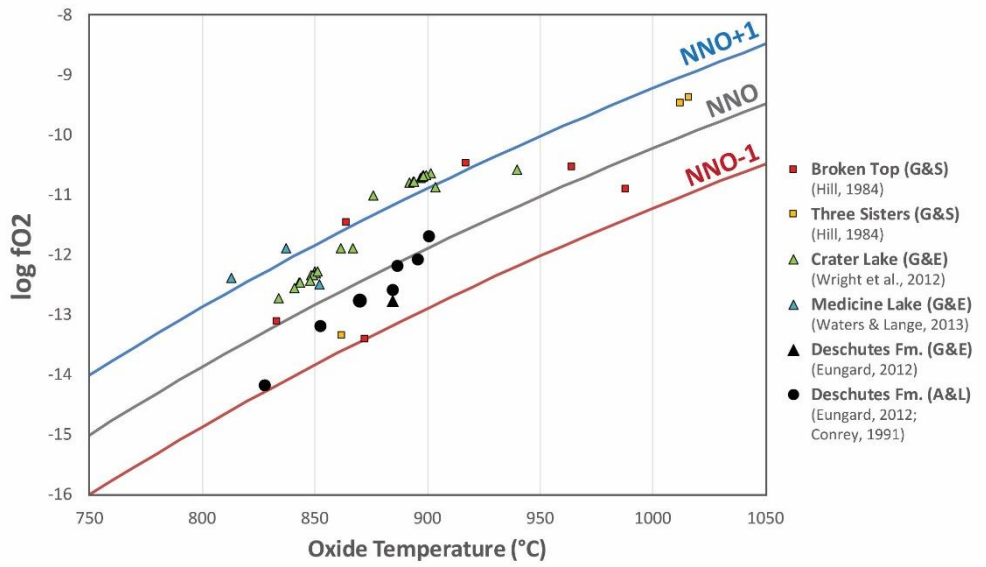

Figure 4.9: Ilmenite-magnetite fO_2 and eruption temperature for Deschutes Formation and High Cascades rhyolites and rhyodacites, compiled from the literature. Methods of calculation are indicated. A&L=Anderson and Lindsley, (1988); G&E= Ghiorso and Evans (2008); G&S= Ghiorso and Sack (1993).

closest were: a CAB with 2 wt.% H_2O, at QFM and 1 or 2 kbar, or an LKT with 1 wt.% H_2O, at QFM and 1 or 2.5 kbar. However, CABs failed reproduce the high FeO vs CaO trend, LKTs couldn't reproduce high Al_2O_3 for felsic compositions, and no experiments could reproduce high FeO*/MgO. The 50:50 mixture of CAB and LKT may have been reproduced the highest proportion of Deschutes Formation major element trends. Admittedly, our test is relatively limited, and a more comprehensive modeling approach including the use of different parental compositions and/or polybaric fractionation could potentially provide a better fit. However, our test indicates that simple FC is not likely to be entirely responsible for the production of Deschutes Formation felsic magmas, and other processes, such as crustal melting or assimilation, must play a role.

4.3.1.3.2 Crustal Melting rather than AFC process

Bimodal volcanism is common in extensional settings (e.g. Iceland, High Lava Plains) and numerous authors suggest that in these settings, crustal melting is

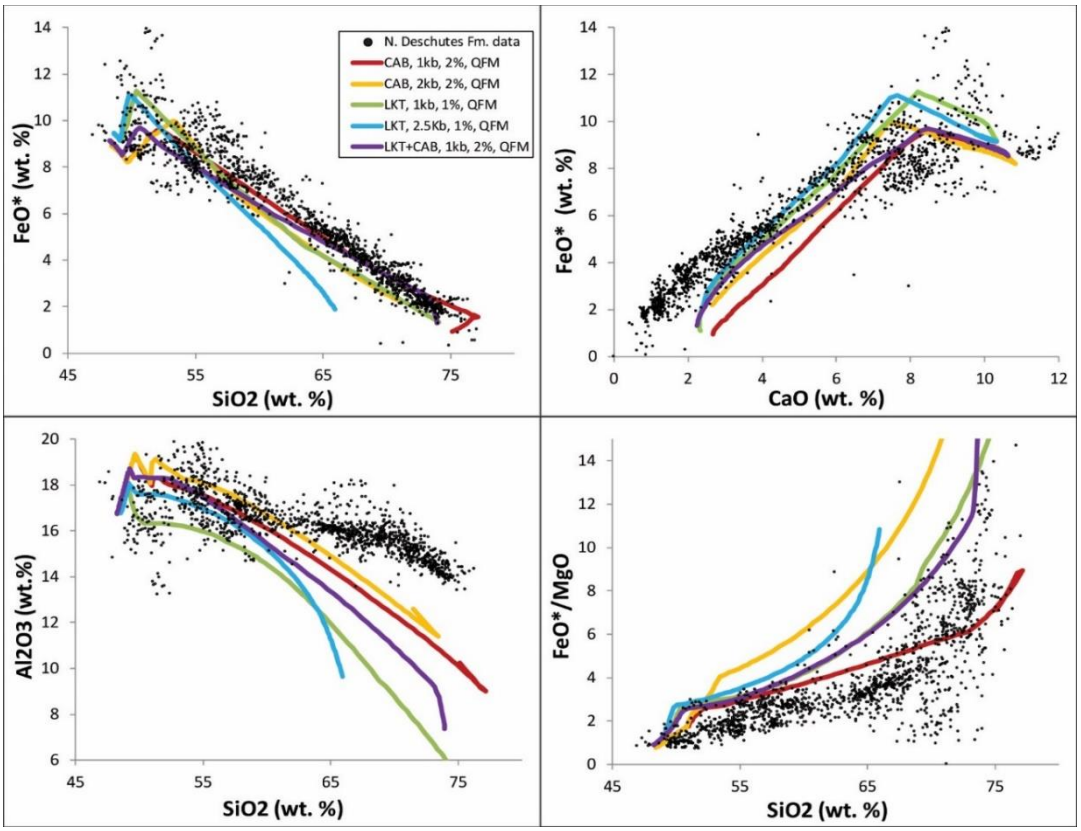

Figure 4.10: The five best MELTS model results compared to data from the Northern-sourced Deschutes Formation. Legend is the same for all four bivariate plots.

the most viable mechanism for rhyolite production (Jonasson, 2007; Streck and Grunder, 2008). Instead, if AFC processes were responsible for rhyolite magma generation, we may expect to see a full compositional range. Experiments by Beard (1995) concluded that the bimodal magmatic compositions and relatively high incompatible trace elements observed at several island arcs, and as observed in Deschutes Formation tuffs (Fig. 4.8), are more easily explained by relatively dry dehydration batch melting over Raleigh Fractionation models. Several Deschutes Formation ignimbrites are bimodal (e.g. Six Creek Tuff, McKenzie Canyon Tuff), lacking intermediate compositions (~62-67 wt.% SiO_2). Furthermore, Deschutes Formation ignimbrites, like those of the High Lava Plains, are crystal poor (most are <5% crystals), which is harder to reconcile with formation in a crystalline mush, compared to the crystal-rich dacites to rhyolites that are more commonly erupted in arc settings (Streck and Grunder, 2008). However, Bachmann and Bergantz (2008) hold that an AFC (mush) model can be invoked to explain bimodal compositions in hot and dry (i.e. extensional) settings. Because a magma will erupt only once it has reached volatile saturation, the authors suggest that in drier settings, a crystallizing mush will reach the point of rheological lock-up at intermediate compositions before volatile saturation occurs, rendering this intermediate magma uneruptable. Then, after continued fractionation, the rhyolite melt reaches volatile saturation and can erupt, leading to a paucity of intermediate compositions in drier settings.

However, trace element trends in Deschutes Formation Tuffs indicate that AFC processes are unlikely. The ratio of two equally incompatible elements, such as Rb/Th or Ba/K, should be relatively invariant during normal FC or AFC processes, since such processes would cause both elements to rise at the same rate (Conrey et al., 2001). Rb and K are highly incompatible except in biotite and alkali feldspar, but neither of these phases are found within any Deschutes Formation units. Ba becomes compatible only in plagioclase in rhyolitic magmas and Th is incompatible until rhyolite compositions, when it is compatible in allanite, clinopyroxene and ilmenite. However, McKenzie Canyon tuff has more than a 50% decrease in Rb/Th and Six Creek Tuff has 35% decrease in Ba/K from mafic to felsic glass compositions.

Although hydration of tephra glass may cause mobility (i.e. decreases) in K and Rb (Cerling et al., 1985; Whitehead et al., 1993) this process cannot be responsible for the observed trends; analytical totals for EMP analysis of Six Creek and McKenzie Canyon Tuff are 98.9% and 97.4%, respectively, indicating that the pumice had not been significantly hydrated. These incompatible element trends suggest that the rhyolitic magmas of these eruptions were formed by partially melting sources that had different ratios of these incompatible elements than the mafic components.

Further evidence against AFC being the dominant processes responsible for rhyolite production in the Deschutes Formation comes from plagioclase compositions in these ignimbrites. If a relatively dry tholeiitic basalt were to fractionate to a rhyolite, we would expect plagioclase to become stable relatively early during differentiation, and thus, to record significant changes in Anorthite (An) content over its history (Mandler et al., 2014; Villiger et al., 2007). This is especially true if the magma resided at shallow depths, as we will demonstrate for the Deschutes Formation in the next section. However, plagioclase from the Deschutes Formation is relatively homogeneous, with 50% of all 654 analyses lying within a narrow range of An27-43 (Fig. 4.11A). In fact, only 11 of the 218 plagioclase crystals that we analyzed had a core-to-rim decrease in An content >10 (Fig. 4.11B). Furthermore, almost all crystals are monotonously zoned, with very minor oscillatory zoning, and disequilibrium textures are almost entirely absent (Streck, 2008). In four of the five tuffs that contain plagioclase with An >55, Anorthite contents are bimodal, with compositional gaps of 10, 15, 33, and 45. One unit, the Meadow Creek Tuff, contains plagioclase compositions that span a full intermediate range (An27-85). However, in this unit, plagioclase from dark grey pumice (average glass SiO_2 of 68 wt.%) have an interquartile range (IQR) of An60-82, and plagioclase from the white pumice population (72 wt. % SiO_2) have an IQR of An30-45. This is much more consistent with two unrelated, bimodal magmas mingling prior to eruption than with a single, continuously-fractionating magma. We suggest that the plagioclase compositions in Deschutes Formation rhyolites are harder to explain via AFC processes, that would be expected to produce more variability in plagioclase compositions than is evident.

4.3.1.3.3 Shallow melting: Evidence from Oxygen Isotopes

Plagioclase oxygen isotope data from numerous Deschutes Formation ignimbrites suggest that crustal melting plays a critical role in the production of the felsic magmas. We collected 36 oxygen isotope laser fluorination analyses of plagioclase from 14 samples of 9 different ignimbrites. Oxygen isotope $\delta^{18}O_{plagioclase}$ values range between 5.01 and 6.27‰ (Fig. 4.12), and thus lack any analyses higher than the "normal array" (i.e. values expected from closed system fractionation of mantle melts, as defined by Bindeman, 2008 and Bindeman et al., 2004). This is consistent with interaction with the young and mafic crust beneath the Cascades, that likely has mantle-like $\delta^{18}O$ values (5.5-5.9‰), rather than the high $\delta^{18}O$ values (>10‰) of sedimentary and metamorphic rocks that have been exposed to meteoric or ocean water at low temperatures (Bindeman, 2008). Therefore, our oxygen isotope data indicate that the reduced fO_2 of Deschutes Formation felsic rocks is not due to partial melting of carbon-bearing meta-sediments, as suggested by Conrey (1991).

A more surprising result is that ~30% of Deschutes formation analyses have $\delta^{18}O$ values lower than the "normal array" (Fig. 4.12). Closed system processes cannot produce magmas with low-$\delta^{18}O$; this requires either melting or assimilation of rocks that have been hydrothermally altered by meteoric water at high temperature

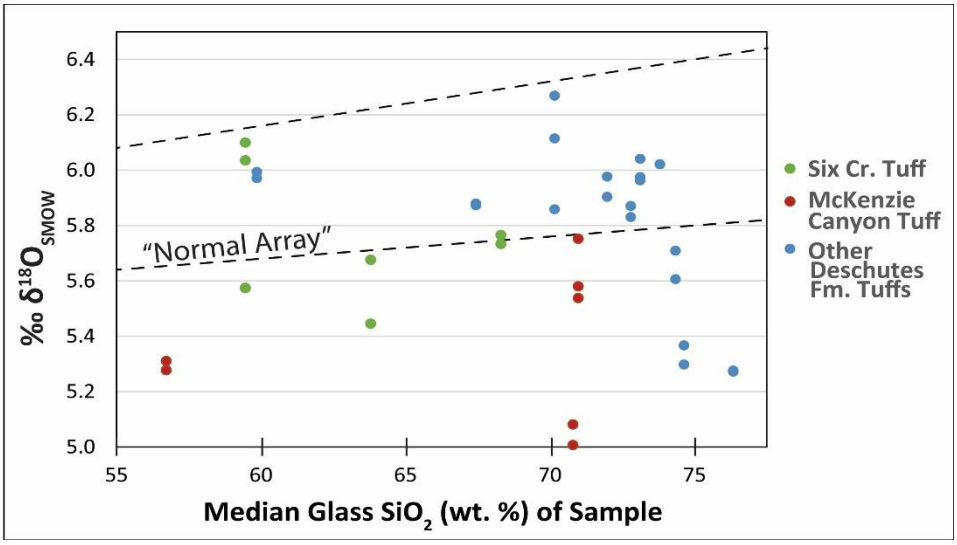

Figure 4.11: plagioclase $\delta^{18}O$ vs. median SiO_2 content of pumice from which the plagioclase was separated from. Errors are <0.1‰. Note that 30% of plagioclase lie below the "normal array" values of $\delta^{18}O$ expected from closed system differentiation of mantle melts (Bindeman, 2004).

(>400°C) (Balsley and Gregory, 1998; Bindeman, 2008; Taylor, 1977). This is because at higher temperatures, there is a much smaller mineral-melt fractionation factor, so interaction with hot, low-$\delta^{18}O$ meteoric water leads to depletion of ^{18}O in the altered rock (Bindeman, 2008). Low $\delta^{18}O$ silicic magmas are relatively rare (Balsley and Gregory, 1998) and tend to occur in locations characterized by caldera activity (e.g. Yellowstone) or extension (e.g. Iceland), such that extensive hydrothermal alteration of the crust can occur (Bacon et al., 1989; Bindeman, 2008; Taylor, 1990). Crustal extension within the central Oregon Cascades provides an efficient mechanism to produce fractures that would act as pathways for meteoric water to hydrothermally alter the uppermost mafic crust. Evidence of intense hydrothermal fluid circulation and high heat flow in the modern central Oregon Cascades is demonstrated by Ingebritsen and Mariner (2010). Subsequent re-melting

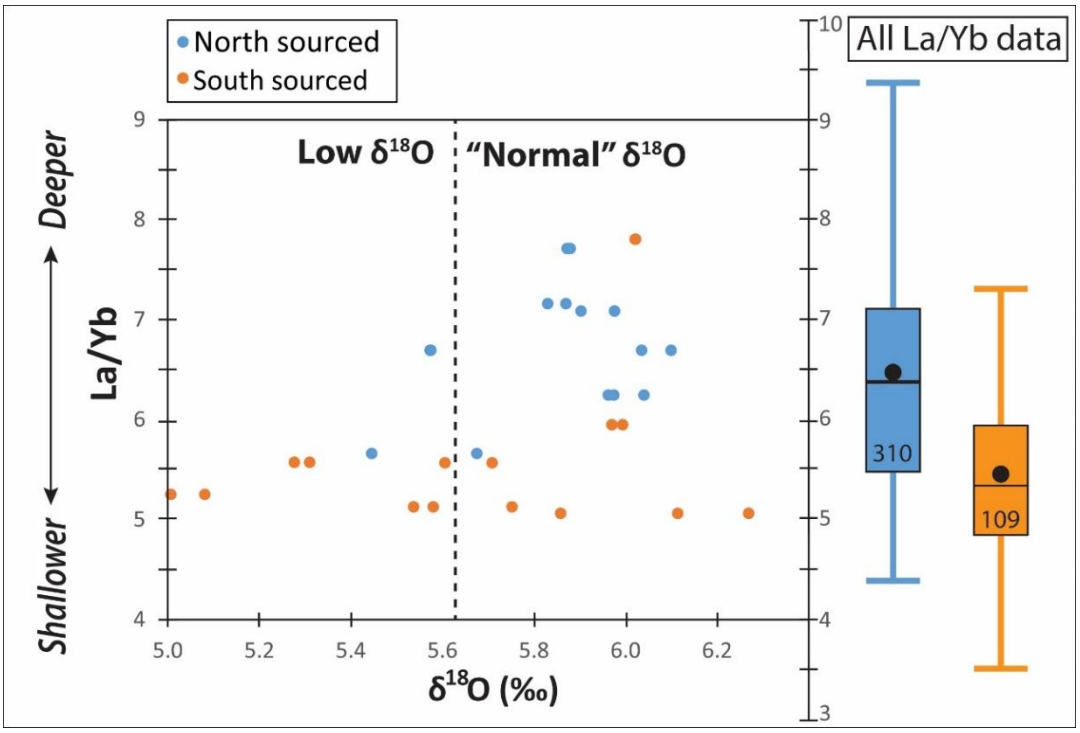

Figure 4.12: $\delta^{18}O$ (plagioclase) is plotted against La/Yb of pumice class from which the plagioclase was separated from. Boxplots on right represent La/Yb values for all North-sourced (blue) vs. south-sourced (orange) ignimbrites, number of analyses is shown in box. Note that only south sourced ignimbrites have low d18O, which corresponds to low La/Yb, consistent with shallow melting of hydrothermally altered rocks.

of this altered crust by shallow-penetrating Deschutes Formation basalts would produce the lower $\delta^{18}O$ silicic magmas seen in the formation.

Oxygen isotope data also provides additional support of crustal melting over AFC processes for rhyolite formation. If AFC were the dominant processes instead of crustal melting, much higher proportions of water would be necessary to produce the low- $\delta^{18}O$ Deschutes Formation rhyolites. Bindeman (2004) estimates that FC of a basalt (1 wt. % H_2O, $\delta^{18}O$=5.7‰) to a rhyolite would cause the $\delta^{18}O_{magma}$ to increase to ~6.0‰. Simple mixing calculations indicate that for ratios of assimilant:magma ranging 0.1 to 0.5, the assimilant would need to have $\delta^{18}O$= -1.5‰ to +4.5‰. To reach these low- $\delta^{18}O$ values, the hot water/rock mass fraction would have to be 0.39-0.05 for MORB and 0.47-0.13 for Siletz basalt, up to 26 times higher mass of hydrothermal water than is needed if crustal melting was the $\delta^{18}O$-lowering process.

Based on magnetotelluric (MT), heat flow, and seismic refraction data, Stanley et al. (1990) suggest that an impermeable zone exists at the brittle-plastic transition zone, ~12 km beneath the Oregon High Cascades, below which fracture permeability is limited and therefore hydrothermal alteration by hot meteoric water is unlikely to occur (Hart et al., 2004). Furthermore, studies of fossilized hydrothermal systems from extensional environments suggest that most hydrothermal alteration occurs shallower than 7 km (Balsley and Gregory, 1998; Criss and Taylor, 1983). This suggests that the crustal melting of hydrothermally altered mafic crust that produced the low-$\delta^{18}O$ silicic magmas of the Deschutes Formation must have occurred at depths shallower than 12 km, but likely occurred shallower than 7 km.

4.3.1.3.4 Shallow melting: Evidence from trace element data:

A shallow crustal melting origin is also corroborated by trace element and REE data. The tuffs of the Deschutes Formation have relatively flat and homogeneous REE patterns (IQR of La/Yb=6.3-7.2), compared to felsic rocks of the Quaternary High Cascades (8.5-12.5). The REE patterns of melts are highly dependent on the residual mineral assemblage that is left behind when a melt is extracted, that, in turn highly depends on the pressure and temperature under which the melting is occurring (Hart et al., 2004). For example, crustal melting at higher

pressures (>1 GPa), tends to create melts with steep REE patterns because garnet and/or amphibole, which are stable at these pressures, strongly partition HREE and MREE, respectively (e.g. Rapp, 1995). The High Cascades felsic rocks have moderate REE slopes and depleted Y contents, indicative of hydrous melting at moderate crustal depths (<30 km) where amphibole (but not garnet) is stable as a residual phase (Wolf and Wyllie, 1995). In contrast, the shallow REE slopes and high Y of Deschutes Formation rhyolites are consistent with melting at shallow crustal pressures (<0.1 GPa), low water content, and relatively high temperatures (Hart et al., 2004). Amphibole is not stable at these conditions, and clinopyroxene becomes the residual phase, producing felsic melts that are only weakly depleted in MREE and HREE, and have relatively high Y contents (Beard and Lofgren, 1991; Wolf and Wyllie, 1995). It is interesting to note that all low-$\delta^{18}O$ values within the Deschutes Formation correspond to the lowest La/Yb ratios (5.0-5.5), providing further evidence of shallow crustal melting of hydrothermally altered rocks (Fig. 4.12).

The major and trace element composition of Deschutes Formation felsic rocks are similar to that of felsic rocks from other intra-arc and back-arc rifts. In fact, Hart et al. (2004) and Lescher et al. (1986) used rhyolites from around the world to propose a rhyolite classification that can be used to infer tectonic settings of ancient rhyolite deposits. Based on this classification scheme, the High Cascades felsic rocks are arc-typical FII-type rhyolites, associated with hydrous melting at moderate crustal depths. However, Deschutes Formation rhyolites, like those from the High Lava Plains, are of the FIIIa-type (high La/Yb, Yb, higher HFSE, low Y), that tend to occur in extensional environments, and are indicative of hot and dry melting at shallow depths. Thus, in summary, the Deschutes Formation was characterized by hot, dry, and shallow crustal melting suggesting extension impacted the magmatic system.

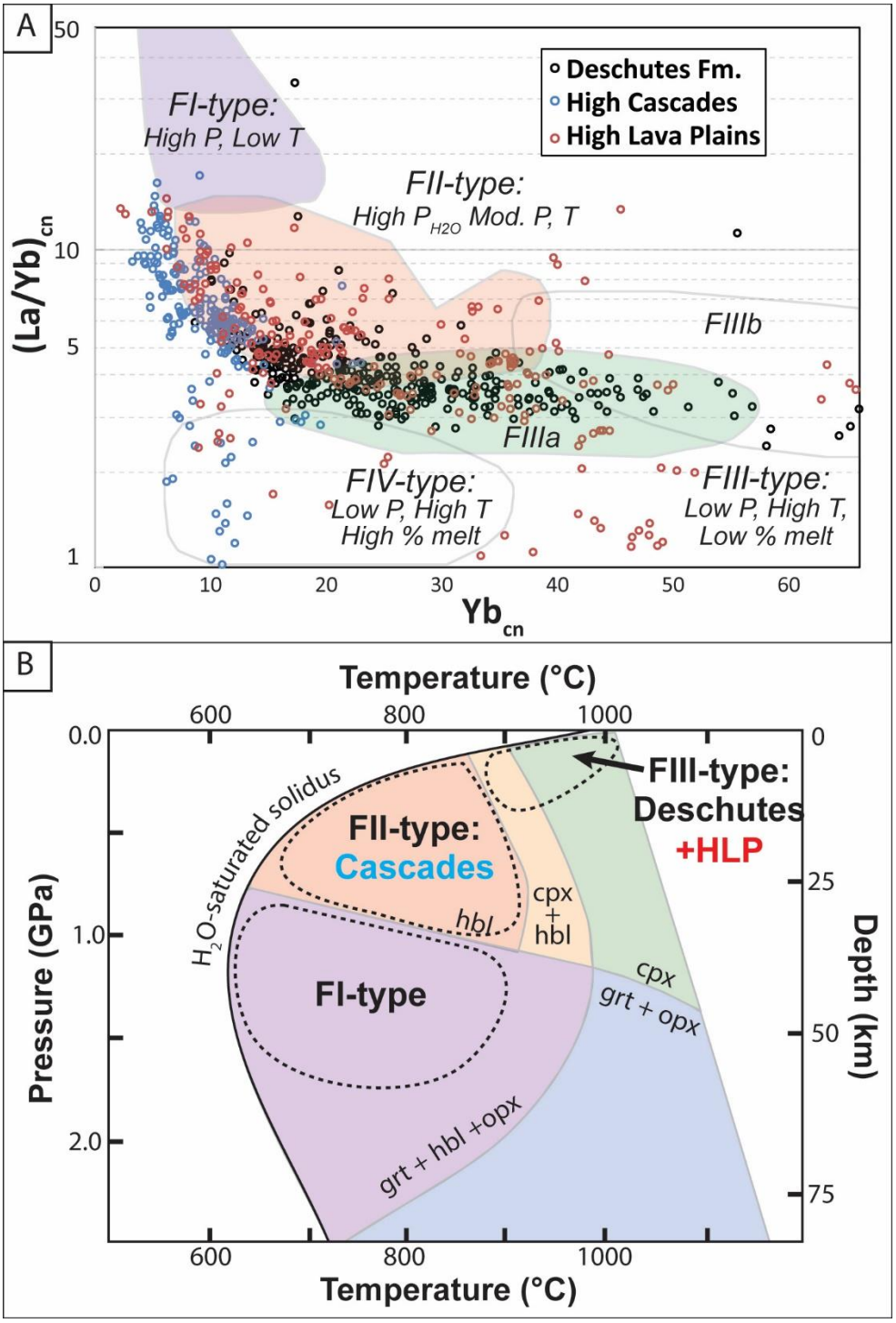

Figure 4.13: (A) Rhyolite discrimination diagram as in Hart et al. (2004). Cascades data is from GEOROC database and HLP data is from Ford (2012). (B) is modified from Hart et al. (2004) and shows phase stability for opx, cpx, hbl, grt compiled from numerous melting experiments. Approximate fields of FI-FIII rhyolites are shown and shading is the same as in (A).

4.3.1.3.5 Potential melting sources

Although trace element and oxygen isotope data suggest melting at shallow depths, it is much harder to constrain the composition of the protolith that was melted. The lack of high- $\delta^{18}O$ values in any Deschutes Formation unit precludes melting of sedimentary rocks or metasedimentary rocks. Conrey (1991) demonstrated that Deschutes Formation ignimbrites from near Green Ridge have $^{87}Sr/^{86}Sr$ compositions of 0.7035-0.7036. This narrow range of non-radiogenic values that are only slightly more radiogenic than average MORB, are consistent with the melting source being young and isotopically primitive. Previous studies have suggested that the Deschutes Formation volcanic sources represent the initial stages of volcanism along the modern High Cascades axis (Priest 1990; Conrey et al., 2002, 2004; Smith, 1986), so the crustal melting source is unlikely to be older plutons (~40-7 Ma) from the Western Cascades. One option that has been proposed by some (Church et al., 1986) is melting mafic crust associated with the Siletz Terrane. The central Oregon Cascades lie within the Columbia Embayment, a region of positive Bouguer gravity anomalies that stretch from central Oregon to central Washington, thought to represent regions of accreted oceanic crust (Trehu et al., 1994). The Late Paleocene-Eocene Siletz Terrain, which outcrops in the forearc from central Oregon to southern British Columbia, has been interpreted to be an oceanic large igneous province (LIP) with a plume-origin (Phillips et al., 2017; Wells et al., 2014). While some authors suggest based on geophysical data that the Siletz Terrane may terminate at the western Cascades-High Cascades boundary (Bedrosian and Feucht, 2014), others suggest it may extend just beneath the Oregon High Cascades arc (Finn, 1990), and others hold that Siletzia lithosphere could extend well east of the arc, almost as far inland as the Idaho border (Gao et al., 2011). Thus, the potential shallow crustal protoliths that could have been partially melted to produce the rhyolites of Deschutes Formation are: greenschist to amphibolite faces metabasalts of oceanic crust (MORB-like) origin (Conrey et al., 2001; Stanley et al., 1990), metabasalts from the oceanic LIP Siletz Terrane (OIB-like), or co-genetic mafic precursors of Deschutes-age (LKTs).

Our trace element and oxygen isotope data indicate that Siletz Terrane basalts were not likely to be the melting source for Deschutes Formation rhyolites. Siletz basalts have OIB-like trace element characteristics such as enriched incompatible trace elements, no negative Nb-Ta anomaly or positive LILE anomaly, and flat-to-enriched REE patterns (Phillips et al., 2017). Petrography and up to 6% loss on ignition indicate that the Siletz basalts are relatively altered, and as such, there has likely been further loss of LILE; Rb and Ba concentrations are lower than other OIBs and are often close to that of primitive mantle (Phillips et al., 2017). Because the trace element concentration of a melt will partially reflect that of the melting source (e.g. Conrey et al., 2001), we would expect a partial melt of Siletz basalt to possess no significant LILE enrichment or HFSE depletion. However, Deschutes Formation rhyolites show a heavy enrichment in LILE and a negative Nb-anomaly, and thus are unlikely to be the result of partial melting of Siletz crust. Instead, Deschutes rhyolites are more consistent with melting a basalt that is transitional between MORB and CAB, like the LKTs erupted during Deschutes time. These rhyolites do not have as strong of a Nb anomaly as Quaternary High Cascades (Fig. 4.8B), but are clearly more enriched in LREE and LILE that would be expected from melting a MORB. As previously mentioned, eastward migration of arc activity likely precludes older Western Cascades CABs from being the melting source. Thus, we suggest that LKT precursors, of similar origin to those erupted within the Deschutes Formation, were re-melted to produce the Deschutes Formation rhyolites. A similar process of re-melting (hydrothermally altered), young co-genetic mafic precursors has been proposed for the Timber Mountain/Oasis Valley caldera complex in Nevada (Bindeman et al., 2006).

Radiogenic isotope data also suggest that the Siletz Terrain is unlikely to be a crustal melting source. Despite having relatively large uncertainties, our LA-ICP-MS plagioclase data for six Deschutes Formation ignimbrites lie along a similar $^{207}Pb/^{206}Pb$ vs. $^{208}Pb/^{206}Pb$ trend and within the range of the Quaternary High Cascades (Fig. 4.14). While we did not collect Sr isotopes, a limited dataset of 5 analyses of Deschutes Formation ignimbrites from Conrey (1991) plot within the

High Cascades field for all Sr-Pb isotope plots. This "High Cascades Array" which is particularly well defined with the high precision data from Mullen et al. (2017) (r^2=0.80) appears to be a linear mixture between two endmembers. MORBs (from the Gorda and Juan de Fuca plates) form the less radiogenic endmember (Davis et al., 2008; White et al., 1987). On the radiogenic side, the High Cascades array tends towards either northern Cascadia sediment (Carpentier et al., 2014), as proposed by Mullen et al. (2017), or towards new Pb isotope data for Siletz basalt (Phillips et al., 2017), that was not compared or discussed by Mullen et al. (2017). However, for other Pb-Sr-Nd isotope plots (e.g. $^{206}Pb/^{204}Pb$ vs. $^{87}Sr/^{86}Sr$), Siletz basalts do not plot along a trend similar to the High Cascades or Deschutes Formation, precluding them from being the radiogenic endmember of the array. Instead, it is more likely that subducted sediment (similar to modern northern Cascadia sediment) has contaminated the mantle under the Cascades, thereby acting as the radiogenic endmember, as suggested by Mullen et al. (2017). Contamination of the mantle source is consistent with the fact that in the Deschutes Formation, as in the High Cascades, there is no systematic difference in Pb isotopes between mafic and felsic rocks.

Oxygen isotope data further contribute skepticism of Siletzia crust being melted. The lowest $\delta^{18}O_{plagioclase}$ value for the Deschutes Formation is 5.0‰. Assuming a temperature of 1,000°C, which is only 100°C higher than the calculated (oxides) eruption temperature (Conrey, 1991; Eungard, 2012), the experimentally determined fractionation factor between rhyolite and plagioclase (avg. An30) is $\Delta_{rhyolite\text{-}plag}$= +0.25‰ (Zhao and Zheng, 2003). Thus, the lowest Deschutes magmatic $\delta^{18}O$ value is 5.25‰. Using the open-system methods of Gregory and Taylor (1981), we can calculate the mass ratio of water to rock necessary to bring the crustal melting source down to 5.25‰. We can assume that the fractionation factor between the partial melt of this source and its restitic mineral assemblage would be relatively close to zero, (Zhao and Zheng, 2003). A study on fossilized horse teeth showed that meteoric water in central Oregon was at $\delta^{18}O$ =-8.1‰ approximately 7.2 Ma (Kohn et al., 2002). Thus, we calculate that Siletz basalt would require six times more

hydrothermal fluid than a MORB to lower their $\delta^{18}O$ to 5.25‰ (water/rock ratios of 0.09 and 0.015, respectively). Although both water/rock ratios are completely reasonable (Gregory and Taylor, 1981), the simpler case would be that which requires

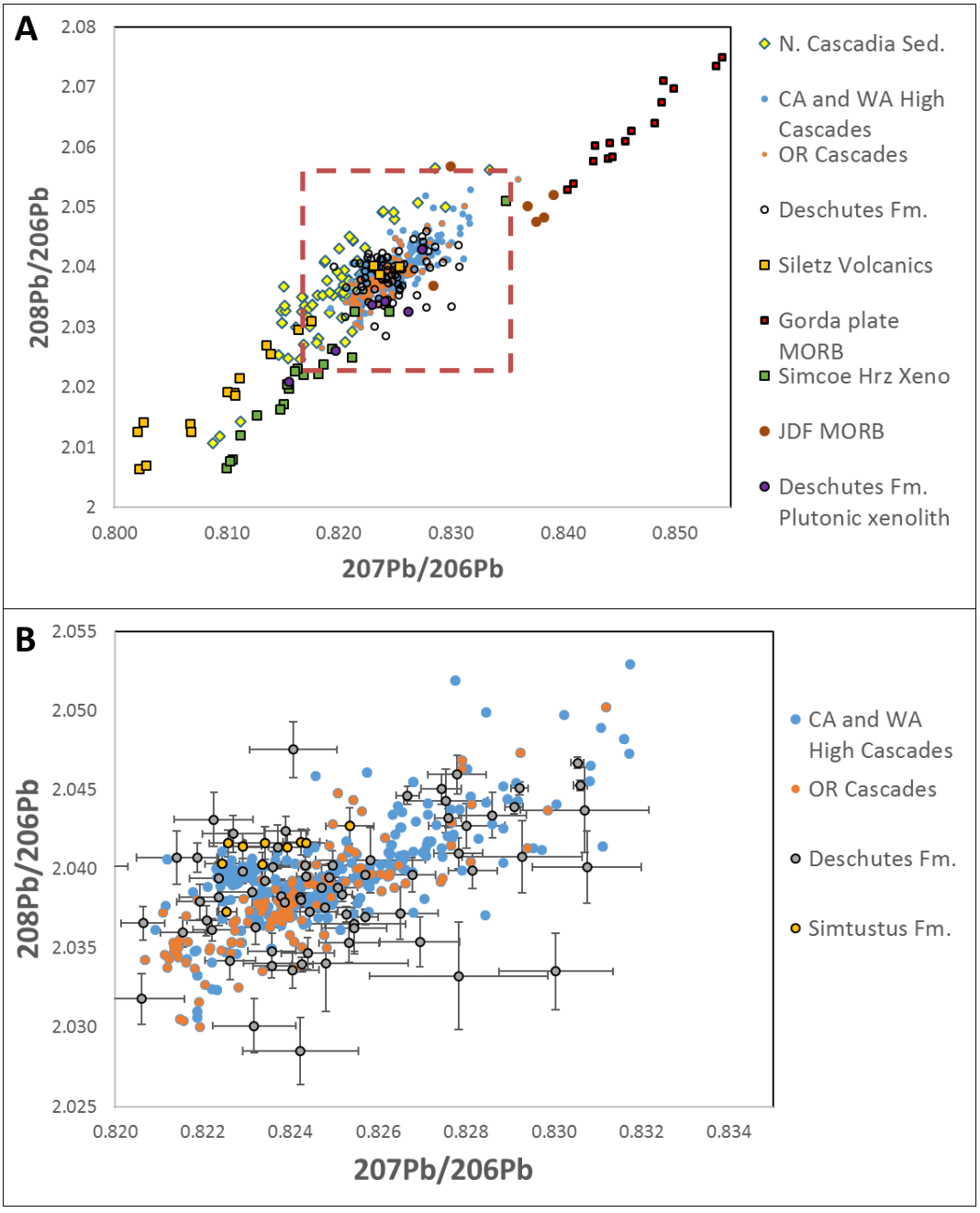

Figure 4.14: Pb isotopes of Deschutes Formation (black circles) compared to Quaternary High Cascades, Siletz Terrane basalts (Phillips et al., 2017), local MORB and subducting sediment (Mullen et al., 2017), and xenoliths from Simcoe volcanic field. Plutonic xenolith from Deschutes Formation tuff is also shown. Dashed box in A is shown in B. Error bars in B are 95% confidence intervals for Deschutes Formation data (see text).

the least amount of hydrothermal fluid circulation at depth (i.e. the MORB-like melting source).

We suggest, based on trace element and isotopic evidence that the Siletz Terrain is not a crustal melting source for the Deschutes Formation rhyolite, and rather it is primarily cogenetic near-solidus LKTs that are partially re-melted. Numerous thick LKT lavas were erupted into the Deschutes Basin for ~1.25 m.y. prior to the first major ignimbrite eruption (Pitcher et al., 2017a). This was interpreted by Pitcher et al. (2017a) to represent a thermal incubation time, during which a high flux of LKTs heated the middle to upper crust to the point when partial melting of stalled LKTs and ambient mafic crust could begin. This is consistent with thermomechanical modeling of high basalt flux within extensional settings, that predicts a ~1 m.y. incubation time before maximum melting efficiency within the crust is reached (Karakas and Dufek, 2015). Thus, stalled LKTs, which may have been just below their solidus, may have provided easily fusible material to produce the cogenetic rhyolites of the Deschutes formation.

4.3.2 Spatial variability: northern vs. southern sourced eruptions

Numerous authors have proposed, based on ignimbrite outcrop distribution, imbrication, and welding variations that the Deschutes Formation ignimbrites came from two separate source regions (Fig. 4.1): one in the south, near the modern Three Sisters, and a northern source just south of Mount Jefferson (Conrey et al., 2002; Pitcher et al., 2017; Smith, 1986). However, no previous studies have completed a detailed comparison of the trace element and isotopic compositions between ignimbrites from each of these sources. Our geochemical data indicate, that while Pb isotopic compositions and many major and trace element trends are similar for the two sources, there are some minor differences in trace elements and oxygen isotopes that may indicate slightly different crustal melting processes and sources.

Felsic pumice (>68 wt.% SiO_2) from the southern source tend to have higher concentrations of all REE and LILE, a larger Eu anomaly, and patterns that are flatter (i.e. lower La/Yb) than those from the north (Fig. 4.12). The difference between north

and south La/Yb is statistically significant (i.e. $p<<0.001$) using a Kolmogorov-Smirnov test (K-S test). Andesitic pumice, however have statistically similar La/Yb ($p=0.06$), indicating that there may be differing processes or source compositions that produce the rhyolitic melts in these two regions. If the northern and southern rhyolites are all partial melts of crustal sources with identical composition, the lower La/Yb in the south could be a result of either shallower melting or a higher degree of partial melting. However, since Pitcher et al. (2017b) calculated that explosive eruptions happened less frequently in the south, we would expect to see lower degree partial melts (higher La/Yb). Instead, oxygen isotopes may indicate that shallower melting may have been occurring in the south. Only one of the 17 oxygen isotope analyses from northern ignimbrites have $\delta^{18}O$ that are lower than the "normal array" of Bindeman (2004). The lack of low- $\delta^{18}O$ in the north as well as higher La/Yb may indicate that the north may have slightly deeper crustal sources for melting that had not been significantly hydrothermally altered. It is possible that higher extension rates in the south (Wells and McCaffrey, 2013) may have caused more significant crustal faulting hydrothermal alteration of shallow rocks, and may have allowed for shallower melting than in the north.

However, northern and southern ignimbrites also have differing high field strength element (HFSE) compositions, possibly indicating slight differences in the crustal melting source. K-S tests indicate that felsic pumice (> 68 wt.% SiO_2) from southern ignimbrites have statistically higher Nb, Zr, Ce, and Th than those sourced in the north. However, Zr and Nb content of andesite pumice from the two source regions are statistically similar, and differences in the other two HFSE (Ce and Th) are much smaller than for the felsic pumice. The fact that these differences are more apparent in felsic pumice, may indicate that the crustal melting source of the southern ignimbrites may have been slightly more enriched in HFSE (and many other trace elements) than northern sources. These differences in HFSE are not likely the result of differing crystallizing phases or restite assemblages during melting. Identical trends in Zr, and no decrease in Th with higher SiO_2 for either source region, indicate that differing degrees of zircon and allanite saturation, respectively, are not

responsible for the HFSE differences. Furthermore, identical trends of TiO_2 and FeO with SiO_2 between the two sources indicate differences in ilmenite crystallization is also not responsible. Biotite is not found in any Deschutes Formation tuffs. However, melting different amounts of biotite could be invoked to produce these north-south differences. Like the HFSE, Ba is also compatible in biotite and shows a similar enrichment within the southern felsic pumice, and only a slight enrichment in the andesitic compositions. A partially melted granite xenolith was found within the Balanced Rocks Tuff by Conrey (1985), who described the rock as containing rare traces of biotite, surrounded by small opaque grains. The author suggested that because "scattered" magnetite is produced during the first stage of biotite melting, that crustal biotite was being melted to produce Deschutes Formation silicic melts. Although further testing is needed, it is possible that the southern crust may have had higher proportions of biotite, a phase that would have been fully consumed during crustal melting (Douce, 1997), thereby enriching the melt in HFSE and Ba.

In summary, we suggest that crustal melting may have occurred at slightly shallower depths in the south and that hydrothermal alteration of these melting sources may have been more significant. Furthermore, the rocks that were melted to produce the southern rhyolites may have been slightly more enriched in HFSE, and limited data from andesitic pumice indicate that the differences in HFSE did not likely come from the mantle.

4.3.3 Temporal changes in magmatic processes of the central Oregon Cascades

We suggest that the magmatic system responsible for the Deschutes Formation ignimbrites was hotter, drier, and likely more extension-driven than Quaternary High Cascades system as a whole. However, significant along-arc differences in the geochemistry of volcanic rocks from the Quaternary arc exist (Pitcher et al., 2017d) and may reflect differences in slab geometry, crustal composition and age, and regional tectonics (e.g. Schmidt et al., 2008). To understand why the unusual pulse of explosive volcanism that is recorded within the Deschutes Formation occurred when it did, we must thus remove the influence of

spatial variability and compare its geochemistry to that of other central Oregon volcanics through time. This, in turn will allow us to infer what changes in the magmatic system led to a short explosive pulse ~6.25-5.45 Ma, and how subsequent changes have led to diminishing pyroclastic volcanism within a single region.

The Quaternary central Oregon High Cascades arc (QCOHC), which includes Mount Jefferson and the Three Sisters volcanoes along the arc axis (43.75-45°N), and Newberry Volcano in the rear arc, continues to experience overall extension today at a rate of ~1 mm/yr (Brocher et al., 2017; Wells et al., 1998). This portion of the arc exhibits unusually high heat flow, and over 25% of hydrothermal heat discharge from the entire Cascades arc comes from just five springs near Mount Jefferson (Ingibritsen and Mariner, 2010). Furthermore, it is characterized the third highest

Table 4.4: Comparison of Deschutes Formation geochemistry to that of the Central Oregon High Cascades, the entire Quaternary arc, and the High Lava Plains. CN indicates value is normalized to C1 chondrite (McDonough and Sun, 1995). $\delta^{18}O$ values are from plagioclase, whole rock or glass analyses only.

	High Lava Plains	Deschutes Formation	Quaternary c. Oregon High Cascades	Whole Quaternary High Cascade arc
Dominant rock types erupted	Bimodal: basalts and rhyolites	Basalts, basaltic-andesite, rhyolites	Basaltic andesite; some basalts and rhyolites	Basaltic andesite through dacite
Primitive lavas: LKTs vs. CABs	80% vs. 10%	74% vs. 26%	20% vs. 45 %	41% vs. 44%
Tholeiitic vs. Calc-alkaline	Mostly tholeiitic	Transitional, more tholeiitic	Mostly Calc-alkaline, some tholeiitic	Predominantly calc-alkaline
Na-enrichment	Yes	Yes	Yes (esp. rear-arc)	No
Felsic Y (ppm): Median (Q1-Q3)	44 (29- 76)	40 (31- 57)	22 (16-28)	20 (15-25)
Rhyolite Zr/Sr	3.2 (1.1-6.6)	2.0 (2.9-3.9)	1.0 (0.8-1.3)	0.8 (0.6-1.1)
La/Yb (CN)	4.4 (3.5-5.6)	4.2 (3.8-4.4)	6.8 (6.7-7.7)	6.8 (6.6-7.5)
Dy/Dy* (CN) Median	0.51	0.67	0.70	0.45
Dy/Yb (CN) Median	0.81	1.04	1.27	0.81
Eu/Eu* (CN) Median	0.53	0.65	0.93	0.73
fO_2 (oxides)	N/A	Reduced: NNO-1 to NNO	Oxidized: NNO to NNO+1	Oxidized: NNO to NNO+1
Rhyodacite eruption temp	N/A	885 (860-890)	860 (850-865)	860 (850-900)
$\delta^{18}O$ ‰	6.5 (6.0-6.9)	5.8 (5.5-6.0)	6.0 (5.8-6.3)	6.4 (5.9-6.9)

volcanic vent density in the arc (only Indian Heaven and Caribou Volcanic field are higher) (Hildreth, 2007) and abundant mafic volcanic vents are generally aligned along normal and strike-slip faults (Trimble, 2015), indicative of the influence that extension still has on the region. In addition, the QCOHC arc has erupted both basalts and true rhyolites, which are relative rare compositions for the Cascades that are predominantly basaltic-andesite to dacite in composition (Hildreth, 2007). However, the eruption rates of both of these compositions during the Quaternary are significantly lower than during Deschutes time (Pitcher et al., 2017a; Priest, 1990). Furthermore, geochemical trends of the QCOHC tend to be intermediate between those of the Deschutes Formation and those of the entire Quaternary arc. Thus, although extension continues to affect regional magmatic processes today, diminished volcanic production and more intermediate geochemical trends indicate that these processes have changed since Deschutes time.

While major and trace element systematics indicate that the early central Oregon High Cascades had a relatively hot-dry-reduced magmatic system, the modern arc in this region is more similar to the rest of the Quaternary arc (Table 4.4). This change is especially apparent in regional primitive lavas, that shifted from being predominantly LKTs to CABs (Fig. 4.3). Amphibole is now a relatively common phase in intermediate to felsic rocks of the QCOHC, and although Y concentrations are slightly elevated above the rest of the arc, concentrations are much lower than the Deschutes Formation (Fig. 4.6). Furthermore, most rhyolite analyses have low Zr/Sr ratios that lie within the field defined by the rest of the Cascades (< 1.5), and only 20% have values (~1-7) that overlap with those of the Deschutes Formation (blue circles, Fig. 4.7). The QCOHC also have FeO* vs. CaO and FeO*/MgO vs. SiO_2 trends that plot between the Deschutes Formation and the rest of the arc, but generally lie within the calc-alkaline field of Myashiro (1974). Like the rest of the arc, the QCOHC tend to be oxidized, lying between NNO and NNO+1 (filled symbols, Fig. 4.9). Thus, although this region may be slightly drier and hotter than the most of the Quaternary arc, these differences are relatively minor compared to the atypical hot-dry-reduced Deschutes Formation.

The depth of crustal melting beneath the Central Oregon High Cascades arc axis has also changed since the Late Miocene. Compared to the deep to mid-crustal two-stage melting model proposed for Quaternary Mount Jefferson by Conrey (2001), crustal melting likely occurred within the shallow crust during Deschutes time. Steeper REE in the younger felsic rocks (median chondrite-normalized La/Yb =6.8 vs. 4.0) (Fig. 4.8), and a complete lack of Eu anomaly (median Eu/Eu*=0.93 vs. 0.65) is indicative of wetter and/or deeper conditions in which plagioclase is not stable. Quaternary felsic pyroclasts from the Tumalo volcanic center (TVC), located ~20 km east of the arc axis share some similarities with the Deschutes Formation, such as relatively high $[La/Yb]_N$~4) and less depletion of MREE (Dy/Dy*=0.75), possibly indicating shallower melting than contemporaneous felsic magmas along the Central Oregon arc axis. However, TVC pumice have very little Eu anomaly (Eu/Eu*=0.84) and low Zr/Sr (~1), indicative of a wetter system than that of the Deschutes Formation.

In addition to different melting depths, differences in Pb and oxygen isotopes between the Late Miocene and Quaternary may provide further evidence of differing melting sources. Although the QCOHC tend to have lower $\delta^{18}O$ than the rest of the arc, there are far fewer analyses that lie below the "normal mantle array," compared to the Deschutes Formation (Fig. 4.15). Thus, the recent magmas had less interaction with shallow hydrothermally altered rocks. Felsic rocks of Quaternary age also tend to be slightly less radiogenic in Pb and Sr than their older regional counterparts (Sr isotopes from Conrey, 1991). Thus, our geochemical data (Table 4.4) suggest that the influence of extension in central Oregon was stronger during Deschutes time than during the Quaternary, causing a higher magmatic flux of hot and dry LKT basalt to shallower regions of the crust, producing larger volumes of felsic crustal melts.

4.3.4 Possible tectonic implications

If the Oregon forearc has been steadily rotating since at least the mid Miocene (Wells and Heller, 1988; Wells and McCaffrey, 2013), then why was the influence of extension on central Oregon Cascades arc magmatism so much greater during Deschutes time than during the Quaternary? Conrey et al. (2002, 2004) suggest that

the Deschutes Formation may be the initial expression of a northward propagating intra-arc rift, that produced a northward-younging trend of LKT lavas and smaller phases of pyroclastic volcanism. However, since the High Cascades graben is so narrow (~30 km wide) and extension rates are relatively low (1-3 mm/yr, Wells et al., 1998 and Conrey et al., 2002, respectively), intra-arc rifting alone is unlikely to produce the immense flux of decompression melts (LKTs) during Deschutes time. We suggest that although extension and arc rifting certainly occurred in the central Oregon Cascades 4-7 Ma, the pulse of decompression melting recorded by the Deschutes Formation was the result of larger-scale mantle upwelling related to the High Lava Plains, and that extension in this region provided pathways for these melts into the shallow crust.

The bimodal volcanism of the High Lava Plains of central and eastern Oregon have been interpreted to be the result of slab-rollback-induced mantle flow (Till et al., 2013; Long et al., 2012). Although there is a well-defined northwest-younging trend

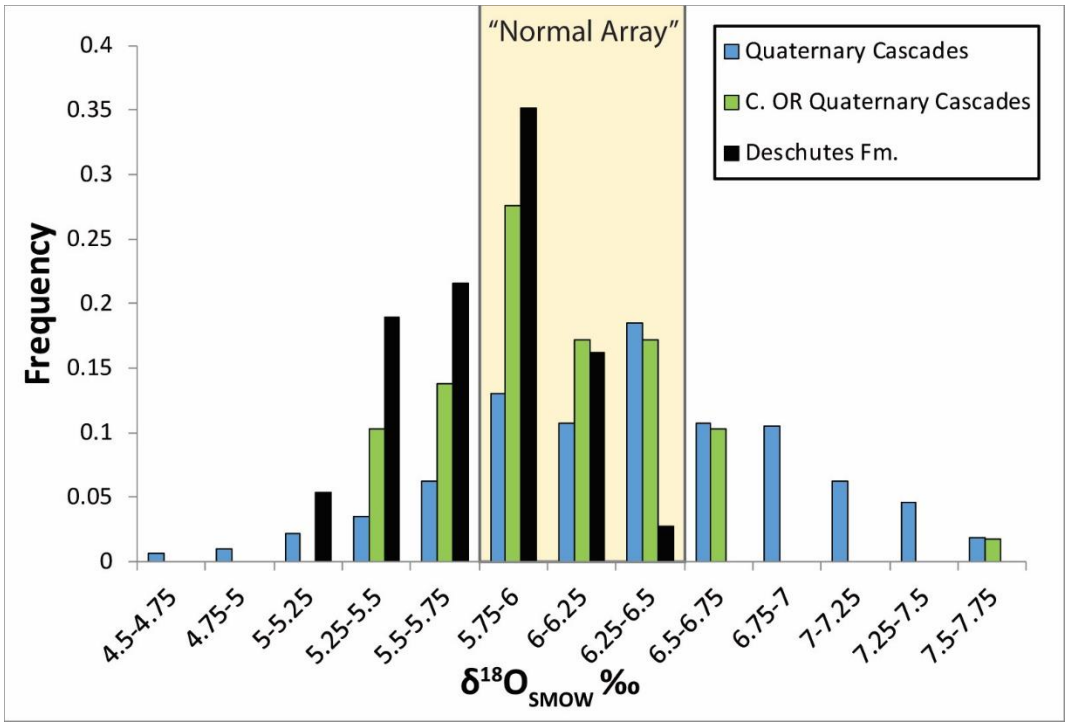

Figure 4.15: frequency histogram of d18O values for Deschutes Formation compared to central Oregon High Cascades and all Quaternary High Cascades (compiled from GeoRoc database). Only plagioclase, whole rock, and glass analyses are shown. In addition, d18O values from Ruscitto et al. (2010) are shown as magmatic values, calculated using the fractionation factor for Cascades LKTs and basaltic andesites from (Martin et al., 2011).

in rhyolites since 10.5 Ma, this is not the case with basalts (Jordan et al., 2004). Following a change in Pacific plate motion ~ 8 Ma (Atwater and Stock, 1998), a major magmatic pulse occurred between 7.8 and 7.4 Ma, in which LKTs erupted across the entire HLP province and into the Cascades rear-arc (Jordan et al., 2004). The timing of these events is contemporaneous with that of the initial eruption of LKTs into the Deschutes Basin 7.5 Ma (Smith et al., 1987), and is unlikely to be a coincidence. We suggest that mantle flow and decompression melting occurred beneath the entire HLP province, reached the region just east of the Western Cascades ancestral arc ~7.5 Ma (Jordan et al., 2004). These melts were then highly focused into the new High Cascades arc axis by crustal extension (Till et al., 2013) occurring at the boundary between northwestern-most Basin and Range extending crust and the non-extended crust that includes the Western Cascades and forearc (Scarberry et al., 2010).

This model is preferable to one in which a northward-propagating intra-arc rift is entirely responsible for the unusual volcanism of the Deschutes Formation for two reasons. First, this would provide a much higher flux of decompression melts than crustal extension alone. Analogue experiments suggest that moderate crustal extension (1.7 mm/yr) above slab-induced mantle flow produces orders-of-magnitude higher thermal anomalies than either process alone (Druken et al., 2011; Long et al., 2012). Second, this mechanism provides a means for this flux of dry decompression melts to eventually wane. If a northward-propagating rift, driven by forearc rotation, were entirely responsible, we may expect a similar flux of decompression melting and relatively hot-dry-reduced magmatic system to persist into the modern day. However, our geochemical results suggest that the central Oregon Cascades were characterized by a more hot-dry-reduced magmatic system during Deschutes time than during the Quaternary.

The mantle flow and subsequent decompression melts responsible for the widely distributed pulse of LKT eruptions across the entire HLP province may have provided the magmatic flux needed to cause partial melting in the shallow crust beneath the newly formed central Oregon High Cascades. This flux of hot and dry

basalts may have overwhelmed the contribution from colder and wetter calc-alkaline primitive magmas, as evident by the higher proportion of LKTs compared to CABs during this time (Fig. 4.3). However, as in the HLP, this mantle upwelling may have then reached a steady-state, providing a lower flux of decompression melts, and eventually allowing for re-establishment of fluid flux melting as a more dominant process. Over time, continued basalt underplating leads to a process of under-accretion (Deering et al., 2010), whereby sills get emplaced progressively deeper into the crust. In addition, the decrease in basaltic flux may have made it more difficult for basalt to ascend to the upper, less-dense crust, thereby leading to the establishment of a deeper magmatic system characterized by more cold-wet-oxidizing conditions. This allowed amphibole to become a stable phase, thereby explaining the change to steeper REE and a depletion in MREE, Y, and Zr/Sr. Continued crustal extension within the region does continue to affect the geochemistry of the arc magmas in the QCOHC, that exhibit some drier trends compared to the rest of the arc (Table 4.3), but these effects are far weaker than they were during Deschutes Formation time.

4.4 Conclusions

Our results indicate that extension likely had a significant influence on the magmatic processes that led to the production of the unusual volume of silicic pyroclastic material that was erupted during Deschutes Formation time. The geochemistry of tephra is consistent with a magmatic system that was much drier than that of the Quaternary Cascades. We propose a petrogenetic model (Fig. 4.2) for the earliest High Cascades in which crustal extension provided the mechanism to focus decompression melts into a new region of the crust and establishment volcanism along the new High Cascades arc axis. The predominance of LKT primitive basalts during this time provides evidence of the influx of these relatively dry decompression melts. Such extension allowed for penetration of these basalts into shallow levels of the crust and thermal priming of this crust under hot-dry-reduced conditions.

Following this thermal maturation period, the high flux of basalt into the upper crust lead to a period of enhanced shallow crustal melting (Pitcher et al., 2017a) and the production of the large volumes of hot-dry-reduced rhyolites of the Deschutes

Formation. These crystal poor rhyolites exhibit high Fe, Na, Y, MREE, and low Eu and Sr, indicative of their formation within this hot and dry environment, and ilmenite-magnetite oxybarometry indicates melting must have occurred under reduced conditions. Furthermore, extensional faulting in the upper crust established a robust hydrothermal system, and melting of these hydrothermally altered rocks lead to the eruption of low-$\delta^{18}O$ felsic magmas.

However, the high flux of decompression melts and efficient crustal melting were temporary, leading to the relatively short duration (800 k.y., Pitcher et al., 2017a) of this silicic pulse of volcanism. Thus, the anomalously high production of silicic magma and rate of explosive volcanism recorded in the Deschutes Formation is mirrored by the unusual geochemistry of the eruptive products, and are indicative of magmatic processes driven by extension, that no longer operate during the Quaternary. By investigating the geodynamic and tectonic causes of this important period of unusual magmatism, we gain a more comprehensive understanding of the Cascades arc and its variability through space and time.

4.4.1 Future Work

Additional geochemical data are needed to fully understand the causes of all geochemical trends within the Deschutes Formation. Collecting trace element and oxygen isotope data for primitive basalts within the formation would allow us to better constrain whether geochemical signals were inherited from the mantle or were the result of crustal melting. Future work may also include the use of EC-RAFC modeling (Spera and Bohrson, 2001) to determine whether trace element and isotopic trends in the rhyolites could be produced via AFC processes instead of, or in addition to crustal melting. We will also collect ilmenite-magnetite oxybarometry data to enhance the relatively limited dataset for the Deschutes formation, and to investigate whether there were spatio-temporal changes in the oxidation state of the Deschutes magmatic system. Furthermore, we plan to collect two-pyroxene thermobarometry data. This will provide depths of pyroxene crystallization and not necessarily that of storage or melting depths. However, if depths for Deschutes pyroxenes are consistently more shallow than those of the Quaternary, it will provide further

evidence of a shallow magmatic system driving the unusual pulsed of volcanism. Collecting FTIR data and comparing the water contents of melt inclusions from the Deschutes formation to the existing dataset for Quaternary central Oregon (Ruscitto et al., 2010), would provide a direct check of our hypothesis of the importance of dry decompression melts driving the geochemical trends of the formation.

References

***Note: This reference list is not complete.*

Arculus, R.J., 2003. Use and Abuse of the Terms Calcalkaline and Calcalkalic. J Petrology 44, 929–935. doi:10.1093/petrology/44.5.929

Arculus, R.J., 1994. Aspects of magma genesis in arcs. Lithos, Tectonics, metamorphism and magmatism in island arcs 33, 189–208. doi:10.1016/0024-4937(94)90060-4

Atwater, T., Stock, J., 1998. Pacific-North America plate tectonics of the NeogenesSouthwestern United States: an update. International Geology Review 40, 375–402. doi:10.1080/00206819809465216

Ayers, J., 1998. Trace element modeling of aqueous fluid – peridotite interaction in the mantle wedge of subduction zones. Contrib Mineral Petrol 132, 390–404. doi:10.1007/s004100050431

Bachmann, O., Bergantz, G.W., 2008. Rhyolites and their Source Mushes across Tectonic Settings. J Petrology 49, 2277–2285. doi:10.1093/petrology/egn068

Bachmann, O., Bergantz, G.W., 2004. On the Origin of Crystal-poor Rhyolites: Extracted from Batholithic Crystal Mushes. J Petrology 45, 1565–1582. doi:10.1093/petrology/egh019

Bacon, C.R., Adami, L.H., Lanphere, M.A., 1989. Direct evidence for the origin of low-18O silicic magmas: quenched samples of a magma chamber's partially-fused granitoid walls, Crater Lake, Oregon. Earth and Planetary Science Letters 96, 199–208. doi:10.1016/0012-821X(89)90132-5

Balsley, S.D., Gregory, R.T., 1998. Low-18O silicic magmas: why are they so rare? Earth and Planetary Science Letters 162, 123–136. doi:10.1016/S0012-821X(98)00161-7

Beard, J.S., 1995. Experimental, geological, and geochemical constraints on the origins of low-K silicic magmas in oceanic arcs. J. Geophys. Res. 100, 15593–15600. doi:10.1029/95JB00861

Beard, J.S., Lofgren, G.E., 1991a. Dehydration Melting and Water-Saturated Melting of Basaltic and Andesitic Greenstones and Amphibolites at 1, 3, and 6. 9 kb. J Petrology 32, 365–401. doi:10.1093/petrology/32.2.365

Beard, J.S., Lofgren, G.E., 1991b. Dehydration Melting and Water-Saturated Melting of Basaltic and Andesitic Greenstones and Amphibolites at 1, 3, and 6. 9 kb. J Petrology 32, 365–401. doi:10.1093/petrology/32.2.365

Bedrosian, P.A., Feucht, D.W., 2014. Structure and tectonics of the northwestern United States from EarthScope USArray magnetotelluric data. Earth and Planetary Science Letters, Special issue on USArray science 402, 275–289. doi:10.1016/j.epsl.2013.07.035

Bindeman, I., 2008. Oxygen Isotopes in Mantle and Crustal Magmas as Revealed by Single Crystal Analysis. Reviews in Mineralogy and Geochemistry 69, 445–478. doi:10.2138/rmg.2008.69.12

Bindeman, I.N., Ponomareva, V.V., Bailey, J.C., Valley, J.W., 2004. Volcanic arc of Kamchatka: a province with high-δ18O magma sources and large-scale 18O/16O

depletion of the upper crust1. Geochimica et Cosmochimica Acta 68, 841–865. doi:10.1016/j.gca.2003.07.009

Bindeman, I.N., Schmitt, A.K., Valley, J.W., 2006. U–Pb zircon geochronology of silicic tuffs from the Timber Mountain/Oasis Valley caldera complex, Nevada: rapid generation of large volume magmas by shallow-level remelting. Contrib Mineral Petrol 152, 649–665. doi:10.1007/s00410-006-0124-1

Bindeman, I.N., Serebryakov, N.S., Schmitt, A.K., Vazquez, J.A., Guan, Y., Azimov, P.Y., Astafiev, B.Y., Palandri, J., Dobrzhinetskaya, L., 2014. Field and microanalytical isotopic investigation of ultradepleted in 18O Paleoproterozoic "Slushball Earth" rocks from Karelia, Russia. Geosphere 10, 308–339. doi:10.1130/GES00952.1

Borg, L.E., Clynne, M.A., 1998. The Petrogenesis of Felsic Calc-alkaline Magmas from the Southernmost Cascades, California: Origin by Partial Melting of Basaltic Lower Crust. J. Petrology 39, 1197–1222. doi:10.1093/petroj/39.6.1197

Bray, E.A. du, John, D.A., 2011. Petrologic, tectonic, and metallogenic evolution of the Ancestral Cascades magmatic arc, Washington, Oregon, and northern California. Geosphere 7, 1102–1133. doi:10.1130/GES00669.1

Brocher, T.M., Wells, R.E., Lamb, A.P., Weaver, C.S., 2017. Evidence for distributed clockwise rotation of the crust in the northwestern United States from fault geometries and focal mechanisms. Tectonics 2016TC004223. doi:10.1002/2016TC004223

Cameron, B.I., Walker, J.A., Carr, M.J., Patino, L.C., Matías, O., Feigenson, M.D., 2003. Flux versus decompression melting at stratovolcanoes in southeastern Guatemala. Journal of Volcanology and Geothermal Research 119, 21–50. doi:10.1016/S0377-0273(02)00304-9

Carpentier, M., Weis, D., Chauvel, C., 2014. Fractionation of Sr and Hf isotopes by mineral sorting in Cascadia Basin terrigenous sediments. Chemical Geology 382, 67–82. doi:10.1016/j.chemgeo.2014.05.028

Cerling, T.E., Brown, F.H., Bowman, J.R., 1985. Low-temperature alteration of volcanic glass: Hydration, Na, K, 18O and Ar mobility. Chemical Geology: Isotope Geoscience section 52, 281–293. doi:10.1016/0168-9622(85)90040-5

Cervantes, P., Wallace, P.J., 2003. Role of H2O in subduction-zone magmatism: New insights from melt inclusions in high-Mg basalts from central Mexico. Geology 31, 235–238. doi:10.1130/0091-7613(2003)031<0235:ROHOIS>2.0.CO;2

Christiansen, E.H., 2005. Contrasting processes in silicic magma chambers: evidence from very large volume ignimbrites. Geological Magazine 142, 669–681. doi:10.1017/S0016756805001445

Conder, J.A., Wiens, D.A., Morris, J., 2002. On the decompression melting structure at volcanic arcs and back-arc spreading centers. Geophys. Res. Lett. 29, 17–1. doi:10.1029/2002GL015390

Conrey, R.M., 1991. Geology and Petrology of the Mt. Jefferson Area, High Cascade Range, Oregon (Ph.D.). Washington State University, Pullman, WA.

Conrey, R.M., Grunder, A.L., Schmidt, M.E., 2004. SOTA field trip guide, State of the Cascade Arc: Stratocone persistence, mafic lava shields, and pyroclastic

volcanism associated with intra-arc rift propagation. DOGAMI Open-File Report O-2004-04 39.
Conrey, R.M., Hooper, P.R., Larson, P.B., Chesley, J., Ruiz, J., 2001. Trace element and isotopic evidence for two types of crustal melting beneath a High Cascade volcanic center, Mt. Jefferson, Oregon. Contrib Mineral Petrol 141, 710–732. doi:10.1007/s004100100259
Conrey, R.M., Taylor, E.M., Donnelly-Nolan, J.M., Sherrod, D.R., 2002. North-central Oregon Cascades: Exploring petrologic and tectonic intimacy in a propagating intra-arc rift. Field guide to geologic processes in Cascadia 36 47–90.
Council, N.R., Sciences, D. on E. and P., Resources, C. on G., Environment and, Committee, G.S., 1990a. The Role of Fluids in Crustal Processes. National Academies Press.
Council, N.R., Sciences, D. on E. and P., Resources, C. on G., Environment and, Committee, G.S., 1990b. The Role of Fluids in Crustal Processes. National Academies Press.
Criss, R.E., Taylor, H.P., 1983. An 18O/16O and D/H study of Tertiary hydrothermal systems in the southern half of the Idaho batholith. Geological Society of America Bulletin 94, 640–663. doi:10.1130/0016-7606(1983)94<640:AOADSO>2.0.CO;2
Davidson, J., Turner, S., Plank, T., 2013. Dy/Dy*: Variations Arising from Mantle Sources and Petrogenetic Processes. J Petrology 54, 525–537. doi:10.1093/petrology/egs076
Davis, A.S., Clague, D.A., Cousens, B.L., Keaten, R., Paduan, J.B., 2008. Geochemistry of basalt from the North Gorda segment of the Gorda Ridge: Evolution toward ultraslow spreading ridge lavas due to decreasing magma supply. Geochem. Geophys. Geosyst. 9, Q04004. doi:10.1029/2007GC001775
Deering, C.D., Bachmann, O., Dufek, J., Gravley, D.M., 2011. Rift-Related Transition from Andesite to Rhyolite Volcanism in the Taupo Volcanic Zone (New Zealand) Controlled by Crystal–melt Dynamics in Mush Zones with Variable Mineral Assemblages. J. Petrology 52, 2243–2263. doi:10.1093/petrology/egr046
Deering, C.D., Cole, J.W., Vogel, T.A., 2008. A Rhyolite Compositional Continuum Governed by Lower Crustal Source Conditions in the Taupo Volcanic Zone, New Zealand. J. Petrology 49, 2245–2276. doi:10.1093/petrology/egn067
Deering, C.D., Gravley, D.M., Vogel, T.A., Cole, J.W., Leonard, G.S., 2010. Origins of cold-wet-oxidizing to hot-dry-reducing rhyolite magma cycles and distribution in the Taupo Volcanic Zone, New Zealand. Contrib Mineral Petrol 160, 609–629. doi:10.1007/s00410-010-0496-0
Deering, C.D., Vogel, T.A., Patino, L.C., Szymanski, D.W., Alvarado, G.E., 2012. Magmatic processes that generate chemically distinct silicic magmas in NW Costa Rica and the evolution of juvenile continental crust in oceanic arcs. Contrib Mineral Petrol 163, 259–275. doi:10.1007/s00410-011-0670-z
Douce, A.E.P., 1997. Generation of metaluminous A-type granites by low-pressure melting of calc-alkaline granitoids. Geology 25, 743–746. doi:10.1130/0091-7613(1997)025<0743:GOMATG>2.3.CO;2

Draper, D.S., Johnston, A.D., 1992. Anhydrous PT phase relations of an Aleutian high-MgO basalt: an investigation of the role of olivine-liquid reaction in the generation of arc high-alumina basalts. Contr. Mineral. and Petrol. 112, 501–519. doi:10.1007/BF00310781

Druken, K.A., Long, M.D., Kincaid, C., 2011. Patterns in seismic anisotropy driven by rollback subduction beneath the High Lava Plains. Geophysical Research Letters 38, L13310. doi:10.1029/2011GL047541

du Bray, E.A., John, D.A., 2011. Petrologic, tectonic, and metallogenic evolution of the Ancestral Cascades magmatic arc, Washington, Oregon, and northern California. Geosphere 7, 1102–1133. doi:10.1130/GES00669.1

Eberle, M.A., Grasset, O., Sotin, C., 2002. A numerical study of the interaction between the mantle wedge, subducting slab, and overriding plate. Physics of the Earth and Planetary Interiors 134, 191–202. doi:10.1016/S0031-9201(02)00157-7

Eungard, D.W., 2012. Early High Cascade Silicic Volcanism: Analysis of the McKenzie Canyon and Lower Bridge Tuff (M.S.). Oregon State University, Corvallis, Oregon.

Finn, C., 1990. Geophysical constraints on Washington Convergent Margin Structure. J. Geophys. Res. 95, 19533–19546. doi:10.1029/JB095iB12p19533

Ford, M.T., Grunder, A.L., Duncan, R.A., 2013. Bimodal volcanism of the High Lava Plains and northwestern Basin and Range of Oregon: distribution and tectonic implications of age-progressive rhyolites. Geochemistry, Geophysics, Geosystems 14, 2836–2857. doi:10.1002/ggge.20175

Gao, H., Humphreys, E.D., Yao, H., van der Hilst, R.D., 2011. Crust and lithosphere structure of the northwestern U.S. with ambient noise tomography: Terrane accretion and Cascade arc development. Earth and Planetary Science Letters 304, 202–211. doi:10.1016/j.epsl.2011.01.033

Glazner, A.F., Coleman, D.S., Bartley, J.M., 2008. The tenuous connection between high-silica rhyolites and granodiorite plutons. Geology 36, 183–186. doi:10.1130/G24496A.1

Gregory, R.T., Taylor, H.P., 1981. An oxygen isotope profile in a section of Cretaceous oceanic crust, Samail Ophiolite, Oman: Evidence for δ18O buffering of the oceans by deep (>5 km) seawater-hydrothermal circulation at mid-ocean ridges. J. Geophys. Res. 86, 2737–2755. doi:10.1029/JB086iB04p02737

Grove, T., Parman, S., Bowring, S., Price, R., Baker, M., 2002. The role of an H2O-rich fluid component in the generation of primitive basaltic andesites and andesites from the Mt. Shasta region, N California. Contrib Mineral Petrol 142, 375–396. doi:10.1007/s004100100299

Grove, T.L., Elkins-Tanton, L.T., Parman, S.W., Chatterjee, N., Müntener, O., Gaetani, G.A., 2003. Fractional crystallization and mantle-melting controls on calc-alkaline differentiation trends. Contrib Mineral Petrol 145, 515–533. doi:10.1007/s00410-003-0448-z

Hart, T.R., Gibson, H.L., Lesher, C.M., 2004. TRACE ELEMENT GEOCHEMISTRY AND PETROGENESIS OF FELSIC VOLCANIC ROCKS ASSOCIATED WITH VOLCANOGENIC MASSIVE Cu-Zn-Pb SULFIDE

DEPOSITS. Economic Geology 99, 1003–1013. doi:10.2113/gsecongeo.99.5.1003

Hildreth, W., 2007. Quaternary Magmatism in the Cascades - Geologic Perspectives. U.S. Geological Survey Professional Paper 1744, Professional Paper.

Hildreth, W., Fierstein, J., Calvert, A., 2012. Geologic map of Three Sisters volcanic cluster, Cascade Range, Oregon. U.S. Geological Survey Scientific Investigations Map 3186.

Hill, B.E., 1984. Petrology of the Bend pumice and Tumalo tuff, a Pleistocene Cascade eruption involving magma mixing (M.S.). Oregon State University, Corvallis, Oregon.

Huber, C., Bachmann, O., Manga, M., 2010. Two Competing Effects of Volatiles on Heat Transfer in Crystal-rich Magmas: Thermal Insulation vs Defrosting. J Petrology 51, 847–867. doi:10.1093/petrology/egq003

Ingebritsen, S.E., Mariner, R.H., 2010. Hydrothermal heat discharge in the Cascade Range, northwestern United States. Journal of Volcanology and Geothermal Research 196, 208–218. doi:10.1016/j.jvolgeores.2010.07.023

Jakesˇ, P., Gill, J., 1970. Rare earth elements and the island arc tholeiitic series. Earth and Planetary Science Letters 9, 17–28. doi:10.1016/0012-821X(70)90018-X

Jónasson, K., 2007. Silicic volcanism in Iceland: Composition and distribution within the active volcanic zones. Journal of Geodynamics, Hotspot Iceland 43, 101–117. doi:10.1016/j.jog.2006.09.004

Jordan, B.T., Grunder, A.L., Duncan, R.A., Deino, A.L., 2004. Geochronology of age-progressive volcanism of the Oregon High Lava Plains: Implications for the plume interpretation of Yellowstone. Journal of Geophysical Research: Solid Earth 109, B10202. doi:10.1029/2003JB002776

Karakas, O., Dufek, J., 2015. Melt evolution and residence in extending crust: Thermal modeling of the crust and crustal magmas. Earth and Planetary Science Letters 425, 131–144. doi:10.1016/j.epsl.2015.06.001

Kelemen, P.B., Rilling, J.L., Parmentier, E.M., Mehl, L., Hacker, B.R., 2004. Thermal Structure due to Solid-State Flow in the Mantle Wedge Beneath Arcs, in: Eiler, J. (Ed.), Inside the Subduction Factory. American Geophysical Union, pp. 293–311. doi:10.1029/138GM13

Kelley, K.A., Plank, T., Grove, T.L., Stolper, E.M., Newman, S., Hauri, E., 2006. Mantle melting as a function of water content beneath back-arc basins. J. Geophys. Res. 111, B09208. doi:10.1029/2005JB003732

Kent, A.J.R., 2008. In-situ analysis of Pb isotope ratios using laser ablation MC-ICP-MS : Controls on precision and accuracy and comparison between Faraday cup and ion counting systems. Journal of Analytical Atomic Spectrometry 23, 968–975. doi:10.1039/B801046C

Kinzler, R.J., Donnelly-Nolan, J.M., Grove, T.L., 2000. Late Holocene hydrous mafic magmatism at the Paint Pot Crater and Callahan flows, Medicine Lake Volcano, N. California and the influence of H2O in the generation of silicic magmas. Contrib Mineral Petrol 138, 1–16. doi:10.1007/PL00007657

Kohn, M.J., Miselis, J.L., Fremd, T.J., 2002. Oxygen isotope evidence for progressive uplift of the Cascade Range, Oregon. Earth and Planetary Science Letters 204, 151–165. doi:10.1016/S0012-821X(02)00961-5

Le Voyer, M., Rose-Koga, E.F., Shimizu, N., Grove, T.L., Schiano, P., 2010. Two Contrasting H2O-rich Components in Primary Melt Inclusions from Mount Shasta. J Petrology 51, 1571–1595. doi:10.1093/petrology/egq030

Lesher, C.M., Goodwin, A.M., Campbell, I.H., Gorton, M.P., 1986. Trace-element geochemistry of ore-associated and barren, felsic metavolcanic rocks in the Superior Province, Canada. Can. J. Earth Sci. 23, 222–237. doi:10.1139/e86-025

Liu, H.-Q., Xu, Y.-G., Tian, W., Zhong, Y.-T., Mundil, R., Li, X.-H., Yang, Y.-H., Luo, Z.-Y., Shang-Guan, S.-M., 2014. Origin of two types of rhyolites in the Tarim Large Igneous Province: Consequences of incubation and melting of a mantle plume. Lithos, Special Issue Permian large igneous provinces: Characteristics, mineralization and paleo-environment effects 204, 59–72. doi:10.1016/j.lithos.2014.02.007

Long, M.D., Till, C.B., Druken, K.A., Carlson, R.W., Wagner, L.S., Fouch, M.J., James, D.E., Grove, T.L., Schmerr, N., Kincaid, C., 2012. Mantle dynamics beneath the Pacific Northwest and the generation of voluminous back-arc volcanism. Geochemistry, Geophysics, Geosystems 13, Q0AN01. doi:10.1029/2012GC004189

Mandler, B.E., Donnelly-Nolan, J.M., Grove, T.L., 2014. Straddling the tholeiitic/calc-alkaline transition: the effects of modest amounts of water on magmatic differentiation at Newberry Volcano, Oregon. Contrib Mineral Petrol 168, 1066. doi:10.1007/s00410-014-1066-7

Martin, E., Bindeman, I., Grove, T.L., 2011. The origin of high-Mg magmas in Mt Shasta and Medicine Lake volcanoes, Cascade Arc (California): higher and lower than mantle oxygen isotope signatures attributed to current and past subduction. Contributions to Mineralogy and Petrology; Heidelberg 162, 945–960. doi:http://dx.doi.org/10.1007/s00410-011-0633-4

McCulloch, M.T., Gamble, J.A., 1991. Geochemical and geodynamical constraints on subduction zone magmatism. Earth and Planetary Science Letters 102, 358–374. doi:10.1016/0012-821X(91)90029-H

Meigs, A., Scarberry, K., Grunder, A., Carlson, R., Ford, M.T., Fouch, M., Grove, T., Hart, W.K., Iademarco, M., Jordan, B., Milliard, J., Streck, M.J., Trench, D., Weldon, R., 2009. Geological and geophysical perspectives on the magmatic and tectonic development, High Lava Plains and northwest Basin and Range. Field Guides 15, 435–470. doi:10.1130/2009.fld015(21)

Miller, C.F., 2014. ZR/SR RATIOS DISTINGUISH COOL & WET FROM HOT & DRY MAGMATIC SUITES. Presented at the Geologic Society of America Annual Meeting, Vancouver, BC.

Miyashiro, A., 1974. Volcanic rock series in island arcs and active continental margins. Am J Sci 274, 321–355. doi:10.2475/ajs.274.4.321

Mullen, E.K., Weis, D., Marsh, N.B., Martindale, M., 2017. Primitive arc magma diversity: New geochemical insights in the Cascade Arc. Chemical Geology 448, 43–70. doi:10.1016/j.chemgeo.2016.11.006

Nichols, A.R.L., Carroll, M.R., Höskuldsson, Á., 2002. Is the Iceland hot spot also wet? Evidence from the water contents of undegassed submarine and subglacial pillow basalts. Earth and Planetary Science Letters 202, 77–87. doi:10.1016/S0012-821X(02)00758-6

Papazachos, C.B., Kiratzi, A.A., 1996. A detailed study of the active crustal deformation in the Aegean and surrounding area. Tectonophysics 253, 129–153. doi:10.1016/0040-1951(95)00047-X

Pearce, J.A., Parkinson, I.J., 1993. Trace element models for mantle melting: application to volcanic arc petrogenesis. Geological Society, London, Special Publications 76, 373–403. doi:10.1144/GSL.SP.1993.076.01.19

Pearce, J.A., Stern, R.J., 2006. Origin of Back-Arc Basin Magmas: Trace Element and Isotope Perspectives, in: Christie, D.M., Fisher, C.R., Lee, S.-M., Givens, S. (Eds.), Back-Arc Spreading Systems: Geological, Biological, Chemical, and Physical Interactions. American Geophysical Union, pp. 63–86. doi:10.1029/166GM06

Phillips, B.A., Kerr, A.C., Mullen, E.K., Weis, D., 2017. Oceanic mafic magmatism in the Siletz terrane, NW North America: Fragments of an Eocene oceanic plateau? Lithos 274–275, 291–303. doi:10.1016/j.lithos.2017.01.005

Pitcher, B.W., Kent, A.J.R., Grunder, A.L., Duncan, R.A., 2017. Frequency and volumes of ignimbrite eruptions following the Late Neogene initiation of the Central Oregon High Cascades. Journal of Volcanology and Geothermal Research 339, 1–22. doi:10.1016/j.jvolgeores.2017.04.019

Plank, T., Kelley, K.A., Zimmer, M.M., Hauri, E.H., Wallace, P.J., 2013a. Why do mafic arc magmas contain ~4 wt% water on average? Earth and Planetary Science Letters 364, 168–179. doi:10.1016/j.epsl.2012.11.044

Plank, T., Kelley, K.A., Zimmer, M.M., Hauri, E.H., Wallace, P.J., 2013b. Why do mafic arc magmas contain ~4 wt% water on average? Earth and Planetary Science Letters 364, 168–179. doi:10.1016/j.epsl.2012.11.044

Priest, G.R., 1990. Volcanic and tectonic evolution of the Cascade Volcanic Arc, central Oregon. Journal of Geophysical Research: Solid Earth 95, 19583–19599. doi:10.1029/JB095iB12p19583

Rapp, R.P., 1995a. Amphibole-out phase boundary in partially melted metabasalt, its control over liquid fraction and composition, and source permeability. J. Geophys. Res. 100, 15601–15610. doi:10.1029/95JB00913

Rapp, R.P., 1995b. Amphibole-out phase boundary in partially melted metabasalt, its control over liquid fraction and composition, and source permeability. J. Geophys. Res. 100, 15601–15610. doi:10.1029/95JB00913

Righter, K., 2000. A comparison of basaltic volcanism in the Cascades and western Mexico: compositional diversity in continental arcs. Tectonophysics 318, 99–117. doi:10.1016/S0040-1951(99)00308-X

Ruscitto, D.M., Wallace, P.J., Johnson, E.R., Kent, A.J.R., Bindeman, I.N., 2010. Volatile contents of mafic magmas from cinder cones in the Central Oregon High Cascades: Implications for magma formation and mantle conditions in a hot arc. Earth and Planetary Science Letters 298, 153–161. doi:10.1016/j.epsl.2010.07.037

Saunders, A.D., Tarney, J., 1984. Geochemical characteristics of basaltic volcanism within back-arc basins. Geological Society, London, Special Publications 16, 59–76. doi:10.1144/GSL.SP.1984.016.01.05

Scarberry, K.C., Meigs, A.J., Grunder, A.L., 2010. Faulting in a propagating continental rift: Insight from the late Miocene structural development of the Abert Rim fault, southern Oregon, USA. Tectonophysics, Extensional Tectonics in the Basin and Range, the Aegean, and Western Anatolia 488, 71–86. doi:10.1016/j.tecto.2009.09.025

Sherrod, D. R., Taylor, E. M., Ferns, M. L., Scott, W. E., Conrey, R. M., Smith, G. A., 2004. Geologic Map of the Bend 30-× 60-Minute Quadrangle. Central Oregon. US Geological Survey Geologic Investigations Series Map I-2683.

Sisson, T.W., Bronto, S., 1998. Evidence for pressure-release melting beneath magmatic arcs from basalt at Galunggung, Indonesia. Nature 391, 883–886. doi:10.1038/36087

Sisson, T.W., Grove, T.L., 1993. Experimental investigations of the role of H2O in calc-alkaline differentiation and subduction zone magmatism. Contr. Mineral. and Petrol. 113, 143–166. doi:10.1007/BF00283225

Sisson, T.W., Layne, G.D., 1993. H2O in basalt and basaltic andesite glass inclusions from four subduction-related volcanoes. Earth and Planetary Science Letters 117, 619–635. doi:10.1016/0012-821X(93)90107-K

Sisson, T.W., Ratajeski, K., Hankins, W.B., Glazner, A.F., 2005. Voluminous granitic magmas from common basaltic sources. Contrib Mineral Petrol 148, 635–661. doi:10.1007/s00410-004-0632-9

Smith, G.A., 1986. Stratigraphy, sedimentology, and petrology of Neogene rocks in the Deschutes basin, central Oregon : a record of continental-margin volcanism and its influence on fluvial sedimentation in an arc-adjacent basin (Ph.D.). Oregon State University, Corvallis, Oregon.

Smith, G.A., Snee, L.W., Taylor, E.M., 1987. Stratigraphic, sedimentologic, and petrologic record of late Miocene subsidence of the central Oregon High Cascades. Geology 15, 389–392. doi:10.1130/0091-7613(1987)15<389:SSAPRO>2.0.CO;2

Spera, F.J., Bohrson, W.A., 2001. Energy-Constrained Open-System Magmatic Processes I: General Model and Energy-Constrained Assimilation and Fractional Crystallization (EC-AFC) Formulation. J Petrology 42, 999–1018. doi:10.1093/petrology/42.5.999

Streck, M.J., 2008. Mineral Textures and Zoning as Evidence for Open System Processes. Reviews in Mineralogy and Geochemistry 69, 595–622. doi:10.2138/rmg.2008.69.15

Streck, M.J., Grunder, A.L., 2008. Phenocryst-poor rhyolites of bimodal, tholeiitic provinces: the Rattlesnake Tuff and implications for mush extraction models. Bull Volcanol 70, 385–401. doi:10.1007/s00445-007-0144-3

Tanton, L.T.E., Grove, T.L., Donnelly-Nolan, J., 2001. Hot, shallow mantle melting under the Cascades volcanic arc. Geology 29, 631–634. doi:10.1130/0091-7613(2001)029<0631:HSMMUT>2.0.CO;2

Taylor, H.P., 1977. Water/rock interactions and the origin of H2O in granitic batholiths Thirtieth William Smith lecture. Journal of the Geological Society 133, 509–558. doi:10.1144/gsjgs.133.6.0509

Till, C.B., Grove, T.L., Carlson, R.W., Donnelly-Nolan, J.M., Fouch, M.J., Wagner, L.S., Hart, W.K., 2013. Depths and temperatures of <10.5 Ma mantle melting and the lithosphere-asthenosphere boundary below southern Oregon and northern California. Geochemistry, Geophysics, Geosystems 14, 864–879. doi:10.1002/ggge.20070

Trehu, A.M., Asudeh, I., Brocher, T.M., Luetgert, J.H., Mooney, W.D., Nabelek, J.L., Nakamura, Y., 1994. Crustal Architecture of the Cascadia Forearc. Science 266, 237–243. doi:10.1126/science.266.5183.237

Trench, D., Meigs, A., Grunder, A., 2012. Termination of the northwestern Basin and Range province into a clockwise rotating region of transtension and volcanism, southeast Oregon. Journal of Structural Geology 39, 52–65. doi:10.1016/j.jsg.2012.03.007

Trimble, J., Meigs, A.J., Wannamaker, P.E., 2015. A REFINED STRUCTURAL MODEL OF THE OREGON CASCADES ARC-BACKARC TECTONIC PROVINCE. Presented at the Geologic Society of America Annual Meeting, Geological Society of America Abstracts with Programs, Baltimore, MD, p. 150.

Vigneresse, J.L., 1999. Understanding Granites: Integrating New and Classical Techniques. Geological Society of London.

Villiger, S., Ulmer, P., Müntener, O., 2007. Equilibrium and Fractional Crystallization Experiments at 0·7 GPa; the Effect of Pressure on Phase Relations and Liquid Compositions of Tholeiitic Magmas. J Petrology 48, 159–184. doi:10.1093/petrology/egl058

Waters, L.E., Lange, R.A., 2015. An updated calibration of the plagioclase-liquid hygrometer-thermometer applicable to basalts through rhyolites. American Mineralogist 100, 2172–2184. doi:10.2138/am-2015-5232

Wells, R., Bukry, D., Friedman, R., Pyle, D., Duncan, R., Haeussler, P., Wooden, J., 2014. Geologic history of Siletzia, a large igneous province in the Oregon and Washington Coast Range: Correlation to the geomagnetic polarity time scale and implications for a long-lived Yellowstone hotspot. Geosphere 10, 692–719. doi:10.1130/GES01018.1

Wells, R.E., Heller, P.L., 1988. The relative contribution of accretion, shear, and extension to Cenozoic tectonic rotation in the Pacific Northwest. Geological Society of America Bulletin 100, 325–338. doi:10.1130/0016-7606(1988)100<0325:TRCOAS>2.3.CO;2

Wells, R.E., McCaffrey, R., 2013. Steady rotation of the Cascade arc. Geology 41, 1027–1030. doi:10.1130/G34514.1

Whitehead, N.E., Seward, D., Veselsky, J., 1993. Mobility of trace elements and leaching rates of rhyolitic glass shards from some New Zealand tephra deposits. Applied Geochemistry 8, 235–244. doi:10.1016/0883-2927(93)90038-I

Wolf, M.B., Wyllie, P.J., 1995. Liquid segregation parameters from amphibolite dehydration melting experiments. J. Geophys. Res. 100, 15611–15621. doi:10.1029/95JB00660

Wright, H.M., Bacon, C.R., Vazquez, J.A., Sisson, T.W., 2012. Sixty thousand years of magmatic volatile history before the caldera-forming eruption of Mount Mazama, Crater Lake, Oregon. Contrib Mineral Petrol 164, 1027–1052. doi:10.1007/s00410-012-0787-8

Yoder, H.S., Tilley, C.E., 1962. Origin of Basalt Magmas: An Experimental Study of Natural and Synthetic Rock Systems. J Petrology 3, 342–532. doi:10.1093/petrology/3.3.342

Zhao, Z.-F., Zheng, Y.-F., 2003. Calculation of oxygen isotope fractionation in magmatic rocks. Chemical Geology 193, 59–80. doi:10.1016/S0009-2541(02)00226-7

5. Statistics and Segmentation: Using Big Data to better assess Cascades arc geochemical variability

5.1 Introduction

The composition of primitive magmas erupted at arc volcanoes bear evidence of the complex interplay between geochemical contributions from the subducted oceanic crust and sediment, liberated fluids, mantle wedge, and the overlying lithosphere. Heterogeneity in the composition and degree of contribution from each of these is highly variable worldwide. This diversity is made even more complex by the fact that other parameters such as the rate and angle of subduction, slab age, mantle flow patterns, and thickness and tectonics of the overlying lithosphere also greatly affect the composition of arc magmas. Thus, the geochemistry of arcs worldwide is highly variable, and significant differences often exist even within a single arc. Comparing along-arc changes in geochemistry to variability in these parameters provides an excellent means by which to identify those that may be most responsible for production of heterogenous magmas within a single arc system. This, in turn, provides a more comprehensive understanding of the complex magmatic processes that occur within arcs.

Systematic changes in the geochemistry of magmas along arcs has been demonstrated for many systems around the world, and numerous causes have been proposed for each system. For example, in the Central American Volcanic Arc (CAVA), systematic trends towards lower La/Yb and higher U/Th and Ba/La in mafic lavas from the Nicaragua portion of the arc, may indicate higher degree partial melting and contribution from the slab (Carr et al., 2003). This has been interpreted to result from a steeper slab angle towards the center of the arc that may result in concentrating the fluid flux (Patino et al., 2000) and more flexure and fracturing and therefore higher flux of liberated fluids (Shaw et al., 2003). Wörner et al. 1(994) explore geochemical variations in volcanoes from the Central Andes (17.5-22°S) and suggest that crustal age is the predominant factor producing heterogeneitiy because crustal thickness, sediment supply, slab depth, and distance from trench are invariant over this portion of the arc. Along-arc changes in the Sunda arc of Indonesia, have

been attributed to mantle heterogeneity and slab depth by Whitford et al. (1979) or differing sediment compositions and degree of melting (Turner and Foden, 2001). Thus, along-strike trends in geochemistry are a common feature in arcs worldwide and provide a window into the effects that each factor has on arc geochemistry.

Numerous authors have also demonstrated along-arc geochemical variability of the Cascades volcanic arc (e.g. Bacon et al., 1997; Leeman et al., 2005; Mullen et al., 2017; Schmidt et al., 2008). Multiple endmember primitive lava types have been identified within the arc (i.e. calc-alkaline, tholeiitic, intraplate, shoshonite, absorokite, primitive basaltic andesite) and the proportion of each type that is erupted varies significantly from north to south (Schmidt et al., 2008). In addition to isotopic and trace element compositions, the arc also exhibits along-strike differences in volcanic spacing, volumetric production, and eruptive style (Hildreth, 2007; Sherrod and Smith, 1990). Based tectonics and volcanic vent density, Guffanti and Weaver (1988) proposed that the arc is physically segmented into five distinct segments, and suggest that tectonic and magmatic processes are similar within each segment, and different between them.

Schmidt et al. (2008) improved on this work by providing a segmentation scheme that divides the Cascades arc spatially into four sections based on abundance of primitive lava types, and trace element and isotopic data (Fig. 5.1). The four segments are: The North Segment (Mt. Meager to Glacier Peak), the Columbia Segment (Mt. Rainier to Mt. Jefferson), the Central Segment (Three Sisters to Medicine Lake), and the South Segment (Mt. Shasta to Lassen Peak). These segment boundaries were defined such that the geochemical composition of primitive lavas is visually similar within a segment but are relatively distinct between segments. The authors suggest that differences in regional tectonics, lithospheric composition, and degree of fluid-flux melting are the primary causes for such geochemical segmentation. The definition of these segments has been adopted by subsequent authors working on Cascades volcanoes, and no studies since then have challenged such the scheme. Although this work made great strides in understanding the geochemical variability of the arc, it is based on a relatively small data set (n=390)

that is spatially biased towards just 14 of the over 3,400 Quaternary volcanic vents of the 1200 km long Cascades arc (Fig. 5.1).

However, to infer robust conclusions about the causes of variability within an arc requires that there is adequate geochemical data to fully characterize the compositional range within each region and provide comprehensive spatial coverage of the entire arc. This requires the compilation of large geochemical datasets. Although larger datasets tend to avoid problems of incomplete sampling, sampling is inherently uneven; certain volcanoes within an arc tend to be oversampled, while other less popular edifices remain poorly studied. This is a problem for studies that seek to address big picture questions such as variability over an entire arc, since the oversampled volcanoes overwhelm the overall trends, while those of the rest of the volcanoes may not be adequately represented. For example, in the Cascades arc, two volcanoes, Mt. Adams and Mt. St. Helens, account for a quarter of all mafic data for the entire arc. Thus, simple calculations involving all arc data are highly skewed towards the compositions of these two volcanoes and the narrow regional processes that produce them. However, rigorous statistical treatment of these data can help avoid the ill-effects of sampling bias and allow for more robust interpretations of larger, more representative datasets.

The Cascades arc is among one of the most highly studied arcs in the world, and the tremendous volume of geochemical data that exists for this arc is underutilized in the literature. The existence of such large data sets for an arc that has been demonstrated to be highly variable provides the perfect opportunity to explore along-arc variability with a more comprehensive dataset. For our study, we compile major and trace element and isotopic data on over 11,000 samples from 175 different publications to more thoroughly assess geochemical variability along the Cascades arc. Our study consists of two parts. We first re-examine the segments proposed by Schmidt et al. (2008) utilizing this more representative dataset, and use a Monte Carlo approach with bootstrap resampling to reduce sampling bias. We then use multivariate statistics to quantify differences among the segments, and to test whether the segments are statistically distinct. In the second part of our study, we develop a

multivariate clustering technique to objectively establish a more statistically significant segmentation scheme. Our study is the first of its kind to use rigorous multivariate statistics to address geochemical variability within a single arc. By utilizing a more representative dataset, reducing the influence of oversampled volcanoes, and partitioning the arc into regions that are most geochemically distinct from each other, we can better assess the petrogenetic causes of geochemical variability across the Cascades arc.

5.2 Background

The eruptive style, volcanic production, spatial distribution and magmatic geochemistry of volcanoes vary significantly along the Cascades arc (Guffanti and Weaver 1988; Hildreth, 2007; Leeman et al., 2005; Mullen et al., 2017). This variability may reflect along-arc changes in subduction geometry, regional tectonics, or the composition of slab, mantle or overlying lithosphere (Fig. 5.1A).

Subduction changes from nearly orthogonal in the north to highly oblique in the south. The age of the slab that is subducted ranges from 3-5 Ma in the northernmost and southernmost regions of the arc, to 10 Ma near the California-Oregon border (Wilson, 2002). In addition, more highly fractured slabs in the north and south may introduce more subduction fluid to the mantle wedge (Schmidt et al., 2008). The slab may be highly segmented, with differing angles, and slab gaps and tears that may allow enriched sub-slab mantle into the overlying wedge (Porritt et al., 2011; Gao and Shen, 2014) Sediment abundance and composition also vary significantly along the arc (Carpentier et al., 2014). The depth of the slab beneath different volcanoes range from <60 km under Mt. St. Helens to >100 km for Garibaldi Belt and back-arc volcanoes (Weaver and Baker, 1988). In addition, multiple authors have suggested that the mantle is highly heterogeneous and may or may not have isotopically distinct domains (e.g. Bacon et al., 1997 and Mullen et al., 2017, respectively). Mantle flow patterns may be toroidal around slab edges, and the degree of melting may be highly dependent on position relative to slab edges or gaps (Long, 2016, and references therein).

Finally, there are significant along-strike differences in the overlying lithosphere. Lithology changes from 50-km thick Paleozoic accreted terranes and old cratonic lithosphere in the north, to ~60 Ma accreted oceanic plateau in the central part of the arc, and the Paleozoic Klamath Terrain in the south (Schmidt et al., 2008). Regional tectonics also change along arc from compressional in the north to extensional in the south (Brocher et al., 2017; Wells and McCaffrey, 2013).

All of these differences, with regard to the slab, mantle and lithosphere, may play a role in the heterogeneity of Cascades arc magmas. Discerning which are most impactful is crucial to our understanding of the Cascades volcanic arc.

5.3 Methods

5.3.1 Data compilation, filtering, and categorization

To fully characterize the geochemical heterogeneity of the Quaternary High Cascades arc, we carefully compiled a comprehensive dataset from the literature. To do this, we used three online data repositories: EarthChem, GeoRoc, and the U.S. Geological Survey (USGS) National Geochemical database. Data from these databases were carefully concatenated such that no repeat analyses were included. The EarthChem Portal (http://www.earthchem.org/portal) offers a "one-stop-shop" that searches six online databases: PetDB, SedDB, NavDat, USGS, GANSEKI, and GeoRoc. To search for High Cascades data, we first set approximate bounding area using the interactive map in the EarthChem Portal (Fig. 5.2). For this area, we included the Simcoe Mountains Volcanic Field, Newberry volcano, and Medicine Lake volcano, and eastern longitudinal borders of these back arc volcanic areas were drawn per USGS scientific investigations maps (Hildreth and Fierstein, 2015; MacLeod et al., 1995; Donnelly-Nolan, 2010). We also limited the search to whole rock or glass analyses of Quaternary volcanic rocks. The EarthChem Portal search returned data from 114 publications, not including USGS, of which 17 were not found by our search using the GeoRoc database alone. Most USGS analyses retrieved by EarthChem were missing FeO and Fe_2O_3 data (n=1929), and some were missing K_2O data (n=75). However, we found these data by manually searching the USGS

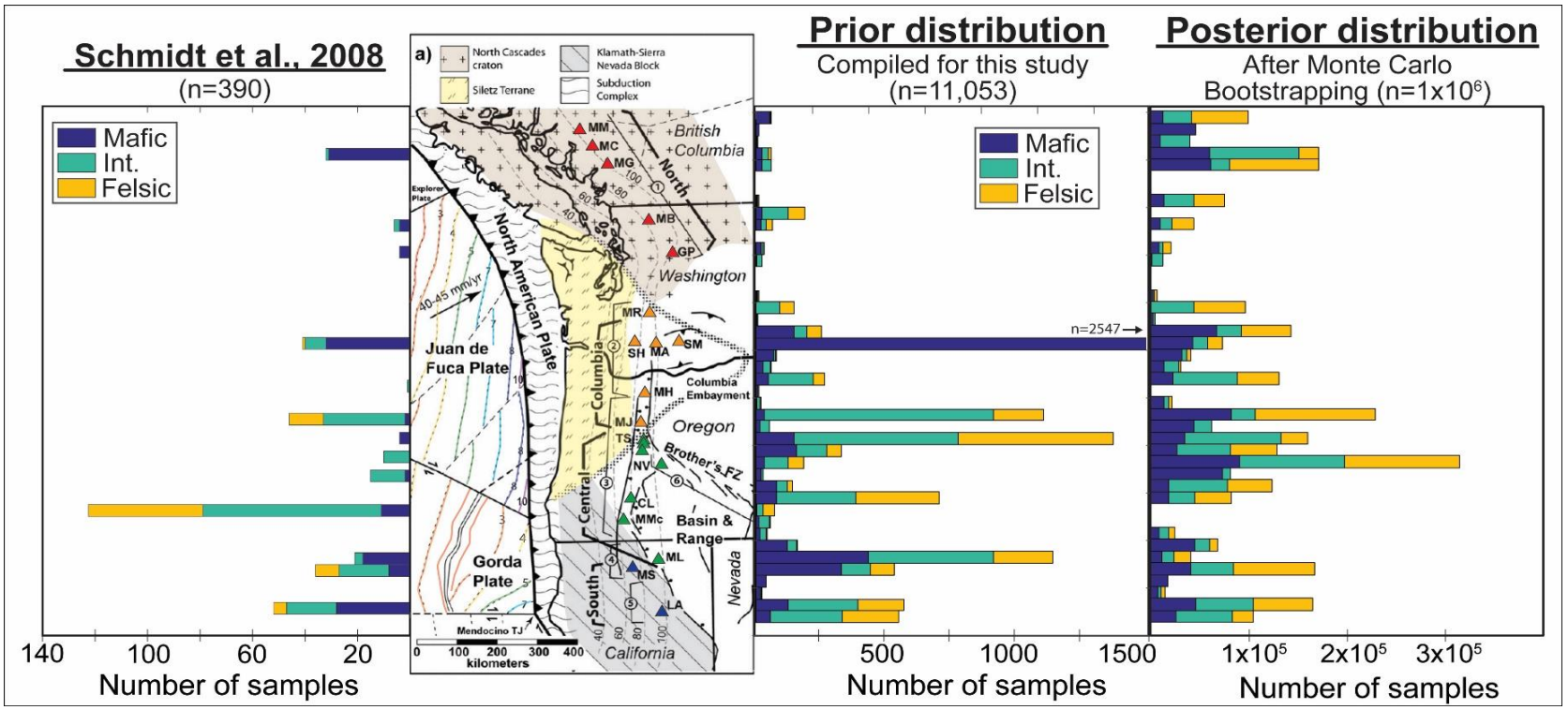

Fig. 5.1: (A) Schematic map modified from Schmidt et al (2008) indicating basement lithology, age of subducting slab, depth to slab, and regional tectonics, which differ along strike. Major Quaternary volcanoes are color coded to Schmidt segments. Sampling distribution from Schmidt et al., 2008 is shown at left. Sampling (prior) distribution from our compilation is shown in the middle histogram. The posterior distribution after completing a Monte Carlo Boot strap re-sampling, with weighting based on new segmentation scheme (see text). Improvement in posterior distribution is limited to 20x because of our choice of minimum weight (see text). Note change of scale for each histogram.

National Geochemical database. This search was made particularly difficult, as EarthChem does not return references to individual USGS studies; it simply returns "USGS National Geochemical database" as the citation. Additionally, data from seven publications were removed because they either were erroneously listed as Quaternary, included only data for SiO_2, or had incorrect longitudes listed and were therefore erroneously included within the bounding area.

We also utilized the GeoRoc (Geochemistry of rocks of the oceans and continents) database (http://georoc.mpch-mainz.gwdg.de/georoc). We did a query by geological setting ("Convergent Margins"), then by location ("Cascades"), Arc Zones ("High Cascades" + "Garibaldi Volcanic Belt", by Region(s)/Site(s) ("British Columbia" + "Washington" + "Oregon" + "California"). We then further constrained the search by rock type ("volcanic rock"), type of material ("volcanic glass" + "whole rock" + "mineral/component"), and constrained the mineral/component to only include "glass" and "groundmass." We selected the "compiled" option, that compiles all analyses for a given sample into one line of data. For each element, priority is given to the most recent data from the most precise analytical method (e.g. decreasing priority methods for major elements are X-ray fluorescence, wet chemistry, electron microprobe, and then atomic emission and absorption spectrometry). We also collected metadata for each analysis including latitude, longitude, rock type, and rock name, each critical for future partitioning of the data. Because we were unable to search by age, we then had to manually remove all data that had age (geological or absolute) that were not Quaternary (n=168). Since many samples did not have ages listed, it is possible that some from the Late Neogene, early High Cascades (2.6-7.5 Ma) may have been accidently included within our database. We chose to limit our study to Quaternary High Cascades as significant changes have occurred in some portions of the arc since the arcs initiation in the late Neogene (e.g. the Central Oregon Cascades, Pitcher et al., 2017c). Overall, our Georoc query returned data from 145 different publications. Although EarthChem Portal claims to search GeoRoc database, the direct search of the database returned data from 86 publications that were not found using the EarthChem portal.

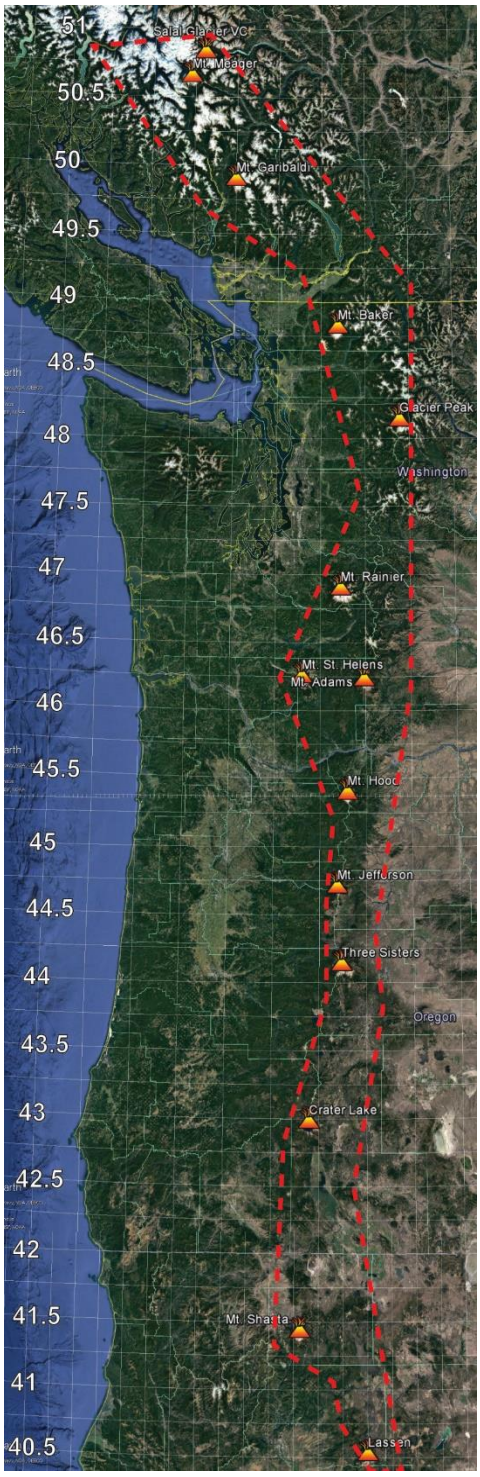

Fig. 5.2: Bounding area chosen for EarthChem Portal search. Conservative outline was drawn as to not include non-Quaternary or non-arc rocks.

Fig. 5.3: Areas that were combined prior to Hierarchical clustering to sparsity of data

We also had to manually enter data from 12 sources that were not found by the databases. We added four datasets from USGS Open-file reports and Scientific Investigations maps, from three theses, and from four other publications (Clynne et al., 2008; Hildreth and Fierstein, 2015; Hildreth, Fierstein, Calvert, 2012; Hildreth, Fierstein, Calvert, 2017; Conrey, 1991; DiGuilio, 2016; Yogodzinski, 1985; Mullen et al., 2017; Mullen and Weis, 2013; Rowe et al., 2009; Ruscitto et al., 2010). We removed analyses that were collected before 1970 (n=245 samples), so as to retain only higher quality data. We converted all iron data to FeO*, normalized all major element data to 100%, and removed all samples with analytical totals <90%, as suggested by WoldeGabriel et al. (2005).

Because the processes of magma generation and differentiation within the rear-arc may differ from those of the volcanic front (e.g. Pearce and Stern, 2006), we created two datasets, one with and one without data from the rear-arc volcanic centers (i.e. Simcoe Volcanic field, Newberry Volcano and Medicine Lake). We used USGS geological maps to constrain the best longitudinal boundary for these three rear-arc provinces. The Simcoe volcanic field (n=1295) was defined as the region east of -121.25° between 46.45 and 45.5°N latitudes (Fig. 5.2). Samples located east of -121.4° and between 41.9 and 45°N, were considered part of the Newberry Volcano (n=423). Medicine Lake area (n=1624) was defined as being east of -121.75°, between 41.9 and 41.1°N. Thus, in our dataset, there is a total of 3341 samples from the rear-arc, which accounts 31% of all Cascades samples (Table 1).

In addition, since compositional differences in felsic rocks may indicate the influence of very different processes than along-arc variability in mafic rocks, we separated the dataset into three compositional groups: mafic (<52 wt.% SiO_2), intermediate (52-62.99 wt.%), and felsic (≥63 wt.%). For the samples that did not have SiO_2 data, we used the rock names given by the author. Our mafic category included those samples listed as: basalt, absorokite, hawaiite, picrite, tholeiite, trachybasalt. Intermediate samples were listed as basaltic-andesite, andesite, shoshonite, trachyandesite, and basaltic trachyandesite. Samples listed as dacite, rhyodacite, rhyolite, or “tuff” were classified as felsic. We deleted the 153 samples

that did not contain any of this information. In addition, we created a separate dataset for primitive samples (SiO_2 <52 wt.% MgO >7wt.%, Mg# >57.5). Schmidt et al (2008) used Mg# >60 as the cutoff for primitive, but this criterion left the northern Cascades (north of Glacier Peak) with very few primitive samples.

Although a major goal of this study is to fully characterize the compositional range of the Cascades, outliers greatly affect the results of multivariate techniques like those implemented in this study (Tryon et al., 2011). Thus, we wanted to remove values that were likely true outliers or analytical errors, without removing "real" compositions that happen to be relatively extreme. To do this, we utilized Chauvenet's criterion for rejection. Unlike methods, such as removing values beyond 2σ from the mean or 1.5*IQR from the median, the cutoff point for Chauvenet's criterion is also dependent on the number of analyses used. This is important because the effect of a single outlier point on larger datasets is much less than for a smaller one. Therefore, we may be more confident in keeping unusual points if we have a larger dataset. We first calculated the mean and standard deviation for each element and isotope and applied the following criterion to each. Suspect values were removed only if they were more than τ standard deviations away from the mean, where τ is the critical Z-score for which the probability $P(\tau) = 1 - \frac{0.25}{n}$, and n is the number of analyses. This means that for a dataset with 200 analyses, outliers are defined as being more than 3σ from the mean, but for a dataset with only 10 analyses, outliers are those that are 1.96σ from the mean. Since mean values of each element differ widely between compositions, we applied the Chauvenet's criterion separately for each of the eight subsets of data (four compositions, each with and without rear-arc data). We also did two iterations to account for the effect that especially large outliers have on the mean and standard deviation.

After the removal of outliers, our data compilation includes over 265,000 analyses on over 11,000 different samples. Of these, 36% are mafic samples, 41% are intermediate, and 23% are felsic (Table 5.1).

Table 5.1: Number of samples and individual major, trace element, or isotopic analyses in our compilation for the Quaternary Cascades

	N of samples			N of analyses
	Back arc	Arc	All data	All Data
Primitive	637	876	1,513	29,149
Mafic	2,406	1,590	3,996	74,026
Intermediate	923	3,542	4,465	85,788
Felsic	400	2,160	2,560	46,929
TOTAL	3,729	7,292	1,1021	265,041

5.3.2 Reducing Sampling bias: Weighted Bootstrap resampling

Because certain volcanoes (e.g. Mt. St. Helens) tend to be more highly studied and sampled than others, our geochemical dataset does not represent an even sampling distribution across the whole Cascades arc. Furthermore, regions that are near major stratovolcanoes tend to be more highly sampled and areas that may include many smaller and/or monogenetic vents may go completely un-sampled. For example, between Mt. Jefferson and Mt. Hood (44.75-45.25°N) there are over 70 mafic to intermediate shield volcanoes and scoria cones and 14 dacite lava domes. However, there are only 23 total samples from this region (Hildreth, 2007; Sherrod and Scott, 1995). In comparison, the region just north of Crater Lake (43-43.25°N) contains only 60 mafic to intermediate vents (Hildreth, 2007), but has over 100 samples with geochemical data. Thus, to better characterize along-arc variability, we must reduce this sampling bias such that there is a more even spatial distribution.

To do this, we used a Monte Carlo method with a weighted bootstrap resampling. Bootstrap resampling, or bootstrapping, refers to any statistical technique that involves iterative random sampling from a population, with replacement after each sample is drawn. Repeating this sampling many times (n>10,000), referred to as a Monte Carlo technique, increases the likelihood that the mean and standard deviation of the sample set accurately represent that of the entire population. This technique is especially powerful in reducing sampling bias when an inverse weighting scheme is used, such that each analysis from under-sampled regions are given a much higher probability of being selected during bootstrapping, compared to those from oversampled regions. Thus, analyses from under-sampled regions are “pulled up by

their bootstraps" to create a new "posterior distribution" that is much more uniform than the original "prior distribution" (Fig. 5.1).

For our study, we first separated the data into bins of 0.25° latitude ("latbins"). Then, we assigned each sample a weight, or probability of selection ($0.05 \leq W \leq 1$), that is inversely proportional to the number of samples within its latbin. This was done separately for each compositional group. The weight given to all analyses within each bin was calculated by dividing the number of samples within that bin by that of the bin that contains the most samples for a given segment, and subtracting that number from one, $\left(W_i = 1 - \frac{N_i}{N_{max}}\right)$. For example, using the Schmidt et al. (2008) segmentation scheme, the latbin (46-46.25°N) that includes both Mount St. Helens and Mt. Adams, has the maximum number of mafic samples, with 774. Thus, the Mt. Hood area (45.25-45.5°N), which has only 56 mafic samples, was given a weight of 0.92 $\left(1 - \frac{56}{774}\right)$ whereas the region just north of Mt. St. Helens and Mt. Adams (46.25-46.5), which has more samples (n=144), was given a lower weight of 0.81. Thus, during the bootstrapping, samples near the Mt. Hood region were more likely to be selected than those from the region north of Mt. St. Helens. We used a minimum weight of 0.05, such that the locations that are most highly sampled (i.e. Mt. St. Helens) are not completely disregarded (Keller and Schoene, 2012). Thus, the improvement in the posterior distribution was limited to 20 times.

To complete this analysis, we wrote a MATLAB code, which is given in Appendix 5.1. Our Monte Carlo bootstrap re-sampling procedure was as follows:
1) For each bootstrap iteration, a random number r between 0 and 1 is assigned to each sample in the dataset. MATLAB uses a Mersenne Twister pseudorandom number generator, which has been shown to be sufficiently close to true randomness (Matsumoto and Nishimura, 1998). New r values are generated for each iteration
2) Each sample for which $W > r$, was "chosen" for that round.
3) For each element of the chosen sample, a random value is drawn from a Gaussian distribution formed by μ=reported value, σ= analytical error, and all these values for a chosen sample are added to the bootstrap subset.
4) Step (3) is done for each chosen sample of that bootstrap iteration.

5) The bootstrap subset from this iteration is concatenated to the subsets from all previous iterations into a single Monte Carlo results set
6) Steps 1-5 are repeated until the number of samples within the Monte Carlo results set >1 million.

Step 3 is necessary because the bootstrap subset must have a continuous normal distribution. We used an analytical uncertainty of 2%, as suggested by Keller and Schoene (2012). To test the effect of this choice of analytical uncertainty, we did two additional test runs, one in which all elements had a 4% uncertainty, and one where major elements had 2% uncertainty and trace elements had 4%. We found that this made almost no difference in the final bootstrapped averages of all elements, and the effect on the bootstrapped confidence intervals was small enough that it could not be visually observed on most bivariate plots.

Because the data distribution for isotopes is quite different from that of major and trace elements, we performed a separate bootstrap analysis for the isotopic data, weighting by number of samples containing such data, rather than just by number of samples within a latbin.

5.3.3 Calculating Confidence intervals for bootstrapped means

Comparing the bootstrapped means of different segments is relatively meaningless without knowing the distribution of data around the mean. Thus, it is important that we calculate a confidence interval around each bootstrapped mean. A 95% confidence interval (CI) suggests that if we repeated our sampling method many more times and calculated means for each of those, we would expect 95% of the mean values to lie within that CI. Confidence intervals are much more useful in statistics than just using $\bar{x}$ ±2σ, because the range depends on the sample size. This is important because larger sample sizes increase the probability that the sample mean ($\bar{x}$) is the same as the true "population mean (μ)." To calculate a 95% CI, we use the following: $\bar{x} \pm t\frac{\sigma}{\sqrt{n}}$, where $\bar{x}$ and σ are the bootstrapped mean and standard deviation, and t is the critical value for a student t distribution at the 0.05 level. We use the original number of samples for n, not the number of samples in the Monte Carlo set

(Keller et al., 2015). For reference, if n=30 the critical t value is 2.04, if n=100 the critical t is 1.98. These CI calculations rely on the assumption of normality. However, even if the original data was not normally distributed, by the Central Limit Theorem, the Monte Carlo set will always be normally distributed due to the high number of samples selected during the Monte Carlo analysis.

5.3.4 Testing the robustness of segmentation schemes

Partitioning the arc into segments should be done in a way that the segments are geochemically dissimilar to one another, so that these segments can be compared and inferences can be made as to the causes for these differences. If two segments are relatively similar, then they should be combined. Thus, to test whether segments are geochemically distinct, we use a multivariate technique called the Hotelling's T^2 test. This test is the multivariate equivalent of the Student's t test and is a "post-hoc test" that follows a multivariate analysis of variance (MANOVA). Hotelling's T^2 test essentially evaluates whether the multivariate means ("mean vector") of two segments, are different enough in n-dimensional space to reject the null hypothesis that the two segments are the same. Before testing this, the variables (elements and isotopes) are transformed by the MANOVA technique, such that the new transformed variables minimize the within-segment variation and maximize the between-segment variation (Fig. 3.3). Thus, instead of just simply comparing the multivariate distances between mean values of each segment, the Hotelling's T^2 compares the means of each element, variance of each element, and multivariate covariance between elements (i.e. multivariate trends) of the data in each segment.

For large populations (N>30), such as the dataset in our study, the Hotelling's T^2 statistic follows a X^2 distribution with k degrees of freedom, where k is the number of geochemical elements, allowing us to calculate a p value. Small p values indicate that two segments are more different than would be expected for two samples drawn from a single population. Specifically, if the $p<0.05$, then we reject the null hypothesis, and the two segments are statistically distinct. The Mahalanobis distance, which is closely related to the Hotelling's T^2, provides the multivariate distance between the mean vectors of the two groups. We used the Hotelling's T^2 test on both

the segmentation scheme of Schmidt et al. (2008) and our new statistically-based scheme and compared the Mahalanobis distances between segments to assess which created more distinct segments groups. We conducted the tests using three different datasets: mafic, with and without the back-arc data, as well as all primitive data. Due to the sparsity of primitive arc-front data in some latbins, covariance matrices could not be calculated, and thus we could only determine MD for primitive compositions if we utilized all data, including the back-arc.

5.3.5 Establishing new segments: modified Hierarchical clustering mechanism

To determine a statistics-based segmentation scheme that best separates the Cascades arc into the geochemically distinct segments, we developed a modified hierarchical clustering technique. For each step in a classic hierarchical clustering analysis, the two individuals or groups that are most similar (e.g. have the shortest distance between their mean values) are combined into a new group and this process is repeated until the desired number of groups are reached or all individuals are combined into a single group. Thus, the process creates groups such that the within-group similarity is maximized. This process can be represented by a dendrogram, in which all individual start out as separate branches on the x axis, and as two individuals are merged together, the distance between their means (distance of fusion) are shown on the y axis (Fig. 5.6). There are multiple techniques for deciding when to stop the process, or to "cut" the dendrogram, which will be discussed later in this section. We had to modify this traditional hierarchical clustering technique to reduce sampling bias, to deal with problems associated with missing data, to ensure that clusters consisted of regions that were proximally close to one another, and the fact that many elements are highly correlated (i.e. differentiation trends). These will be discussed in detail below.

In a classic hierarchical cluster analysis, one has a choice of "linkage method," which is the way that one determines the distance between groups to combine those that are closest to one another. In one method, called centroid linkage, the Euclidean distance between each clusters' centroid is used to determine which are closest together. However, this method is best suited for data that is multidimensional

spheres. That is, data where the dispersion around the centroid is approximately equal in all directions (Everitt et al., 2001). This is not the case for geochemical data, since there is significant covariation between elements. Thus, we chose to use the Mahalanobis distance (MD) as the measure of distance between groups in our hierarchical clustering. MD measures the distance between the centroids of two groups while also considering the dispersion around the centroids. This dispersion is measured by a dataset's covariance matrix. A dataset will have k by k covariance matrix, which contains the variance of each of the k elements (σ^2) is along the diagonal, and correlation coefficients between each element is in the other matrix positions. MD between groups i and j is given by:

$MD_{ij} = \sqrt{(\bar{x}_i - \bar{x}_j)^T S^{-1} (\bar{x}_i - \bar{x}_j)}$ where S is the covariance matrix and $\bar{x}_i$ is the mean vector for sample i, which contains the means of each element. We could not calculate the MD for any latbin that had less samples than number of elements (N<45) because the covariance matrix would be "singular", meaning it is not invertible. Thus, for these latbins we had to use the covariance matrix calculated for all mafic data. This is permissible, however, because the covariation of elements is not likely to change significantly between latbins (e.g. MgO will always decrease with increasing SiO_2). Because most samples had data for only a subset of elements, there was a lot of missing data. The covariance matrix of a dataset can become singular if it has excessive missing values. This was the case with our dataset. In order to calculate the covariance matrix, we used the Expectation Conditional Maximization (ECM) algorithm of Meng and Rubin (1993) to calculate a non-singular covariance matrix. This algorithm imputes values for these missing data, based on the mean and variance of that element, and then iteratively changes these imputed values until the log-likelihood function is maximized. Further explanation of the theory can be found in Little and Rubin (2014)

We wanted to reduce the effects of sampling bias when creating our new segments. Thus, every time two groups of latbins were combined, we performed a Monte Carlo analysis with bootstrap re-sampling to find that new group's bootstrapped mean values for each element. This portion of our procedure was almost

identical to the one described above in section 3.2. The only difference was that instead of assigning the same weight to all elements, based on the number of samples within the latbin, for this bootstrapping, we assigned a different weight to each element. This is preferable because if a latbin has a lot of major element data, but very little trace element data, latter data can then be given a higher weight. This allows the posterior distribution of each individual element to be much closer to uniform. This was ideal for the clustering because we do not care about keeping data from each sample together. However, for the final bootstrap means of each of our new segments, we will return to using a single weight for all elements of all samples in a latbin, as it is important in this case to keep all data from a sample row together, in order to calculate elemental ratios.

To create the clusters (segments), we used mafic data, but excluded the back-arc data. We chose not to cluster based on primitive data because such data are relatively sparse in some parts of the arc. We also chose to not include back arc data because it skews the clustering results such that regions without back-arc data are rarely clustered with regions that do have it. Additionally, this allows us to focus on the processes that may be responsible for arc variability, without adding complications from the additional processes involved in back arc magma generation.

For the purpose of clustering, we removed the 15 elements/isotopes in our data compilation for which there were more than 4 latbins that had no data, leaving us with 29 elements. We did this because when calculating the MD between two latbins, if a particular element was missing, the difference in means for that element was given a value of 0, making the two latbins appear identical for that element. Although this does not affect whether a latbin with less data gets combined to the north or to the south, it does artificially decrease the MD, which could cause that latbin to get clustered earlier in the hierarchical process.

Before beginning the clustering process, latbins that had little to no data ($n<5$) were merged with the neighboring bin to the south (Fig. 5.3). We also did a test to see if segment boundaries were different if these under-sampled bins were combined with their northern neighbor instead. We found that this choice made no difference in the

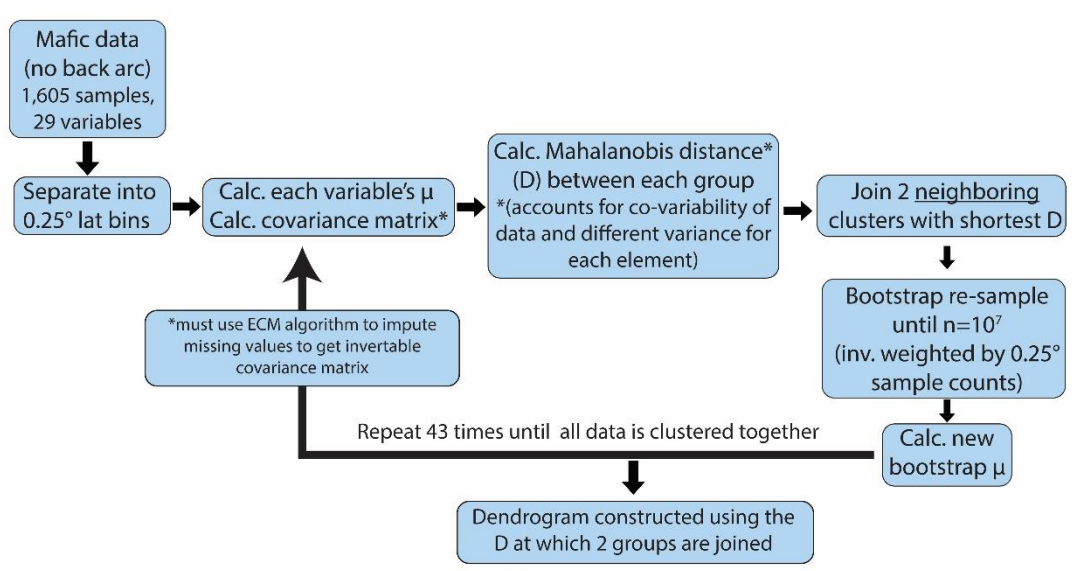

Fig 5.4: Flow chart indicating steps taken in our modified hierarchical clustering technique. Fully annotated Matlab script is given in Appendix 5.2.

final segment boundaries. After merging latbins with little to no data to their southern neighbors, we had 33 initial bins of data to subject to our modified hierarchical clustering technique.

We wrote a MATLAB script for our clustering technique (Appendix 5.2). The modified hierarchical clustering process can be summarized as follows (Fig. 5.4):

1) Means and standard deviations were calculated for each element of each latbin.

2) The covariance matrix was calculated using all mafic data from all latbins and utilizing the ECM algorithm to impute missing values

3) MDs between each neighboring latbin are calculated

4) The two with the lowest MD are combined

5) New weights are calculated for samples in this newly combined segment

6) Monte Carlo simulation with boot strap re-sampling for this newly combined segment to calculate its bootstrapped mean

7) New MDs are calculated for all neighboring segments using the bootstrapped means

8) Steps 4-7 are repeated until all are combined into a single segment.

To determine the ideal number of clusters, we use the upper-tail stopping rule of Mojena (1977). This rule states that the clustering should be cut when, for the first

time, $\alpha_{j+1} > \bar{\alpha} + k(s_\alpha)$, where $\bar{\alpha}$ and s_α are the mean and standard deviation of all the j previous distances of fusion. The k value is the upper-tail critical value for a t distribution that is defined by the number of original separate groups, and a choice in confidence level. Since we start with 33 separate latbins (after combining the ones with little to no data), the critical k value at the 99% confidence level is 2.44. In other words, we stopped the hierarchical clustering once the closest segments are separated by a MD that is larger than the average of all previous steps' distance of fusion +2.44s.

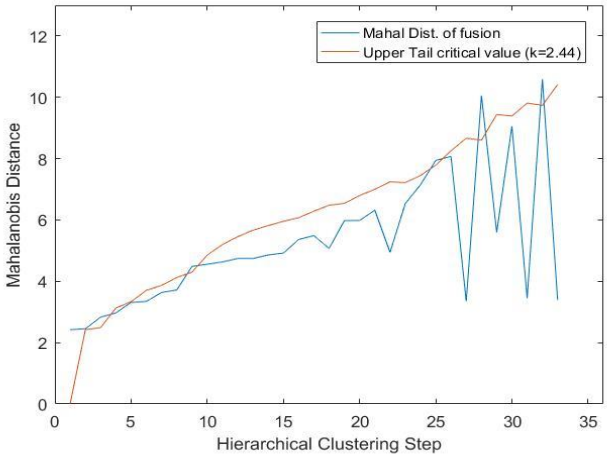

Fig. 5.5: Plot demonstrating our use of the upper-tail cutoff technique of Mojena (1977). At step 25, the MD of fusion (blue line) is finally higher than the mean of all previous MD+2.44*s (red line). Thus, we chose to cut-off the dendrogram at this step (MD=7.95). See text for further description of method.

5.4 Results

Bootstrapped means and standard errors of the Schmidt et al. (2008) segments are provided in Appendix 5.2 and those of the new segmentation scheme are given in Appendix 5.3.

5.4.1 Statistical test of the previous segmentation scheme

Our Hotelling's T^2 tests indicate that all four of the segments defined by Schmidt et al. (2008) are statistically distinct for mafic and primitive compositions (Table 5.2). For all neighboring segments, $p << 0.05$. Bootstrapped MD values, based on 29 elements, for neighboring segments range from 2.6 to 4.8 for mafic compositions and 3.6 to 6.7 for primitive compositions. These MDs indicate that for mafic and primitive compositions the Columbia and North segments are more similar

(MD=2.6-3.6) than the other pairs of neighboring segments. The South and Central portions of the arc are the most geochemically dissimilar (MD=4.2-6.7).

5.4.2 The new statistically-derived Segmentation Scheme

Using our modified hierarchical clustering technique, we establish a new statistically-based segmentation scheme for the Cascades arc. The upper-tail stopping rule designated that the clustering should stop at step 25, at which point the distance of fusion (MD=7.95) became higher than $\bar{\alpha} + 2.44(s_\alpha)$ (7.79) (Fig. 5.5). Ending the clustering at this point produced 6 segments. Although these represent the most statistically distinct partitioning, it produced two separate segments near Crater Lake, which include only 2 latbins each (42.75-43.25°N and 43.25-43.75°N). However, when we applied hierarchical clustering on primitive data, these two were combined with a MD of 6.83, which is below the cut-off point determined for the mafic data. On this basis, we choose to combine these into a single segment (Fig. 5.6).

Thus, we propose a new segmentation scheme that includes five segments: (1) the North Segment (51-49°N) from Mt. Meager to the United States-Canada border, (2) the Washington Segment (48.75-45.5°N) from Glacier Peak to the Columbia River, (3) the Graben Segment (45.5-43.75°N) from Mt. Hood to the region south of Three Sisters volcanoes, (4) the Mazama Segment (43.75-42.75°N) including the regions north and south of Crater Lake, and (5) the South Segment (42.25-40.25°N) including Mt. Shasta and Lassen Peak (Fig. 5.6). Two latbins (48.75-49°N and 42.25-42.75°N) each with very sparse mafic data remained statistically distinct, so we will consider these to be transitional zones between the segments

We performed Monte Carlo bootstrap analysis for all compositions, assigning weights based on the new segmentation scheme (Appendix 5.4). Hotelling's T^2 tests indicate that for all compositions, $p << 0.05$ and thus, these new segments are statistically distinct (Table 5). MD values for mafic compositions range from 3.6 to 7.2 (Table 5.2) and primitive data range from 3.8 to 7.7 (Appendix 5.4).

5.5 Discussion

5.5.1 Comparison of Segmentation Schemes

The primary objective of partitioning the arc into segments is to explore the causes for the geochemical differences between each segment. Thus, it is most useful if the partitioning is done such that the geochemical differences between segments is maximized. Although the segments defined by Schmidt et al. (2008) are statistically

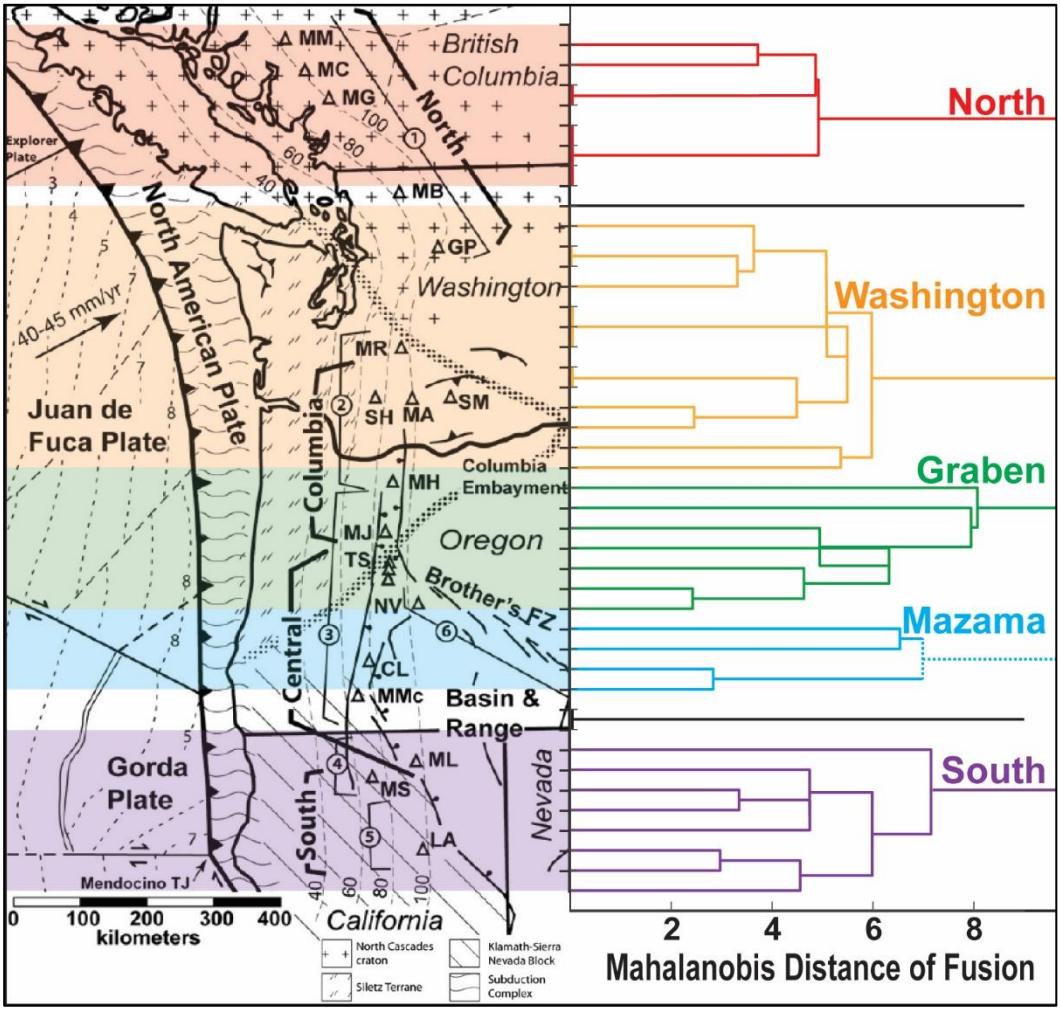

Fig. 5.6: Dendrogram from our modified hierarchical clustering and the resulting new segments. Distance along the x axis represents the MD between two groups when they were combined. Schematic map from Schmidt et al (2008) is shown on left to compare different segmentation schemes.

distinct from each other, our new statistically-derived segments tend to have higher Mahalanobis distances between them, indicating that they are more statistically dissimilar. If we consider the arc-front mafic data that we used to create our new segments, the new scheme has inter-group MDs that are up to 2.7 times higher than that of Schmidt et al. (2008) (Table 5.2). The MD between the Washington and North segments is the lowest (3.6), but is still higher than the MD between the Columbia and North segments of Schmidt et al. (2008). Primitive MD values are higher in the new scheme except for between the Mazama and Graben segments (Appendix 5.4). This is likely because the segment boundary, which was established based on arc-front data only, is at the latitude of Newberry Caldera. Thus, since this boundary causes Newberry Volcano to contribute 53 primitive samples to the Graben Segment and 47 to the Mazama Segment, the segments appear more geochemically similar when the back-arc is included (lower MD).

5.5.2 Preliminary discussion of Geochemical Trends

By calculating the bootstrapped means of our dataset, we have removed significant sampling bias, and therefore established mean compositions that best represent each arc segment as a whole. Thus, we can begin to explore the geochemical differences between each arc segment and infer the regional processes affecting these segments, rather than processes at individual volcanoes. Although the

Table 5.2: Hotelling's T^2 test results for mafic data (excluding back arc) utilizing each segmentation scheme. In both cases 29 elements were used and the critical X^2 value is 42.6 and critical F value is 1.5. Note that the Mahalanobis distance between each segment is higher in the new scheme. Hotelling's results for primitive data and for back arc data can be found in appendix 5.4

	Schmidt Segments			New Segments			
	South vs. Central	Central vs. Columbia	Columbia vs. North	South vs. Mazama	Mazama vs. Graben	Graben vs. Washington	Washington vs. North
n	913	1177	677	848	1010	416	418
MD	4.8	3.4	2.7	5.3	7.2	7.1	4.5
D2	22.9	11.7	7.2	28.4	52.5	49.9	20.3
T2	3339.7	3238.0	1096.0	2880.5	10624.6	4565.7	5439.1
X^2 p	<<0.01	<<0.01	<<0.01	<<0.01	<<0.01	<<0.01	<<0.01
F	111.6	109.0	36.2	96.0	356.2	146.8	60.0
F p	<<0.01	<<0.01	<<0.01	<<0.01	<<0.01	<<0.01	<<0.01

purpose of this paper is to develop and demonstrate the power of a new statistics-based methodology for exploring along-arc variability, we present a preliminary discussion of some of the geochemical differences between segments here. Significant future work in this regard will be required to fully interpret the trends produced by our new methodology.

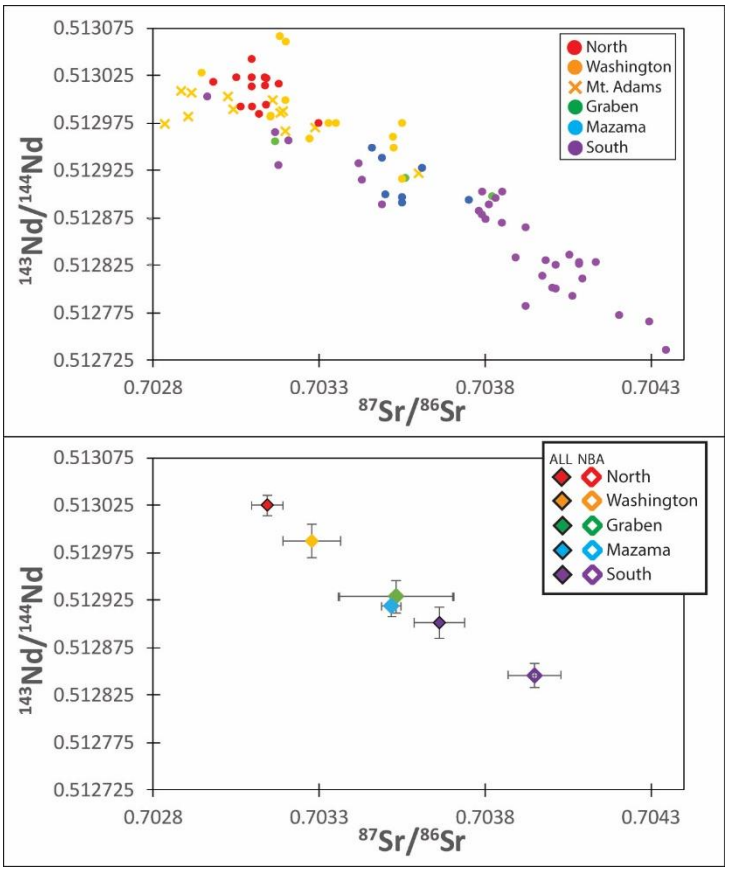

Figure 5.7: Sr vs. Nd isotopes. (A) shows actual data from Primitive Cascades. Note that Mt. Adams (x) greatly skews Washington segment data towards less radiogenic Sr. However, when we remove this sampling bias, the bootstrapped means (B) demonstrate striking north-south trend

5.5.2.1 Along-arc variability

Segment means of primitive data reveal a striking north-to-south linear trend towards more evolved Sr and Nd isotopic compositions (Fig. 5.7). Although this trend has been discussed by numerous previous authors (e.g. Bacon et al., 1997; Mullen et al., 2017; Schmidt et al., 2008), we demonstrate that by removing sampling bias, overall north-south trends can be made more clear. Isotopic data for the Washington segment of the arc is highly skewed by Mt. Adams; 58% of all primitive Sr and Nd isotope data for the segment comes from the volcano. Because Mt. Adams tends to have primitive lavas that are less radiogenic in Sr (mean=0.70315) than the rest the Washington segment (0.70330), the trend of the regional volcanoes is skewed in that direction. However, our bootstrapped mean avoids this bias and provides a more representative mean value for the segment as a whole.

Scarcity of isotope data in some segments, (e.g. n=3 in the Graben Segment), limits the power of the bootstrap technique for these regions. Conversely, the bootstrap technique is very effective at creating even sampling distributions for major and trace element data, for which there are hundreds of data points for many latbins. In addition, the bootstrapped mean and 95% confidence interval provide a much simpler way to display large quantities of data. These data can be thought of as an unbiased representation of the relative contributions of various primitive lava types in the High Cascades. Several end-member primitive basalt compositions have been proposed for the Cascades including low-K tholeiites (LKTs), calc-alkaline basalts (CABs), and intraplate-type basalts (IPBs), and the differing major and trace element compositions may be the result of differing mantle

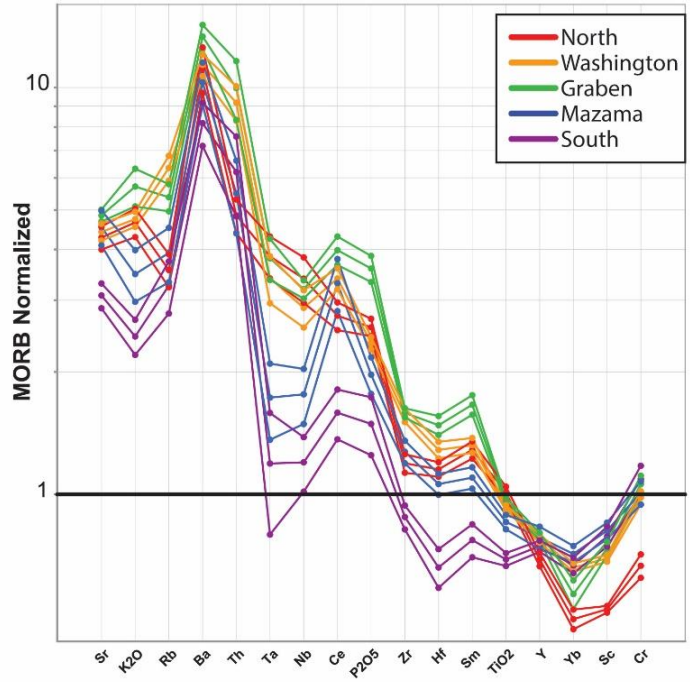

Figure 5.8: Trace element spider diagram, normalized to MORB (Pearce, 1983). Middle line for each segment is the bootstrapped mean, and upper and lower bounds represent 95% confidence interval.

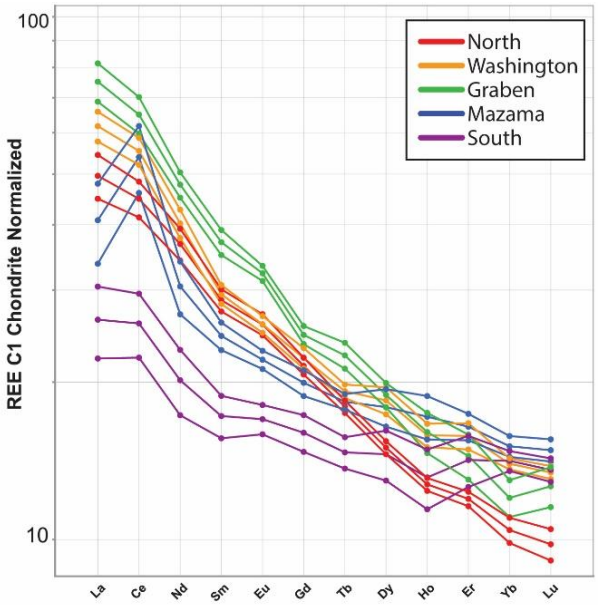

Figure 5.9: REE diagram, normalized to C1 Chondrite (Sun and McDonough, 1995). Symbols as in fig. 5.8.

processes or compositions (e.g. Bacon et al. 1997; Conrey et al. 1997; Leeman et al., 1990, 2005; Mullen et al., 2017; Rowe et al., 2009; Schmidt et al., 2008). A brief discussion of each is given in section 4.3.1.1 of this thesis, but for a detailed description of these end-members, the reader is referred to Mullen et al. (2017). Our bootstrapped mean allows us to determine which primitive type has the largest overall influence within a segment and begin to infer the processes or source heterogeneities responsible.

The southern two segments demonstrate a much larger influence of fluid-flux melting. These segments are characterized by an arc-typical negative Nb and Ta anomaly (Fig. 5.8), as well as an enrichment in LILE, with the highest high Ba/Ce (Fig. 5.10), Ba/Nb, and Sr/P in the arc, indicative of the influence of slab fluids (Borg et al., 1997). In addition, these segments likely record the highest degree mantle melts, as they have the flattest REE (Fig. 5.9 and 5.10). The flatter REE patterns are not likely to be simply the result of shallower melting since HREE abundances of the southern segment are similar to others (Fig. 5.9). Intense fracturing and deformation of the subducting Gorda Plate due to motion along the Mendocino Fracture Zone may lead to increased fluid penetration and higher delivery of subduction fluids into this segment (Schmidt et al., 2008). Fluid flux melting in these regions is likely assisted by hotter mantle temperatures due to toroidal flow around the slab edge (Mullen and Weis, 2014). Although the southern and Mazama segments share very similar fluid flux signatures, the Mazama segment seems to exhibit a lower degree of partial melting. This could be because the boundary between these segments lies at the boundary of the Juan deFuca and Gorda subducting plates. The age of the slab in the Mazama segment is the oldest in the arc and is 4-6 m.y. older than the young slab that is subducted in the south (Wilson, 2002). It is possible that despite having similarly high fluid flux, the Southern Segment has higher degree melts because the mantle is hotter due to a younger slab and hot toroidal flow around the slab edge.

A similar mechanism of toroidal flow was invoked by Mullen and Weis (2014) to explain north-to-south trends in the North Segment. Our Bootstrapped

averages support the idea that toroidal flow around the slab edge is likely an important process in generating primitive basalts there. The segment has anomalously high Nb/Zr and Nb/Yb compared to the rest of the arc (Fig. 5.11), consistent with enriched, fertile mantle entering the sub-arc wedge by toroidal flow around the slab. The North segment also has the lowest fluid-flux signal in the arc (low Ba/Ce, Ba/Nb, high HFSE), which may result from the slab being young and hot, and may result in dehydration significantly trenchward of the arc. In addition, our data suggest that slab melting may be occurring in the North Segment, since it has significantly lower HREE, Y, Sc, Cr abundances than all other segments, indicative of melting with garnet residual (Mullen et al., 2017).

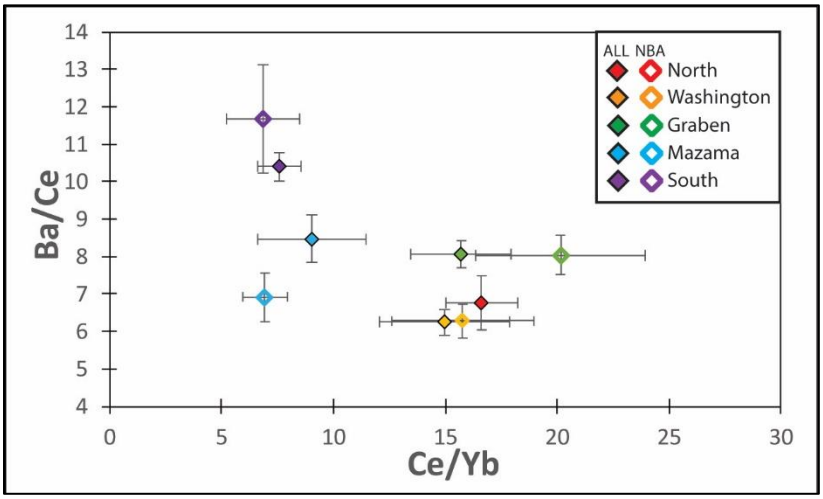

Figure 5.10: Ba/Ce vs. Ce/Yb for primitive data. Closed symbols represent all data for the segment (ALL) and open symbols are with no back arc (NBA). Error bars represent 95% confidence intervals

Although Wallowski et al. (2015) demonstrated that slab melting likely occurs in the southernmost Cascades beneath Lassen Peak, our bootstrapped data indicate that this may not be a dominant process throughout the entire segment, since the bootstrapped mean has relatively high HREE and Sc, and the lowest Dy/Yb and Sr/Y of any segment (Fig. 5.11). Thus, it is possible that slab melting in the Southern segment is more localized to the region beneath Lassen Peak, where deeper slab depths and hot toroidal flow may allow for more melting.

Schmidt et al. (2008) demonstrated the dominant role of LKTs in their Central Segment (Three Sisters to Medicine Lake). However, our statistically-based segmentation scheme placed a segment boundary south of Three Sisters, and the relative role of LKTs compared to IPBs may be the reason. The Mazama Segment has

geochemical trends that indicate the importance of both CABs (as discussed above) and LKTs, including low Nb/Zr and K_2O/TiO_2, and HFSE abundances that approximate N-MORB (Fig. 5.8). However, the Graben segment, which includes Three Sisters, has bootstrapped mean compositions that indicate the importance of enriched, IPB-type primitive compositions, including the highest HFSE, LREE, K_2O, and relatively high K_2O/TiO_2 and Nb/Zr (Mullen et al., 2017) (Fig. 5.8 and 5.9). Thus, lower degree partial melting of an enriched mantle source may be occurring beneath central but not southern Oregon, and this discrepancy may be the reason our statistically-based segmentation technique established a boundary here.

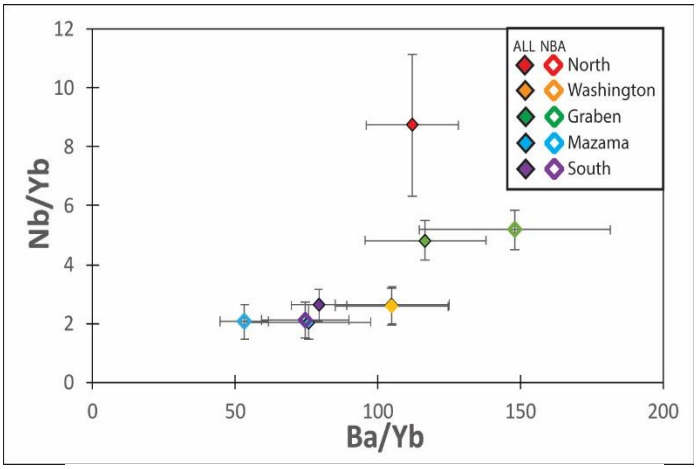

Figure 5.11: Nb/Yb vs. Ba/Yb for primitive data. Symbols as in Fig. 5.10.

A similar enrichment trend to that of the Graben Segment is seen in the bootstrapped compositions of the Washington Segment. Both of these lie within the Columbia Embayment, a region of positive Bouguer gravity anomalies that are thought to represent regions of accreted oceanic crust. This may include the Late Paleocene-Eocene Siletz Terrain, which has been interpreted to be an oceanic large igneous province (LIP) with a plume-origin (Phillips et al, 2017; Wells et al., 2014). Interaction of primitive basalts with Siletzia lithosphere would be expected to impart an IPB-like signature (Schmidt et al., 2008). Alternatively, a slab gap such the one suggested by Gao and Shen (2014) to underlie the latitude of the Columbia River, could provide both segments with enriched sub-slab mantle material.

5.3.2 The effect of back-arc data

We performed Monte Carlo Bootstrap analysis for each composition, both with, and without back arc data. While Schmidt et al. (2008) included back arc volcanoes such as the Newberry and Medicine Lake, our bootstrapped data indicate

that geochemical trends differ significantly depending on the inclusion of such data. This means that inclusion of the back-arc data may dilute along-arc geochemical trends as they include additional melt-generating processes . However, comparing data within a segment, both with and without the back arc, reveals interesting trends.

In general, back-arc inclusive data are lower or similar Ba/Nb and Ba/Ce, consistent with less subduction influence (Fig. 5.10). However, in the Mazama segment, these are higher in the back arc. The High Lava Plains (HLP), which stretch across southern Oregon and terminate with the youngest center at Newberry volcano (Jordan et al., 2004), have been shown to have unusually high Ba content for a back-arc (e.g. Jordan, 2011; Streck and Grunder, 2012). In addition, the back arc of the Mazama Segment also has enriched Nb/Ta (18.8), which is higher than chondrite values (~17), indicating a more fertile mantle source than is beneath the arc-front (Pearce and Stern, 2006). Slab-induced corner flow has been suggested to be the cause for HLP volcanism (e.g. Long et al., 2012), and our data are consistent with the flow of fertile, Ba-enriched mantle, into the back-arc, where it is depleted before proceeding to the arc-front (Pearce and Stern, 2006).

Further investigation of the geochemical differences between our new segments may allow for more inferences as to the processes that lead to along-arc variability. The preceding discussion is preliminary, but provides evidence of the value of our statistically-based techniques in highlighting key geochemical differences between arc segments.

5.6 Conclusions

In this study, we have demonstrated the need to approach important petrologic questions, such as along-arc variability, using statistically rigorous methodology. With the continual growth of online data repositories, scientists now have access to massive datasets that can allow for much more detailed studies of particular regions, or at the global scale. While these data can be quite powerful, great care should be taken in assessing the quality of data and reducing sampling bias.

Our work improves on previous studies of Cascades arc trends because we compiled a massive dataset of over 11,000 samples and utilize a Monte Carlo

approach with bootstrap resampling to reduce the bias that over-sampled volcanoes have on overall trends. In in doing so, we can assess regional, rather than local processes. Our study develops a novel approach to assessing along-arc geochemical variability using entirely objective and statistically-based methodology. Using this new approach, we separate the Cascades arc into 5 segments such that the geochemical differences between each is maximized. Although we demonstrate that the segments proposed by Schmidt et al. (2008) are statistically distinct form one another, our new segmentation scheme, which includes the North, Washington, Graben, Mazama, and South Segments is more statistically robust. By separating the arc into the most statistically distinct regions, we can better assess the different processes that lead to geochemical heterogeneity. This, in turn, allows us to better understand the fundamental processes involved in arc magma generation.

5.6.1 Future Work

The primary purpose of this work was to utilize a large dataset and develop a new statistical methodology for assessing along-arc variability. While we are confident in our new segmentation scheme and statistical methodology, there is still significant work to be done. The study was hampered by the inability to calculate Mahalanobis distances for some regions and compositions due to the lack of analyses in some portions of the arc. Further investigation of better algorithms for imputing missing values to calculate covariance matrices, or a different proximity measure, could prove to be useful.

Significant future work will be directed at interpreting geochemical trends for primitive data. In addition, we plan to compare felsic compositions between these new arc segments to see if the parental composition or crustal reprocesses are most important in developing along-arc heterogeneity on felsic magmas.

We also plan to investigate a segmentation scheme utilizing the back-arc data. Comparing the two schemes could provide insight into the processes that lead to differing back arc compositions, and to explore how north-south trends affect arc-front volcanoes differently than those of the back arc.

In addition, we have separated data into the three endmember types (Fig. 4.3), and plan to use our bootstrap analysis to investigate along-arc differences within a single endmember primitive type. Previous studies, (e.g. Leeman et al., 2005; Mullen et al., 2017; Schmidt et al. 2008), have assessed these differences, but with much smaller datasets, and such analysis has proven fruitful. These studies could be improved upon with the use of a comprehensive dataset and statistical methodology.

We have also begun exploring changes in the arc through time. We have conducted preliminary bootstrap analyses on data from the Western Cascades ancestral arc (~40-5 Ma), and plan to compare how geochemical trends change, within each region, through time.

References

Brocher, T.M., Wells, R.E., Lamb, A.P., Weaver, C.S., 2017. Evidence for distributed clockwise rotation of the crust in the northwestern United States from fault geometries and focal mechanisms. Tectonics 2016TC004223. doi:10.1002/2016TC004223

Carpentier, M., Weis, D., Chauvel, C., 2014. Fractionation of Sr and Hf isotopes by mineral sorting in Cascadia Basin terrigenous sediments. Chemical Geology 382, 67–82. doi:10.1016/j.chemgeo.2014.05.028

Carr, M.J., Feigenson, M.D., Patino, L.C., Walker, J.A., 2004. Volcanism and Geochemistry in Central America: Progress and Problems, in: Eiler, J. (Ed.), Inside the Subduction Factory. American Geophysical Union, pp. 153–174. doi:10.1029/138GM09

Everitt, B., Landau, S., Leese, M., 2001. Cluster analysis, 4th ed. ed. Arnold ; Oxford University Press, London : New York.

Gardner, M.J., Altman, D.G., 1986. Confidence intervals rather than P values: estimation rather than hypothesis testing. Br Med J (Clin Res Ed) 292, 746–750. doi:10.1136/bmj.292.6522.746

Hildreth, W., Fierstein, J., 2015. Geologic map of the Simcoe Mountains Volcanic Field, main central segment, Yakama Nation, Washington (USGS Numbered Series No. 3315), Scientific Investigations Map. U.S. Geological Survey, Reston, VA.

Keller, C.B., Schoene, B., 2012. Statistical geochemistry reveals disruption in secular lithospheric evolution about 2.5 Gyr ago. Nature 485, 490–493. doi:10.1038/nature11024

Keller, C.B., Schoene, B., Barboni, M., Samperton, K.M., Husson, J.M., 2015. Volcanic-plutonic parity and the differentiation of the continental crust. Nature 523, 301–307. doi:10.1038/nature14584

Little, R.J.A., Rubin, D.B., 2014. Statistical Analysis with Missing Data. John Wiley & Sons.

Matsumoto, M., Nishimura, T., 1998. Mersenne Twister: A 623-dimensionally Equidistributed Uniform Pseudo-random Number Generator. ACM Trans. Model. Comput. Simul. 8, 3–30. doi:10.1145/272991.272995

Meng, X.-L., Rubin, D.B., 1993. Maximum likelihood estimation via the ECM algorithm: A general framework. Biometrika 80, 267–278. doi:10.1093/biomet/80.2.267

Mojena, R., 1977. Hierarchical grouping methods and stopping rules: an evaluation. Comput J 20, 359–363. doi:10.1093/comjnl/20.4.359

Mullen, E.K., Weis, D., 2015. Evidence for trench-parallel mantle flow in the northern Cascades arc from basalt geochemistry. Earth and Planetary Science Letters 414, 100–107. doi:10.1016/j.epsl.2015.01.010

Patino, L.C., Carr, M.J., Feigenson, M.D., 2000. Local and regional variations in Central American arc lavas controlled by variations in subducted sediment input. Contrib Mineral Petrol 138, 265–283. doi:10.1007/s004100050562

Schmidt, M.E., Grunder, A.L., Rowe, M.C., 2008. Segmentation of the Cascades arc as indicated by Sr and Nd isotopic variation among diverse primitive basalts. Earth and Planetary Science Letters 266, 166–181. doi:10.1016/j.epsl.2007.11.013

Shaw, A.M., Hilton, D.R., Fischer, T.P., Walker, J.A., Alvarado, G.E., 2003. Contrasting He–C relationships in Nicaragua and Costa Rica: insights into C cycling through subduction zones. Earth and Planetary Science Letters 214, 499–513. doi:10.1016/S0012-821X(03)00401-1

Sherrod, D.R., Smith, J.G., 1990. Quaternary extrusion rates of the Cascades Range, northwestern United States and southern British Columbia. J. Geophys. Res. 95, 19465–19474. doi:10.1029/JB095iB12p19465

Streck, M.J., Grunder, A.L., 2012. Temporal and crustal effects on differentiation of tholeiite to calcalkaline and ferro-trachytic suites, High Lava Plains, Oregon, USA. Geochem. Geophys. Geosyst. 13, Q0AN02. doi:10.1029/2012GC004237

Turner, S., Foden, J., 2001a. U, Th and Ra disequilibria, Sr, Nd and Pb isotope and trace element variations in Sunda arc lavas: predominance of a subducted sediment component. Contrib Mineral Petrol 142, 43–57. doi:10.1007/s004100100271

Turner, S., Foden, J., 2001b. U, Th and Ra disequilibria, Sr, Nd and Pb isotope and trace element variations in Sunda arc lavas: predominance of a subducted sediment component. Contrib Mineral Petrol 142, 43–57. doi:10.1007/s004100100271

Weaver, C.S., Baker, G.E., 1988. Geometry of the Juan de Fuca plate beneath Washington and northern Oregon from seismicity. Bulletin of the Seismological Society of America 78, 264–275.

Wells, R.E., McCaffrey, R., 2013. Steady rotation of the Cascades arc. Geology 41, 1027–1030. doi:10.1130/G34514.1

Whitford, D.J., Nicholls, I.A., Taylor, S.R., 1979. Spatial variations in the geochemistry of quaternary lavas across the Sunda arc in Java and Bali. Contr. Mineral. and Petrol. 70, 341–356. doi:10.1007/BF00375361

Wörner, G., Moorbath, S., Horn, S., Entenmann, J., Harmon, R.S., Davidson, J.P., Lopez-Escobar, L., 1994. Large- and Fine-Scale Geochemical Variations Along the Andean Arc of Northern Chile (17.5°– 22°S), in: Reutter, P.D.K.-J., Scheuber, D.E., Wigger, D.P.J. (Eds.), Tectonics of the Southern Central Andes. Springer Berlin Heidelberg, pp. 77–92. doi:10.1007/978-3-642-77353-2_5

6. Conclusions

Determining the causes for geochemical differences within arcs worldwide and the role that tectonics and geodynamics play in producing such heterogeneities is crucial to our understanding of arc processes. Assessing changes in the behavior of a single arc, both along-strike and through time can be an excellent tool to elucidate these petrogenetic causes.

In this thesis, I have demonstrated that the pyroclastic record contained within the Deschutes Formation of central Oregon records an 800 k.y. pulse (6.25-5.45 Ma) of heightened silicic and explosive volcanism that is significantly higher, both in volumetric rate and frequency of eruptions, than anywhere in the arc for the last 17 Ma. I used statistical correlation methods to establish basin-wide tephrostratigraphy which helps to constrain the pace of volcanism during this pulse. We have found that volcanism had begun to wane prior to the creation of the High Cascades graben. The timing, duration and geochemistry of this silicic pulse was likely due to intra-arc extension, which focused decompression mantle melts into a new arc location. This high flux of hot-dry-reduced basalt, ushered into the shallow crust by extension, allowed for a temporary period of heightened crustal melting and silicic magma generation. Geochemical trends, including major and trace element and isotopic data indicate that extension influenced every level of the magmatic system during this time. By comparing the geochemistry and eruptive volumes to that of the Quaternary we have demonstrated that very different magmatic processes acted to produce the unusual magmatism of the Deschutes Formation, compared with those of the Quaternary. This work has acted to constrain the timing, magnitude, and tectonic and petrogenetic causes of this critical period in the history of the Cascades arc. This is important not only for understanding Cascades arc, but also helps us to infer processes that can cause an arc to shift from the steady-state to a period of heightened explosive volcanism, which is critical for hazard assessment of arcs worldwide.

In addition to assessing the causes for an unusually explosive time interval in Cascades arc history, this thesis also aimed to investigate the spatial variability of arc magmatic geochemistry. To do this, we compiled a massive dataset of Cascades

major element, trace element, and isotopic data, and developed a new robust statistical methodology to establish a new segmentation scheme of the Cascades arc. By establishing these statistically distinct segments, we can begin to infer the tectonic and geodynamic differences along the arc that may be responsible for such geochemical heterogeneity.

Thus, this thesis acts to address the variability of magmatic geochemistry and eruption style within a single arc, both through time and space. In doing so, we have not only filled gaps in knowledge about an important transitional period of Cascades arc history, but we have also illuminated petrogenetic causes for arc variability, which addresses fundamental themes in the field of igneous petrology and geochemistry.